

Synthesis and Study of Electro-Active Organic Molecules for Optoelectronic Applications

Shriya Wadumethrige
Marquette University

Recommended Citation

Wadumethrige, Shriya, "Synthesis and Study of Electro-Active Organic Molecules for Optoelectronic Applications" (2012).
Dissertations (2009 -). Paper 203.
http://epublications.marquette.edu/dissertations_mu/203

SYNTHESIS AND STUDY OF ELECTRO-ACTIVE ORGANIC MOLECULES FOR
OPTOELECTRONIC APPLICATIONS

by

Shriya Hemalika Wadumethrige B. Sc. (Hons.)

A Dissertation submitted to the Faculty of the Graduate School,
Marquette University,
in Partial Fulfillment of the Requirements for
the Degree of Doctor of Philosophy

Milwaukee, Wisconsin

May 2012

ABSTRACT
SYNTHESIS AND STUDY OF ELECTRO-ACTIVE ORGANIC MOLECULES FOR
OPTOELECTRONIC APPLICATIONS

Shriya Hemalika Wadumethrige B.Sc. (Hons.)

Marquette University, 2012

Electro-active organic materials have received considerable attention in the emerging area of molecular electronics and nanotechnology not only because of the attractive optical and electronic properties but also the advantages of organic materials such as low cost, easy processing, and great opportunities for structural modification. These materials are now being considered as active components in electronic and optoelectronic devices such as light emitting diodes for display applications, thin film transistors for low-cost and ultra-dense logic and memory circuits, photodiodes for optical information processing, and photovoltaic cells for solar energy harvesting. Therefore the electro-active organic materials have become a focus of intense research. This thesis concentrates the synthesis and study of optoelectronic properties of several classes of novel electro-active organic materials.

A series of electro-active tetraarylbenzo[1,2-*b*:4,5-*b'*]difuran (BDF) and model diarylbenzofuran derivatives have been synthesized and their structures were established by X-ray crystallography. The single charge stabilization by benzodifuran and coplanar α -aryl groups lying on the longitudinal suggests that the linear arrays of BDFs may allow the construction of molecular wires suitable for long-range electron transport. The synthesis of hexa alkyloxy substituted hexa-*peri*-hexabenzocoronene (HBC), a larger and electron rich chromophore, via oxidative cyclodehydrogenation of *hexakis*(4-alkyloxyphenyl)-benzene produced a quantitative yield of an indenofluorene derivative rather than the expected HBC. The mechanistic considerations for the formation of the indenofluorene derivative led us to devise an alternative synthesis of elusive alkoxy-substituted HBC. Furthermore a series of alkyloxy substituted HBCs were prepared and their electronic properties were studied. A series of aryloxy-substituted tetraphenylethylenes (TPEs), tetraphenylethylene based dendrimers and a series of phenyl ethers were prepared and the effect of the diarylether linkage on their electronic and optical properties was studied. Although the diarylether linkage in TPEs did not affect the properties significantly, these linkages in poly-*p*-phenyl ethers seem to mediate the delocalization of the cationic charges. A series of cycloannulated aromatic donors were prepared for the preparation of stable cation radical salts. The availability of wide range of donors with varied redox potentials (0.82 V- 1.85 V) and spectroscopic features make these cation radicals to be valuable oxidants for variety of organic, inorganic and organometallic donors.

DEDICATION

To the memory of my late father

*I remember the big smile on your face upon my success which always encouraged
me.....*

ACKNOWLEDGMENTS

Shriya Hemalika Wadumethrige B. Sc. (Hons.)

I am heartily thankful to my supervisor, Prof. Rajendra Rathore who was abundantly helpful and offered invaluable assistance, support and guidance throughout my research work. My deepest gratitude is also due to the members of my dissertation committee, Prof. James R. Gardinier, Prof. Mark G. Steinmetz and Prof. Adam Fiedler for their generously given time and expertise to better my work. I would like to give my sincere thanks to all my teachers who pointed me in the right direction to get where I am today. It is a pleasure to thank to all my group members Ruchi, Vijay, Tushar, Linyi, Mathew, Khushabu, Rekha and Anita for sharing the literature and invaluable assistance. I would like to acknowledge Department of Chemistry, Marquette University for financial sources and laboratory facilities. I am much grateful to Prof. John Eisch for his generous support as “Eisch research fellowship”. I owe my deepest gratitude to Todd and Tracy who helped me adjust to a new country. I greatly value their support, care and friendship which helped me overcome setbacks in the beginning of my graduate study.

I would like to express my heart-felt gratitude to my family, specially my mother who has been a constant source of love, concern, support and strength throughout my life. My sincere gratitude is due to my husband, Sarath for his support, encouragement, help and love throughout this endeavor. I would like to convey my love and blessings for my little son, Nirad for giving me strength and happiness in my life. Lastly, I offer my regards and blessings to all of those who supported me in any respect during the completion of my graduate study.

TABLE OF CONTENTS

DEDICATION.....	i
ACKNOWLEDGMENTS.....	ii
LIST OF TABLES.....	iv
LIST OF FIGURES.....	v
INTRODUCTION.....	1
CHAPTER 1. Synthesis, Electronic Properties and X-ray Structural Characterization of Tetrarylbenzo[1,2-b:4,5-b']-difuranCation Radicals.....	6
Introduction	6
Results and Discussion	7
Experimental Section	19
CHAPTER 2A. A Facile Synthesis of Elusive Alkoxy-substituted Hexa-<i>peri</i>- hexabenzocoronene.....	44
Introduction	44
Results and Discussion	45
Experimental Section	56
CHAPTER 2B. Intramolecular Scholl reactions of alkoxy-substituted hexaarylbenzenes via cation radical (electron transfer) mechanism.....	78
Introduction	78
Results and Discussion	85
Experimental Section	91
CHAPTER 2C. Dodecaalkoxy-hexa-<i>peri</i>-hexabenzocoronene: A non-planar PAH with six easily accessible oxidation states.....	104
Introduction	104
Results and Discussion	108

Experimental Section	121
CHAPTER 3A. Preparation of tetraaryloxyphenylethylene based dendrimers	131
Introduction	131
Results and Discussion	132
Experimental Section	148
CHAPTER 3B. Structure and optoelectronic properties of acyclic and cyclic polyphenyl ethers (PPE)	161
Introduction	161
Results and Discussion	162
Experimental Section	175
CHAPTER 4. Cycloannulated aromatic donors and their highly robust cation radical salts as redox tunable oxidants.....	188
Introduction	188
Results and Discussion	192
Experimental Section	212
BIBLIOGRAPHY.....	242

LIST OF TABLES

CHAPTER 1

- Table 1a** Experimental and theoretical bond lengths of the centrosymmetric neutral and cation radical of **BDF1** in picometers (pm).
The average esd's are shown in parenthesis.....17
- Table 1b** Experimental and theoretical bond lengths of the centrosymmetric Neutral and cation radical of **BDF2** in picometers (pm).
The average esd's are shown in parenthesis.....18

CHAPTER 3A

- Table 1** Electrochemical Oxidation Potentials and substituent constant σ of tetraaryloxyphenylethylenes.....139

CHAPTER 3B

- Table 1** Oxidation potential values of E1-E_{cyclic}, PE3, PE4, DHB.....170
- Table 2** λ_{\max} values for the bands observed for linear and cyclic poly p-phenyl ethers.....171

CHAPTER 4

- Table 1** Electrochemical Oxidation Potentials of the cycloannulated aromatic donos **I-XIII**.....198
- Table 2** Radical cation data of various cycloannulated aromatic donors.....201

LIST OF FIGURES

INTRODUCTION

Figure 1	Structures of some ladder type organic compounds.....	2
Figure 2	Structures of polyphenylenevinylenes (PPV) and poly[2-methoxy -5-(2'- ethylhexyloxy)-1,4-phenylene vinylene] (MEH-PPV).....	3
Figure 3	Structures of substituted triphenylenes and substituted hexa- <i>peri</i> -hexabenzocoronenes.....	4

CHAPTER 1

Figure 1	Showing the structural similarities between polyphenylenevinylenes and tetraarylbenzo[1,2-b:4,5-b']-difurans.....	6
Figure 2	Comparison of the emission and excitation spectra of BDF1-3 (left) and M1-3 (right) in dichloromethane at 22 °C.....	10
Figure 3	Comparison of the cyclic voltammograms of various benzodifuran (2 mM) and benzofuran (3 mM) derivatives in CH ₂ Cl ₂ (0.1 M <i>n</i> -Bu ₄ NPF ₆) at a scan rate of 200 mV s ⁻¹ . Note that the first oxidation wave of BDF1 is completely reversible (red curve) if the scanning is terminated before the start of the second oxidation event.....	10
Figure 4A	Left: Spectral changes upon the reduction of 3.2 × 10 ⁻⁵ M NAP ^{•+} (blue line) by incremental addition of 1.0 × 10 ⁻³ M BDF1 to its radical cation (green line) in CH ₂ Cl ₂ at 22 °C. Right: A plot of depletion of absorbance of NAP ^{•+} (blue squares, at 672 nm) and an increase of the absorbance of BDF1 ^{•+} (green circles, at 1100 nm) against the equivalent of added neutral BDF1	12
Figure 4B	A comparison of the absorption spectra of BDF1-3 cation radicals (left) and M1-3 cation radicals (right).....	13
Figure 5	The ORTEP diagrams showing the arrangement of BDF1 ^{•+} SbCl ₆ ⁻ (right) and BDF2 ^{•+} SbCl ₆ ⁻ (left) unit cells.....	14
Figure 6	Showing the HOMO's of BDF1 (right) and BDF2 (left), obtained by DFT calculations at the B3LYP-631G* level.....	16
Figure 7	UV-vis absorption spectra of various benzodifurans and benzofurans obtained in dichloromethane at 22 °C. The absorption maxima and extinction coefficients are: BDF1 , λ _{max} = 354 nm, ε ₃₅₄ = 7.8 × 10 ⁴ M ⁻¹ cm ⁻¹ ; BDF2 , λ _{max} = 363 nm, ε ₃₆₃ = 7.29 × 10 ⁴ M ⁻¹ cm ⁻¹ ; BDF3 ,	

$\lambda_{\max} = 365 \text{ nm}$, $\epsilon_{365} = 8.4 \times 10^4 \text{ M}^{-1} \text{ cm}^{-1}$; **M1**, $\lambda_{\max} = 314 \text{ nm}$,
 $\epsilon_{314} = 2.5 \times 10^4 \text{ M}^{-1} \text{ cm}^{-1}$; **M2**, $\lambda_{\max} = 317 \text{ nm}$, $\epsilon_{317} = 3.6 \times 10^4$
 $\text{M}^{-1} \text{ cm}^{-1}$; **M3**, $\lambda_{\max} = 315 \text{ nm}$, $\epsilon_{315} = 2.6 \times 10^4 \text{ M}^{-1} \text{ cm}^{-1}$21

- Figure 8** Spectral changes upon the reduction of $6.85 \times 10^{-5} \text{ M MA}^{*\cdot+}$ (Black line) by incremental addition of $1.0 \times 10^{-3} \text{ M BDF1}$ to its radical cation (green line) in CH_2Cl_2 at $22 \text{ }^\circ\text{C}$. Note that the growth of the absorption bands due to **BDF1**⁺⁺ was only ceased after the addition of excess **BDF1** (i.e. roughly 3 equivalents).....22
- Figure 9** Spectral changes upon the reduction of $6.87 \times 10^{-5} \text{ M MA}^{*\cdot+}$ (Black line) by incremental addition of $1.0 \times 10^{-3} \text{ M BDF2}$ to its radical cation (red line) in CH_2Cl_2 at $22 \text{ }^\circ\text{C}$. Note that the growth of the absorption bands due to **BDF2**⁺⁺ completely ceased after the addition of one equivalent of neutral **BDF2**.....23
- Figure 10** Spectral changes upon the reduction of $6.62 \times 10^{-5} \text{ M MA}^{*\cdot+}$ (Black line) by incremental addition of $1.0 \times 10^{-3} \text{ M BDF3}$ to its radical cation (green line) in CH_2Cl_2 at $22 \text{ }^\circ\text{C}$. Note that the growth of the absorption bands due to **BDF3**⁺⁺ completely ceased after the addition of one equivalent of neutral **BDF3**.....23
- Figure 11** Spectral changes upon the reduction of $6.85 \times 10^{-5} \text{ M MA}^{*\cdot+}$ (Black line) by incremental addition of $1.0 \times 10^{-3} \text{ M M2}$ to its radical cation (green line) in CH_2Cl_2 at $22 \text{ }^\circ\text{C}$. Note that the growth of the absorption bands due to **M2**⁺⁺ completely ceased after the addition of one equivalent of neutral **M2**.....24
- Figure 12** Spectral changes upon the reduction of $7.33 \times 10^{-5} \text{ M MA}^{*\cdot+}$ (Black line) by incremental addition of $1.0 \times 10^{-3} \text{ M M3}$ to its radical cation (green line) in CH_2Cl_2 at $22 \text{ }^\circ\text{C}$. Note that the growth of the absorption bands due to **M3**⁺⁺ completely ceased after the addition of one equivalent of neutral **M3**.....24
- Figure 13** **Left:** Spectral changes upon the reduction of $3.2 \times 10^{-5} \text{ M NAP}^{*\cdot+}$ (blue line) by incremental addition of $1.0 \times 10^{-3} \text{ M BDF1}$ to its radical cation (green line) in CH_2Cl_2 at $22 \text{ }^\circ\text{C}$. **Right:** A plot of depletion of absorbance of $\text{NAP}^{*\cdot+}$ (blue squares, at 672 nm) and an increase of the absorbance of **BDF1**⁺⁺ (green circles, at 1100 nm) against the equivalent of added neutral **BDF1**.....25
- Figure 14** Spectral changes upon the reduction of $5.61 \times 10^{-5} \text{ M NAP}^{*\cdot+}$ (blue line) by incremental addition of $1.0 \times 10^{-3} \text{ M M1}$ to its radical cation (black line) in CH_2Cl_2 at $22 \text{ }^\circ\text{C}$. Note that the growth of the absorption bands due to **M1**⁺⁺ completely ceased after the addition of one equivalent of neutral **M1**.....26

- Figure 15** **Left:** Spectral changes upon the reduction of 4.83×10^{-5} M $\text{NAP}^{\bullet+}$ (blue line) by incremental addition of 1.0×10^{-3} M **BDF2** to its dication (green lines) and radical cation (pink line) in CH_2Cl_2 at 22 °C. **Right:** A comparison of the spectra of dication (green line) and radical cation (pink line) of **BDF2** showing that intense NIR transition at 1368 nm is absent in the **BDF2** dication.....26
- CHAPTER 2A
- Figure 1A** Showing the similarity of the aromatic region of the ^1H NMR spectra of indenofluorenes **7a** and **7b**.....47
- Figure 1B** Showing the similarity of the aromatic region of the ^{13}C NMR spectra of indenofluorenes **7a** and **7b**.....47
- Figure 1C** Showing the similarity of the aromatic region of the ^1H NMR spectra of indenofluorenes **7a** and **7b** in $\text{DMSO}-d_6$. Note that the aromatic region of reported ^1H NMR spectrum of supposed phenanthroquinone **4** ($\text{R} = \text{C}_{12}\text{H}_{25}$) in $\text{DMSO}-d_6$ was identical to that of **7a** and **7b**. [Compare: Weiss, K.; Beernink, G.; Dötz, F.; Birkner, A.; Müllen, K.; Wöll, C. H. *Angew. Chem. Int. Ed.* **1999**, *38*, 3748-3752.].....48
- Figure 2** Cyclic voltammogram of indenofluorene **7b** in CH_2Cl_2 containing 0.1 M $n\text{-Bu}_4\text{NPF}_6$ (as the supporting electrolyte) at a scan rate of 100 mV s^{-1} . The E_{ox} values of **7b** (i.e. $E_{\text{ox}1} = 1.18$ and $E_{\text{ox}2} = 1.41$ V vs. SCE) were referenced with ferrocene ($E_{\text{ox}} = 0.45$ V vs. SCE) as an added internal standard.....50
- Figure 3** UV-vis-NIR absorption spectrum of the cation radical of indenofluorene **7b** ($\text{7b}^{\bullet+}$, $\lambda_{\text{max}} = 1108, 952, 504, \text{ and } 466 \text{ nm}$; $\epsilon_{1108} = 44,300 \text{ M}^{-1} \text{ cm}^{-1}$) in CH_2Cl_2 generated using a hindered naphthalene cation radical ($\text{NAP}^{\bullet+}$, $E_{\text{red}} = 1.34$ V vs. SCE, $\lambda_{\text{max}} = 672, 616, 503, \text{ and } 396 \text{ nm}$; $\epsilon_{672} = 9300 \text{ M}^{-1} \text{ cm}^{-1}$).....51
- Figure 4A** Variable temperature ^1H NMR spectra of HBC **2** in toluene- d_8 obtained at 20, 40, 60, 80, and 90 °C. Temperatures are indicated on the spectra.....53
- Figure 4B** ^{13}C NMR spectrum of **2** in CDCl_3 at 60 °C was rather broad and therefore the spectrum was recorded in toluene- d_8 at 90 °C. Also note that the peaks belonging to HBC **2** are labeled with red circles.....54
- Figure 5** The MALDI mass spectra of HBC **2** (top) and the calculated isotope distribution for the mass ion of HBC **2** (bottom).....54

CHAPTER 2B

- Figure 1** (A) Energies of various intermediates formed in the cyclo-dehydrogenation of hexaphenylbenzene by Benjamin King and coworkers. (B) Energies of various intermediates formed during cyclodehydrogenation of the HPB by DFT calculations at the B3LYP/6-31G* level.....80
- Figure 2** A. ¹H NMR spectrum of hexakis(4-isobutylphenyl)benzene (**1m**) in CDCl₃. B. ¹H NMR spectrum of the crude product obtained after a reaction of **1m** with 6 equivalents of DDQ in CH₂Cl₂ in the presence of CH₃SO₃H showing the quantitative formation of the corresponding HBC **2m**. C. ¹H NMR spectrum of the crude product obtained after a reaction of **1m** with 2 equivalents of DDQ in CH₂Cl₂ in the presence of CH₃SO₃H showing that only 1/3 of **1m** is transformed to corresponding HBC**2m**.....82
- Figure 3** X-ray crystal structures of products obtained by oxidative cyclodehydrogenation of (A) 4-methoxy substituted, (B) 3,4-di-methoxy substituted, and (C) 3,5-dimethoxy substituted hexaarylbenzenes.....88

CHAPTER 2C

- Figure 1A** Structures of A and B.....105
- Figure 1B** The molecular structures of non-planar alkoxy substituted HBCs C and D obtained by DFT calculations at B3LYP/6-31G* level.....106
- Figure 2** (A) The molecular structure of **3a** shown as ORTEP diagram (thermal ellipsoids drawn in 50% probability). (B)/(C) Two views showing that one pair of 3,5-dimethoxyphenyls (with syn oriented methoxy groups) lie at a dihedral angle of ~89.4° relative to central phenyl ring (middle) while the other two pairs of 3,5-dimethoxyphenyls (with anti oriented methoxy groups) lie at the dihedral angles of 74.6° and 72.7°.....109
- Figure 3** (A) The molecular structure of **4a** shown as ORTEP diagram (thermal ellipsoids drawn in 50% probability). (B)/(C)/(D) Three views showing the distortion of the HBC core from mean plane of the molecule.....111
- Figure 4** Comparison of variable temperature ¹H NMR spectra of **4a** in CDCl₃ recorded at 20, 30, 40, 50, and 60 °C. Temperatures are indicated on the spectra.....112
- Figure 5** Comparison of the ¹³C NMR spectra of **4b** in CDCl₃ recorded at 20 and 60 °C. Temperatures are indicated on the spectra.....113
- Figure 6** Cyclic (red curve) and square-wave (blue curve) voltammo-grams of a 0.18 mM solution of **4a** in CH₂Cl₂ containing 0.1 M

	<i>n</i> -Bu ₄ NPF ₆ as the supporting electrolyte at a scan rate of 200 mV s ⁻¹ and at 20 °C.....	114
Figure 7	Cyclic (red curve) and square-wave (blue curve) voltammograms of a 1 mM solution of 4b in CH ₂ Cl ₂ containing 0.1 M <i>n</i> -Bu ₄ NPF ₆ as the supporting electrolyte at a scan rate of 200 mV s ⁻¹ and at 20 °C. The <i>E</i> _{ox} values of 4b were referenced to ferrocene (<i>E</i> _{ox} = 0.45 V vs. SCE) as an added internal standard.....	115
Figure 8	Spectral changes upon the reduction of 3.6 x 10 ⁻⁵ M MB ^{•+} by an incremental addition of 5.3 x 10 ⁻⁴ M 4b in CH ₂ Cl ₂ at 22 °C. The coloring scheme in the above Figure is as follows: addition of 0 to 0.25 equiv of 4b (pink spectra); addition of 0.25 to 0.5 equiv of 4b (green spectra); addition of 0.5 to 0.75 equiv of 4b (red spectra); addition of 0.75 to 1.0 equiv of 4b (blue spectra).....	116
Figure 9	The UV-vis absorption spectra of tetracationic 4b ⁺⁴ , tricationic 4b ⁺³ , dicationic 4b ⁺² , and finally the cation radical 4b ^{•+} , produced upon treatment of a solution of MB ^{•+} to 0.25, 0.33, 0.50, and 1.00 equivalents of 4b , respectively, in CH ₂ Cl ₂ at 22 °C.....	119
Figure 10	A. UV-vis absorption spectrum of neutral 4b (λ _{max} = 285, 315, 425, 464, and 495 nm; ε ₄₂₅ = 4.1 x 10 ⁵ M ⁻¹ cm ⁻¹) in CH ₂ Cl ₂ . B. Emission spectrum of the 4b in dichloromethane at 22 °C.....	120
CHAPTER 3A		
Figure 1	The molecular structure of A , B and D shown as ORTEP diagram.....	134
Figure 2	Cyclic voltammograms of 1.25 x 10 ⁻³ M A-D in CH ₂ Cl ₂ containing 0.2 M (<i>n</i> -Bu) ₄ NPF ₆ at 22 °C at scan rate of 100 mV s ⁻¹	138
Figure 3	The Hammett plot of the oxidation potentials of various tetraaryloxyphenylethylenes in dichloromethane solutions at 22 °C vs substituent constant σ (regression coefficient = 0.99).....	140
Figure 4	Left. Spectral changes upon the reduction of 4.1 x 10 ⁻⁵ M MB ^{•+} by incremental addition of 2.0 x 10 ⁻³ M D to its radical cation in CH ₂ Cl ₂ at 22 °C Right. A plot of depletion of absorbance of MB ^{•+} (blue triangles, at 728 nm) and an increase of the absorbance of D ^{•+} (red squares, at 964 nm) against the equivalent of added neutral D	141
Figure 5	Comparison of the absorption spectra of radical cation of A-D obtained upon reduction of 6.85 x 10 ⁻⁵ M CRET ^{•+} by one equivalent of TAEs in CH ₂ Cl ₂ at 22 °C.....	142

Figure 6	Showing HOMOs of B obtained by AM1 calculations.....	143
Figure 7	The crystal structure of D ²⁺ (SbCl ₆ ⁻) ₂ shown as ORTEP diagram.....	144
Figure 8	UV-vis absorption spectrum of a solution of D ²⁺ obtained by dissolving the dicationic crystals isolated for X-ray diffraction in dichloromethane..	144
Figure 9	Cyclic voltammograms of 2.5 mM G1 and G2 in CH ₂ Cl ₂ containing 0.2 M (<i>n</i> -Bu) ₄ NPF ₆ at 22 °C at scan rate of 100 mV s ⁻¹	146
Figure 10	Comparison of the absorption spectra of radical cation of G1 and G2 obtained upon reduction of 6.85 x 10 ⁻⁵ M CRET ^{•+} and 7.10 x 10 ⁻⁵ M MB ^{•+} by one equivalent of G1 and G2 respectively in CH ₂ Cl ₂ at 22 °C....	147
Figure 11	Comparison of Emission properties of dendrimers (G1 , G2) with D	147
CHAPTER 3B		
Figure 1	The ball and stick display of X-ray crystal structures of E2, E3 and E4 respectively.....	165
Figure 2	Cyclic voltammograms and square wave voltammograms of the <i>p</i> -PPEOs obtained from 2.5 x10 ⁻³ mM solution in dichloromethane in the presence of 0.2 M Tetra- <i>n</i> -butylammoniumhexafluorophosphate as the supporting electrolyte at 22°C.....	167
Figure 3	Comparison of Cyclic voltammograms of E1 and 1,4-dihexyloxybenzene obtained from 2.5 x10 ⁻³ mM solution in dichloromethane in the presence of 0.2 M Tetra- <i>n</i> -butylammoniumhexafluorophosphate as the supporting electrolyte at 22°C.....	168
Figure 4	Comparison of Cyclic voltammograms of E3 with PE3 obtained from 2.5 x10 ⁻³ mM solution in dichloromethane in the presence of 0.2 M Tetra- <i>n</i> -butylammoniumhexafluorophosphate as the supporting electrolyte at 22°C.....	168
Figure 5	Cyclic voltammograms of E4 and PE4 obtained from 2.5 x10 ⁻³ mM solution in dichloromethane in the presence of 0.2 M Tetra- <i>n</i> -butylammoniumhexafluorophosphate as the supporting electrolyte at 22°C.....	169
Figure 6	The HOMO Pictures of linear and cyclic ether oligomers.....	170
Figure 7	(a) Comparison of the UV-Vis spectra of neutral ethers E1-E6, (b) E6- Eyclic (c) PE3 and E3 (d) PE4 and E4 (e) Emission spectra of E1-E _{cyclic} in 4.5 x 10 ⁻⁵ M in dichloromethane at 22 °C.....	172

Figure 8	The absorption spectra of 3.02×10^{-4} M Cation radical of linear poly - phenylether oligomers generated by using $\text{NO}^+\text{SbCl}_6^-$	173
Figure 9	The absorption spectra of Cation radical of cyclic poly –phenylether oligomers generated by using $\text{NO}^+\text{SbCl}_6^-$	174
Figure 10	Comparison of The absorption spectra of Cation radical of poly- <i>p</i> -phenylether oligomers generated by using $\text{NO}^+\text{SbCl}_6^-$ and Laser flash photolysis.....	174
Figure 11	Comparison of the absorption spectra of Cation radical of poly- <i>p</i> -phenylether oligomers generated by using $\text{NO}^+\text{SbCl}_6^-$ (red) and Laser flash photolysis(blue).....	175
CHAPTER 4		
Figure 1	A-D Representative X-ray crystal structures of cycloannulated hydrocarbons showing that steric hindrance prevents face-face contact of aromatic moities.....	197
Figure 2A	Cyclic voltammograms and square wave voltammograms of I, II, V, VII, VIII-X, XII, and XIII as a 2.5×10^{-3} M solution in dichloromethane containing 0.2 M tetra- <i>n</i> -butylammonium hexafluorophosphate (<i>n</i> -Bu ₄ NPF ₆) as the supporting electrolyte at sweep rate of 200 mV s ⁻¹	199
Figure 2B	Cyclic voltammograms of (a) VII (b) XI (c) III and (d) IV as a 2.5×10^{-3} M solution in dichloromethane containing 0.2 M tetra- <i>n</i> -butylammonium hexafluorophosphate (<i>n</i> -Bu ₄ NPF ₆) as the supporting electrolyte at sweep rates 50-1000 mV s ⁻¹	200
Figure 3	The electronic absorption spectra of radical cations of (II- XIII) obtained by oxidizing with or $\text{NO}^+\text{SbCl}_6^-$ under argon atmosphere at 22 °C.....	202
Figure 4	X-ray crystal structures of (a) [V] ⁺⁰ SbCl ₆ ⁻ and (b) [VII] ⁺⁰ SbCl ₆ ⁻	203
Figure 5	(left) Spectral changes attendant upon the reduction of 1.5×10^{-4} M naphthalene cation radical (NAP ⁺⁰) by incremental addition of 1.2×10^{-3} M TAM to its tetracation radical TAM ^{4+•} in dichloromethane at 22 °C. (right) A plot of depletion of absorbance of NAP ⁺⁰ (open triangles), monitored at 672 nm) and an increase of the absorbance of TAM ^{4+•} (filled triangles, monitored at 1000 nm) against the equivalent of added TAM.....	204

- Figure 6** (left) Spectral changes attendant upon the reduction of 1.5×10^{-4} M naphthalene cation radical ($\text{NAP}^{+\cdot}$) by incremental addition of 1.2×10^{-3} M HAB to its hexacation radical $\text{HAB}^{6+\cdot}$ in dichloromethane at 22°C . (right) A plot of depletion of absorbance of $\text{NAP}^{+\cdot}$ (open circles), monitored at 672 nm) and an increase of the absorbance of $\text{TAM}^{6+\cdot}$ (filled circles, monitored at 1000 nm) against the equivalent of added HAB.....205
- Figure 7** (left)Spectral change upon the addition of $\text{NAP}^{+\cdot}$ to a solution of biaryl compound in dichloromethane at 22°C . (right) The appearance of the band (464 nm) due to monocation(open circles) and appearance and disappearance of the band (1530 nm)due to the charge transfer complex formation(filled circles).....206
- Figure 8** (left) Spectral changes attendant upon an incremental addition of neutral octamethoxytetraphenylene(1.61×10^{-3} M) to a M solution of VIII^{0+} (1.08×10^{-4} M) in dichloromethane at 25°C .(right) The depletion of VIII^{0+} (blue square) and increase in the absorption at 518 nm in dichloromethane at 25°C207
- Figure 9** Spectral changes attendant upon an incremental addition of neutral octamethylbiphenylene(3.22×10^{-3} M) to a M solution of XII^{0+} (5.38×10^{-5} M) in dichloromethaneat 25°C208
- Figure 10** Spectral changes attendant upon an incremental addition of neutral octamethoxychrysene(8.22×10^{-4} M) to a M solution of VII^{0+} (6.85×10^{-5} M) in dichloromethaneat 25°C209
- Figure 11** Spectral changes attendant upon an incremental addition of neutral tetramethylbiphenylene(3.22×10^{-3} M) to a M solution of V^{0+} (1.08×10^{-4} M) in dichloromethaneat 25°C210
- Figure 12** The UV-vis spectra of the compounds (**I-XIII**).....227

LIST OF SCHEMES

CHAPTER 1

Scheme 1	Preparation of various BDFs and model compounds.....	9
-----------------	------------------------------------------------------	---

CHAPTER 2A

Scheme 1	Postulated Synthesis of Hexaalkoxy-HBC 2.....	45
Scheme 2	Postulated mechanism for the formation of 7	49
Scheme 3A	Synthesis of hexaalkoxy HBC 2 and its precursor 10	52
Scheme 3B	An electron transfer mechanism for the formation HBC 2 from precursor.....	55

CHAPTER 2B

Scheme 1	Arenium ion (or proton transfer) mechanism for the Scholl reactions proposed by King and coworkers ¹¹	79
Scheme 2	Cation radical (or electron transfer) mechanism for the oxidative cyclodehydrogenation of hexaarylbenzene to HBC.....	83
Scheme 3	Synthesis of 3,5-dihexyloxyiodobenzene.....	85
Scheme 4	Synthesis of hexakis(alkoxyphenyl)benzenes.....	86
Scheme 5	Different products obtained from differently substituted Hexaarylbenzenes.....	87
Scheme 6	The proposed cation radical mechanism for the cyclization of Z₁ and Z₂	89
Scheme 7	The proposed cation radical mechanism for the cyclization of X	90
Scheme 8	The proposed cation radical mechanism for the cyclization of Y	91

CHAPTER 2C

Scheme 1	Synthesis of dodecamethoxy and dodecahexyloxy HBCs 4a and 4b	108
Scheme 2	Disproportionation of 4b⁺⁴ to tricationic 4b⁺³ , dicationic 4b⁺² , and finally to cation radical 4b^{+•} upon continued incremental addition	

	of neutral 4b to a solution of MB⁺ (see Figure 8).....	117
CHAPTER 3A		
Scheme 1	Synthesis of tetraaryloxyphenylethylenes (A-D).....	133
Scheme 2	Synthesis of dendrimers (G1-G4).....	136
CHAPTER 3B		
Scheme 1	Synthesis of E1-E6 by using Ullman coupling.....	164
Scheme 2	Synthesis of precursors PE3, PE4, B3, B4	164
Scheme 3	Synthesis of the cyclic ether oligomer.....	165
CHAPTER 4		
Scheme 1	Indirect routes for the syntheses of selected cycloannulated polycyclic aromatic hydrocarbons.....	193
Scheme 2	The formation and disappearance of charge transfer complex upon oxidation of the biaryl compound.....	206
Scheme 3	Reversible C-C bond formation in octamethoxytetraphenylene upon oxidation.....	208
Scheme 4	Formation of octamethylbiphenylene cation radical.....	209
Scheme 5	Formation of octamethoxychrysene cation radical using VII⁰⁺SbCl₆⁻ as the oxidant.....	210
Scheme 6	Formation of tetramethylbiphenylene cation radical using V⁰⁺ SbCl₆⁻ as the oxidant.....	211

INTRODUCTION

Over the past decades, an intense scientific investigation has been focused on the organic optoelectronic materials owing to their potential for the development of flexible modern display devices, field effect transistors and photovoltaic devices.¹⁻⁵ The study of organic molecules for such applications stems from the fact that they can be easily processed, they are light weight in comparison to silicon-based devices, and their properties can be readily modulated by appropriate substituent modifications onto a given organic structure. Most importantly, the advances in modern organic synthesis techniques allow one to synthesize such tailored organic molecule with relative ease.

A vast variety of linear (1-D), planar (2-D) and globular (3-D) chemical structures with varied functionalities⁶ can be prepared by either covalent or non-covalent assemblies of simpler molecules. Organic materials such as conducting polymers and oligomers derived from simple aromatic hydrocarbons, dendrimers, and liquid crystals have played an important role in the development of modern photovoltaic devices.⁶

Conjugated conducting polymers can be easily obtained by coupling arenes through their *para* positions. For example, polyphenylenes and their derivatives have been widely investigated for optoelectronic applications over the past 50 years.⁷ Unfortunately, the applications of *p*-polyphenylenes have been hampered due to their poor solubility. Although the solubility can be increased by substituting solubilizing groups, it affects the properties and stability of these materials due to additional torsional strain in the polymer backbone.⁸ To overcome the issue of torsional strain, the ladder-like compound (Figure 1) have been prepared by introducing a bridging atom between two conjugated phenylene units. For example, as shown in Figure 1, 6,12-dihydroindeno[1,2-

b]fluorene, a ladder-like structure, has shown promise as a building block for the OLEDs and Organic Field Effect Transistors (OFETs)⁴. The ladder type compounds also provide the possibility of incorporating hetero atoms at the bridging position or in the π -backbone to enhance the optical properties as well as electrochemical properties.⁹

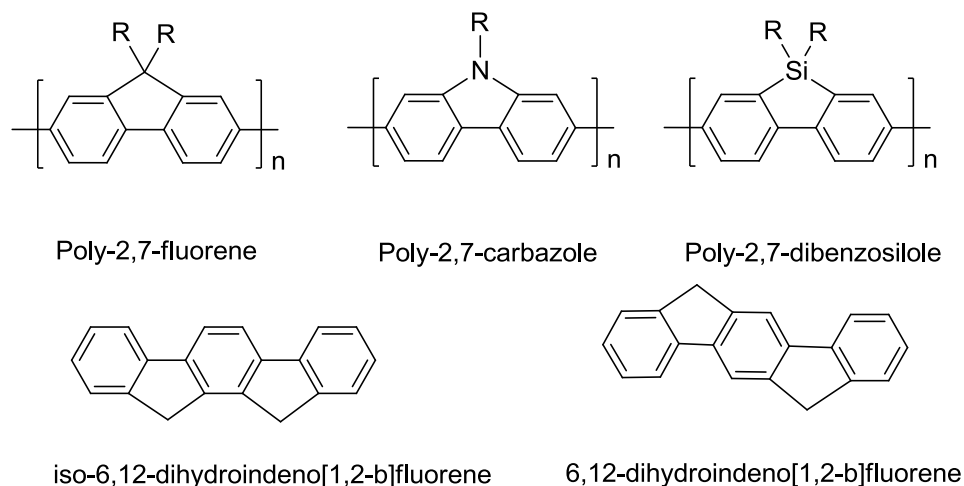


Figure1. Structures of some ladder type organic compounds.

Polyphenylenevinylenes (PPV), is another class of well-known conjugated materials which have been widely employed in various electronic and optoelectronic devices owing to their unique properties such as efficient electroluminescence (EL), easy preparation, and high solubility.¹⁰ The soluble poly[2-methoxy-5-(2'-ethylhexyloxy)-1,4-phenylenevinylene] (MEH-PPV) has been extensively studied on its applicability for the preparation of flat display devices.¹¹ Many research studies have been carried out to improve the EL performance of PPV by changing its structure by substituting different groups.¹²

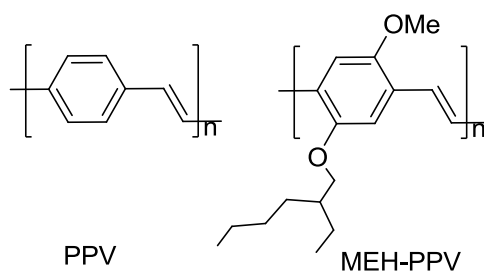


Figure 2. Structures of polyphenylenevinylenes (PPV) and poly[2-methoxy-5-(2'-ethylhexyloxy)-1,4-phenylene vinylene] (MEH-PPV).

Polycyclic aromatic hydrocarbons (PAHs) exhibit strong π - π stacking interactions that promote self-assembly in solution and in films. Thus, these disk-shaped molecules with flexible chains on the periphery readily form columnar mesophases which can serve as nanowires for one-dimensional transport process along the column axes and they are promising candidates for applications in field-effect transistors, hole-conducting layers in photovoltaic devices and in light-emitting diodes.^{13,14} Large PAHs such as triphenylenes¹⁵ and hexa-peri-hexabenzocoronenes(HBCs)¹⁶ show attractive charge-transporting properties owing to the formation of discotic liquid crystals. Alkyl and alkylphenyl substituted HBCs possess excellent properties such as higher order columnar packing and the highest charge-carrier mobility (up to $1.13 \text{ cm}^2 \text{ V}^{-1} \text{ s}^{-1}$) of all known discotic liquid crystalline materials due to the large π -orbital overlap between the discs in the column.

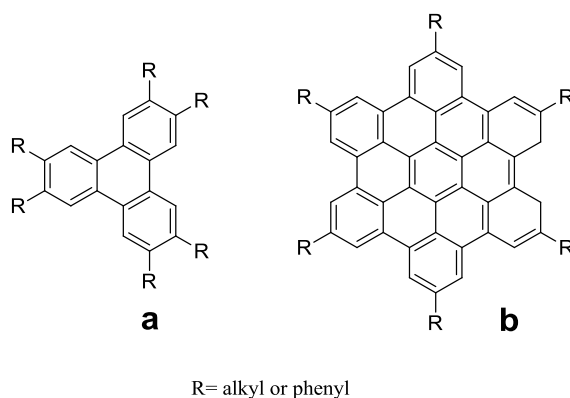


Figure 3. Structures of substituted triphenylenes and hexa *peri*-hexabenzocoronenes.

Dendritic macromolecules, also known as dendrimers, are a new class of hyper-structured material which have also been explored for modern photovoltaic applications.¹⁷ The long branching chains and the high degree of control over their molecular weight makes it possible to create three-dimensional purely organic structures that are roughly spherical or globular. In optical and optoelectronic applications, functional chromophores can be introduced at branches, core, or the ends of the dendrimers to control their optical properties. Tetraphenylethylene (TPE) has been explored for decades due to rich electrochemical¹⁸, aggregation induced emission¹⁹ and excited state properties²⁰ as well as its extensive usage as an electron transfer catalyst in a variety of polymerizations.²¹ Unfortunately, however, tetraphenylethylene (TPE)-based dendrimers are largely unexplored.²²⁻²⁴

The goal of my research projects has been geared towards synthesizing next generation of organic molecules which hold potential for applications in the photovoltaic devices. Accordingly, various new compounds reported in this thesis have been carefully characterized using NMR spectroscopy and mass spectrometry and studied via a variety of spectroscopic methods such as electrochemistry, X-ray crystallography and time-

resolved laser spectroscopy.

The work towards achieving this fundamental goal is divided in the following 4 chapters.

- **Chapter 1.** Synthesis, electronic properties and X-ray structural characterization of tetraarylbenzodifuran cation radicals
- **Chapter 2A.** A facile synthesis of elusive alkoxy-substituted hexa-*peri*-hexabenzocoronene
- **Chapter 2B.** Intramolecular Scholl reactions of alkoxy-substituted hexaarylbenzenes via cation radical (electron transfer) mechanism
- **Chapter 2C.** Dodecaalkoxy-hexa-*peri*-hexabenzocoronene: A non-planar PAH with six easily accessible oxidation states.
- **Chapter 3A.** Preparation of tetraaryloxyphenylethylene based dendrimers
- **Chapter 3B.** Structure and optoelectronic properties of acyclic and cyclic polyphenyl ethers (PPE)
- **Chapter 4.** Cycloannulated aromatic donors and their highly robust cation radical salts as redox tunable oxidants

CHAPTER 1

Synthesis, Electronic Properties and X-ray Structural Characterization of Tetraarylbenzo[1,2-b:4,5-b']-difuran Cation Radicals

Introduction

The design and syntheses of new electro-active chromophores have attracted considerable attention over the past decade owing to their potential for the practical applications in the emerging areas of molecular electronics and nanotechnology.¹ Tetraarylbenzo[1,2-b:4,5-b']difurans (simply referred to hereafter as **BDF**), a largely unexplored^{2,3} class of electro-active chromophores, possess close structural similarities to the electro-active moieties utilized for the construction of, extensively explored, polyphenylenevinylene (**PPV**) and its alkoxy-substituted derivatives (i.e. Figure 1).⁴

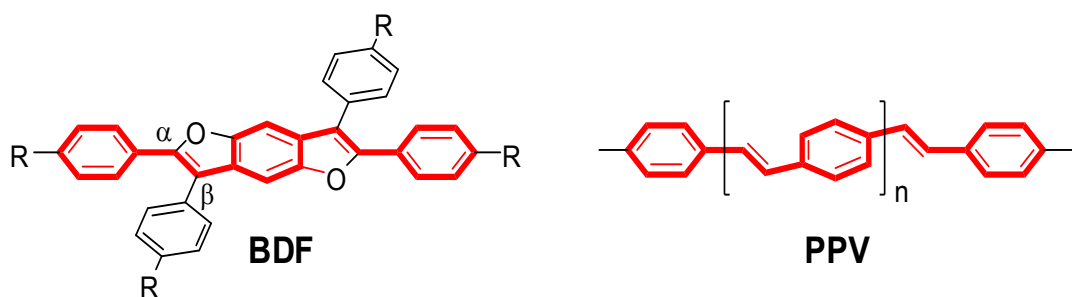


Figure 1. Showing the structural similarities between polyphenylenevinylenes and tetraarylbenzo[1,2-b:4,5-b']-difurans.

Although **BDF** derivatives have been known for over a century² and can be easily prepared in excellent yields via Lewis acid-catalyzed condensations of benzoin or substituted benzoin with *p*-hydroquinone, their potential as electro-active materials has received little attention.³

Our continuing interest in the design and syntheses of chromophores that form stable organic cation radicals led us to explore the potential of **BDF** derivatives as hole carriers. As such, the cation radicals, or hole carriers, are of fundamental importance to organic material science since they constitute the smallest unit that stabilizes a cationic charge as well as an unpaired electron.⁵

Accordingly, in this chapter we describe the preparation of various tetraarylbenzodifurans (**BDFs**) as well as diarylbenzofurans (as model compounds), and show that **BDFs** are highly luminescent materials that undergo reversible electrochemical oxidations and form stable cation-radical salts that can be isolated in crystalline form. The structures of various neutral **BDFs** and their cation radicals are determined by X-ray crystallography and further corroborated by DFT calculations. The structural studies of **BDF** cation radicals allow us to delineate that a single charge in **BDFs** is stabilized largely by benzodifuran and the α -aryl groups lying on the longitudinal axis (shown in red in Figure 1) while the β -aryl groups on the vertical axis (shown in black in Figure 1) contribute little to the stabilization of the cationic charge. The details of these findings are described herein.

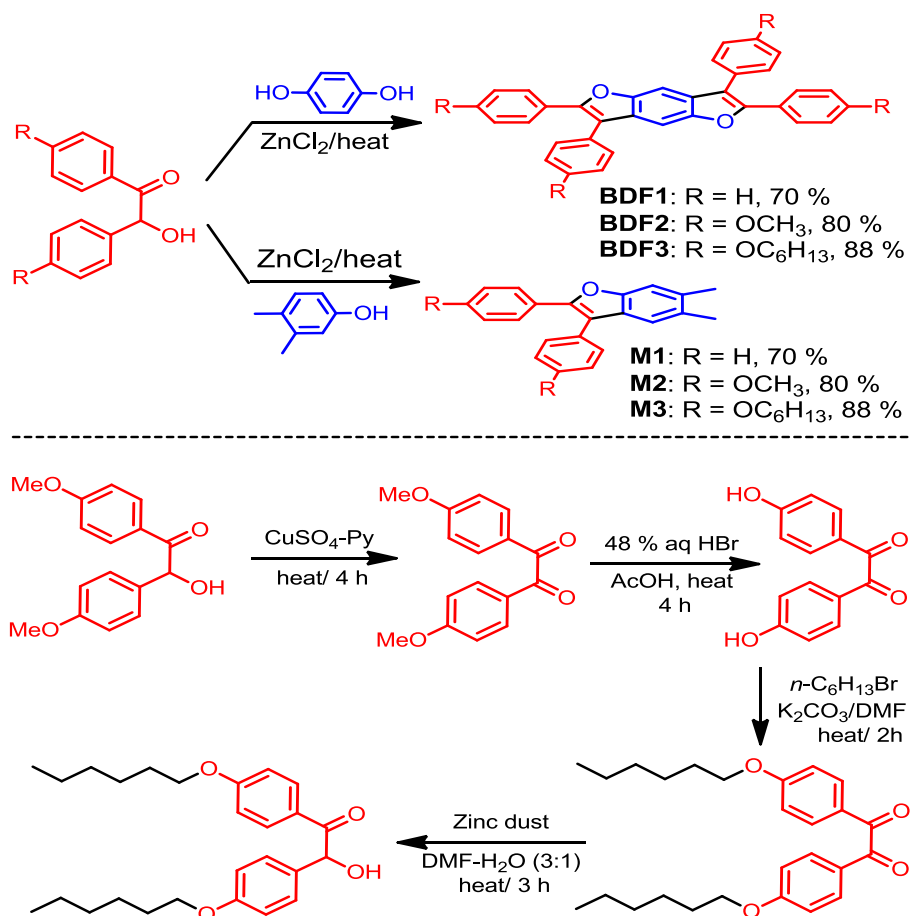
Results and Discussion

Thus, tetraphenylbenzodifuran (**BDF1**) was obtained by simply heating an intimate mixture of benzoin, *p*-hydroquinone, and zinc chloride in 2:1:2.5 molar ratio for 5-15 min. The resulting mixture was cooled to 22 °C and was triturated with dichloromethane and water. The dichloromethane layer was separated and washed with a 10% aqueous sodium hydroxide solution and evaporated to afford a solid residue which

was recrystallized from a mixture of dichloromethane and acetonitrile to afford **BDF1** in 70% isolated yield. A similar reaction with commercially-available anisoin afforded **BDF2** in excellent yield. It was noted that both **BDF1** and **BDF2** have limited solubility in dichloromethane, chloroform, benzene or toluene. For example, **BDF1** has a solubility of 30 mg/ 10 mL of CH₂Cl₂ and **BDF2** has a solubility of 40 mg/ 10 mL in CH₂Cl₂. Hence, a readily soluble benzodifuran derivative **BDF3** was also prepared using 4,4'-dihexyloxybenzoin (Scheme 1) which in turn was obtained from anisoin using standard procedures.⁶ The model diarylbenzofurans (**M1-3**) were obtained by a reaction of various benzoin derivatives with 3,4-dimethylphenol in excellent yields (Scheme 1).

The molecular structures of **BDF1-3** and **M1-3** were established with the aid of ¹H/¹³C NMR spectroscopy, mass spectrometry, and further confirmed by X-ray crystallography (see Experimental section for the full details).

Scheme 1. Preparation of various BDFs and model compounds.



With the various **BDF** derivatives at hand, we next examined their emission and excitation spectra in dichloromethane at 22 °C. The highly luminescent **BDFs** showed structured emission/excitation bands with a modest bathochromic shift going from the tetraphenyl derivative (i.e. **BDF1**) to the corresponding alkoxy-substituted derivatives (i.e. **BDF2-3**) (see Figure 2, left). In contrast, the model benzofuran derivatives (**M1-3**) showed only broad emission/excitation bands (see Figure 2, right).

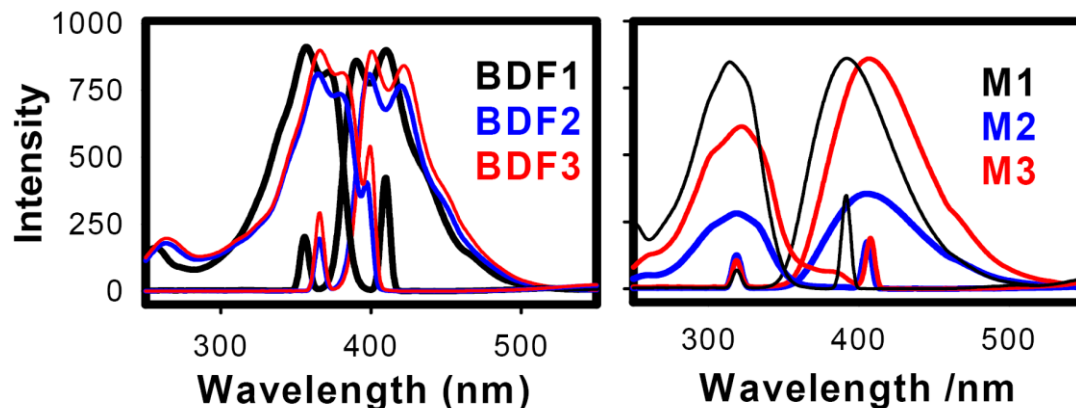


Figure 2. Comparison of the emission and excitation spectra of **BDF1-3** (left) and **M1-3** (right) in dichloromethane at 22 °C.

The electron-donor strengths of various **BDF** derivatives and the initial indication of the stability of their cation radicals were evaluated by cyclic voltammetry.

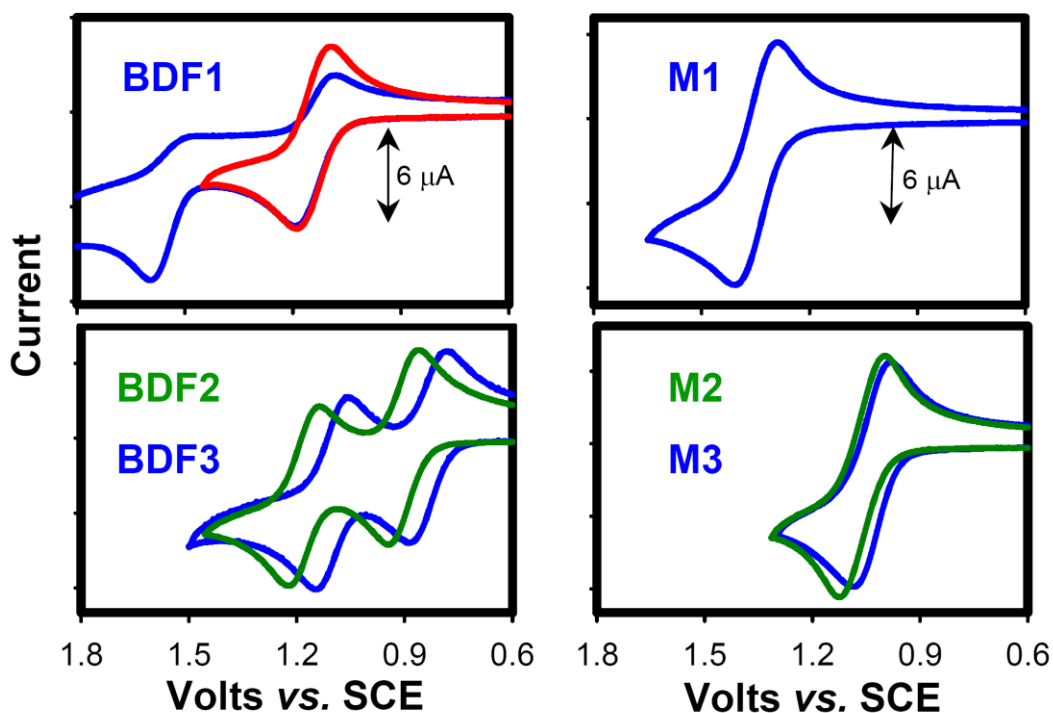


Figure 3. Comparison of the cyclic voltammograms of various benzodifuran (2 mM) and benzofuran (3 mM) derivatives in CH_2Cl_2 (0.1 M $n\text{-Bu}_4\text{NPF}_6$) at a scan rate of 200 mV s^{-1} . Note that the first oxidation wave of **BDF1** is completely reversible (red curve) if the scanning is terminated before the start of the second oxidation event.

Thus, each benzodifuran and benzofuran derivative was subjected to electrochemical oxidation at a platinum electrode as a 2-3 mM solution in dichloromethane containing 0.1 M *n*-Bu₄NPF₆ as the supporting electrolyte. Figure 3 compiles the cyclic voltammograms of **BDF1-3** (left) and benzofuran derivatives **M1-3** (right). The benzodifuran derivatives, **BDF1-3**, showed two oxidation waves corresponding to the formation of mono cation radicals and dications, respectively. The phenyl substituted **BDF1** showed that its first oxidation wave corresponding to the formation of the cation radical is completely reversible ($E_{\text{ox1}} = 1.17$ V vs. SCE, see Figure 3, red curve) while the second oxidation to the dication occurs irreversibly (at ~ 1.6 V vs. SCE). Expectedly, the alkoxy-substituted **BDF2** and **3** showed two reversible oxidation waves at very similar and relatively lower potentials (i.e. **BDF2**: 0.91 and 1.19; **BDF3**: 0.89 and 1.15 volts vs. SCE) as compared to the **BDF1** owing to the presence of electron donating alkoxy substituents. The cyclic voltammograms of the corresponding model benzofuran derivatives **M1-3** showed at least one reversible oxidation wave occurring at relatively higher potentials (**M1**: 1.34; **M2**: 1.07; and **M3**: 1.04 V vs. SCE) as compared to the corresponding **BDF** derivatives.

The electrochemical reversibility and relatively low oxidation potentials of benzodifuran and benzofuran derivatives prompted us to generate their cation radicals using a hydroquinone ether cation radical ($\text{MA}^{\bullet+}$, $E_{\text{red}} = 1.11$ V vs. SCE)⁷ or a naphthalene cation radical ($\text{NAP}^{\bullet+}$, $E_{\text{red}} = 1.34$ V vs. SCE)⁸ as stable (aromatic) one-electron oxidants.

Thus Figure 4A (left) shows the spectral changes attendant upon an incremental addition of sub-stoichiometric amounts of **BDF1** to a 1.3×10^{-5} M $\text{NAP}^{\bullet+}$ ($\lambda_{\text{max}} = 672$,

616, 503, and 396 nm; $\epsilon_{672} = 9300 \text{ M}^{-1} \text{ cm}^{-1}$)⁸ in dichloromethane at 22 °C. Furthermore a plot of formation of the **BDF1** cation radical (i.e. increase in the absorbance at 1100 nm) against the increments of added neutral **BDF1** (see Figure 4A, right), established that $\text{NAP}^{\bullet+}$ was completely consumed after the addition of 1 equiv. of **BDF1**; and the resulting highly structured absorption spectrum of **BDF1**^{•+} [$\lambda_{\text{max}} = 502, 545, 610(\text{sh}),$ and 1100 (log $\epsilon = 3.81$) nm] remained unchanged upon further addition of neutral **BDF1** (i.e. eq 1).

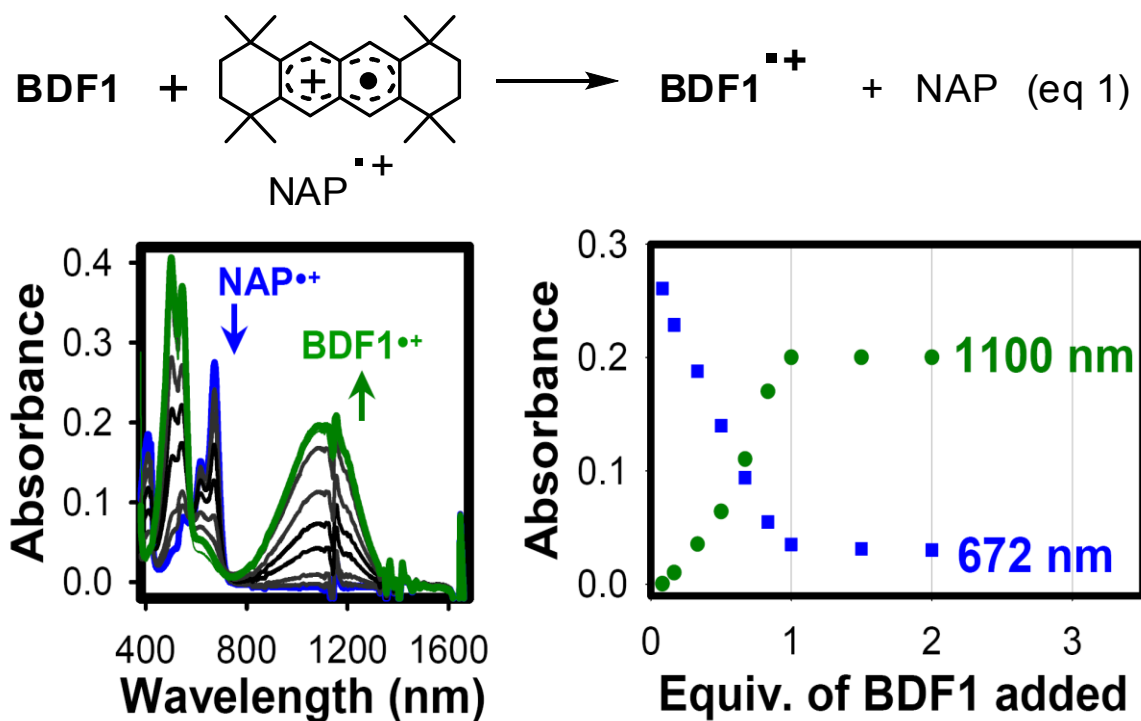


Figure 4A. Left: Spectral changes upon the reduction of $3.2 \times 10^{-5} \text{ M}$ $\text{NAP}^{\bullet+}$ (blue line) by incremental addition of $1.0 \times 10^{-3} \text{ M}$ **BDF1** to its radical cation (green line) in CH_2Cl_2 at 22 °C. Right: A plot of depletion of absorbance of $\text{NAP}^{\bullet+}$ (blue squares, at 672 nm) and an increase of the absorbance of **BDF1**^{•+} (green circles, at 1100 nm) against the equivalent of added neutral **BDF1**.

Similarly, the cation radicals of various **BDFs** and benzofuran derivatives were generated using $\text{NAP}^{\bullet+}$ as well as $\text{MA}^{\bullet+}$ (see experimental section) and are compared in Figure 4. The absorption spectrum of green-colored $\text{BDF1}^{\bullet+}$ was expectedly similar to that of the alkoxy substituted $\text{BDF2}^{\bullet+}$ [$\lambda_{\text{max}} = 540(\text{sh}), 572, 676, \text{ and } 1368$ ($\log \epsilon = 4.37$) nm] and $\text{BDF3}^{\bullet+}$ [$\lambda_{\text{max}} = 541(\text{sh}), 576, 705, \text{ and } 1375$ ($\log \epsilon = 4.47$) nm] as shown in Figure 4 (middle). A compilation of the absorption spectra of the cation radicals of benzofurans $\text{M1}^{\bullet+}$ [$\lambda_{\text{max}} = 442, 720$ ($\log \epsilon = 3.74$), and 950 nm], $\text{M2}^{\bullet+}$ [$\lambda_{\text{max}} = 478, 685(\text{sh}), 750$ ($\log \epsilon = 4.11$), and 1050 nm], and $\text{M3}^{\bullet+}$ [$\lambda_{\text{max}} = 480, 695(\text{sh}), 760$ ($\log \epsilon = 4.17$), and 1055 nm] in Figure 4 (right) show that they contain similar spectral transitions, as in the spectra of the cation radicals of **BDF** derivatives. However, they lack the intense NIR transition (1180-1400 nm) which is attributed to a Robin Day III type inter-valence transition in **BDF** cation radicals.⁹

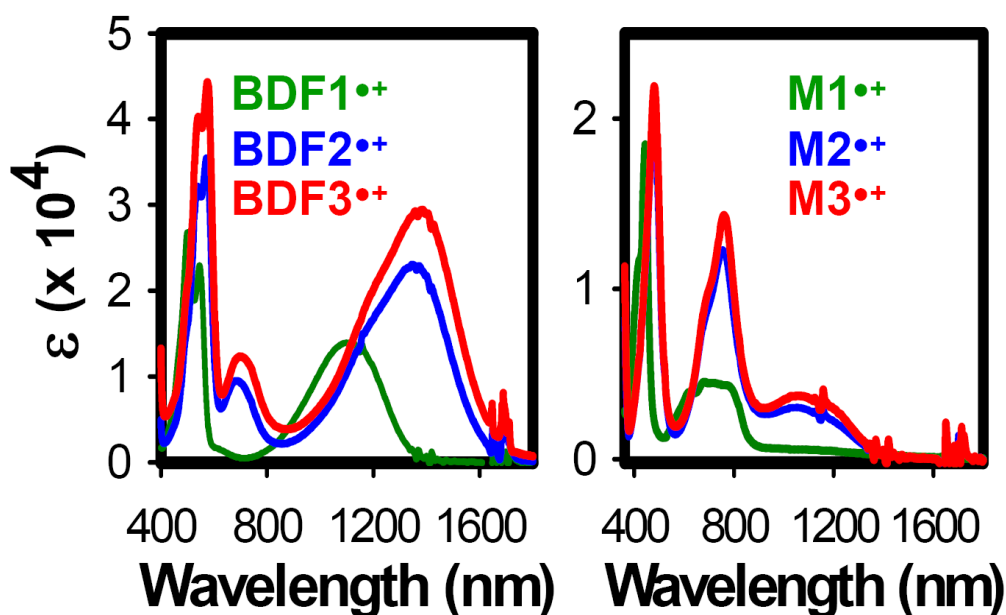


Figure 4B. A comparison of the absorption spectra of **BDF1-3** cation radicals (left) and **M1-3** cation radicals (right).

The **BDF** cation radicals, obtained according to eq 1, are highly persistent at ambient temperatures and did not show any decomposition during a 24 h period at 22 °C, as confirmed by UV-vis spectroscopy. The single crystals of the **BDF1**^{•+} and **BDF2**^{•+}, suitable for X-ray crystallography, were obtained by a slow diffusion of toluene into the dichloromethane solutions of **BDF1**^{•+} SbCl₆⁻ and **BDF2**^{•+} SbCl₆⁻ at -10 °C during the course of 2 days (see Experimental Section).

The crystallographic analysis of the dark-colored crystals of **BDF1**^{•+} SbCl₆⁻ and **BDF2**^{•+} SbCl₆⁻ revealed that they pack by the formation of translational stacks where peripheral α -aryl groups overlap with the central benzodifuran moieties of the neighboring molecules at a relatively large dihedral angle ($\sim 20^\circ$), see Figure 5.

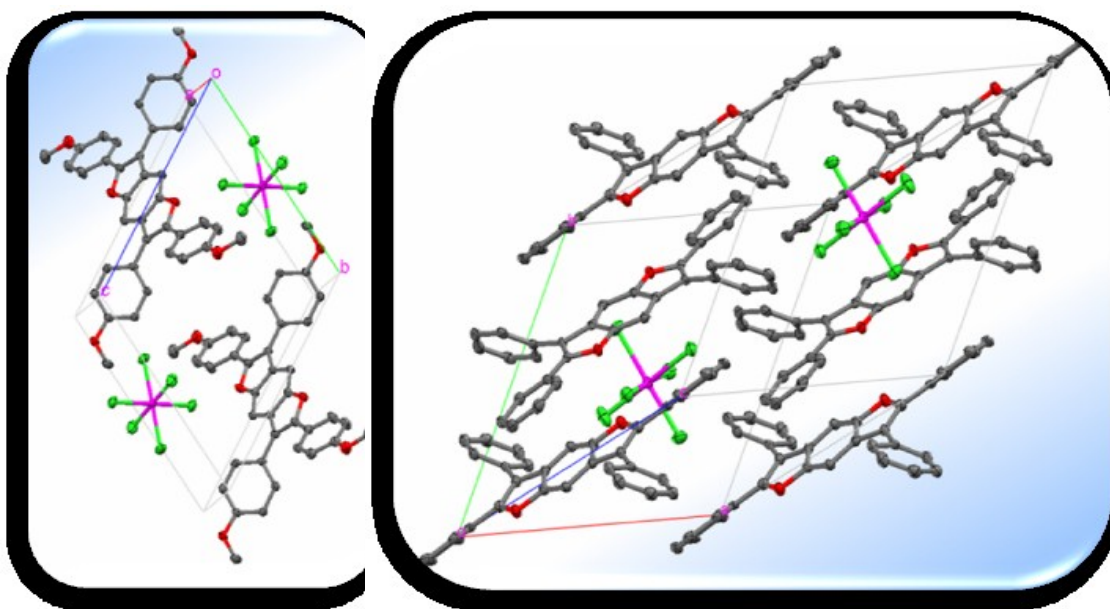


Figure 5. The ORTEP diagrams showing the arrangement of **BDF1**^{•+} SbCl₆⁻ (right) and **BDF2**^{•+} SbCl₆⁻ (left) in unit cells.

A closer look at the bond length changes in the **BDF** cation radicals, together with a comparison of the corresponding neutral forms, the structures of which were

established by X-ray crystallography, points to the following important observations: (i) The bond lengths in the central benzodifuran nuclei are identical in both **BDF** derivatives (see Table 1a and 1b). (ii) In the cation radicals, the “olefinic” bonds (in the furan rings denoted ‘e’ in the generic structure in Table 1) undergo increased delocalization with the central aromatic ring that leads to their elongation by ~3 pm and the shortening of adjacent bonds ‘f’ and ‘d’ by ~2 and ~3 pm, respectively (see Table 1a and 1b). (iii) The central benzene ring acquires a quinoidal structure, i.e. bonds labeled ‘b’ shorten by ~2 pm whereas the other four bonds (labeled ‘a’ and ‘c’) become elongated by ~1 pm and ~2 pm, respectively. (iv) Interestingly, the structural changes (described above) in the benzodifuran moiety in **BDF1^{•+}** are roughly 1.5 times more pronounced than in the case of **BDF2^{•+}** (see Table 1a and 1b), and such a difference can be readily attributed to the fact that the unsubstituted phenyl groups in **BDF1^{•+}** are less involved in the stabilization of the positive charge as compared to the electron-rich *p*-anisyl groups in **BDF2^{•+}**.

It is noteworthy that the α -aryl groups, which are more coplanar with the benzodifuran ring ($\phi_{\alpha} = 10\text{-}34^{\circ}$), undergo a pronounced quinoidal change owing to the delocalization of the cationic charge as compared to the less coplanar β -aryl groups ($\phi_{\beta} = 44\text{-}61^{\circ}$) which show almost no change in their bond lengths (see Table S1 and S2).

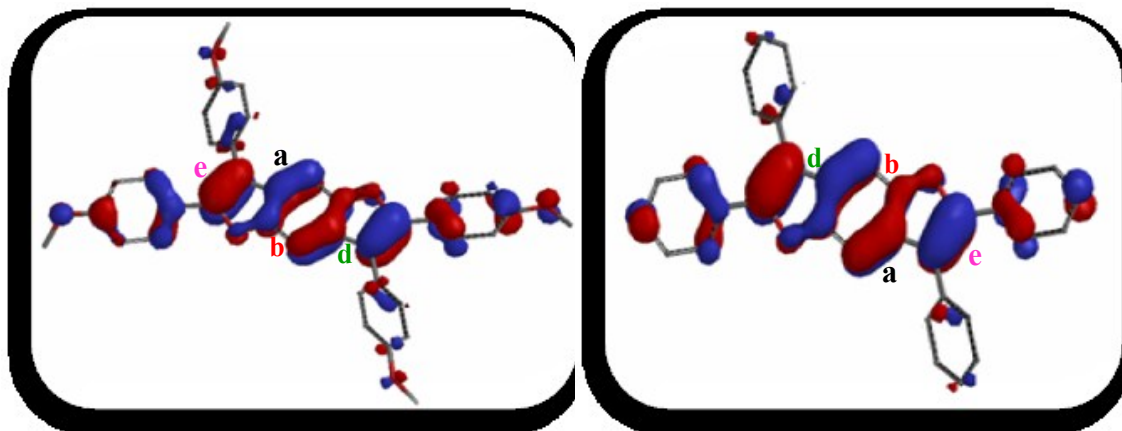
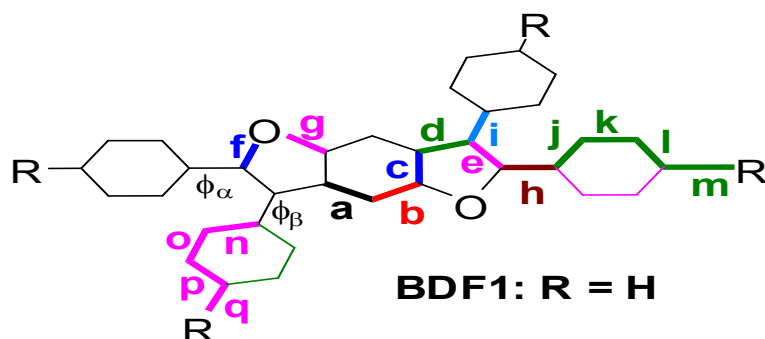


Figure 6. Showing the HOMO's of **BDF1** (right) and **BDF2** (left), obtained by DFT calculations at the B3LYP-631G* level.

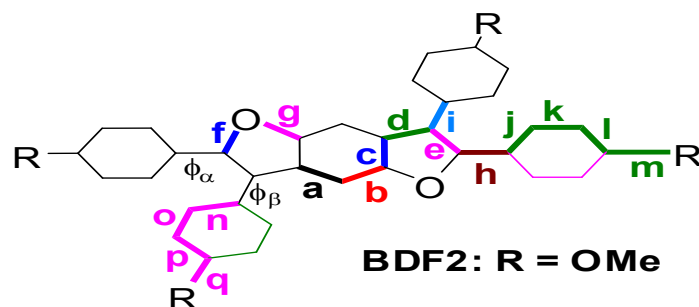
The experimental observations of the bond length changes in **BDF** cation radicals were found to be in reasonable agreement with the calculated values using DFT calculations at the B3LYP-631G* level (see Table 1a and 1b).¹⁰ Furthermore, it is noted that the bonds which undergo the most dramatic lengthening (*i.e.* bonds 'a' and 'e') and shortening (*i.e.* bonds 'b' and 'd') in **BDF** cation radicals are the bonds on which the HOMO shows the largest bonding and antibonding character, respectively (*i.e.* Figure 6).¹¹

Table 1a. Experimental and theoretical bond lengths of the centrosymmetric neutral and cation radical of **BDF1** in picometers (pm). The average esd's are shown in parenthesis.



Bond Type	B3LYP/6-31G*			X-Ray Data		
	BDF1	BDF1 ⁺	Δ	BDF1	BDF1 ⁺	Δ
a	140.3	141.8	+1.5	139.9(1)	142.2(5)	+2.3
b	138.5	137.1	-1.4	137.8(1)	135.3(5)	-2.5
c	141.6	142.6	+1.0	140.7(1)	142.1(5)	+1.4
d	144.8	142.0	-2.8	144.9(1)	141.6(5)	-3.3
e	137.7	141.1	+3.4	136.7(1)	140.3(5)	+3.6
f	138.4	136.7	-1.7	138.6(1)	136.7(4)	-1.9
g	136.8	137.1	+0.3	137.5(1)	137.9(4)	+0.4
h	146.3	144.5	-1.8	146.4(1)	144.9(5)	-1.5
i	147.8	147.3	-0.5	147.4(1)	147.5(5)	+0.1
j	140.8	141.4	+0.6	139.6(1)	140.2(5)	+0.6
k	139.2	138.9	-0.3	138.6(2)	138.5(5)	-0.1
l	139.7	139.9	+0.2	138.3(2)	138.7(6)	+0.4
m	--	--	-	--	--	--
n	140.5	140.7	+0.2	139.4(1)	140.3(5)	+0.9
o	139.4	139.3	-0.1	138.6(2)	138.3(5)	-0.3
p	139.6	139.7	+0.1	138.3(2)	138.1(5)	-0.2
q	--	--	--	--	--	--
ϕ_α	24°	20°	-4°	32.7(2)°	21.8(6)°	-11°
ϕ_β	53°	52°	-1°	50.2(2)°	49.9(5)°	0°

Table 1b. Experimental and theoretical bond lengths of the centrosymmetric neutral and cation radical of **BDF2** in picometers (pm). The average esd's are shown in parenthesis.



bond type	B3LYP/6-31G*			X-ray data		
	BDF2	BDF2 ⁺	Δ	BDF2	BDF2 ⁺	Δ
a	140.3	141.5	+1.2	140.0(1)	141.7(2)	+1.7
b	138.5	137.3	-1.2	138.1(1)	136.5(2)	-1.6
c	141.5	142.4	+0.9	140.9(1)	141.7(2)	+0.8
d	144.8	142.5	-2.3	144.7(1)	141.7(2)	-3.0
e	137.7	140.8	+3.1	137.1(1)	139.9(2)	+2.8
f	138.5	137.2	-1.3	138.6(1)	137.3(2)	-1.3
g	136.9	137.0	+0.1	137.3(1)	137.8(2)	+0.5
h	146.1	144.0	-2.1	145.9(1)	144.3(2)	-1.6
i	147.7	147.0	-0.7	147.8(1)	145.8(2)	-2.0
j	140.7	141.6	+0.9	140.1(1)	140.6(2)	+0.5
k	139.0	138.3	-0.7	138.7(1)	137.9(2)	-0.8
l	140.2	140.9	+0.7	139.3(1)	139.9(2)	+0.6
m	136.4	134.4	-2.0	136.6(1)	135.0(2)	-1.6
n	140.5	140.8	+0.3	139.8(1)	139.9(2)	+0.1
o	139.2	138.9	-0.3	139.1(1)	138.2(2)	-0.9
p	140.1	140.5	+0.4	139.3(1)	139.1(2)	-0.2
q	136.6	135.2	-1.4	137.2(1)	136.3(2)	-0.9
ϕ_α	23°	18°	-5°	9.8(1)°	21.4(2)°	+11°
ϕ_β	51°	50°	-1°	61.0(1)°	44.3(2)°	-17°

In summary, we have demonstrated that various tetraarylbenzodifuran (**BDF**) and benzofuran derivatives can be easily prepared from readily available starting materials. These highly luminescent **BDFs** undergo reversible electrochemical oxidation and form stable cation-radical salts. The isolation and X-ray crystal structure determination of the neutral and cation radicals of **BDF** derivatives as well as the DFT calculations provide unequivocal evidence that a single charge (or polaron) in **BDFs** is stabilized largely by the benzodifuran and the α -aryl groups. Efforts are now underway to construct linear arrays of **BDF** derivatives to explore their conducting properties for potential applications in the emerging areas of molecular electronics and nanotechnology.¹²

Experimental

The General Experimental Methods.

Dichloromethane (Aldrich) was repeatedly stirred with fresh aliquots of conc. sulfuric acid (~10 % by volume) until the acid layer remained colorless. After separation, it was washed successively with water, aqueous sodium bicarbonate, water, and saturated aqueous sodium chloride and dried over anhydrous calcium chloride. The dichloromethane was distilled twice from P₂O₅ under an argon atmosphere and stored in a Schlenk flask equipped with a Teflon valve fitted with Viton O-rings. The hexanes and toluene were distilled from P₂O₅ under an argon atmosphere and then refluxed over calcium hydride (~12 hrs). After distillation from CaH₂, the solvents were stored in Schlenk flasks under an argon atmosphere.

Cyclic Voltammetry.

Cyclic voltammetry (CV) was performed on an Electrochemical Analyser. The CV cell was of an airtight design with high vacuum Teflon valves and Viton *O*-rings seals to allow an inert atmosphere to be maintained without contamination by grease. The working electrode consisted of an adjustable platinum disk embedded in a glass seal to allow periodic polishing (with a fine emery cloth) without changing the surface area ($\approx 1 \text{ mm}^2$) significantly. The reference SCE electrode (saturated calomel electrode) and its salt bridge were separated from the catholyte by a sintered glass frit. The counter electrode consisted of platinum gauze that was separated from the working electrode by $\approx 3 \text{ mm}$.

The CV measurements were carried out in a solution of 0.1 M supporting electrolyte (tetra-*n*-butylammonium hexafluorophosphate, TBAH) and 2.5 mmol electron donor in dichloromethane under an argon atmosphere. All cyclic voltammograms were recorded at the sweep rate of 200 mV sec^{-1} , unless otherwise specified and were IR compensated. The oxidation potentials ($E_{1/2}$) were referenced to SCE that was calibrated with added (equimolar) ferrocene ($E_{1/2} = 0.450 \text{ V vs. SCE}$). The $E_{1/2}$ values were calculated by taking the average of anodic and cathodic peak potentials in the reversible cyclic voltammograms.

UV-vis Absorption Spectra of Various Benzodifuran and Benzofuran Electron Donors.

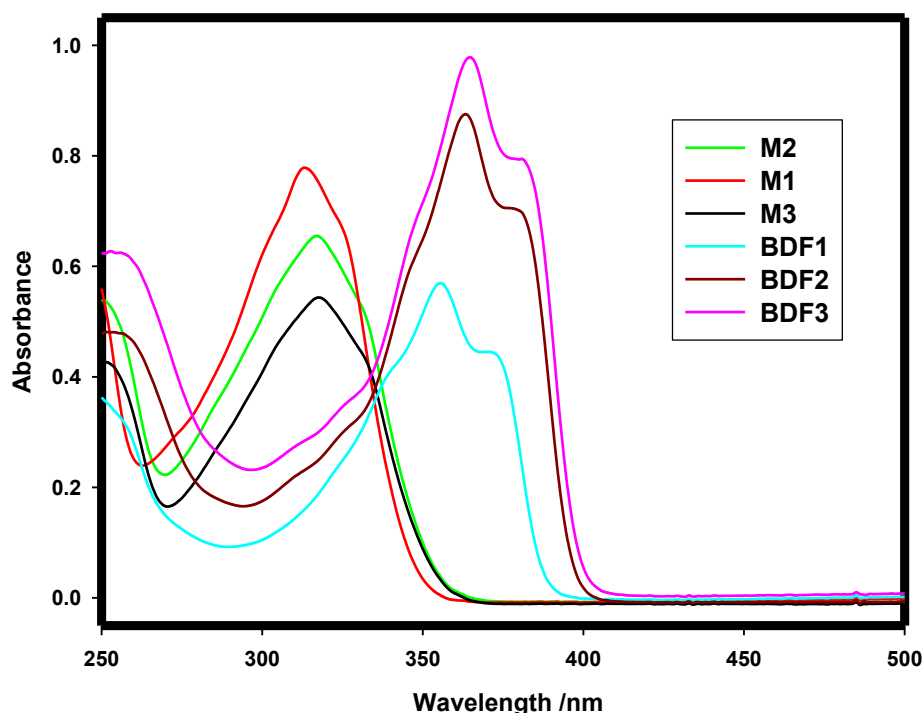


Figure 7. UV-vis absorption spectra of various benzodifurans and benzofurans obtained in dichloromethane at 22 °C. The absorption maxima and extinction coefficients are: **BDF1**, $\lambda_{\max} = 354 \text{ nm}$, $\epsilon_{354} = 7.8 \times 10^4 \text{ M}^{-1} \text{ cm}^{-1}$; **BDF2**, $\lambda_{\max} = 363 \text{ nm}$, $\epsilon_{363} = 7.29 \times 10^4 \text{ M}^{-1} \text{ cm}^{-1}$; **BDF3**, $\lambda_{\max} = 365 \text{ nm}$, $\epsilon_{365} = 8.4 \times 10^4 \text{ M}^{-1} \text{ cm}^{-1}$; **M1**, $\lambda_{\max} = 314 \text{ nm}$, $\epsilon_{314} = 2.5 \times 10^4 \text{ M}^{-1} \text{ cm}^{-1}$; **M2**, $\lambda_{\max} = 317 \text{ nm}$, $\epsilon_{317} = 3.6 \times 10^4 \text{ M}^{-1} \text{ cm}^{-1}$; **M3**, $\lambda_{\max} = 315 \text{ nm}$, $\epsilon_{315} = 2.6 \times 10^4 \text{ M}^{-1} \text{ cm}^{-1}$.

General Procedure for the Spectral Titration of $[\text{MA}^{++} \text{SbCl}_6^-]$ with various electron donors.

An orange-red solution of $\text{MA}^{++} \text{SbCl}_6^-$ in dichloromethane (3 mL, $2.0 \times 10^{-4} \text{ mM}$) was transferred under an argon atmosphere in a 1-cm quartz cuvette equipped with a Schlenk adaptor at room temperature. A dichloromethane solution ($2.0 \times 10^{-3} \text{ M}$) of dibenzofuran **BDF1** in 10 μL increments was added to this solution. The electronic spectra of the resulting solutions, after the addition of each substoichiometric increment,

were recorded at 22 °C [see Figure 3 (left) in the text]. The spectral titration data for various benzodifuran and benzofuran electron donors are compiled below:

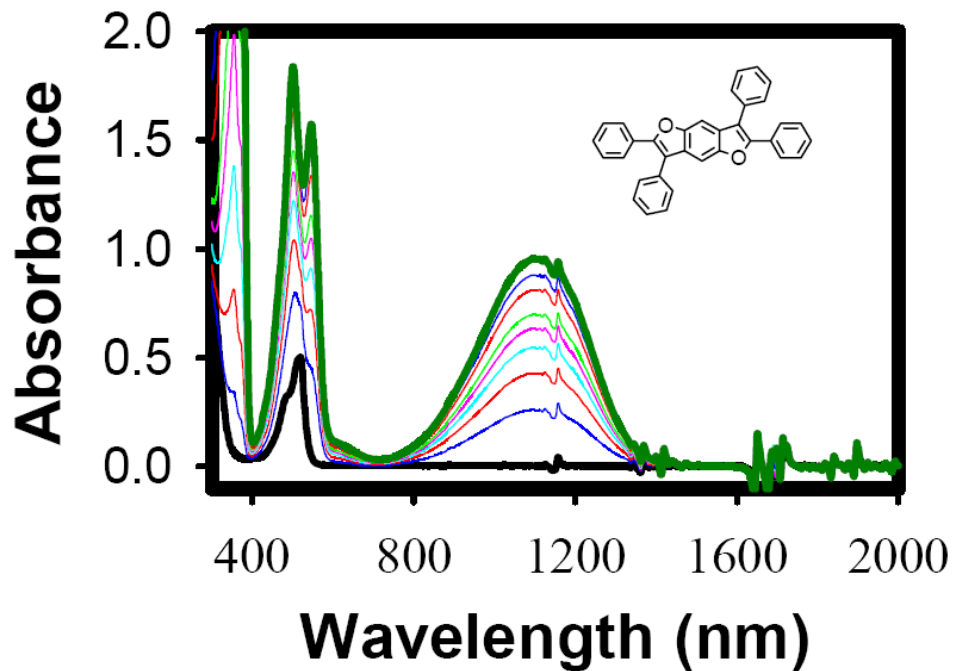


Figure 8. Spectral changes upon the reduction of 6.85×10^{-5} M $\text{MA}^{+\bullet}$ (Black line) by incremental addition of 1.0×10^{-3} M **BDF1** to its radical cation (green line) in CH_2Cl_2 at 22 °C. Note that the growth of the absorption bands due to $\text{BDF1}^{+\bullet}$ was only ceased after the addition of excess **BDF1** (i.e. roughly 3 equivalents).

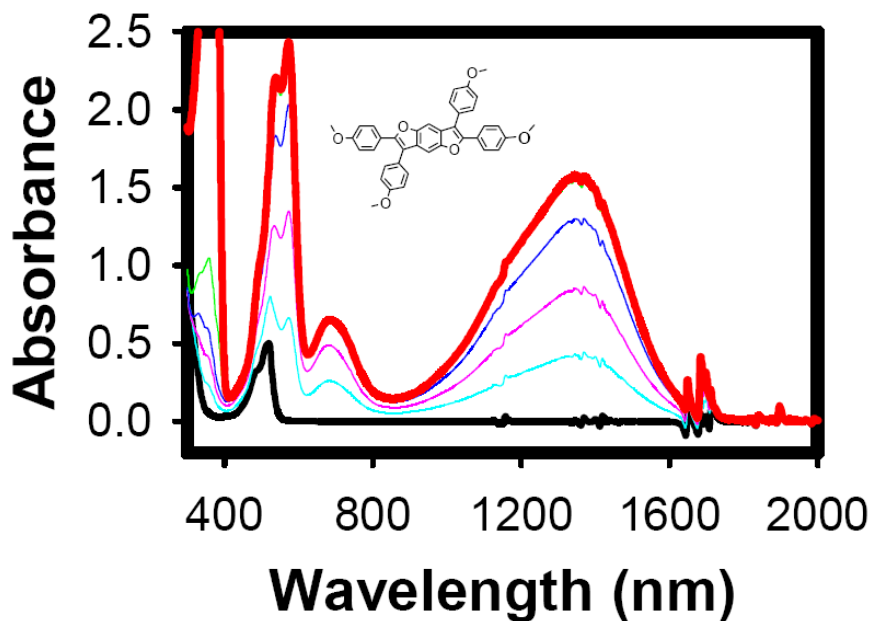


Figure 9. Spectral changes upon the reduction of 6.87×10^{-5} M $\text{MA}^{\bullet+}$ (Black line) by incremental addition of 1.0×10^{-3} M BDF2 to its radical cation (red line) in CH_2Cl_2 at 22°C . Note that the growth of the absorption bands due to $\text{BDF2}^{\bullet+}$ completely ceased after the addition of one equivalent of neutral BDF2 .

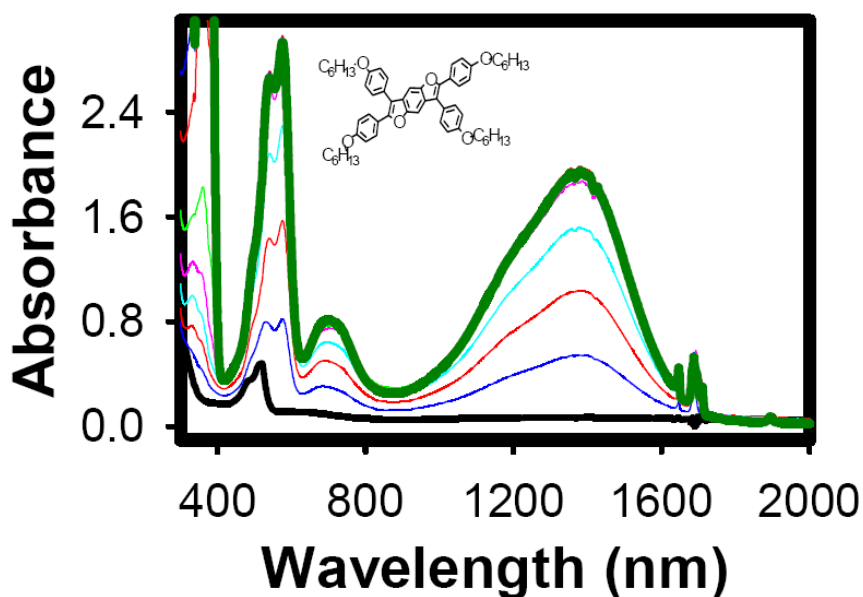


Figure 10. Spectral changes upon the reduction of 6.62×10^{-5} M $\text{MA}^{\bullet+}$ (Black line) by incremental addition of 1.0×10^{-3} M BDF3 to its radical cation (green line) in CH_2Cl_2 at 22°C . Note that the growth of the absorption bands due to $\text{BDF3}^{\bullet+}$ completely ceased after the addition of one equivalent of neutral BDF3 .

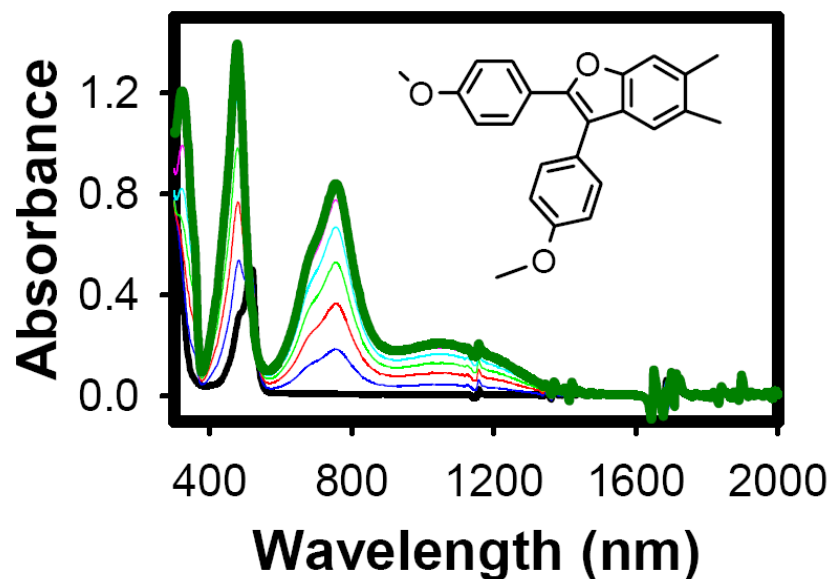


Figure 11. Spectral changes upon the reduction of 6.85×10^{-5} M $\text{MA}^{+\bullet}$ (Black line) by incremental addition of 1.0×10^{-3} M M2 to its radical cation (green line) in CH_2Cl_2 at 22°C . Note that the growth of the absorption bands due to $\text{M2}^{+\bullet}$ completely ceased after the addition of one equivalent of neutral M2 .

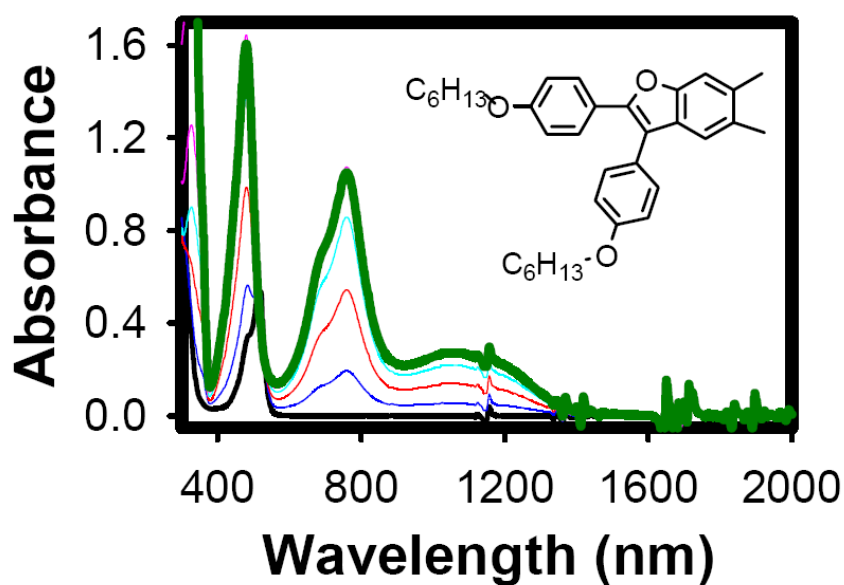


Figure 12. Spectral changes upon the reduction of 7.33×10^{-5} M $\text{MA}^{+\bullet}$ (Black line) by incremental addition of 1.0×10^{-3} M M3 to its radical cation (green line) in CH_2Cl_2 at 22°C . Note that the growth of the absorption bands due to $\text{M3}^{+\bullet}$ completely ceased after the addition of one equivalent of neutral M3 .

General Procedure for the Spectral Titration of $[\text{NAP}^{+\cdot} \text{SbCl}_6^-]$ with various electron donors.

A deep blue solution of $\text{NAP}^{+\cdot} \text{SbCl}_6^-$ in dichloromethane (3 mL, 4.3×10^{-5} M) was transferred under an argon atmosphere in a 1-cm quartz cuvette equipped with a Schlenk adaptor at room temperature. A dichloromethane solution (8.6×10^{-4} M) of **BDF1** in 5 μL increments was added to this solution. The electronic spectra of the resulting solutions, after the addition of each substoichiometric increment, were recorded at 22 °C (see Figure below). The spectral titration data for various benzodifuran and benzofuran electron donors using $[\text{NAP}^{+\cdot} \text{SbCl}_6^-]$ are compiled below:

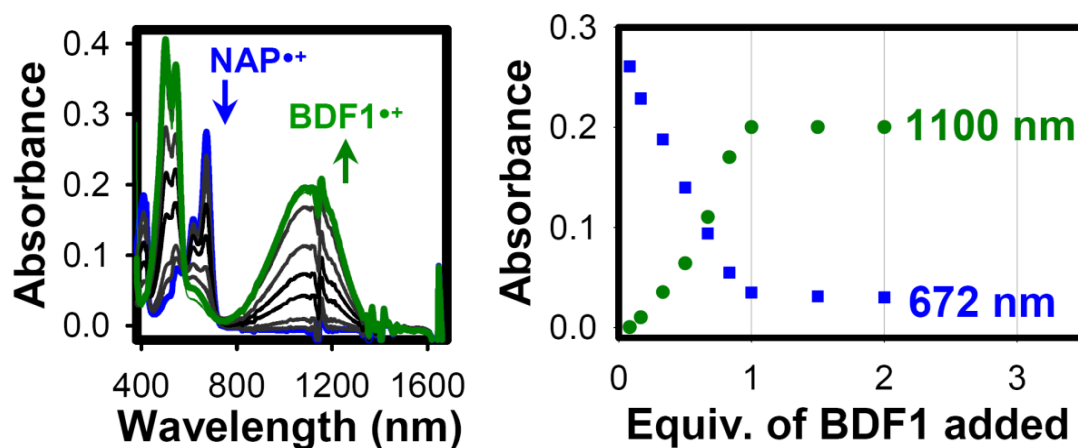


Figure 13. Left: Spectral changes upon the reduction of 3.2×10^{-5} M $\text{NAP}^{+\cdot}$ (blue line) by incremental addition of 1.0×10^{-3} M **BDF1** to its radical cation (green line) in CH_2Cl_2 at 22 °C. Right: A plot of depletion of absorbance of $\text{NAP}^{+\cdot}$ (blue squares, at 672 nm) and an increase of the absorbance of $\text{BDF1}^{+\cdot}$ (green circles, at 1100 nm) against the equivalent of added neutral **BDF1**.

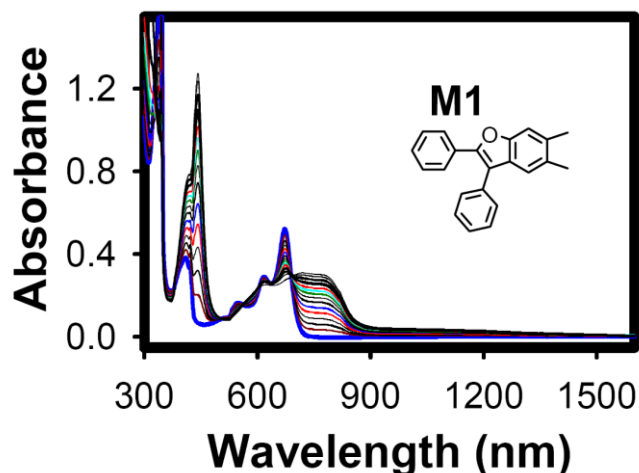


Figure 14. Spectral changes upon the reduction of 5.61×10^{-5} M NAP^{++} (blue line) by incremental addition of 1.0×10^{-3} M **M1** to its radical cation (black line) in CH_2Cl_2 at 22 °C. Note that the growth of the absorption bands due to M1^{++} completely ceased after the addition of one equivalent of neutral **M1**.

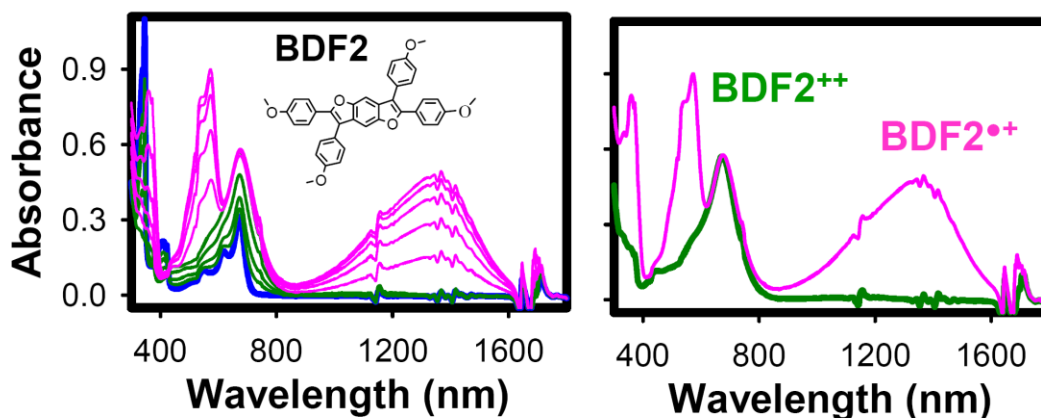


Figure 15. Left: Spectral changes upon the reduction of 4.83×10^{-5} M NAP^{++} (blue line) by incremental addition of 1.0×10^{-3} M **BDF2** to its dication (green lines) and radical cation (pink line) in CH_2Cl_2 at 22 °C. **Right:** A comparison of the spectra of dication (green line) and cation radical (pink line) of **BDF2** showing that intense NIR transition at 1368 nm is absent in the **BDF2** dication.

Crystallization of [BDF1^{•+} SbCl₆⁻] and [BDF2^{•+} SbCl₆⁻] using [MA^{•+} SbCl₆⁻]

A 25-mL Schlenk tube was charged with MA^{•+} SbCl₆⁻ (30.0 mg, 0.05 mmol), and a cold solution of **BDF1** (28.9 mg, 0.05 mmol) in anhydrous dichloromethane (5 mL) was added under argon atmosphere at ~0 °C. The solution immediately took on a dark green coloration, spectrophotometric analysis of the green-colored solution indicated the quantitative formation of [BDF1^{•+} SbCl₆⁻]. The green-colored solution was carefully layered with dry hexanes or toluene (15 mL) and placed in a refrigerator (-10 °C). During the course of 2 days, single crystals of cation radical salt suitable for X-ray crystallography were obtained. The single crystals of **BDF2^{•+} SbCl₆⁻** were obtained using a similar protocol. Note that solutions of [BDF1^{•+} SbCl₆⁻] and **BDF2^{•+} SbCl₆⁻** can also be prepared using NO⁺ SbCl₆⁻ in dichloromethane.

General method for the Synthesis of benzodifurans and benzofurans

An intimate mixture of hydroquinone (1 equiv.), zinc chloride (2 equiv.), and benzoin or its derivatives (2 equiv.) was heated under an argon atmosphere over a flame for 2-3 minute. After the mixture melts, precaution was taken to heat gently (5-10 min.) in such a way as to prevent the charring of the reaction mixture. The resulting mixture was cooled to room temperature, dissolved in dichloromethane (50 mL) and washed with aqueous sodium hydroxide (2 x 25 mL). Organic layer was separated and dried over anhydrous magnesium sulfate and evaporated under reduced pressure. The resulting residue was purified by crystallization with dichloromethane and methanol or acetonitrile. The characterization data for various benzodifurans and benzofurans thus prepared are summarized below:

BDF1: Yield (70 %); mp 279-281 °C; ^1H NMR (CDCl_3) δ : 7.26 – 7.69 (Ar, 22H); ^{13}C NMR (CDCl_3) δ : 100.99, 118.04, 127.09, 127.98, 128.53, 128.66, 129.25, 129.32, 130.03, 130.96, 133.18, 151.43, 151.55. **BDF2:** Yield (82 %); mp 282-285 °C; ^1H NMR (CDCl_3) 3.81 (s, 6H), 3.90 (s, 6H), 6.84 (d, 2H), 7.03 (d, 4H) 7.46 (d, 4H), 7.49 (s, 2H), 7.59 (d, 4H); ^{13}C NMR (CDCl_3) δ : 55.46, 55.53, 55.55, 55.61, 100.51, 114.13, 114.74, 116.16, 123.92, 125.58, 128.43, 129.18, 131.17, 151.17, 151.36, 159.28, 159.76. **BDF3:** Yield (65 %); mp 148-150°C; ^1H NMR (CDCl_3) δ : 0.91 (m, 6H), 1.36 (m, 12H), 1.82 (m, 4H), 3.94 (t, 2H), 4.02 (t, 2H), 6.82 (d, 2H), 7.00 (d, 2H) 7.44 (d, 2H), 7.48 (d, 2H), 7.58 (d, 2H); ^{13}C NMR (CDCl_3) δ : 14.27, 14.31, 22.84, 22.89, 25.95, 26.06, 29.43, 29.58, 31.81, 31.90, 68.24, 68.31, 100.47, 114.62, 115.23, 116.10, 123.70, 125.37, 128.39, 129.13, 131.11, 151.18, 151.33, 158.83, 159.33. **MI:** Yield (65 %); mp 144-146°C; ^1H NMR (CDCl_3) δ : 2.31 (s, 3H), 2.38 (s, 3H), 7.20 – 7.70 (Ar, 12H); ^{13}C NMR (CDCl_3) δ : 20.21, 20.76, 111.80, 117.45, 120.25, 127.03, 127.70, 128.22, 128.36, 128.59, 129.15, 129.99, 131.20, 131.76, 133.48, 134.14, 149.96, 153.18. **M2:** Yield (75 %); mp 144-147°C; ^1H NMR (CDCl_3) δ : 2.31 (s, 3H), 2.39 (s, 3H), 3.81 (s, 3H), 3.88 (s, 3H), 6.73 (s, 1H), 6.84 (d, 2H), 7.00 (d, 2H) 7.21 (s, 1H), 7.31 (s, 1H), 7.41 (d, 2H), 7.58 (d, 2H); ^{13}C NMR (CDCl_3) δ : 20.21, 20.74, 55.47, 55.50, 111.65, 114.05, 114.58, 115.53, 120.00, 124.03, 125.76, 128.36, 128.67, 131.09, 131.52, 149.88, 152.93, 159.08, 159.55. **M3:** Yield (70 %); mp 78-80°C; ^1H NMR (CDCl_3) δ : 0.91 (m, 6H), 1.36 (m, 12H), 1.79 (m, 4H), 2.29 (s, 3H), 2.36 (s, 3H), 3.97 (t, 2H), 3.99 (t, 2H), 6.80 (d, 2H), 6.97 (d, 2H) 7.19 (s, 1H), 7.28 (s, 1H), 7.37 (d, 2H), 7.55 (d, 2H); ^{13}C NMR (CDCl_3) δ : 14.26, 14.29, 20.68, 22.82, 22.87, 25.94, 26.04, 29.42, 29.56, 31.87, 68.18, 68.21, 111.62, 114.56,

115.08, 115.13, 115.49, 120.00, 123.82, 125.56, 128.32, 128.74, 131.04, 131.14, 133.37, 149.96, 152.94, 158.68, 159.16.

Synthesis of 4,4'-dihydroxybenzil

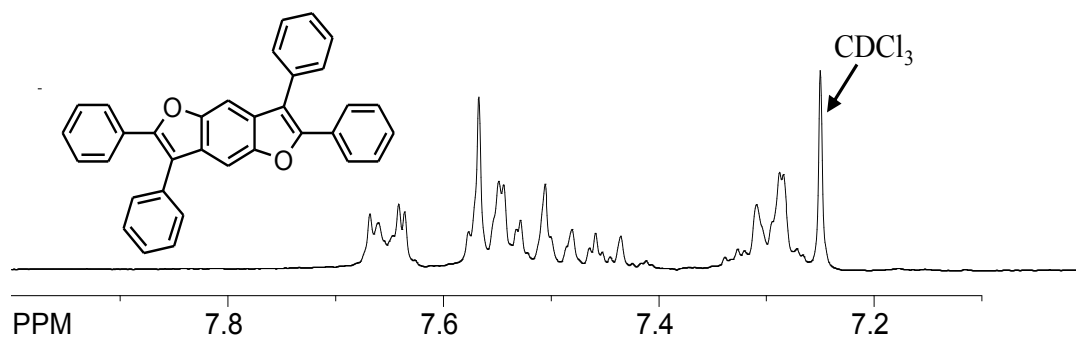
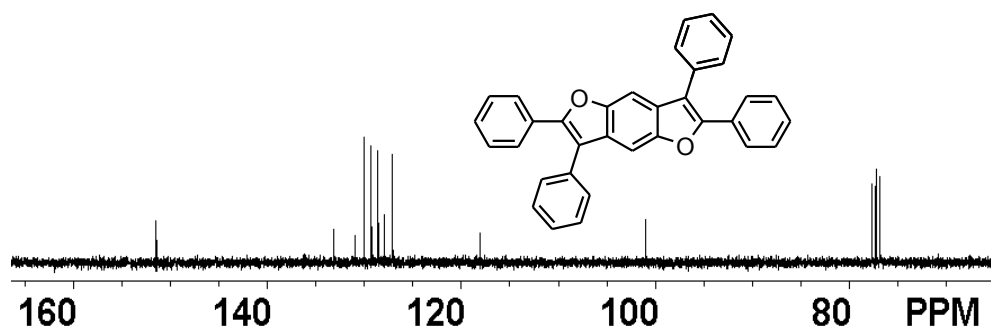
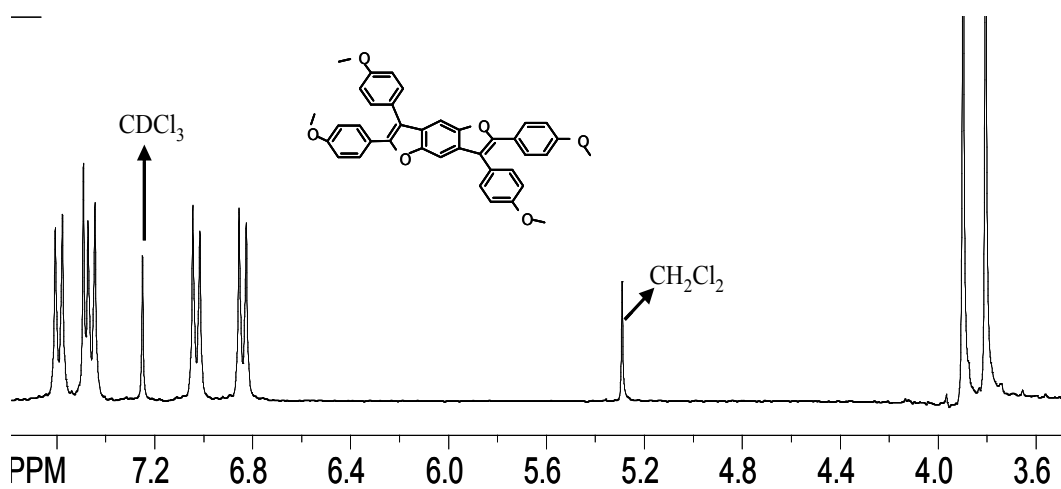
Following a literature procedure [Moylan, C.R.; Miller, R. D.; Twieg, R. J. ; Betterton, K. M. ; Lee, V. Y. ; Matray, T. J. ; Nguyen, C. *Chem. Mater.* **1993**, *5*, 1499-1508], a suspension of 4,4'-dimethoxybenzil (6.0 g, 20 mol) in a mixture of acetic acid (60 mL) and 48 % aqueous HBr (240 mL) was heated to reflux for 4 h. The homogeneous mixture was cooled and diluted with water (200 mL) and the resulting precipitate was filtered, washed with water and dried to give 4.5 g (84%) of 4,4'-dihydroxybenzil as a light tan solid: mp 248-250 °C; ¹H NMR (actone-d₆) δ: 6.99 (d, 4H), 7.82 (d, 4H); ¹³C NMR (CDCl₃) δ: 194.58, 164.62, 133.06, 126.09, 116.77.

Synthesis of 4,4'-dihexyloxybenzil

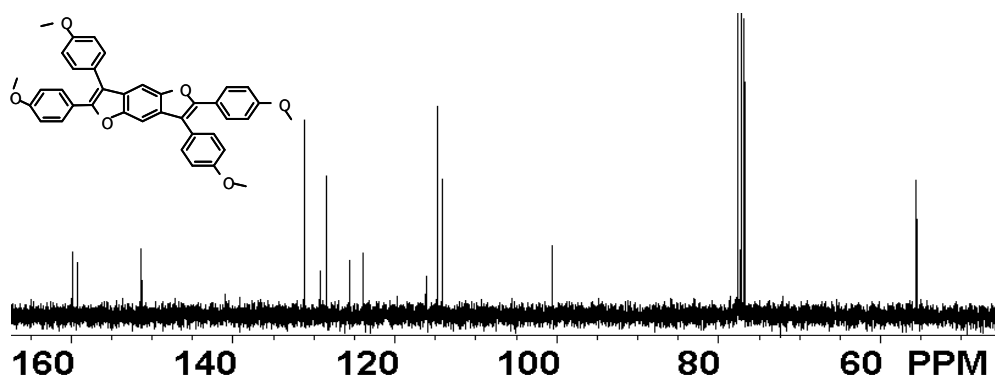
A mixture of 4,4'-dihydroxybenzil (4.0 g, 17 mmol), 1-bromohexane (6.0 g, 36 mmol), tetra-*n*-butylammonium bromide (2.67 g, 8 mol), and potassium carbonate (5.0 g, 36 mol) in DMF (120 mL) was stirred at 100-120 °C for 1.5 h. The reaction mixture was diluted with water, and the resulting precipitate was filtered and washed with water (3 x 50 mL). The resulting syrupy liquid was used in the next step without further purification. Yield (6.3 g, 93 %); mp 54-56 °C; ¹H NMR (CDCl₃) δ: 0.87 (t, 6H), 1.31 (m, 8H), 1.43 (m, 4H), 1.77 (m, 4H), 4.00 (t, 4H), 6.92 (d, 4H), 7.90 (d, 4H). ¹³C NMR (CDCl₃) δ: 14.18, 22.73, 25.77, 31.66, 68.63, 114.87, 126.23, 132.51, 164.67, 193.74.

Synthesis of 4,4'-dihexyloxybenzoin

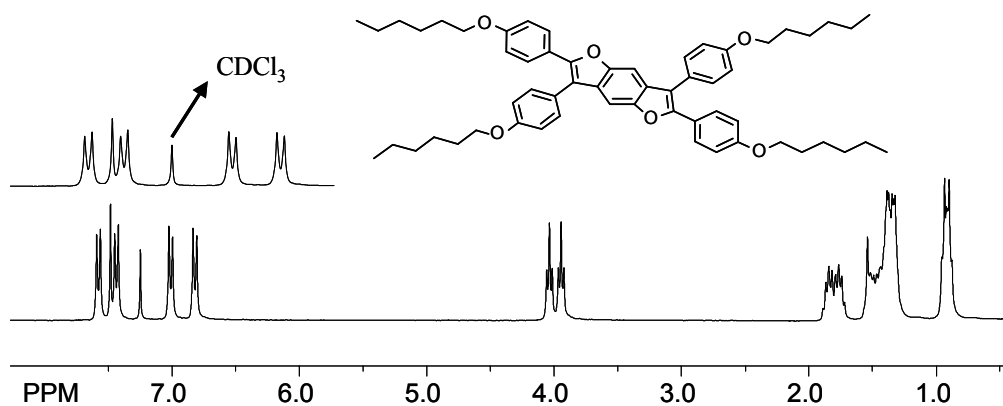
Zinc dust (5.7 g, 88 mol) was added to a vigorously stirred solution of 4,4'-dihexyloxybenzil (6.0 g, 15 mol) in a 3:1 mixture of DMF (180 mL) and water (60 mL). The resulting mixture was heated to reflux for 3 h and then cooled to room temperature. The zinc-dust residue was filtered and washed with dichloromethane (300 mL). The organic layer was separated and washed repeatedly with water and dried over anhydrous magnesium sulfate. Evaporation of the solvent under reduced pressure afforded 4,4'-dihexyloxybenzoin as a syrupy liquid which was used in the next step without further purification. Yield (5.3 g, 88 %); mp 30-32 °C; ¹H NMR (CDCl₃) δ: 0.88 (m, 6H), 1.30 (m, 8H), 1.40 (m, 4H), 1.73 (m, 4H), 3.88 (t, 2H), 3.95 (t, 2H), 4.57 (d, 2H), 5.83 (d, 2H), 6.82 (2d, 4H), 7.22 (d, 2H), 7.87 (d, 2H); ¹³C NMR (CDCl₃) δ: 14.09, 14.29, 22.63, 22.65, 25.67, 25.76, 29.02, 29.23, 31.55, 31.62, 67.97, 68.32, 75.28, 114.35, 115.02, 126.12, 129.03, 131.61, 131.75, 159.24, 163.66, 197.37.

NMR Spectroscopic Data**¹H NMR spectrum of 2,3,6,7-tetraphenylbenzo[1,2-b:4,5-b']difuran (BDF1)****¹³C NMR spectrum of 2,3,6,7-tetraphenylbenzo[1,2-b:4,5-b']difuran (BDF1)****¹H NMR spectrum of 2,3,6,7-tetrakis(4-methoxyphenyl)benzo[1,2-b:4,5-b']difuran (BDF2)**

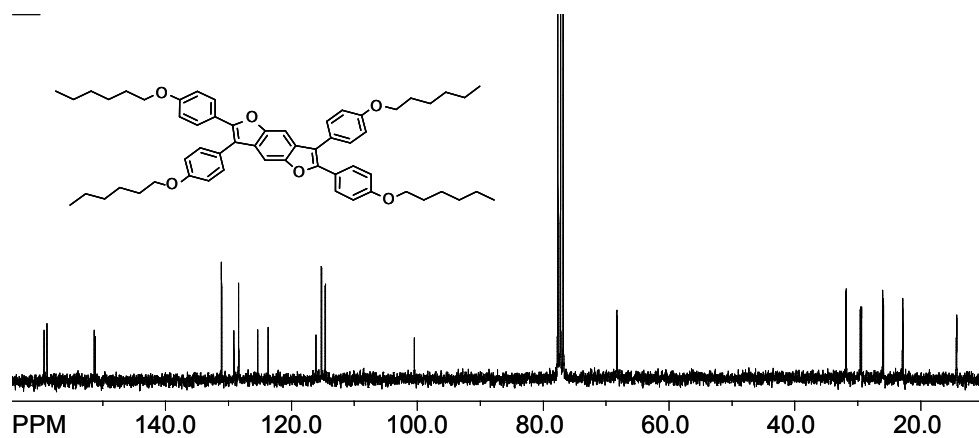
¹³C NMR spectrum of 2,3,6,7-tetra(4-methoxyphenyl)benzo[1,2-b:4,5-b']difuran (BDF2)

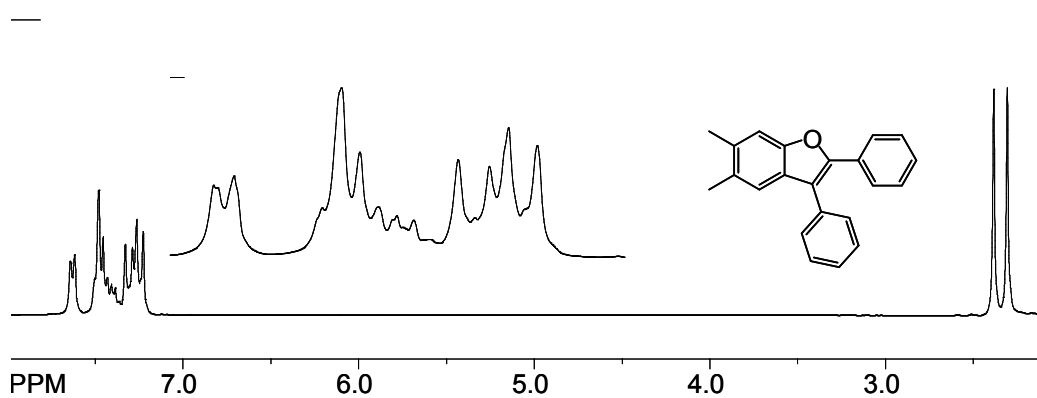
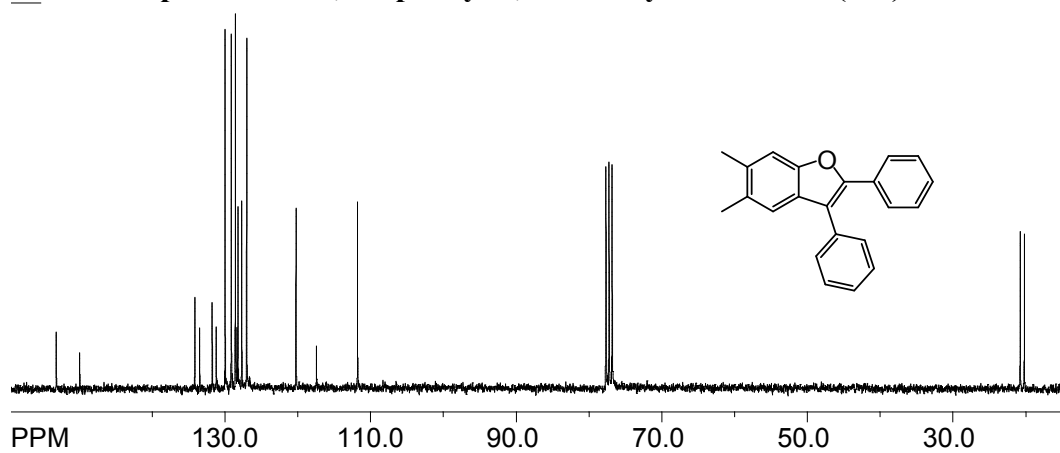
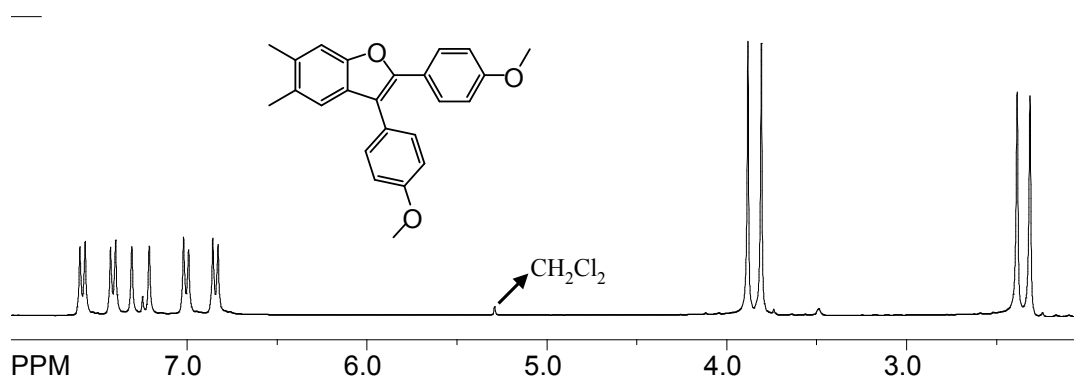


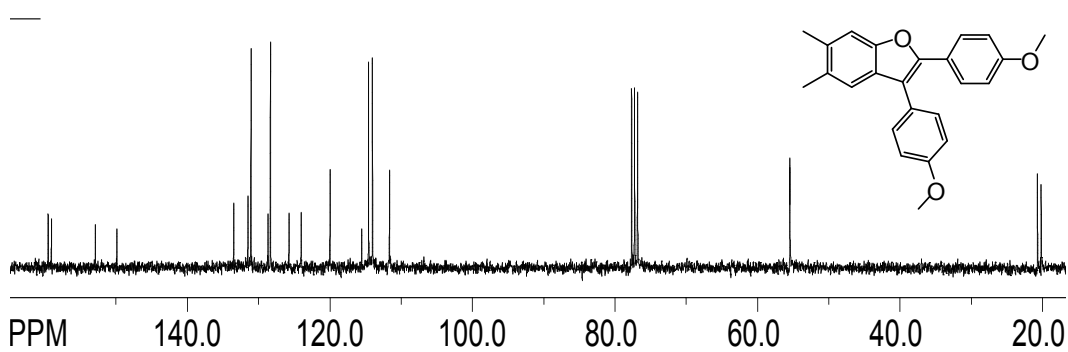
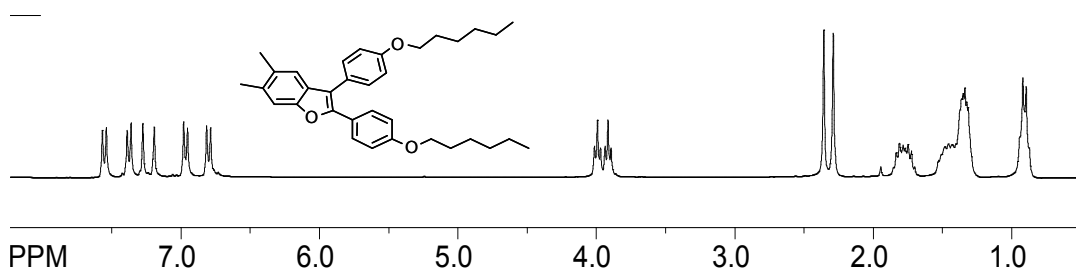
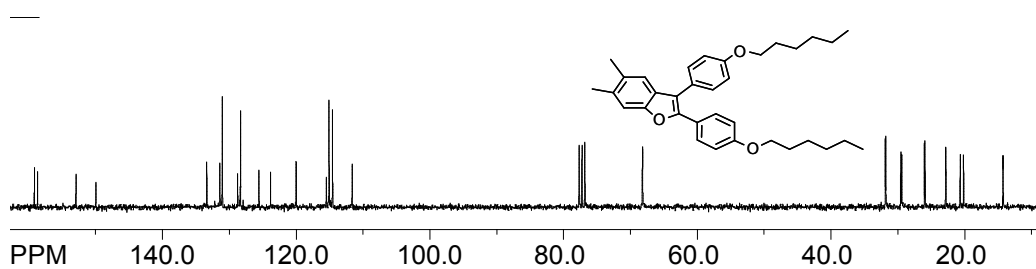
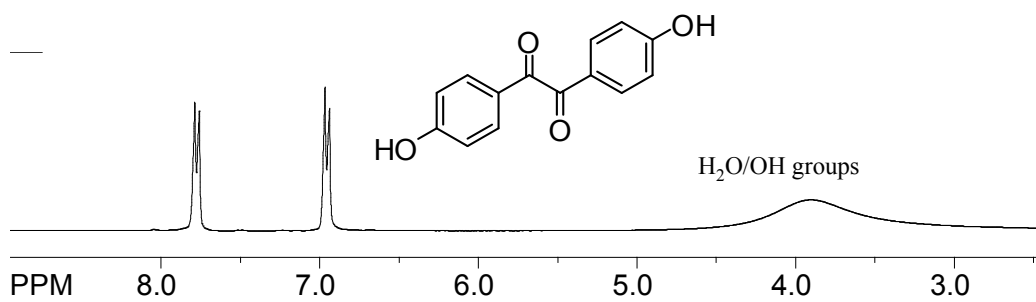
¹H NMR spectrum of 2,3,6,7-tetra(4-hexyloxyphenyl)benzo[1,2-b:4,5-b']difuran (BDF3)

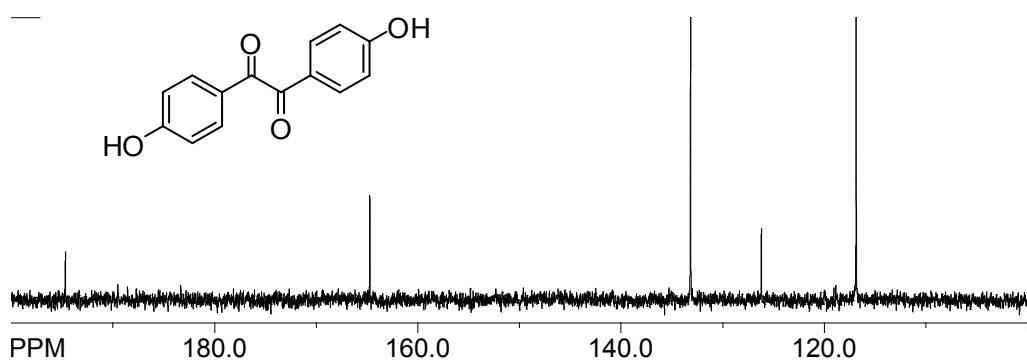
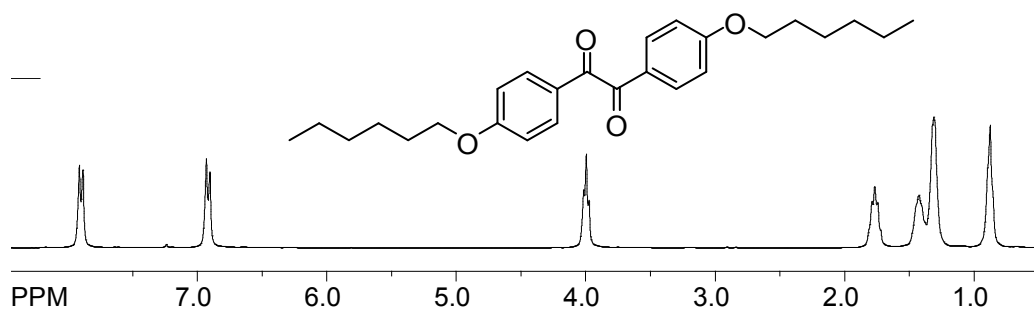
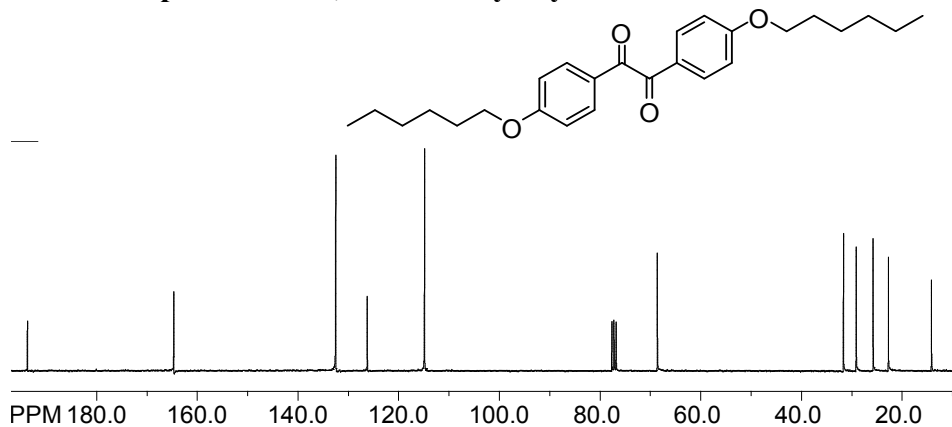
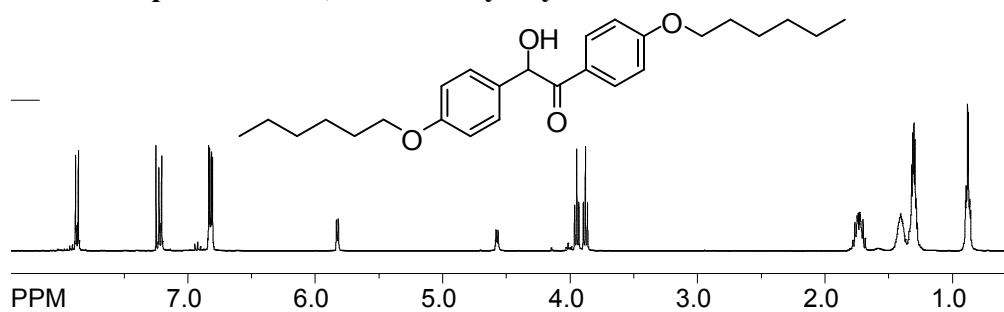


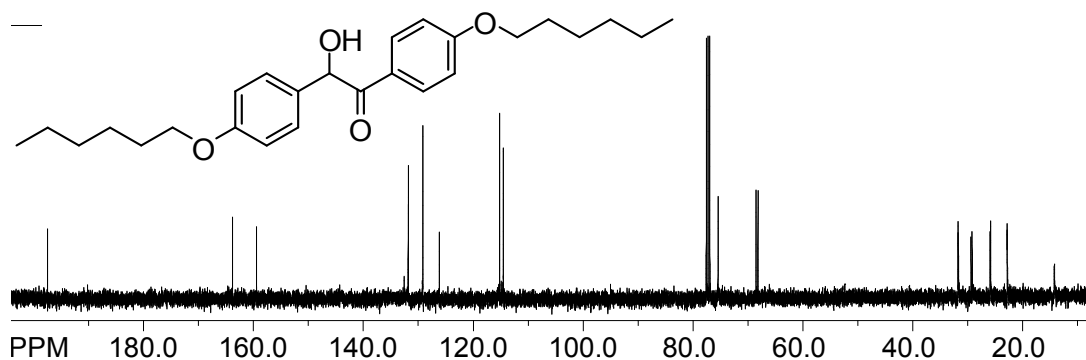
¹³C NMR spectrum of 2,3,6,7-tetra(4-hexyloxyphenyl)benzo[1,2-b:4,5-b']difuran (BDF3)



¹H NMR spectrum of 2,3-diphenyl-5,6-dimethylbenzofuran (M1)**¹³C NMR spectrum of 2,3-diphenyl-5,6-dimethylbenzofuran (M1)****¹H NMR spectrum of 2,3-di-(4-methoxyphenyl)-5,6-dimethylbenzofuran (M2)**

^{13}C NMR spectrum of 2,3-di-(4-methoxyphenyl)-5,6-dimethylbenzofuran (M2) **^1H NMR spectrum of 2,3-di-(4-hexyloxyphenyl)-5,6-dimethylbenzofuran (M3)** **^1H NMR spectrum of 2,3-di-(4-hexyloxyphenyl)-5,6-dimethylbenzofuran (M3)** **^1H NMR spectrum of 4,4'-dihydroxybenzil**

^{13}C NMR spectrum of 4,4'-dihydroxybenzil **^1H NMR spectrum of 4,4'-di-*n*-hexyloxybenzil** **^{13}C NMR spectrum of 4,4'-di-*n*-hexyloxybenzil** **^1H NMR spectrum of 4,4'-di-*n*-hexyloxybenzoil**

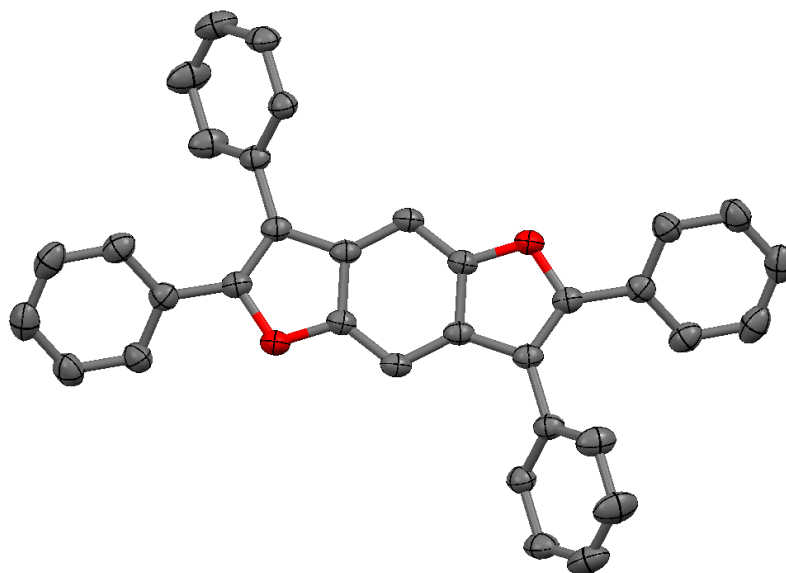
^{13}C NMR spectrum of 4,4'-di-*n*-hexyloxybenzoin**Crystal Structure Determinations.****General considerations**

X-ray intensity was measured at 100(2) K using a Bruker AXS 3-circle diffractometer equipped with a SMART2^{S1} CCD detector using Cu K α radiation ($\lambda = 1.54178 \text{ \AA}$). Raw data frame integration and Lp corrections were performed with SAINT+.^{S2} For each, analysis of the data showed negligible crystal decay during collection. Numerical absorption corrections were applied to the data whenever needed. Direct methods structure solutions, difference Fourier calculations and full-matrix least-squares refinements against F^2 were performed with SHELXTL.^{S2} All non-hydrogen atoms were refined with anisotropic displacement parameters. Hydrogen atoms were placed in geometrically idealized positions and included as riding atoms.

[S1] SMART Version 5.630, SAINT+ Version 6.45, and SADABS Version 2.05. Bruker Analytical X-ray Systems, Inc., Madison, Wisconsin, USA, 2003.

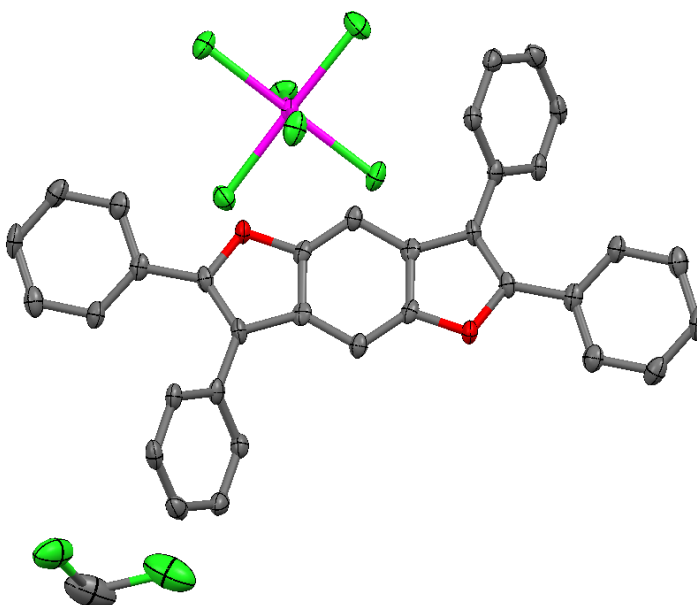
[S2] Sheldrick, G. M. SHELXTL Version 6.14; Bruker Analytical X-ray Systems, Inc., Madison, Wisconsin, USA, 2000.

Crystal data and structure refinement for BDF1.



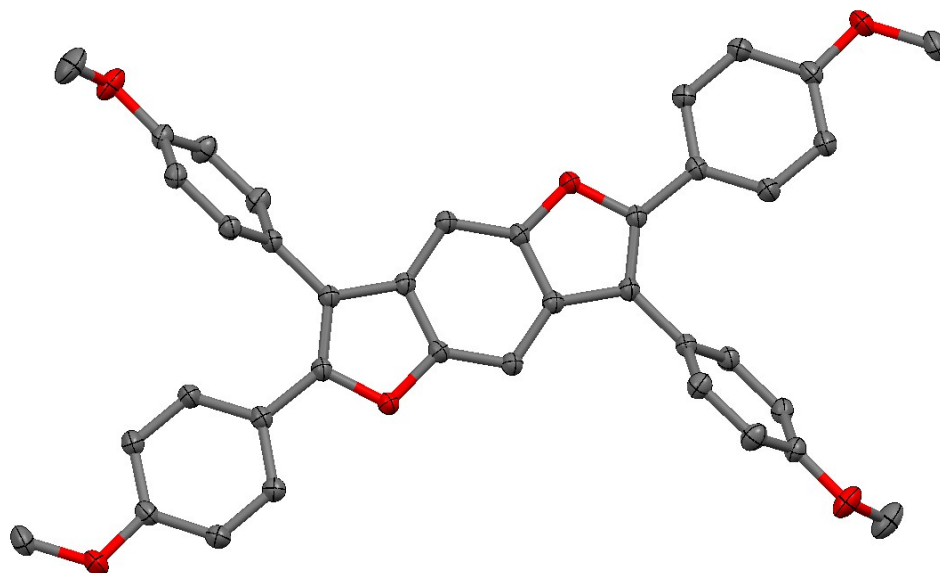
Identification code	rajf	
Empirical formula	C ₃₄ H ₂₂ O ₂	
Formula weight	462.52	
Temperature	100(2) K	
Wavelength	0.71073 Å	
Crystal system	Triclinic	
Space group	P -1	
Unit cell dimensions	a = 9.5994(9) Å	$\alpha = 93.7300(10)^\circ$
	b = 10.9712(11) Å	$\beta = 106.4600(10)^\circ$
	c = 11.9451(12) Å	$\gamma = 95.153(2)^\circ$
Volume	1196.2(2) Å ³	
Z	2	
Density (calculated)	1.284 Mg/m ³	
Absorption coefficient	0.079 mm ⁻¹	
F(000)	484	
Crystal size	0.35 x 0.16 x 0.12 mm ³	
Theta range for data collection	1.79 to 31.95°	
Index ranges	-14 ≤ h ≤ 13, -16 ≤ k ≤ 16, 0 ≤ l ≤ 17	
Reflections collected	19414	
Independent reflections	7636 [R(int) = 0.0262]	
Completeness to theta = 25.0°	99.2 %	
Absorption correction	Semi-empirical from equivalents	
Max. and min. transmission	0.989 and 0.970	
Refinement method	Full-matrix least-squares on F ²	
Data / restraints / parameters	7636 / 0 / 325	
Goodness-of-fit on F ²	1.086	
Final R indices [I > 2σ(I)]	R1 = 0.0488, wR2 = 0.1296	
R indices (all data)	R1 = 0.0660, wR2 = 0.1386	
Largest diff. peak and hole	0.373 and -0.218 e.Å ⁻³	

Crystal data and structure refinement for $\text{BDF1}^{\bullet+} \text{SbCl}_6^- \cdot \text{CH}_2\text{Cl}_2$.



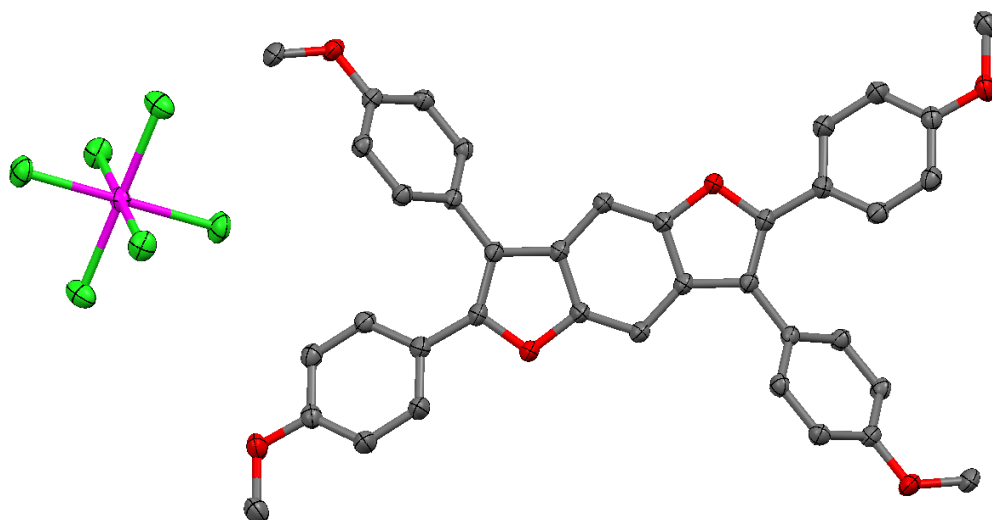
Identification code	raj10ba	
Empirical formula	C ₃₅ H ₂₄ Cl ₈ O ₂ Sb	
Formula weight	881.89	
Temperature	100(2) K	
Wavelength	1.54178 Å	
Crystal system	Triclinic	
Space group	P -1	
Unit cell dimensions	a = 11.9744(6) Å	α = 65.734(3)°.
	b = 12.3225(7) Å	β = 74.646(3)°.
	c = 14.8492(9) Å	γ = 62.175(2)°.
Volume	1759.28(17) Å ³	
Z	2	
Density (calculated)	1.665 Mg/m ³	
Absorption coefficient	12.072 mm ⁻¹	
F(000)	874	
Crystal size	0.73 x 0.07 x 0.04 mm ³	
Theta range for data collection	3.28 to 66.71°.	
Index ranges	-13 ≤ h ≤ 14, -12 ≤ k ≤ 14, 0 ≤ l ≤ 16	
Reflections collected	14172	
Independent reflections	5722 [R(int) = 0.0370]	
Completeness to theta = 67.00°	99.7 %	
Absorption correction	Numerical	
Max. and min. transmission	0.6773 and 0.0356	
Refinement method	Full-matrix least-squares on F ²	
Data / restraints / parameters	5722 / 0 / 415	
Goodness-of-fit on F ²	1.039	
Final R indices [I > 2σ(I)]	R1 = 0.0344, wR2 = 0.0856	
R indices (all data)	R1 = 0.0413, wR2 = 0.0882	
Largest diff. peak and hole	1.100 and -0.718 e.Å ⁻³	

Crystal data and structure refinement for BDF2.



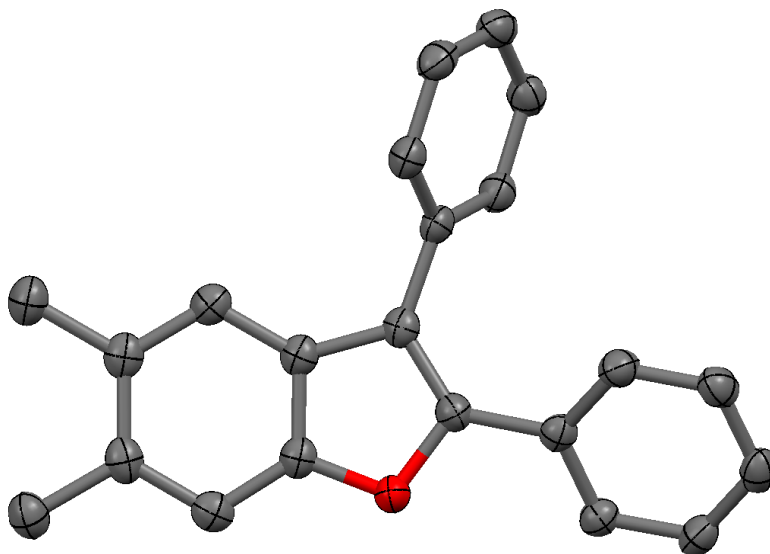
Identification code	rajb	
Empirical formula	C ₃₈ H ₃₀ O ₆	
Formula weight	582.62	
Temperature	100(2) K	
Wavelength	0.71073 Å	
Crystal system	Monoclinic	
Space group	P 2(1)/n	
Unit cell dimensions	a = 7.6547(9) Å	$\alpha = 90^\circ$.
	b = 7.7335(9) Å	$\beta = 94.224(2)^\circ$.
	c = 24.521(3) Å	$\gamma = 90^\circ$.
Volume	1447.7(3) Å ³	
Z	2	
Density (calculated)	1.337 Mg/m ³	
Absorption coefficient	0.090 mm ⁻¹	
F(000)	612	
Crystal size	0.75 x 0.25 x 0.1 mm ³	
Theta range for data collection	1.67 to 31.96°.	
Index ranges	-11 ≤ h ≤ 11, 0 ≤ k ≤ 11, 0 ≤ l ≤ 35	
Reflections collected	23524	
Independent reflections	4757 [R(int) = 0.0349]	
Completeness to theta = 25.00°	99.8 %	
Absorption correction	Semi-empirical from equivalents	
Max. and min. transmission	0.986 and 0.931	
Refinement method	Full-matrix least-squares on F ²	
Data / restraints / parameters	4757 / 0 / 201	
Goodness-of-fit on F ²	1.039	
Final R indices [I > 2σ(I)]	R1 = 0.0466, wR2 = 0.1304	
R indices (all data)	R1 = 0.0524, wR2 = 0.1359	
Largest diff. peak and hole	0.574 and -0.195 e.Å ⁻³	

Crystal data and structure refinement for BDF2^{•+} SbCl₆⁻.



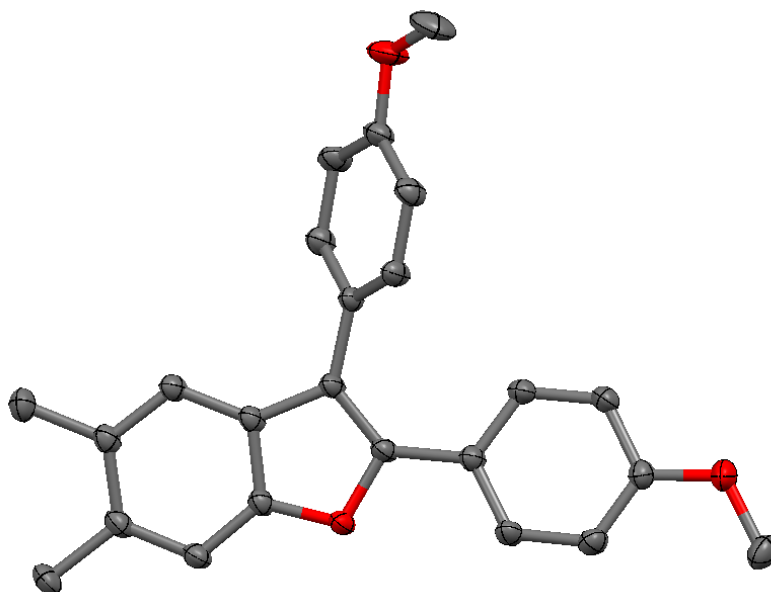
Identification code	raj_z	
Empirical formula	C ₃₈ H ₃₀ Cl ₆ O ₆ Sb	
Formula weight	917.07	
Temperature	100(2) K	
Wavelength	0.71073 Å	
Crystal system	Triclinic	
Space group	P-1	
Unit cell dimensions	a = 7.3249(8) Å	α = 68.992(1)°.
	b = 11.5799(12) Å	β = 86.057(1)°.
	c = 11.8128(12) Å	γ = 78.314(1)°.
Volume	915.98(17) Å ³	
Z	1	
Density (calculated)	1.663 Mg/m ³	
Absorption coefficient	1.238 mm ⁻¹	
F(000)	459	
Crystal size	0.13 x 0.13 x 0.10 mm ³	
Theta range for data collection	1.85 to 31.87°.	
Index ranges	-10 ≤ h ≤ 10, -15 ≤ k ≤ 17, 0 ≤ l ≤ 17	
Reflections collected	14889	
Independent reflections	5818 [R(int) = 0.0217]	
Completeness to theta = 25.00°	99.6 %	
Absorption correction	Semi-empirical from equivalents	
Max. and min. transmission	0.8862 and 0.8556	
Refinement method	Full-matrix least-squares on F ²	
Data / restraints / parameters	5818 / 0 / 292	
Goodness-of-fit on F ²	1.051	
Final R indices [I > 2σ(I)]	R1 = 0.0274, wR2 = 0.0703	
R indices (all data)	R1 = 0.0320, wR2 = 0.0726	
Largest diff. peak and hole	0.823 and -0.296 e.Å ⁻³	

Crystal data and structure refinement for M1.



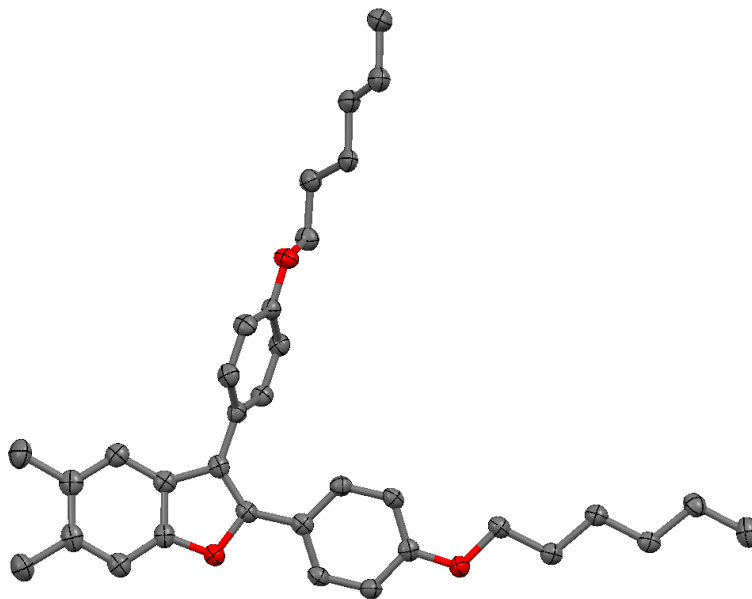
Identification code	raj10h5	
Empirical formula	C ₂₂ H ₁₈ O	
Formula weight	298.36	
Temperature	100(2) K	
Wavelength	1.54178 Å	
Crystal system	Triclinic	
Space group	P -1	
Unit cell dimensions	a = 6.0367(5) Å	$\alpha = 97.099(5)^\circ$.
	b = 7.5110(6) Å	$\beta = 94.814(5)^\circ$.
	c = 17.5810(15) Å	$\gamma = 96.725(5)^\circ$.
Volume	781.67(11) Å ³	
Z	2	
Density (calculated)	1.268 Mg/m ³	
Absorption coefficient	0.587 mm ⁻¹	
F(000)	316	
Crystal size	0.43 x 0.38 x 0.08 mm ³	
Theta range for data collection	2.55 to 67.09°.	
Index ranges	-7 ≤ h ≤ 7, -8 ≤ k ≤ 8, 0 ≤ l ≤ 20	
Reflections collected	7078	
Independent reflections	3855 [R(int) = 0.0331]	
Completeness to theta = 68.00°	99.7 %	
Absorption correction	Semi-empirical from equivalents	
Max. and min. transmission	0.9546 and 0.7865	
Refinement method	Full-matrix least-squares on F ²	
Data / restraints / parameters	3855 / 0 / 212	
Goodness-of-fit on F ²	0.991	
Final R indices [I > 2σ(I)]	R1 = 0.0420, wR2 = 0.1087	
R indices (all data)	R1 = 0.0457, wR2 = 0.1108	
Extinction coefficient	0.0050(7)	
Largest diff. peak and hole	0.182 and -0.190 e.Å ⁻³	

Crystal data and structure refinement for M2.



Identification code	rajq	
Empirical formula	C ₂₄ H ₂₂ O ₃	
Formula weight	358.42	
Temperature	100(2) K	
Wavelength	0.71073 Å	
Crystal system	Monoclinic	
Space group	P2(1)/c	
Unit cell dimensions	a = 17.600(5) Å	$\alpha = 90^\circ$.
	b = 6.1125(16) Å	$\beta = 99.252(4)^\circ$.
	c = 17.536(5) Å	$\gamma = 90^\circ$.
Volume	1862.0(9) Å ³	
Z	4	
Density (calculated)	1.279 Mg/m ³	
Absorption coefficient	0.083 mm ⁻¹	
F(000)	760	
Crystal size	0.7 x 0.4 x 0.15 mm ³	
Theta range for data collection	2.34 to 31.81°.	
Index ranges	-24 ≤ h ≤ 24, 0 ≤ k ≤ 9, 0 ≤ l ≤ 25	
Reflections collected	18029	
Independent reflections	5883 [R(int) = 0.0559]	
Completeness to theta = 25.00°	99.6 %	
Absorption correction	Semi-empirical from equivalents	
Max. and min. transmission	0.987 and 0.933	
Refinement method	Full-matrix least-squares on F ²	
Data / restraints / parameters	5883 / 0 / 270	
Goodness-of-fit on F ²	0.999	
Final R indices [I > 2σ(I)]	R1 = 0.0744, wR2 = 0.2058	
R indices (all data)	R1 = 0.0900, wR2 = 0.2213	
Largest diff. peak and hole	0.748 and -0.528 e.Å ⁻³	

Crystal data and structure refinement for M3.



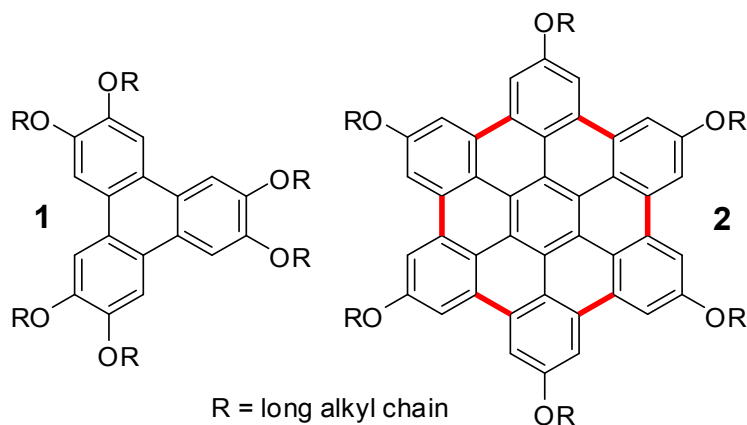
Identification code	raj0w	
Empirical formula	C ₃₄ H ₄₂ O ₃	
Formula weight	498.68	
Temperature	100(2) K	
Wavelength	1.54178 Å	
Crystal system	Triclinic	
Space group	P -1	
Unit cell dimensions	a = 8.8124(2) Å	α = 98.402(2)°.
	b = 9.1581(2) Å	β = 103.073(2)°.
	c = 18.5645(5) Å	γ = 96.722(2)°.
Volume	1426.13(6) Å ³	
Z	2	
Density (calculated)	1.161 Mg/m ³	
Absorption coefficient	0.560 mm ⁻¹	
F(000)	540	
Crystal size	0.61 x 0.42 x 0.07 mm ³	
Theta range for data collection	2.48 to 66.63°.	
Index ranges	-10 ≤ h ≤ 9, -10 ≤ k ≤ 10, 0 ≤ l ≤ 22	
Reflections collected	11523	
Independent reflections	4631 [R(int) = 0.0248]	
Completeness to theta = 67.00°	99.7 %	
Absorption correction	Semi-empirical from equivalents	
Max. and min. transmission	0.9618 and 0.7262	
Refinement method	Full-matrix least-squares on F ²	
Data / restraints / parameters	4631 / 0 / 339	
Goodness-of-fit on F ²	1.043	
Final R indices [I > 2σ(I)]	R1 = 0.0389, wR2 = 0.1004	
R indices (all data)	R1 = 0.0485, wR2 = 0.1049	
Extinction coefficient	0.0004(1)	
Largest diff. peak and hole	0.449 and -0.161 e.Å ⁻³	

CHAPTER 2A

A Facile Synthesis of Elusive Alkoxy-substituted Hexa-*peri*-hexabenzocoronene

Introduction

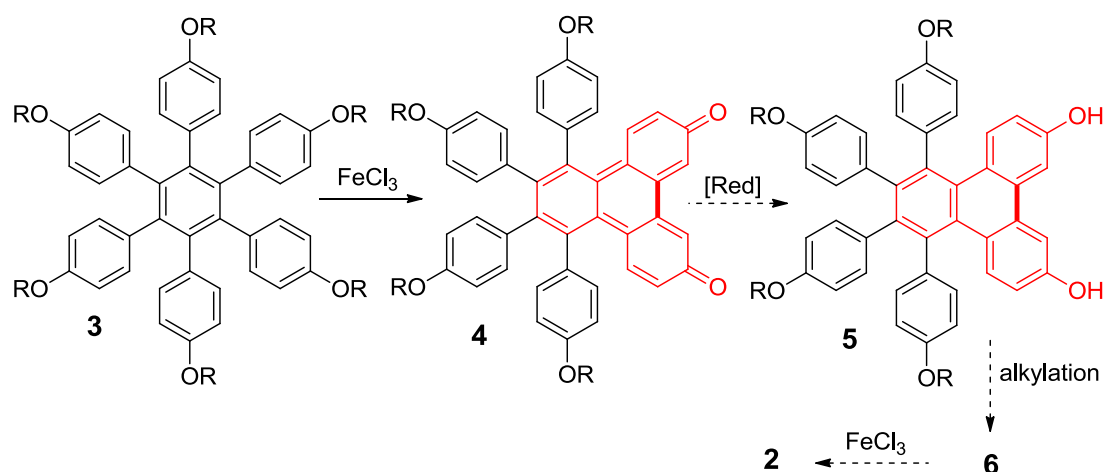
The study of polycyclic aromatic hydrocarbons (PAH), such as triphenylenes (TP) and hexa-*peri*-hexabenzocoronenes (HBC), has attracted considerable attention¹ since these materials hold promise for applications in the emerging area of molecular electronics and nanotechnology.²



It is noteworthy that hexaalkoxytriphenylenes (**1**) have been extensively explored as building blocks for the preparation of liquid crystalline materials, owing to their disc-shaped structure which allows efficient columnar packing.³ Columnar discotic liquid crystals have received considerable attention as functional materials for applications such as photovoltaic solar cells, light emitting diodes, and field effect transistors.⁴ It can be envisioned that a corresponding HBC analog (**2**), possessing a disc of relatively large size, may prove to be superior for the preparation of liquid crystalline materials.^{3,4}

Unfortunately, the synthesis of the parent hexaalkoxy HBC (**2**) has thus far eluded chemists.⁵ Müllen and coworkers have reported⁶ that attempted preparation of **2** from hexakis(4-alkoxyphenyl)benzene via oxidative cyclodehydrogenation led to a quantitative yield of a phenanthroquinone **4**, i.e. Scheme 1.

Scheme 1. Postulated Synthesis of Hexaalkoxy-HBC **2**.

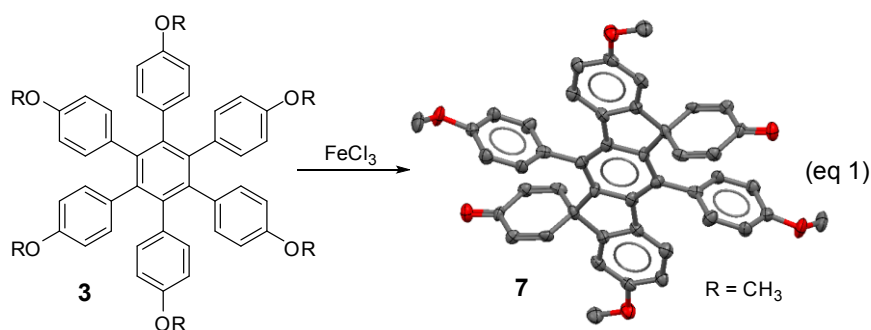


Results and Discussion

It was conjectured that a reduction of quinone **4** to the corresponding hydroquinone **5** followed by *O*-alkylations and oxidative cyclization, may allow the preparation of the long-sought hexaalkoxy-HBC **2** (Scheme 1). However, we now uncover that the oxidative cyclization of **3** unfortunately does not produce quinone **4**, but rather an unexpected indeno[1,2-*b*]fluorene derivative (**7**), whose structure is confirmed by X-ray crystallography. Mechanistic consideration for the formation of indenofluorene **7** via oxidative cyclodehydrogenation of **3** now leads us to an alternative route to access the elusive **2**. The details of these preliminary findings are described herein.

Thus, an addition of a solution of FeCl_3 in nitromethane to a solution of **3** in dichloromethane at $\sim 0^\circ\text{C}$ produces a green colored solution which was stirred for 1 h

while a slow stream of argon was bubbled through the solution to remove gaseous hydrochloric acid, which was formed in the reaction. The standard workup⁷ afforded a pale yellow solid in quantitative yield. The ¹H/¹³C NMR analysis of the above solid suggested that it is a single compound that has lost two alkyl groups and two 'H' atoms (See Figure 1A-1C). As such, the preliminary spectral analysis was in accord with the phenanthroquinone-like structure **4**, however, further experimentation⁸ and X-ray crystallography showed that it is indenofluorene **7** (i.e. eq 1). Note that the thermal ellipsoids for the ORTEP representation of **7** (R = CH₃), in eq 1, are shown in 50 % probability and hydrogens are omitted for the sake of clarity.



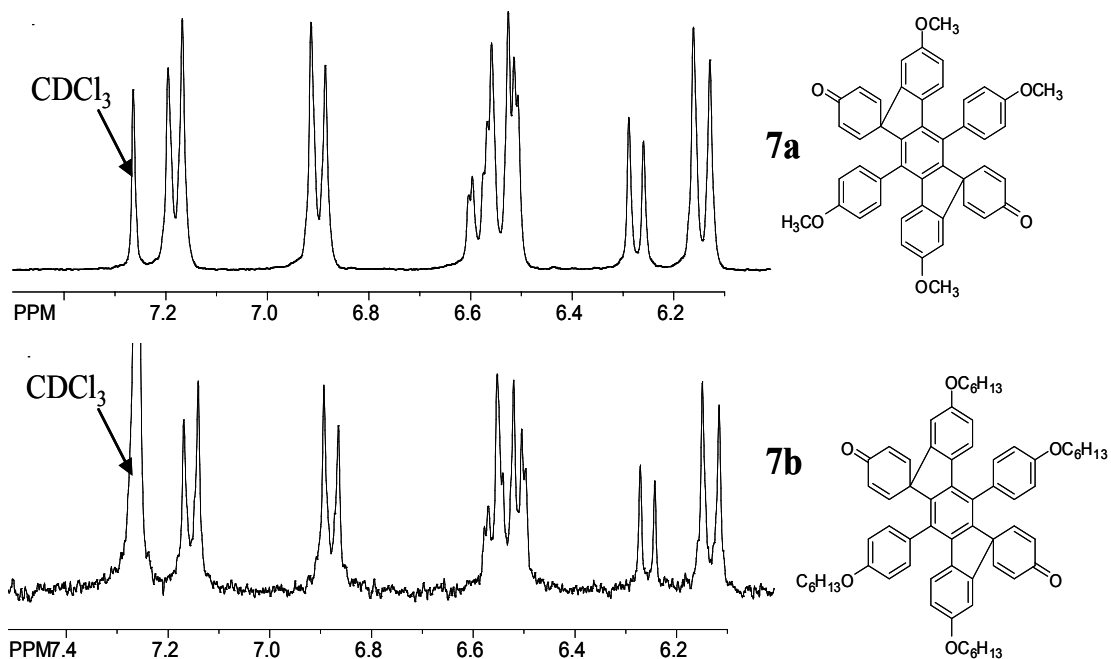


Figure 1A. Showing the similarity of the aromatic region of the ^1H NMR spectra of indenofluorenes **7a** and **7b**.

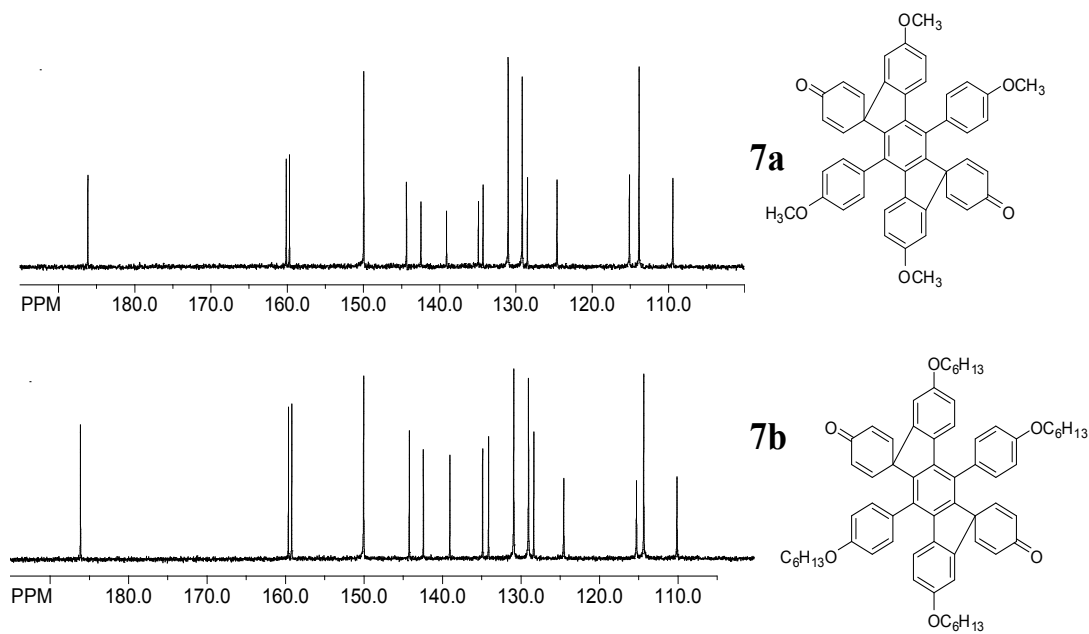


Figure 1B. Showing the similarity of the aromatic region of the ^{13}C NMR spectra of indenofluorenes **7a** and **7b**.

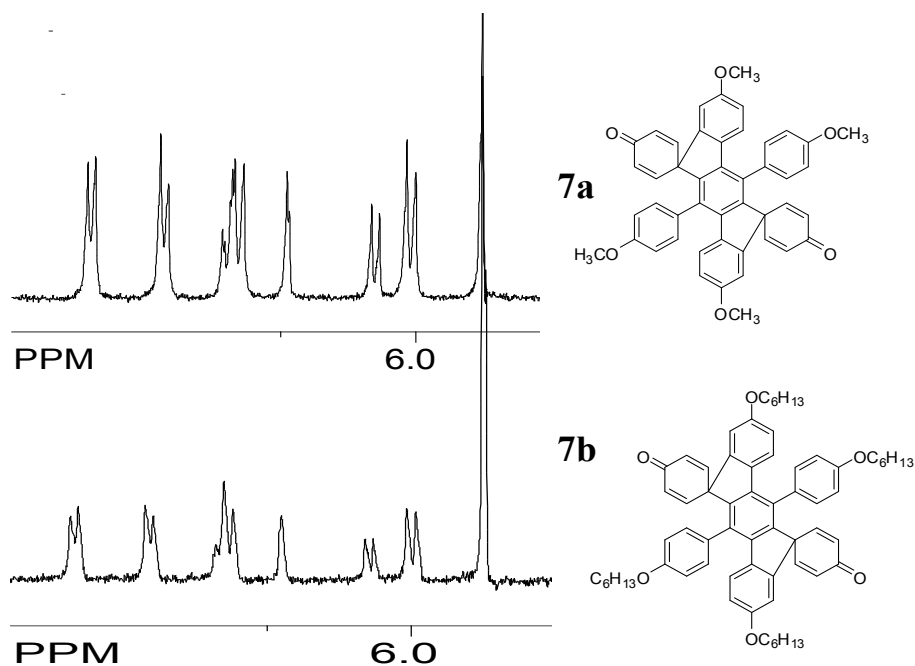
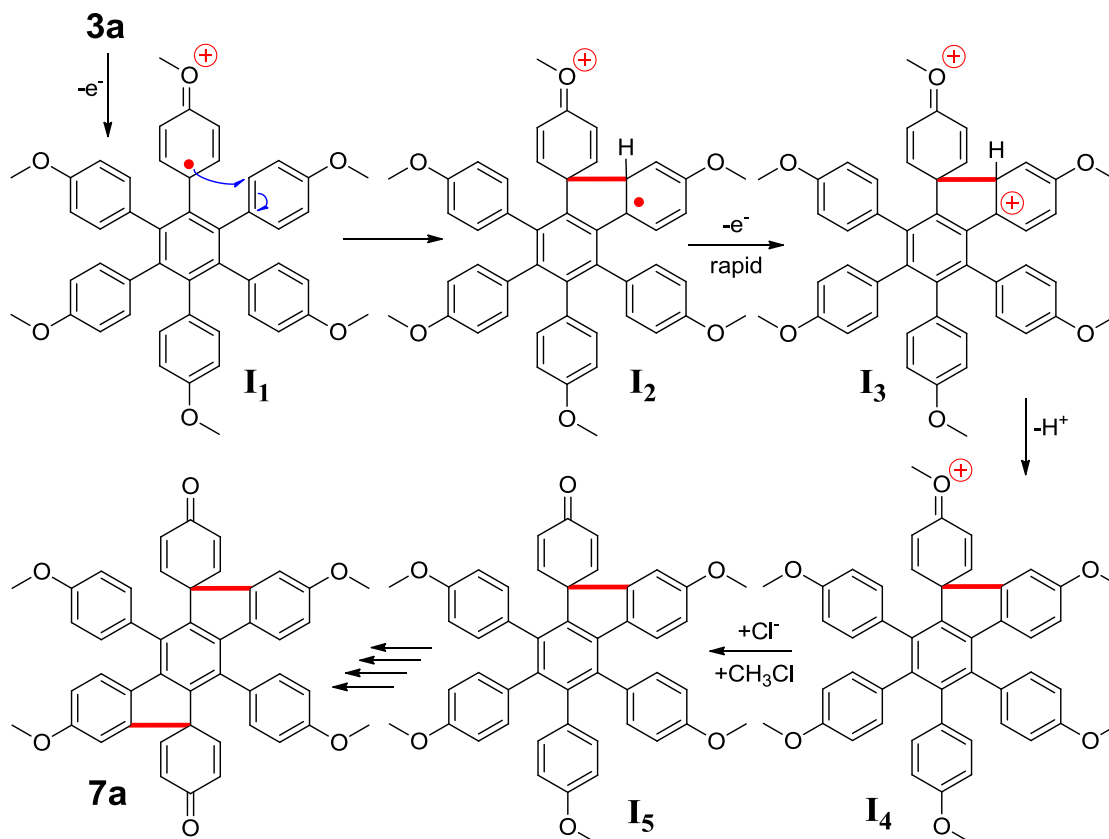


Figure 1C. Showing the similarity of the aromatic region of the ^1H NMR spectra of indenofluorenes **7a** and **7b** in $\text{DMSO-}d_6$. Note that the aromatic region of reported ^1H NMR spectrum of supposed phenanthroquinone **4** ($\text{R} = \text{C}_{12}\text{H}_{25}$) in $\text{DMSO-}d_6$ was identical to that of **7a** and **7b**. [Compare: Weiss, K.; Beernink, G.; Dötz, F.; Birkner, A.; Müllen, K.; Wöll, C. H. *Angew. Chem. Int. Ed.* **1999**, *38*, 3748-3752.]

Moreover, both **3a** ($\text{R} = \text{methyl}$) and **3b** ($\text{R} = n\text{-hexyl}$) formed the corresponding indenofluorenes (**7a** and **7b**) upon oxidative cyclodehydrogenation as judged by the similarity of their $^1\text{H}/^{13}\text{C}$ NMR spectra (Figure 1A-1C) and further confirmed by mass spectrometry.

The transformation in eq 1 can be carried out using a variety of 1-e^- oxidants such as $\text{NO}^+\text{SbCl}_6^-$,⁹ $\text{PhI}(\text{OCOCF}_3)_2$,¹⁰ DDQ-TFA ,¹¹ and FeCl_3 as well as electrochemical oxidation.

Scheme 2. Postulated mechanism for the formation of **7**.



The oxidative transformation in eq 1 can be reconciled according to an ECECC mechanism (Scheme 2)¹² based on the spectroscopic and structural data. Thus, one electron oxidation of **3** generates its radical cation where a single charge is stabilized via quinoidal distortion in such a way that the radical character is largest at the *p*-carbon of the anisyl group (see **I₁**).¹³ The radical cation **I₁** undergoes an intramolecular C-C bond formation to yield a distonic radical cation (**I₂**).¹⁴ It is the distonic nature of this rearranged radical cation which facilitates the removal of a second electron at a much lower potential,¹⁵ and leads to the formation of a dication (**I₃**). The loss of a proton and an alkyl group produces the fluorene derivative (**I₅**), which in turn undergoes a similar sequence of ECECC events to produce indeno[1,2-*b*]fluorene **7**. Note that indeno[1,2-*b*]fluorene **7** does

not suffer further oxidative transformations owing to the fact that it undergoes oxidation ($E_{\text{ox}} = 1.18$ V vs. SCE) at a relatively low potential to its cation radical which is stable under the reaction conditions. [See Figures 2 and 3 for a cyclic voltammogram and the cation radical spectrum of **7**, respectively.]

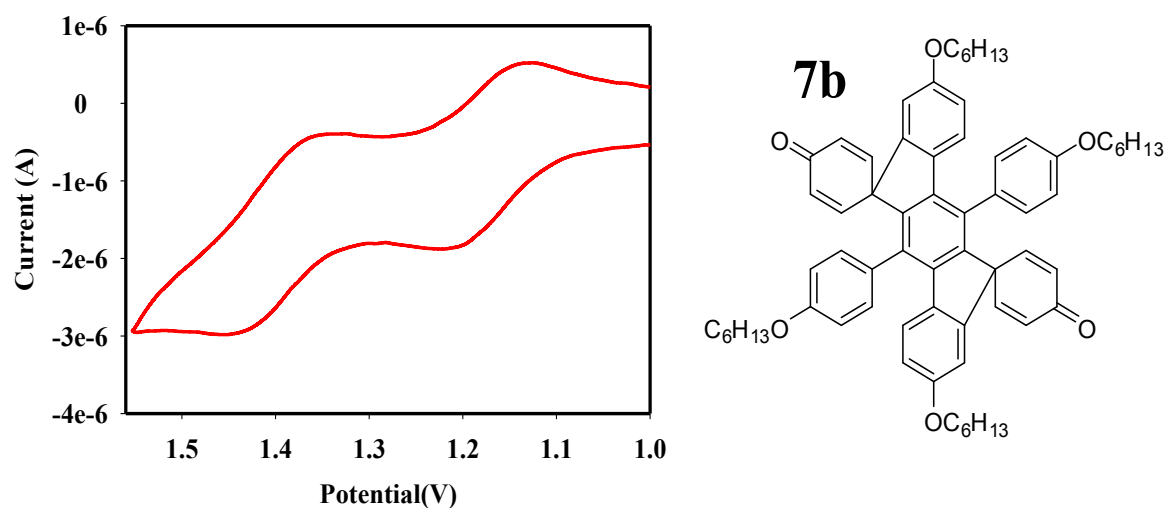


Figure 2. Cyclic voltammogram of indenofluorene **7b** in CH_2Cl_2 containing 0.1 M $n\text{-Bu}_4\text{NPF}_6$ (as the supporting electrolyte) at a scan rate of 100 mV s^{-1} . The E_{ox} values of **7b** (i.e. $E_{\text{ox}1} = 1.18$ and $E_{\text{ox}2} = 1.41$ V vs. SCE) were referenced with ferrocene ($E_{\text{ox}} = 0.45$ V vs. SCE) as an added internal standard.

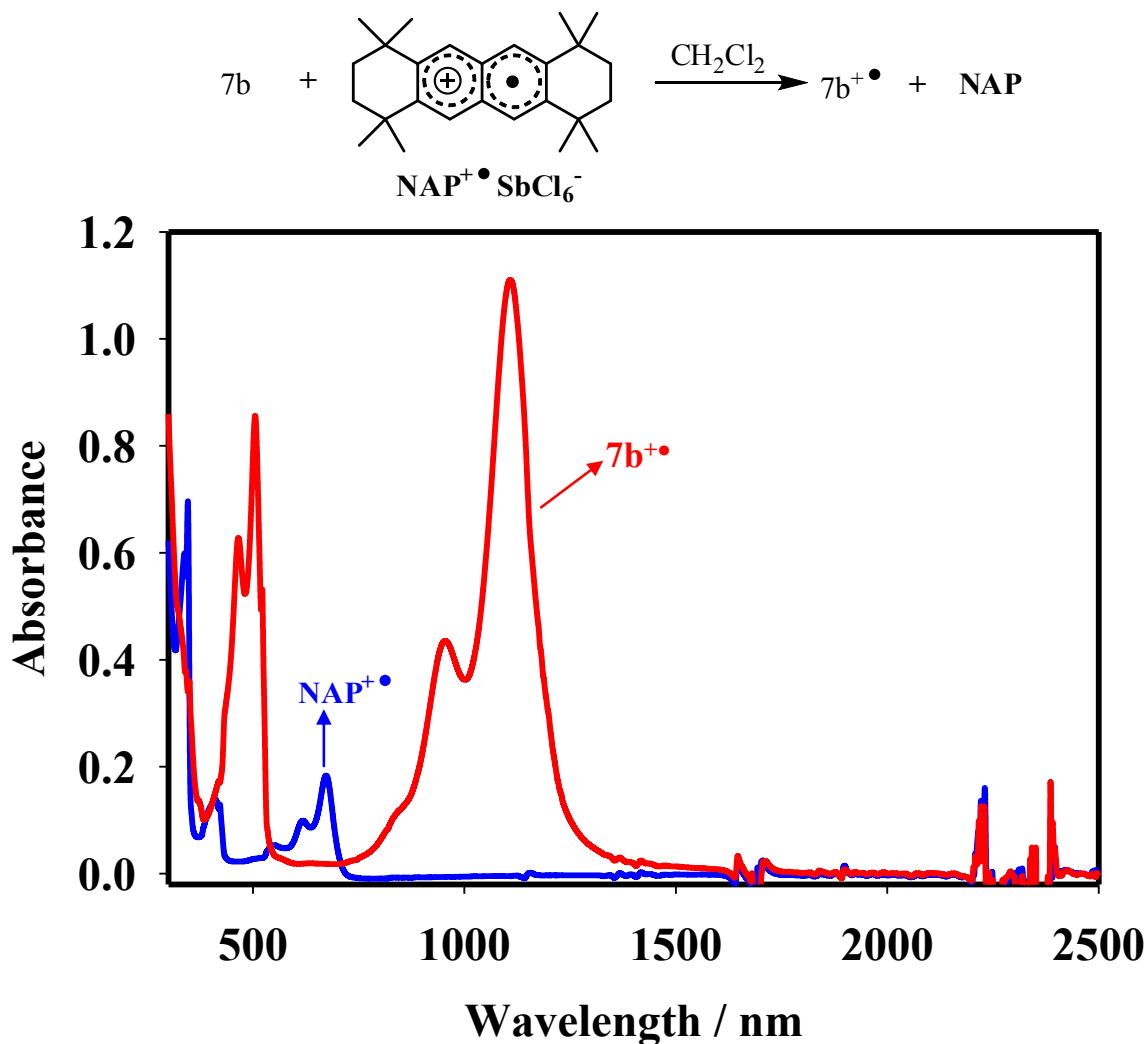
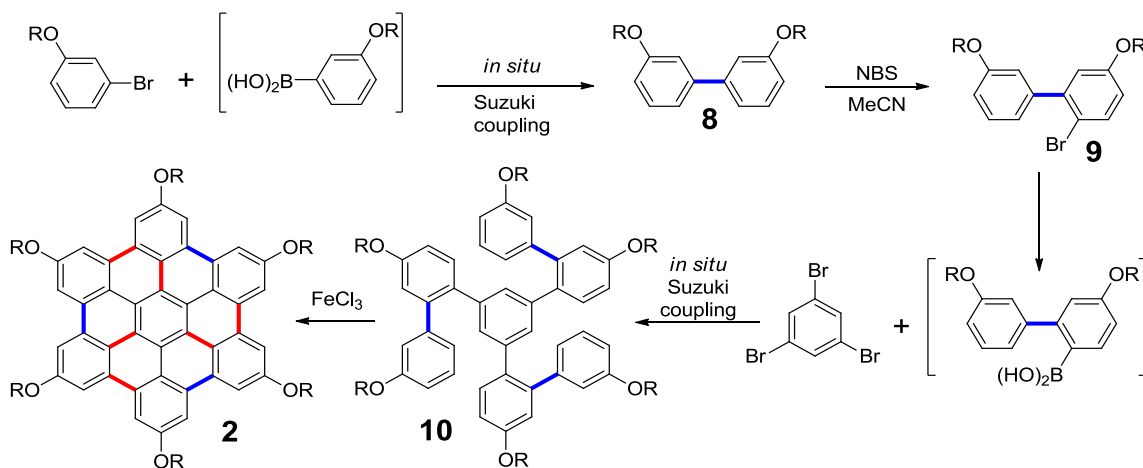


Figure 3. UV-vis-NIR absorption spectrum of the cation radical of indenofluorene **7b** ($7b^{\bullet+}$, $\lambda_{\text{max}} = 1108, 952, 504,$ and 466 nm; $\epsilon_{1108} = 44,300 \text{ M}^{-1} \text{ cm}^{-1}$) in CH_2Cl_2 generated using a hindered naphthalene cation radical ($\text{NAP}^{\bullet+}$, $E_{\text{red}} = 1.34$ V vs. SCE, $\lambda_{\text{max}} = 672, 616, 503,$ and 396 nm; $\epsilon_{672} = 9300 \text{ M}^{-1} \text{ cm}^{-1}$).

From the mechanistic considerations in Scheme 2, it was clear that an alternative C-C bond forming sequence was desired to access HBC **2**. It was conjectured that if some of the C-C bonds were pre-formed in a new precursor of HBC **2**, it should be feasible to produce **2** rather than indenofluorene **7**.

Accordingly, we chose 1,3,5-tris(5,5'-di-*n*-hexyloxy-2-biphenyl)-benzene (**10**) as a precursor to HBC **2**, which was obtained by a one-pot Suzuki coupling¹⁶ of 3 equiv of boronic acid, derived from 5,5'-dihexyloxy-2-bromobiphenyl (**9**) with 1 equiv of 1,3,5-tribromobenzene in the presence of Pd(0) catalyst. The desired brombiphenyl **9**, in turn, was obtained by a one-pot Suzuki coupling of 3-bromohexyloxybenzene followed by a bromination using NBS in acetonitrile in excellent yield (see Scheme 3A). Indeed, when **10** (R = *n*-hexyl) was subjected to an oxidative cyclodehydrogenation using FeCl₃ in a mixture of dichloromethane-nitromethane (3:1), it yielded a readily soluble hexahexyloxy-HBC **2** as a yellow-orange solid in nearly quantitative yield (see Scheme 3A).

Scheme 3A. Synthesis of hexaalkoxy HBC **2** and its precursor **10**.



The molecular structure of HBC **2** was established by the simplicity of its ¹H/¹³C NMR spectra (Figure 4)¹⁷ and was further confirmed by MALDI mass spectrometry (see Figure 5). Note that a calculated isotope distribution for mass ion of HBC **2** matches the prediction quite well (see Figure 5).

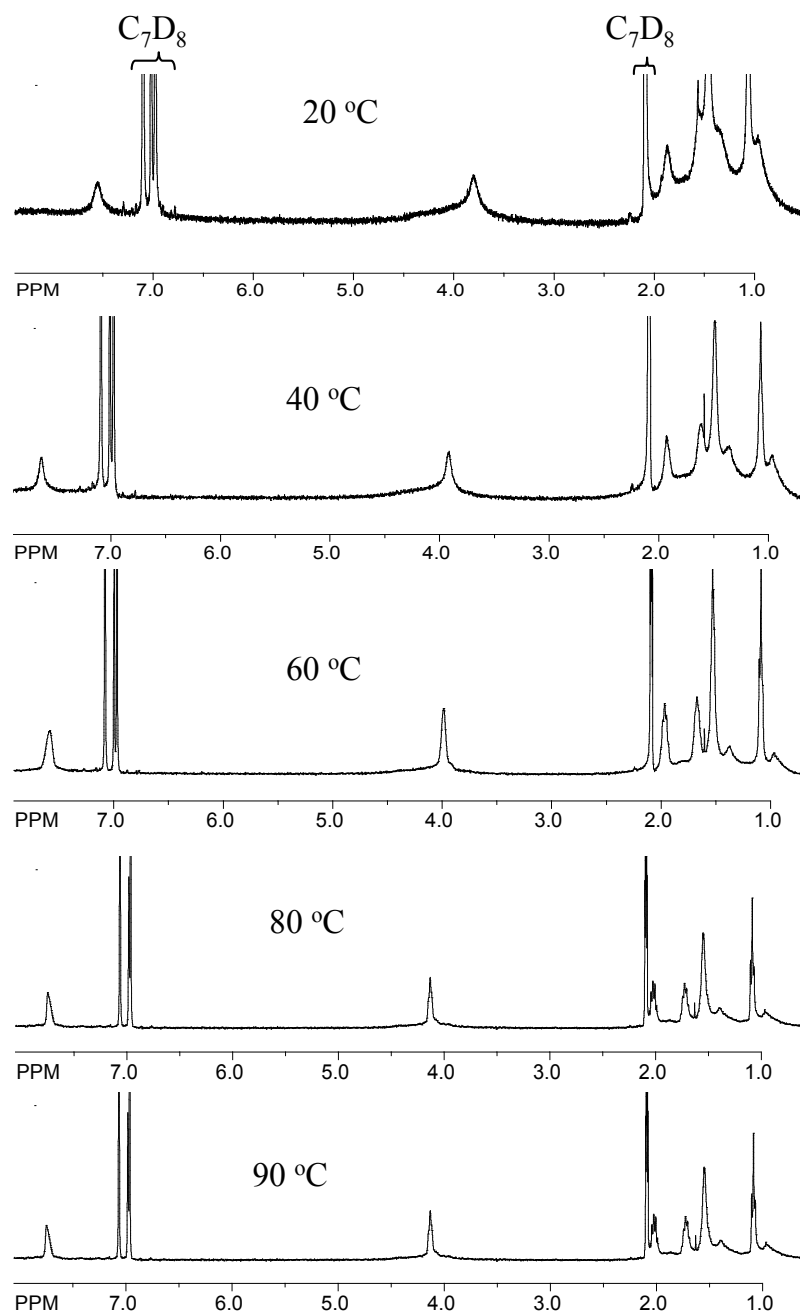


Figure 4A. Variable temperature ^1H NMR spectra of HBC 2 in toluene- d_8 obtained at 20, 40, 60, 80, and 90 °C. Temperatures are indicated on the spectra.

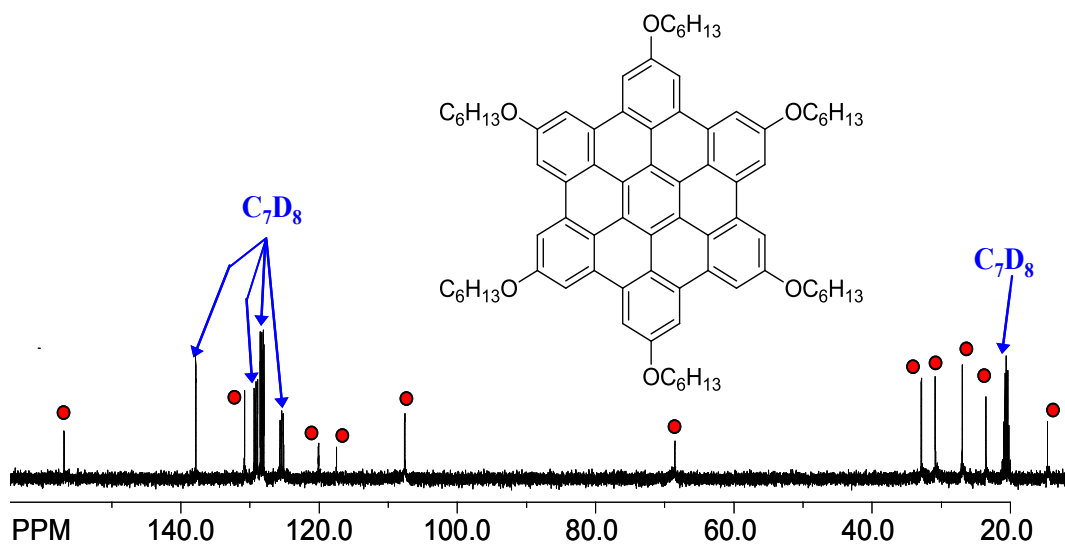


Figure 4B. ^{13}C NMR spectrum of **2** in CDCl_3 at $60\text{ }^\circ\text{C}$ was rather broad and therefore the spectrum was recorded in toluene- d_8 at $90\text{ }^\circ\text{C}$. Also note that the peaks belonging to HBC **2** are labeled with red circles.

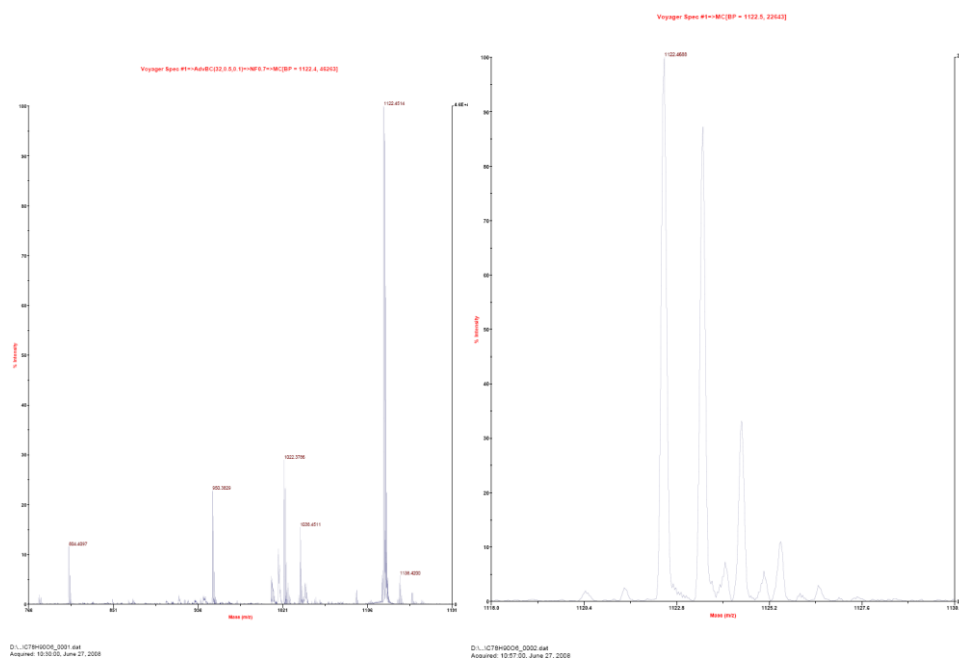
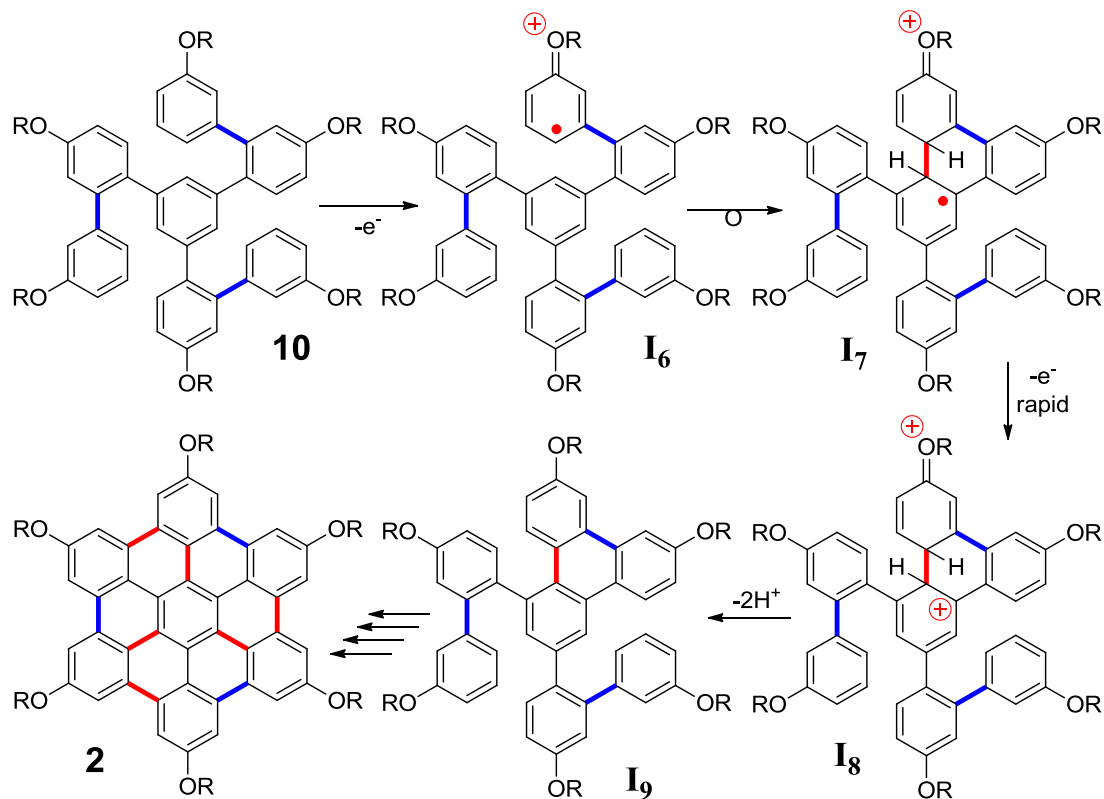


Figure 5. The MALDI mass spectra of HBC **2** (top) and the calculated isotope distribution for the mass ion of HBC **2** (bottom).

As detailed in Scheme 3B, the mechanism for conversion of **10** to HBC **2** simply followed a standard ECE mechanism applicable to other (oxidative) biaryl

syntheses.^{12,14} Thus, a coupling of an anisyl-type cation radical (**I₆**) with the central benzene ring produces a distonic cation radical (**I₇**) which undergoes a ready loss of an electron (**I₈**) followed by two proton (**I₉**) to form a biaryl-type bond. Multiple repetitions of the ECE sequence finally produce HBC **2** (Scheme 3B).

Scheme 3B. An electron transfer mechanism for the formation HBC **2** from precursor **10**.



In summary, we have demonstrated that the oxidative cyclodehydrogenation of *hexakis*(4-alkoxyphenyl)benzenes (**3**) produce indenofluorenes **7** in quantitative yields rather than HBC **2**, as confirmed by X-ray crystallography. This finding led us to design an alternative (simple) synthesis of HBC **2** from an easily synthesized 1,3,5-tris(dialkoxybiphenyl)benzene **10**. The ready availability of hexaalkoxy HBC **2** should spur theoretical and experimental interest in the exploration of its materials' properties.

Experimental

General Experimental Methods and Materials

Dicobaltoctacarbonyl, *p*-iodophenol, 1-bromohexane, ferric chloride, nitromethane, anhydrous benzene, 1,8-diazobicyclo[5,4,0]undec-7-ene (DBU), CuI, trimethylsilylacetylene, *n*-BuLi, trimethylborate, ethanol, sodium carbonate, *tetrakis*(triphenylphosphine)palladium(0), acetonitrile, *N*-bromosuccinamide, *bis*(triphenyl-phosphine)palladium dichloride and anhydrous dioxane were commercially available and were used without further purification.

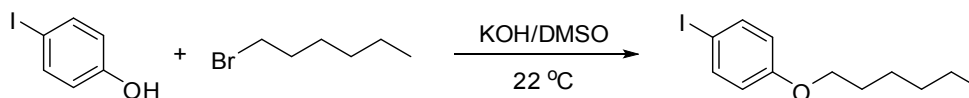
Anhydrous tetrahydrofuran (THF) was prepared by refluxing the commercial tetrahydrofuran over lithium tetrahydroaluminate under an argon atmosphere for 24 hours followed by distillation. It was stored under an argon atmosphere in a Schlenk flask equipped with a Teflon valve fitted with Viton *O*-rings. Dichloromethane was repeatedly stirred with fresh aliquots of conc. sulfuric acid (~10 % by volume) until the acid layer remained colorless. After separation it was washed successively with water, aqueous sodium bicarbonate, water, and saturated aqueous sodium chloride and dried over anhydrous calcium chloride. The dichloromethane was distilled twice from P₂O₅ under an argon atmosphere and stored in a Schlenk flask equipped with a Teflon valve fitted with Viton *O*-rings. The hexanes and toluene were distilled from P₂O₅ under an argon atmosphere and then refluxed over calcium hydride (~12 hrs). After distillation from CaH₂, the solvents were stored in Schlenk flasks under argon atmosphere.

Cyclic Voltammetry

Cyclic voltammetry (CV) was performed on an Electrochemical Analyser. The CV cell was of an air-tight design with high vacuum Teflon valves and Viton O-rings seals to allow an inert atmosphere to be maintained without contamination by grease. The working electrode consisted of an adjustable platinum disk embedded in a glass seal to allow periodic polishing (with a fine emery cloth) without changing the surface area ($\sim 1 \text{ mm}^2$) significantly. The reference SCE electrode (saturated calomel electrode) and its salt bridge were separated from the catholyte by a sintered glass frit. The counter electrode consisted of platinum gauze that was separated from the working electrode by $\sim 3 \text{ mm}$. The CV measurements were carried out in a solution of 0.1 M supporting electrolyte (tetra-*n*-butylammonium hexafluorophosphate, TBAH) and 2 mmol substrate in dichloromethane and under an argon atmosphere. All cyclic voltammograms were recorded at a sweep rate of 100 mV sec^{-1} , unless otherwise specified and were IR compensated. The oxidation potentials ($E_{1/2}$) were referenced to SCE which was calibrated with added (equimolar) ferrocene ($E_{1/2} = 0.45 \text{ V vs. SCE}$). The $E_{1/2}$ values were calculated by taking the average of anodic and cathodic peak potentials in the reversible cyclic voltammograms.

Synthesis of various compounds in Schemes 1-3

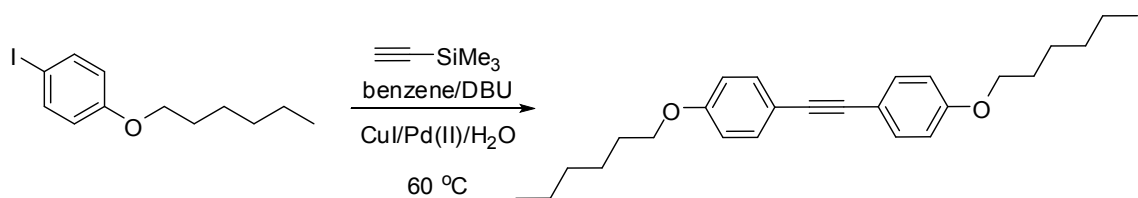
4-(Hexyloxy)iodobenzene



A suspension of potassium hydroxide (4.4 g, 80 mmol) in DMSO (80 mL) was treated with *p*-iodophenol (4.4 g, 20 mmol) and 1-bromohexane (2.8 mL, 20 mmol). The

resulting mixture was stirred vigorously at room temperature for 30 minutes and then quenched with water. The product was extracted with dichloromethane (2 x 25 mL), washed with water (3 x 25 mL), dried over anhydrous magnesium sulfate and evaporated to produce a pale yellow oil. Yield (5.4 g, 90 %) ; ^1H NMR (CDCl_3) δ : 0.90 (t, 3H), 1.33 (m, 4H), 1.44 (m, 2H), 1.76 (qn, 2H), 3.90 (t, 2H), 6.66 (d, $J = 9.0$ Hz, 2H), 7.53 (d, $J = 9.0$ Hz, 2H). ^{13}C NMR (CDCl_3) δ : 14.24, 22.80, 25.88, 29.32, 31.77, 68.33, 82.59, 117.14, 138.35, 159.22.

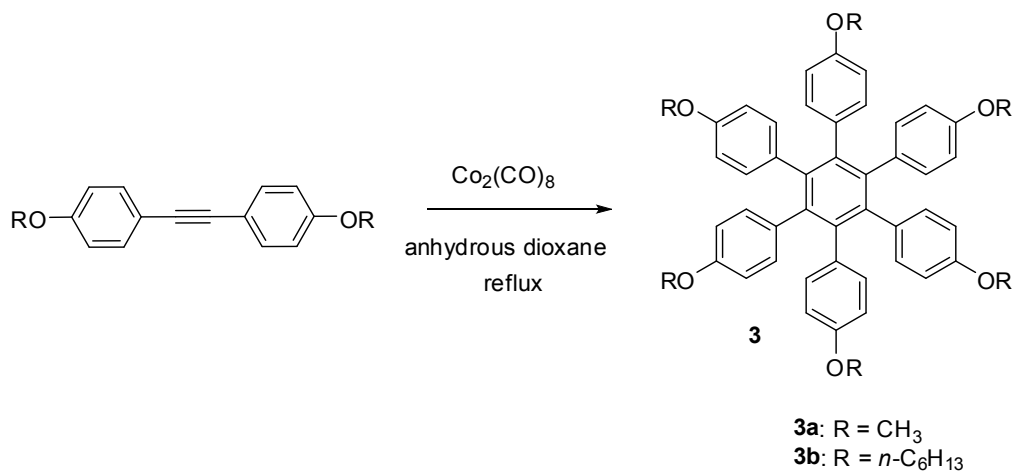
Bis-(4-hexyloxyphenyl)acetylene



4-(Hexyloxy)iodobenzene (8.4 g, 27.6 mmol) was dissolved in anhydrous benzene (140 mL) in a Schlenk flask under argon atmosphere. DBU (25 mL, 166 mmol), CuI (0.26 g, 1.4 mmol, 5% mol) and Pd(PPh_3) $_2\text{Cl}_2$ (0.86 g, 0.83 mmol, 3% mol) were added to the flask, and it was evacuated and refilled with argon three times. To this mixture was then added distilled water (0.2 mL, 11 mmol, 40 mol %) followed by trimethylsilylacetylene (1.35 mL, 13.8 mmol). The resulting mixture was first stirred for 1 hour at room temperature, and then at 60 °C for 24 hours. The solvent was evaporated under reduced pressure and the dark-colored residue was extracted with dichloromethane (2 x 50 mL). The dichloromethane layer was dried with anhydrous magnesium sulfate, filtered, and evaporated to afford a dark colored syrup. Purification of the product by column chromatography using hexanes as eluent afforded a white solid. Yield (2.8 g, 56 %); mp 85-86 °C ; ^1H NMR (CDCl_3) δ : 0.91 (t, 6H), 1.34 (m, 8H), 1.45 (m, 4H), 1.78 (qn, 4H),

3.95 (t, 4H), 6.85 (d, $J = 9.1$ Hz, 4H), 7.42 (d, $J = 9.1$ Hz, 4H). ^{13}C NMR (CDCl_3) δ : 14.26, 22.82, 25.92, 29.39, 31.79, 68.27, 88.15, 114.69, 115.69, 133.04, 159.17.

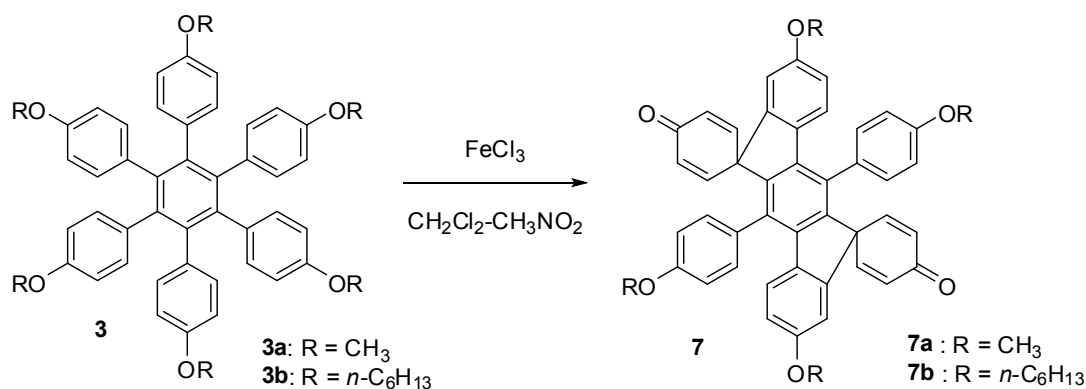
Preparation of hexakis(4-alkoxyphenyl)benzenes by trimerization of bis-(4-alkoxyphenyl)-acetylenes



For example, *bis*-(4-hexyloxyphenyl)acetylene (1.93 g, 5.1 mmol) was dissolved in anhydrous dioxane (50 mL) in an oven dried Schlenk flask under an argon atmosphere and the flask was evacuated and filled with argon repeatedly (3x). Then, $\text{Co}_2(\text{CO})_8$ (80 mg) was added to the flask under an argon atmosphere and the flask was evacuated and filled with argon again (3 x). The resulting mixture was refluxed for 14 h and the dioxane was evaporated. The resulting residue was dissolved in dichloromethane and filtered through a short pad of silica gel. Evaporation of the solvent afforded a dark colored solid which was recrystallized using a mixture of dichloromethane/methanol (1:1) to yield *hexakis*(4-hexyloxyphenyl)benzene (**3b**) as a white solid. Yield (1.1 g, 57 %); mp 102-103 °C ; ^1H NMR (CDCl_3) δ : 0.88 (t, 18H), 1.33 (m, 36H), 1.66 (qn, 12H), 3.75 (t, 12H), 6.39 (d, $J = 8.6$ Hz, 12H), 6.64 (d, $J = 8.6$ Hz, 12H). ^{13}C NMR (CDCl_3) δ : 14.24, 22.79, 25.89, 29.43, 31.83, 67.85, 112.99, 132.64, 133.68, 140.42, 156.41.

Hexakis(4-methoxyphenyl)benzene (**3a**) was prepared by an identical procedure using *bis*-(4-methoxyphenyl)acetylene (3 g, 12.6 mmol) as above. Yield (2.75 g, 92 %); mp 378 °C (decomp.) ([lit^{S1} mp 390 °C (decomp.)]; ¹H NMR (CDCl₃) δ: 3.63 (s, 18H), 6.41 (d, *J* = 8.4 Hz, 12H), 6.67 (d, *J* = 8.4 Hz, 12H). ¹³C NMR (CDCl₃) δ: 55.13, 112.36, 132.64, 133.77, 140.46, 156.94. [^{S1}Kobayashi, K.; Shirasaka, T.; Sato, A.; Horn, E.; Furukawa, N. *Angew. Chem. Int. Ed.* **1999**, *38*, 3483-3486.]

Oxidative cyclodehydrogenation of hexakis(4-alkoxyphenyl)benzenes (**3a** and **3b**) to indenofluorenes **7a** and **7b**

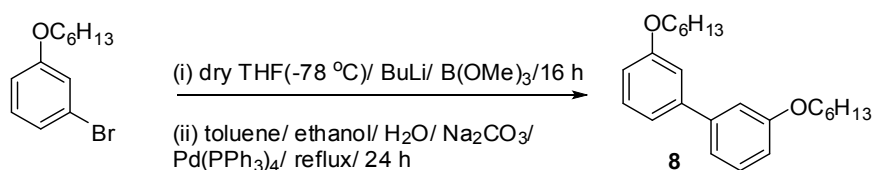


For example, *hexakis*(4-hexyloxyphenyl)benzene (0.5 g, 0.44 mmol) was dissolved in dry dichloromethane (30 mL) and cooled to ~0 °C in an ice bath under an argon atmosphere. A solution of ferric chloride (1.43 g, 8.82 mmol) in nitromethane (20 mL) was added dropwise into the above mixture. When the addition was completed, the ice bath was removed and the resulting mixture was stirred for 1 h at room temperature. [Note that throughout the reaction period, a slow stream of argon was passed through the reaction mixture to remove gaseous HCl formed in the reaction.] The reaction was quenched by addition of methanol (30 mL) followed by water (30 mL). The organic layer was separated and the aqueous layer was extracted with dichloromethane (3 x 25 mL). The combined dichloromethane extracts were dried over anhydrous MgSO₄, filtered and

evaporated to produce a pale yellow solid. Recrystallization of the solid by 1:1 dichloromethane/methanol mixture afforded **7b** as a pale yellow solid. Yield (0.4 g, 94 %); mp 228-230 °C; ¹H NMR (CDCl₃) δ: 0.86 (t, 6H), 0.95 (t, 6H), 1.28 (m, 8H), 1.39 (m, 8H), 1.51 (m, 8H), 1.68 (qn, 4H), 1.87 (qn, 4H), 3.79 (t, 4H), 4.00 (t, 4H), 6.13 (d, *J* = 9.7 Hz, 4H), 6.25 (d, *J* = 8.7 Hz, 2H), 6.53 (m, 8H), 6.88 (d, *J* = 8.3 Hz, 4H), 7.15 (d, *J* = 8.3 Hz, 4H). ¹³C NMR (CDCl₃) δ: 14.16, 14.28, 22.71, 22.83, 25.77, 25.93, 29.25, 29.46, 31.66, 31.88, 56.74, 68.41, 110.12, 114.36, 115.29, 124.55, 128.37, 129.05, 130.92, 134.13, 134.89, 139.06, 142.44, 144.23, 150.05, 159.21, 159.63, 186.13.

Similarly, *hexakis*(4-methoxyphenyl)benzene, afforded **7a** in nearly quantitative yield. mp 399 -403 °C (decomp.); ¹H NMR (CDCl₃) δ: 3.68 (s, 6H), 3.88 (s, 6H), 6.14 (d, *J* = 9.4 Hz, 4H), 6.27 (d, *J* = 8.9 Hz, 2H), 6.55 (m, 8H), 6.90 (d, *J* = 8.4 Hz, 4H), 7.18 (d, *J* = 8.4 Hz, 4H). ¹³C NMR (CDCl₃) δ: 55.65, 56.77, 109.42, 113.85, 115.12, 124.61, 128.49, 129.17, 131.02, 134.32, 134.93, 139.10, 142.46, 144.36, 149.96, 159.69, 160.12, 186.15.

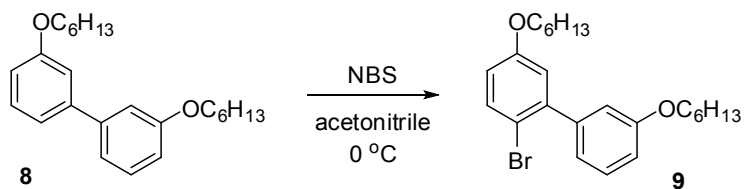
Preparation of 3,3'-*n*-hexyloxybiphenyl (**8**) from 3-*n*-hexyloxybromobenzene



One-pot Suzuki coupling was performed following a slightly modified literature procedure (Anderson, N.G.; Maddaford, S. P.; Keay, B.A. *J. Org. Chem.* **1996**, *61*, 9556-9559). To a solution of 3-hexyloxy-bromobenzene (8.0 g, 31.1 mmol) in dry THF (35 mL) at -78 °C was added *n*-BuLi (6.2 mL of 2.5 M in hexane, 15.6 mmol) followed by trimethylborate (5.2 mL, 47 mmol) under an argon atmosphere. The resulting mixture

was stirred for 4 h at $-78\text{ }^{\circ}\text{C}$ and the stirring mixture was allowed to warm to room temperature, gradually, during a course of 12 h. To the resulting solution at room temperature were added anhydrous toluene (35 mL), ethanol (35 mL), water (14 mL), sodium carbonate (4.9 g, 47 mmol) and $\text{Pd}(\text{PPh}_3)_4$ (0.34 g, 0.3 mmol) under an argon atmosphere and the mixture was refluxed for 24 h. The reaction mixture was cooled to room temperature and diluted with water (50 mL). The aqueous mixture was extracted with dichloromethane (3 x 50 mL), organic layers were dried over anhydrous MgSO_4 and evaporated to afford a pale yellow liquid which was purified by column chromatography using hexanes as the eluent to afford **8** as a colorless oil. Yield (3.8 g, 69 %); ^1H NMR (CDCl_3) δ : 0.91 (t, 6H), 1.35 (m, 8H), 1.47 (m, 4H), 1.80 (qn, 4H), 4.00 (t, 4H), 6.88 (dd, $J = 2.5$ and 8.2 Hz, 2H), 7.14 (m, 4H), 7.32 (t, 2H). ^{13}C NMR (CDCl_3) δ : 14.27, 22.83, 25.97, 29.51, 31.82, 68.25, 113.54, 113.71, 119.69, 129.84, 142.82, 159.65.

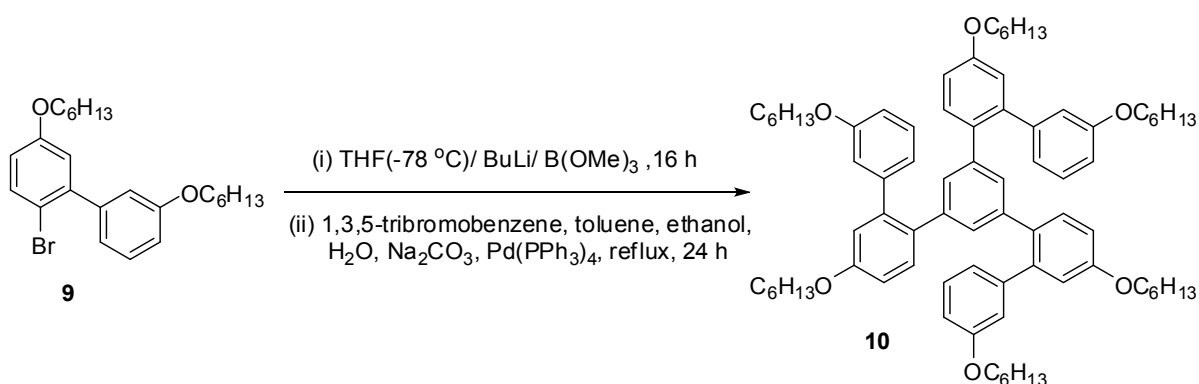
Preparation of 6-bromo-3,3'-hexyloxybiphenyl (**9**)



3,3'-Hexyloxybiphenyl (3.6 g, 10.2 mmol) was dissolved in acetonitrile (40 mL) and cooled to $0\text{ }^{\circ}\text{C}$. A solution of *N*-bromosuccinimide (1.8 g, 10.2 mmol) in acetonitrile (40 mL) was added drop-wise to the above solution over a period of 1 h and the resulting mixture was stirred for an additional 30 min. The reaction mixture was diluted with water (50 mL) and extracted with dichloromethane (3 x 50 mL). The dichloromethane layer was dried over anhydrous MgSO_4 and evaporated to afford a pale yellow liquid in nearly

quantitative yield which contained mostly mono bromo-biphenyl **9** together with a small quantity of (~5%) the corresponding di-bromo derivative. This material was used in the next step without further purification. ^1H NMR (CDCl_3) δ : 0.90 (m, 6H), 1.33 (m, 8H), 1.45 (m, 4H), 1.78 (m, 4H), 3.94 (t, 2H), 3.99 (t, 2H), 6.76 (dd, $J = 3.1$ and 8.7 Hz, 1H), 6.92 (m, 4H), 7.32 (t, 1H), 7.51 (d, $J = 8.7$ Hz, 1H). ^{13}C NMR (CDCl_3) δ : 14.25, 14.26, 22.80, 22.82, 25.88, 25.95, 29.35, 29.46, 31.75, 31.81, 68.25, 68.54, 112.87, 114.10, 115.52, 115.65, 117.34, 121.71, 129.12, 133.82, 142.65, 143.44, 158.51, 158.87.

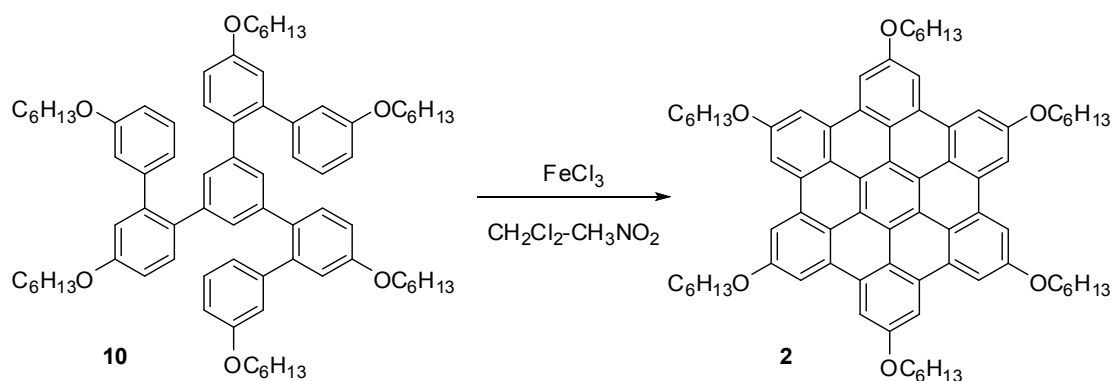
Preparation of **10**



To a solution of 6-bromo-3,3'-hexyloxybiphenyl (3.3 g, 7.6 mmol) in dry THF (30 mL) at $-78\text{ }^\circ\text{C}$ was added *n*-BuLi (3.1 mL, 2.5 M, 7.7 mmol) followed by trimethylborate (1.3 mL, 11.4 mmol) under an argon atmosphere. The resulting mixture was stirred for 4 h at $-78\text{ }^\circ\text{C}$ and it was allowed to warm to room temperature during a 12 h period. To this mixture at room temperature were then added 1,3,5-tribromobenzene (0.6 g, 1.9 mmol), toluene (30 mL), ethanol (30 mL), water (12 mL), sodium carbonate (1.2 g, 11.4 mmol) and $\text{Pd}(\text{PPh}_3)_4$ (0.09 g, 0.07 mmol) under an argon atmosphere and the resulting mixture was refluxed for 24 h. The reaction mixture was cooled to room temperature and diluted

with water (50 mL) and extracted with dichloromethane. The combined dichloromethane extracts were dried over anhydrous MgSO_4 and evaporated to yield pale yellow oil which was purified by column chromatography (hexane/ ethyl acetate) to afford **10** as colorless oil. Yield (2.0 g, 93 %); ^1H NMR (CDCl_3) δ : 0.89 (m, 18H), 1.35 (m, 36H), 1.74 (m, 12H), 3.83 (t, 6H), 3.97 (t, 6H), 6.51 (d, $J = 7.7$ Hz, 3H), 6.67 (m, 6H), 6.77 (m, 9H), 6.89 (d, 3H), 7.15 (t, 3H). ^{13}C NMR (CDCl_3) δ : 14.43, 23.03, 26.16, 29.63, 31.93, 68.35, 113.06, 113.70, 116.33, 116.49, 123.14, 129.12, 129.13, 131.87, 133.39, 140.57, 141.85, 143.44, 158.61, 159.27.

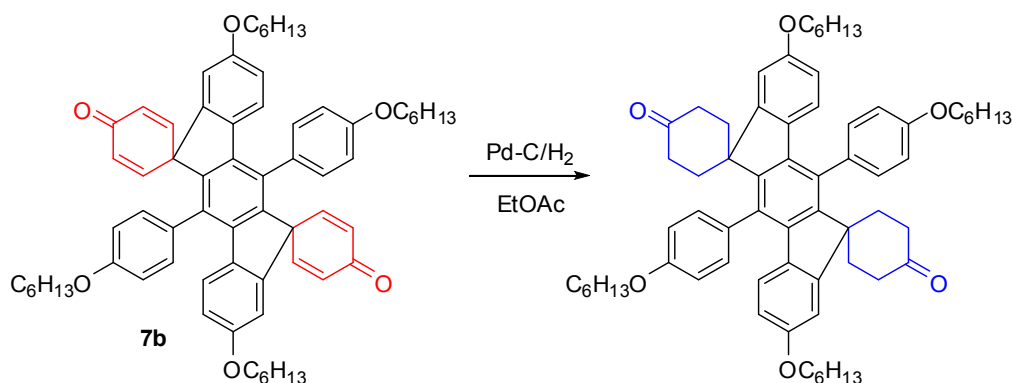
Preparation of hexakis-*n*-hexyloxy-hexa-peri-hexabenzocoronene **2**



1,3,5-Tris(5,5'-dihexyloxy-2-biphenyl)benzene (**10**) (1.0 g, 0.88 mmol) was dissolved in dry dichloromethane (30 mL) and cooled to 0°C in an ice/acetone bath under an argon atmosphere. A solution of ferric chloride (2.86 g, 17.6 mmol) in nitromethane (20 mL) was added drop-wise to the above solution at 0°C and the mixture was stirred for 1 h at room temperature. During the course of the reaction, a constant stream of argon was passed through the mixture to remove gaseous HCl formed in the reaction. To the resulting mixture was added methanol (30 mL) followed by water (100 mL) and dichloromethane (30 mL). The dichloromethane layer was separated and dried

over anhydrous MgSO_4 and evaporated to produce a brown solid. The purification of the crude solid by column chromatography using hexanes as eluent afforded HBC **2** as dark orange-red solid. Yield (0.82 g, 82 %); mp 240-250 °C (decomp.) ^1H NMR (CDCl_3) δ : 1.07 (t, 18H), 1.54 (m, 24H), 1.66 (m, 12H), 1.94 (m, 12H), 3.95 (t, 12H), 7.35 (s, 12H). [Note that the spectrum was recoded at 60 °C]. ^{13}C NMR (C_7D_8) δ : 14.63, 23.52, 26.96, 30.84, 32.87, 68.54, 107.63, 117.49, 120.09, 130.79, 156.89. [Note that the spectrum was recoded at 90 °C].

Hydrogenation of cyclohexadienone moieties in indenofluorene **7b** to the cyclohexanones

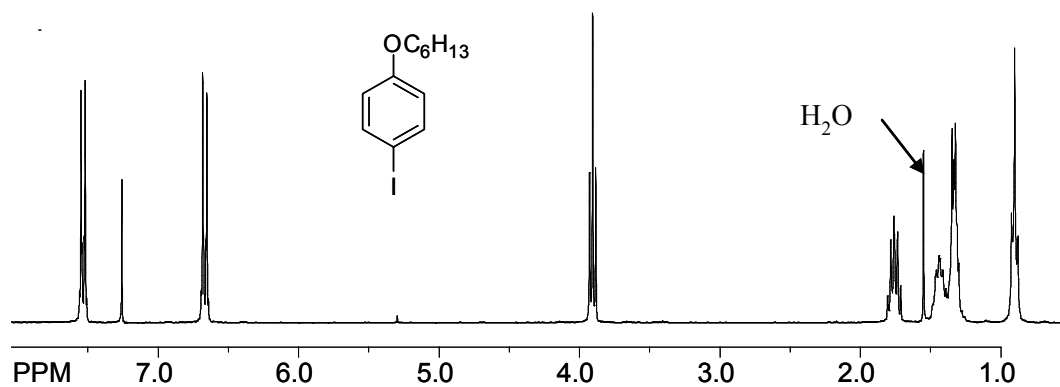


Indeno[1,2-*b*]fluorene **7b** (100 mg, 0.1 mmol) was dissolved in 100 mL ethyl acetate and mixed with 18 mg of 10% Pd on charcoal. The resulting suspension was subjected to a pressure of ~30 psi hydrogen gas for 3 h in a high pressure bottle after which an aliquot showed complete disappearance of **7b** as adjudged by ^1H NMR spectroscopy. The mixture was then passed through a pad of celite and the pad was further washed with dichloromethane (3 x 10 mL). The solvent was evaporated to afford ~100 mg of product which was analyzed by NMR spectroscopy to confirm that cyclohexadienone groups in **7b** were hydrogenated to the corresponding cyclohexanone groups (see structures in the above equation). Mp 187-188 °C; ^1H NMR (CDCl_3) δ : 0.89

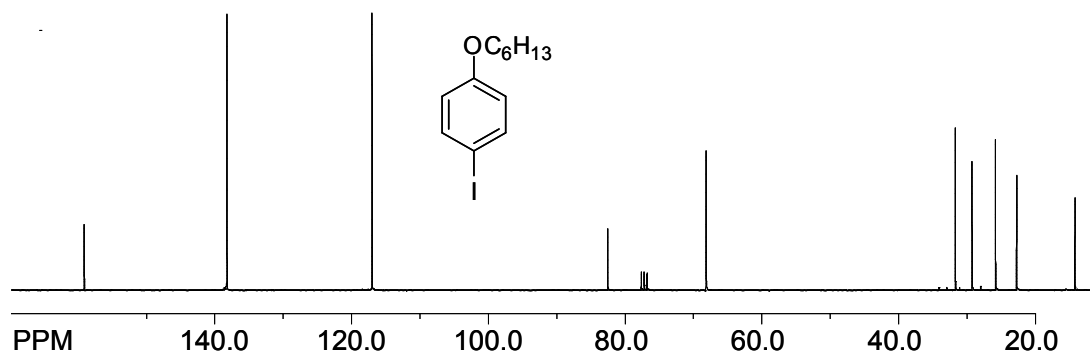
(t, 6H), 0.96 (t, 6H), 1.21-1.58 (m, 20H), 1.56 (sym m, 4H), 1.69-2.02 (m, 16H), 2.53 (m, 4H), 2.82 (m, 4H), 3.86 (t, 4H), 4.09 (t, 4H), 5.81 (d, $J = 8.8$ Hz, 2H), 6.51 (dd, $J = 2.4$ and 8.8 Hz, 2H), 6.88 (d, $J = 2.3$ Hz, 2H), 7.08 (d, $J = 8.7$ Hz, 4H), 7.37 (d, $J = 8.7$ Hz, 4H). ^{13}C NMR (CDCl_3) δ : 14.27, 22.82, 25.85, 25.98, 29.40, 29.47, 31.71, 31.89, 32.23, 37.65, 49.15, 68.33, 68.38, 111.11, 112.04, 115.28, 124.10, 130.83, 131.86, 132.27, 132.71, 137.74, 149.47, 155.87, 158.14, 159.02, 213.83.

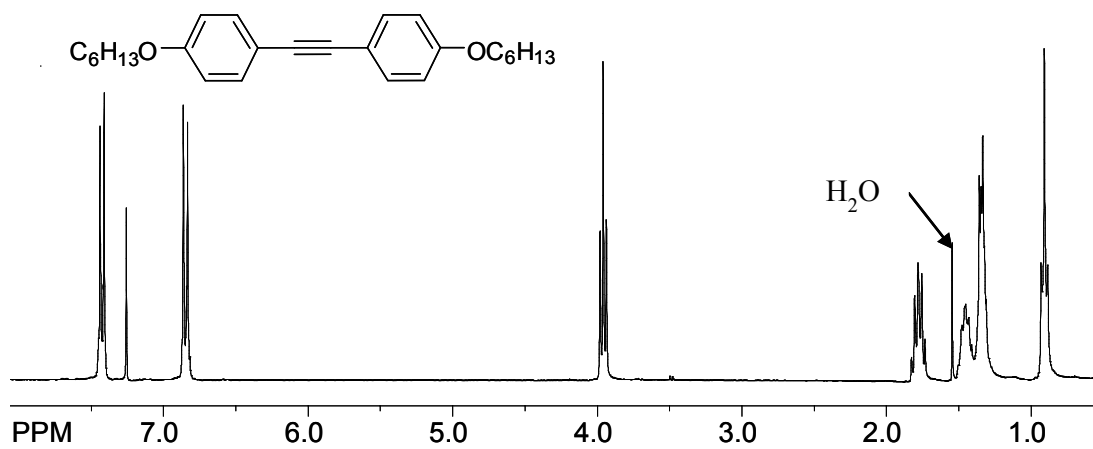
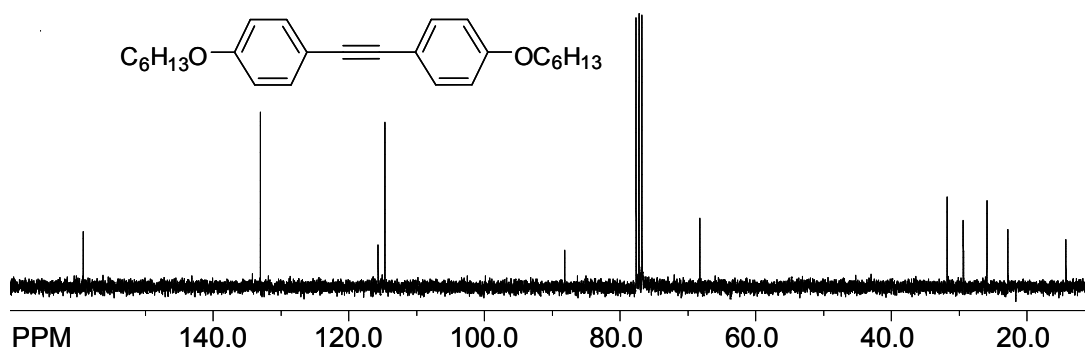
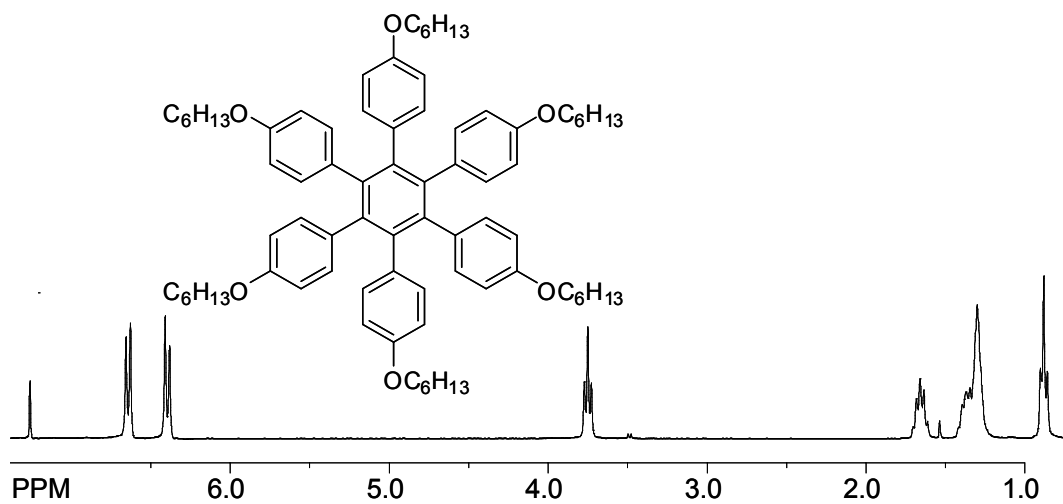
Spectral data for the compounds in Schemes 1-3

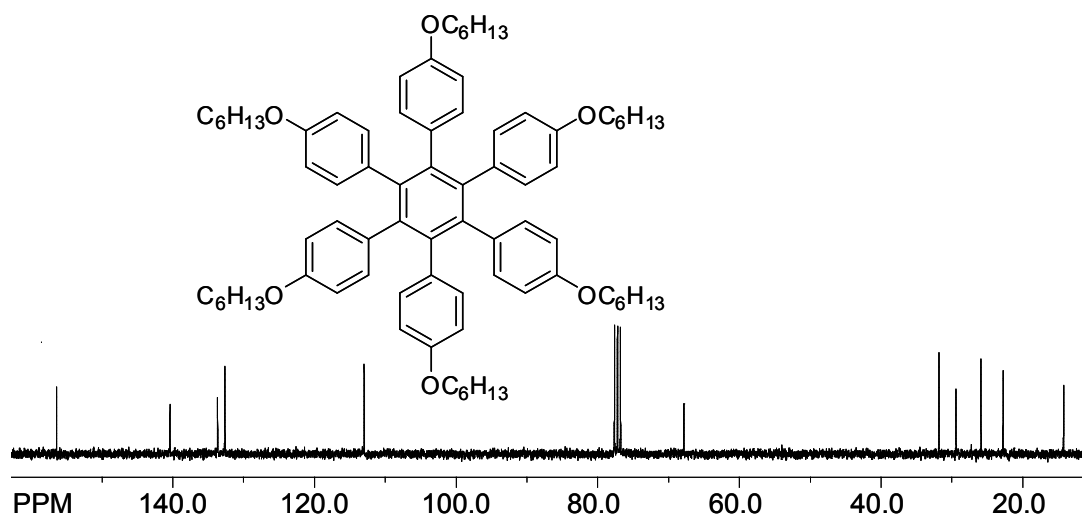
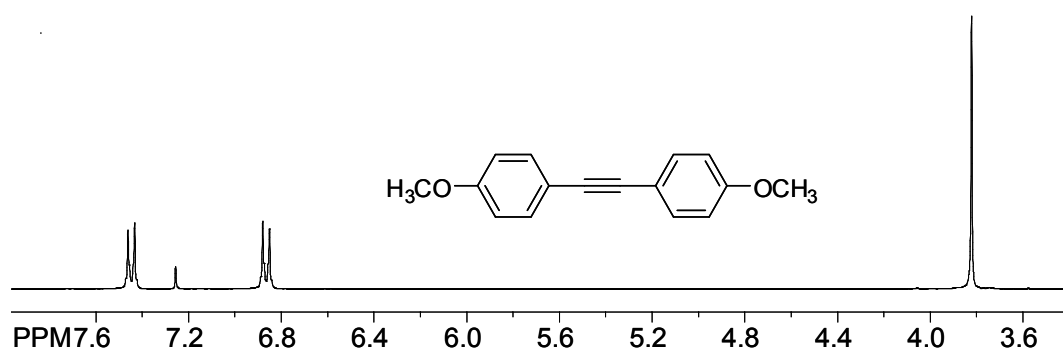
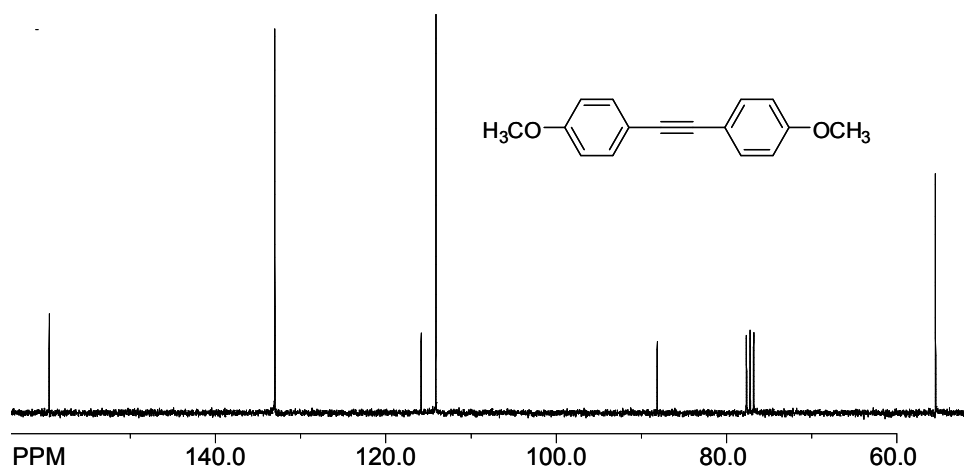
^1H NMR spectrum of 4-(hexyloxy)iodobenzene

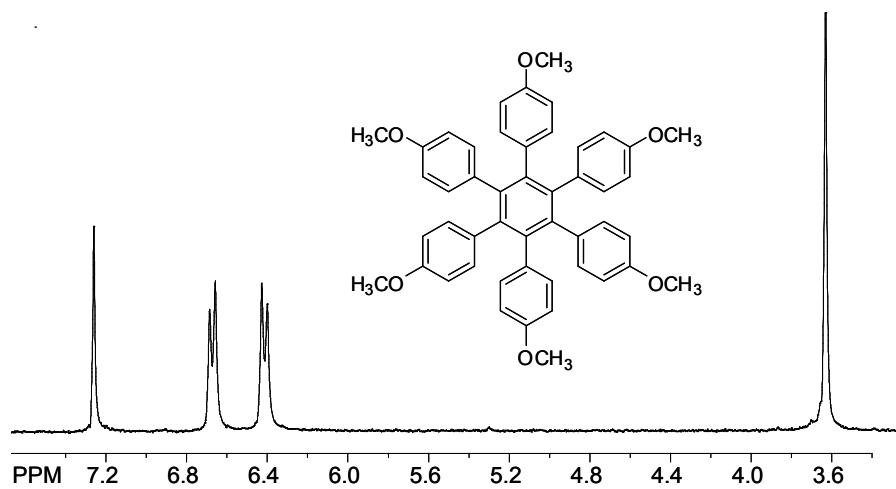
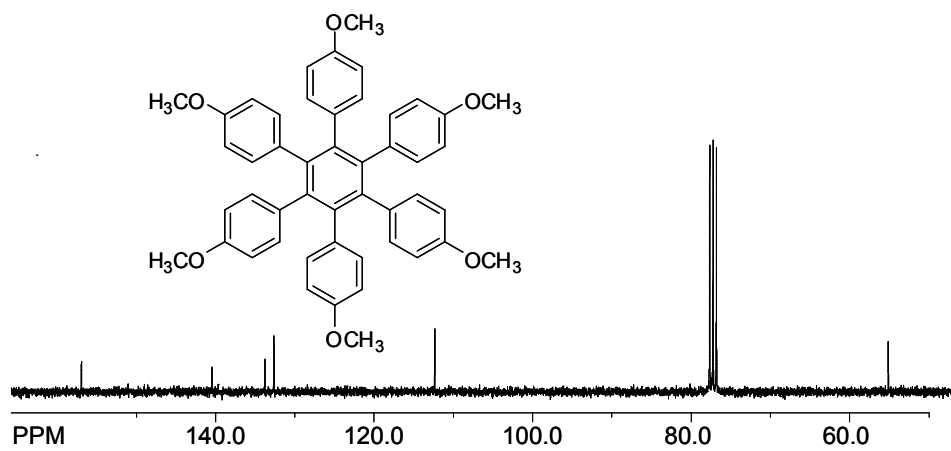


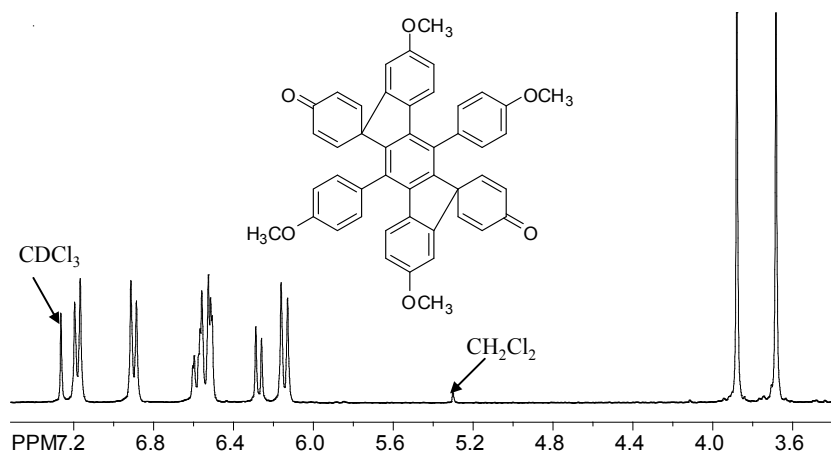
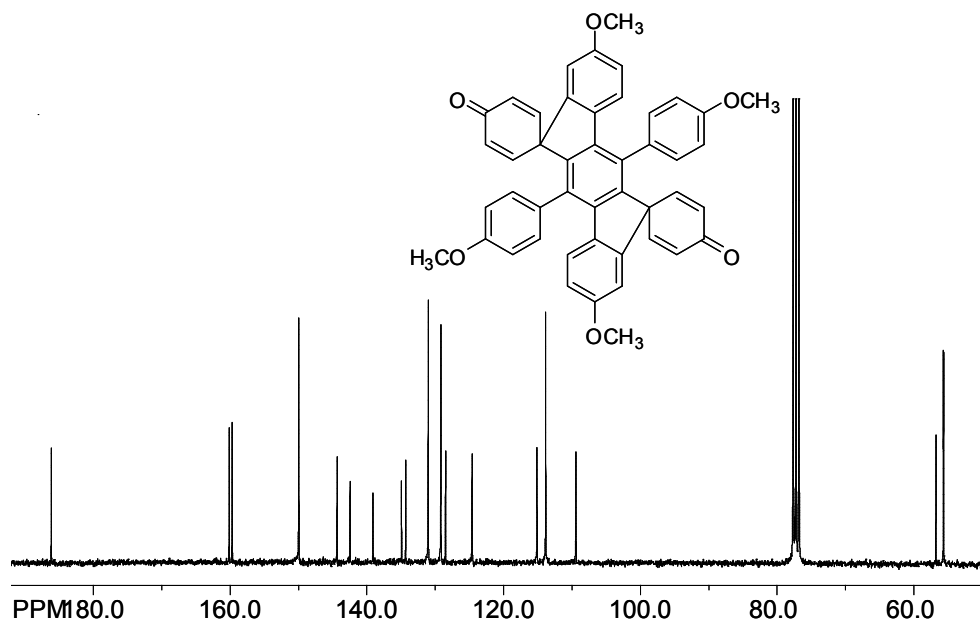
^{13}C NMR spectrum of 4-(hexyloxy)iodobenzene

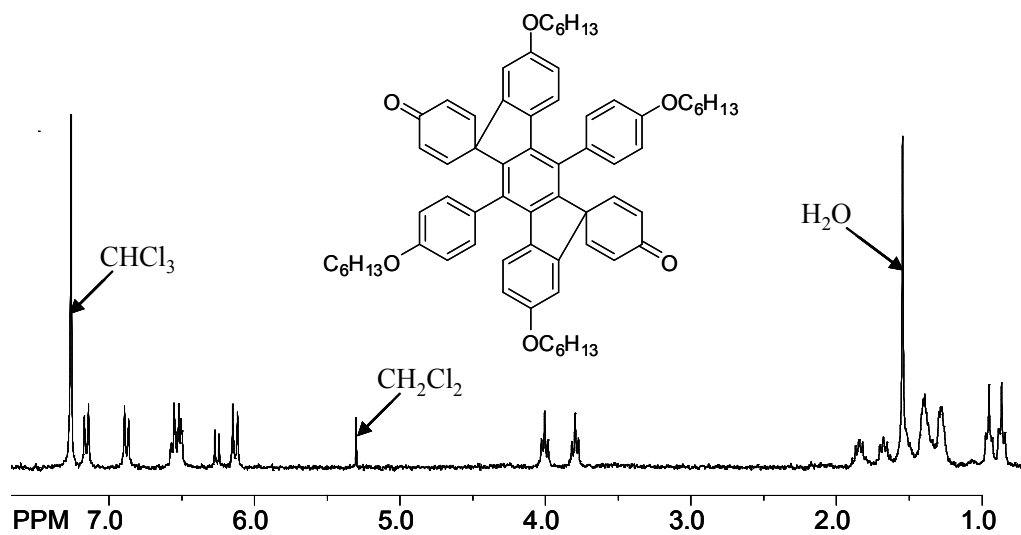
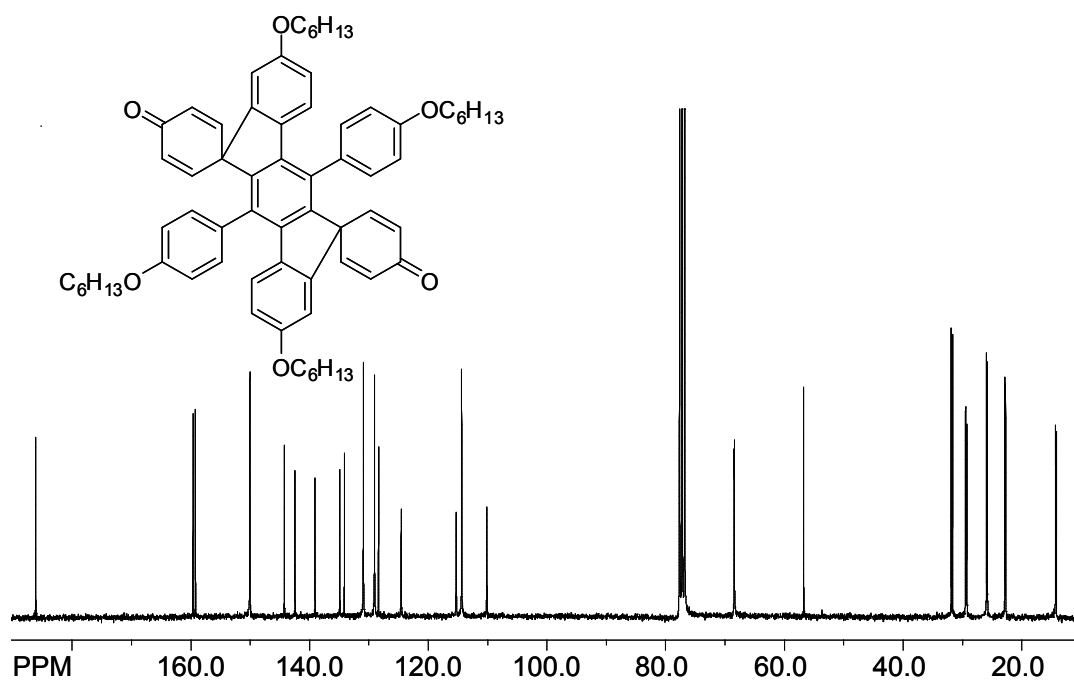


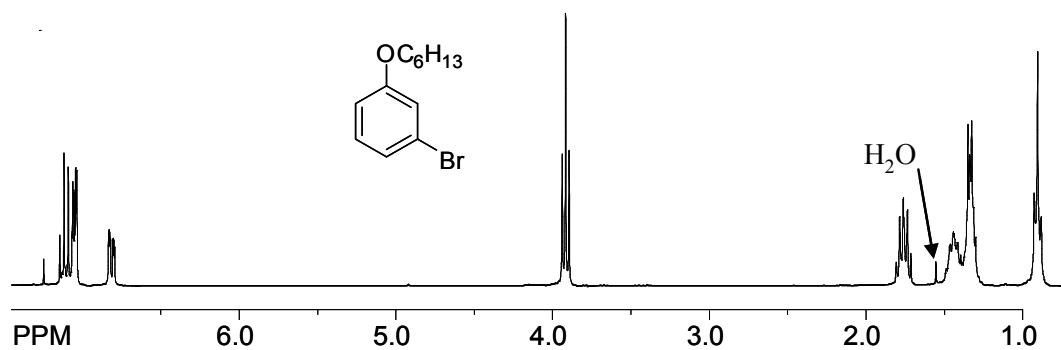
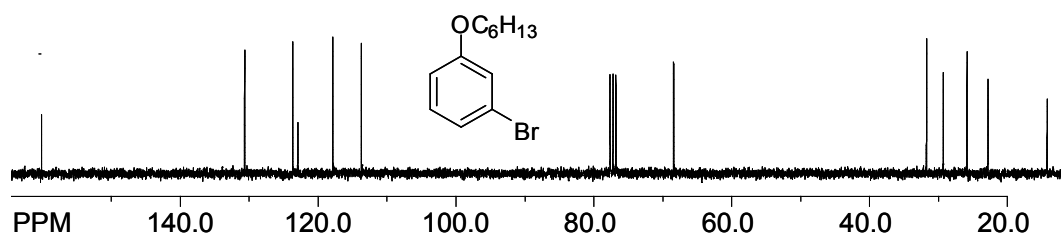
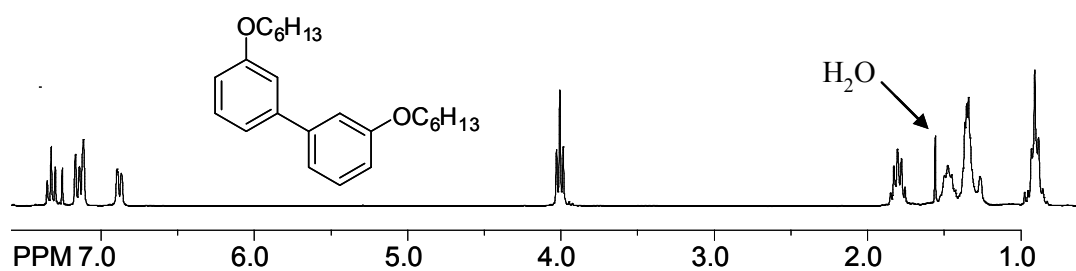
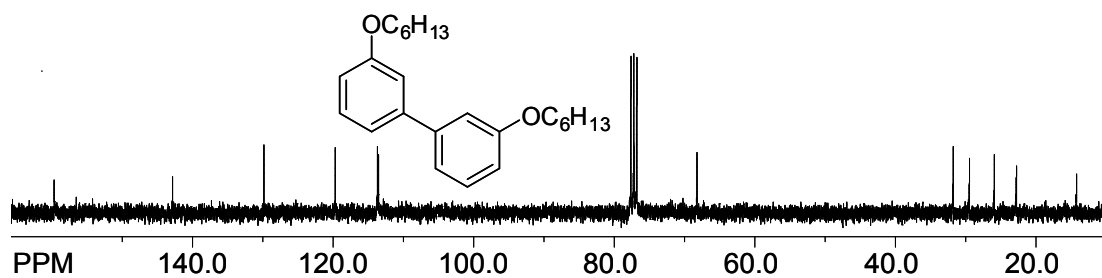
^1H NMR spectrum of bis(4-hexyloxyphenyl)acetylene **^{13}C NMR spectrum of bis(4-hexyloxyphenyl)acetylene** **^1H NMR spectrum of hexakis(4-hexyloxyphenyl)benzene**

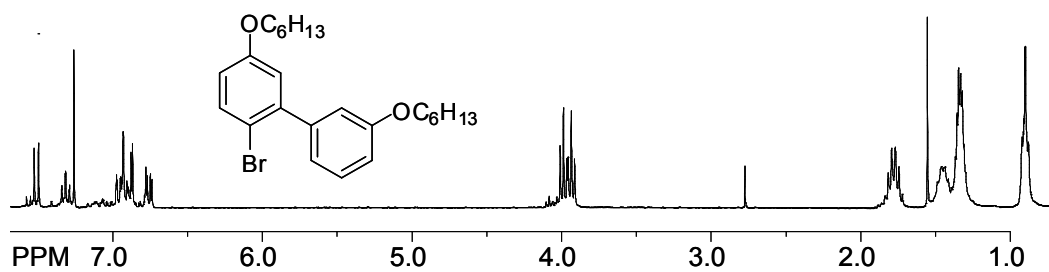
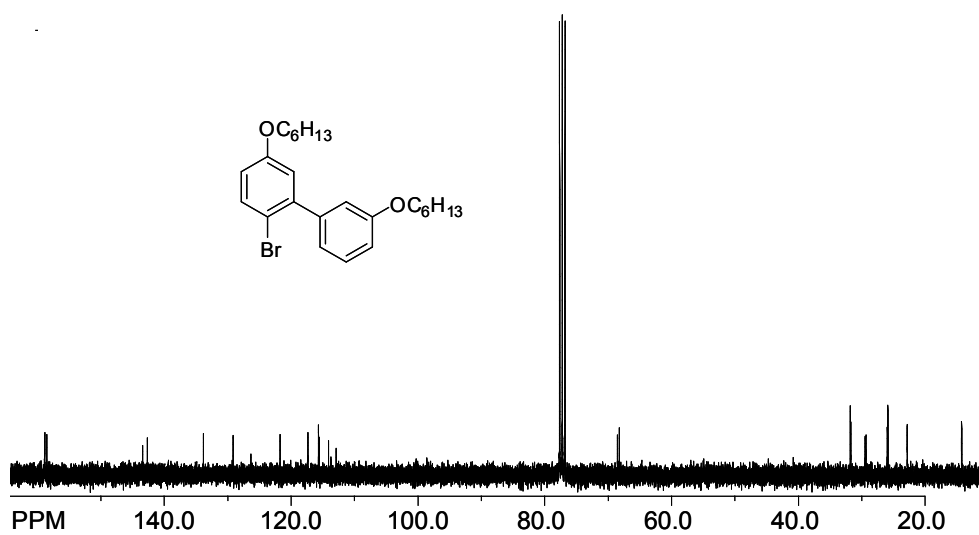
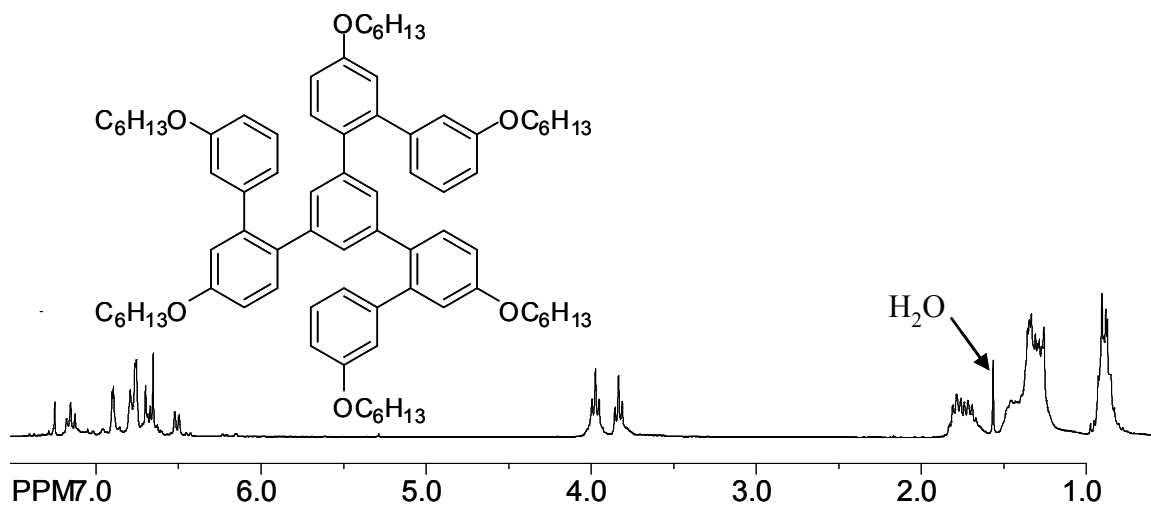
^{13}C NMR spectrum of hexakis(4-hexyloxyphenyl)benzene **^1H NMR spectrum of bis(4-methoxyphenyl)acetylene** **^{13}C NMR spectrum of bis(4-methoxyphenyl)acetylen**

^1H NMR spectrum of hexakis(4-methoxyphenyl)benzene **^{13}C NMR spectrum of hexakis(4-methoxyphenyl)benzene**

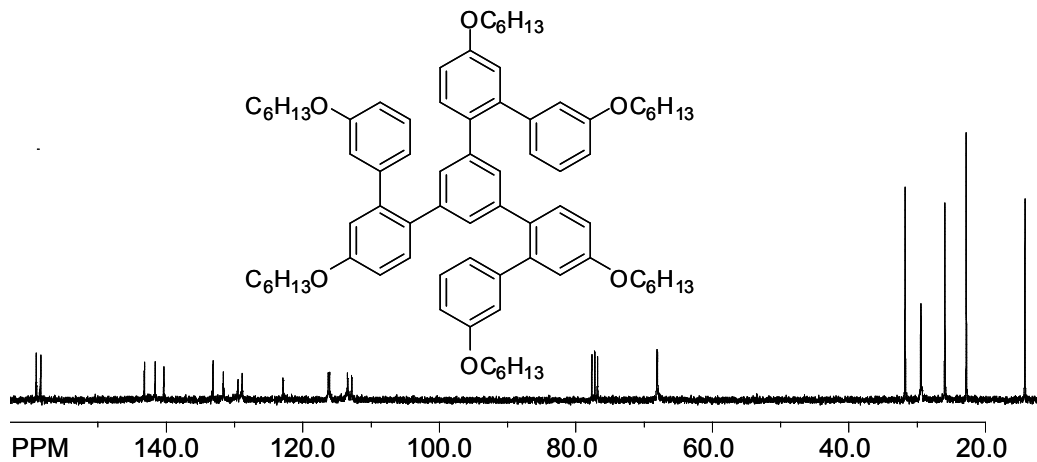
^1H NMR spectrum of the indenofluorene 7a **^{13}C NMR spectrum of the compound indenofluorene 7a**

^1H NMR spectrum of the indenofluorene 7b **^{13}C NMR spectrum of indenofluorene 7b**

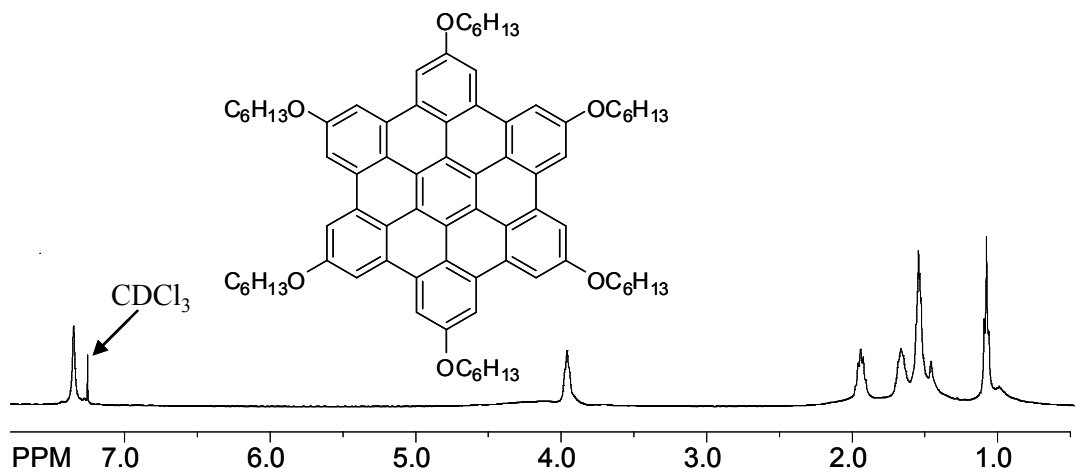
^1H NMR spectrum of 3-bromohexyloxybenzene **^{13}C NMR spectrum of 3-bromohexyloxybenzene** **^1H NMR spectrum of 3,3'-hexyloxybiphenyl (8b)** **^{13}C NMR spectrum of 3,3'-hexyloxybiphenyl (8b)**

^1H NMR spectrum of 5,5'-dialkyloxy-2-bromobiphenyl **^{13}C NMR spectrum of 5,5'-dialkyloxy-2-bromobiphenyl** **^1H NMR spectrum of 1,3,5-tris(5,5'-dihexyloxy-2-biphenyl)benzene (10)**

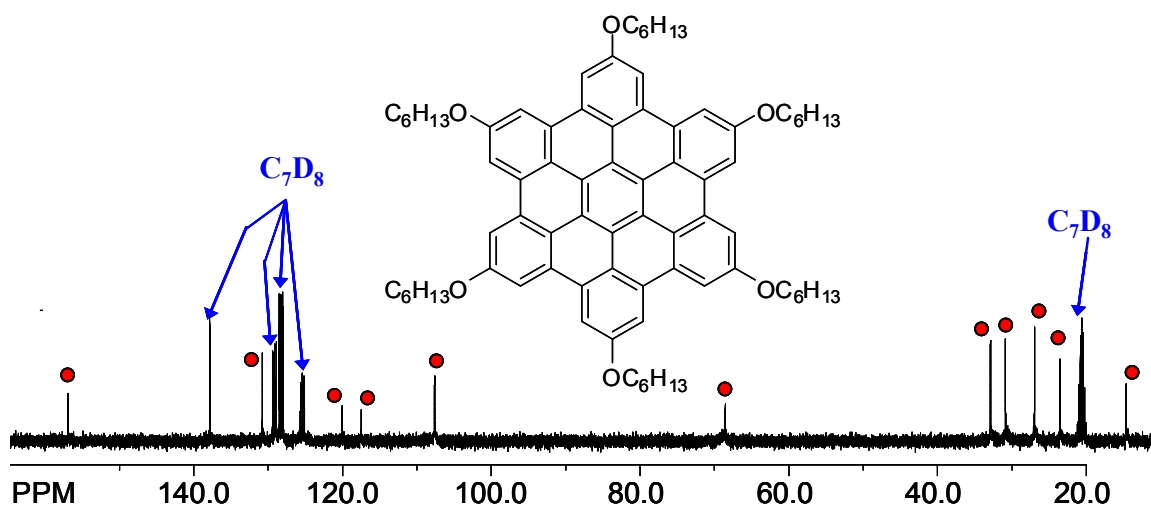
^{13}C NMR spectrum of 1,3,5-tris(5,5'-dihexyloxy-2-biphenyl)benzene (10)



^1H NMR spectrum of HBC 2 in CDCl_3 at 60°C



^{13}C NMR spectrum of HBC 2 in C_7D_8 at 90°C



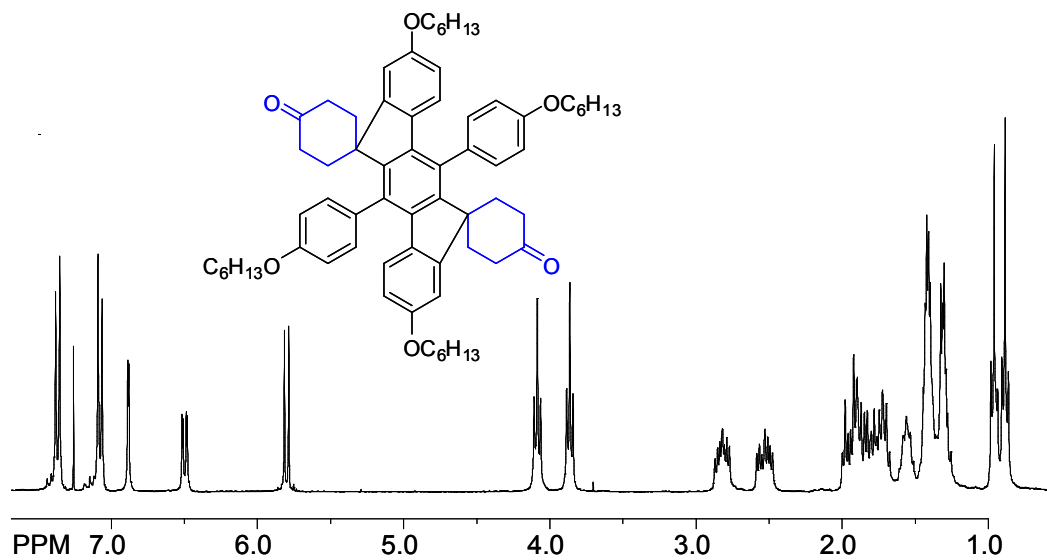
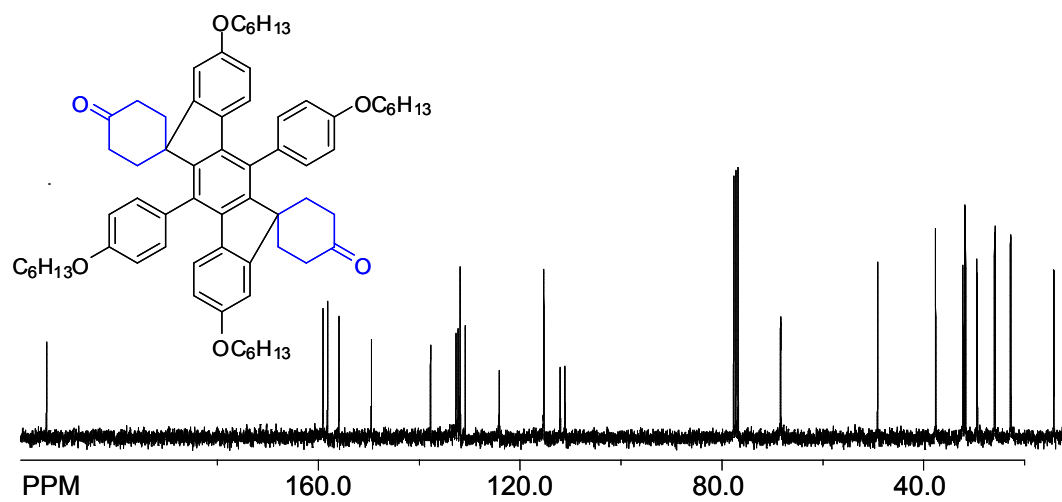
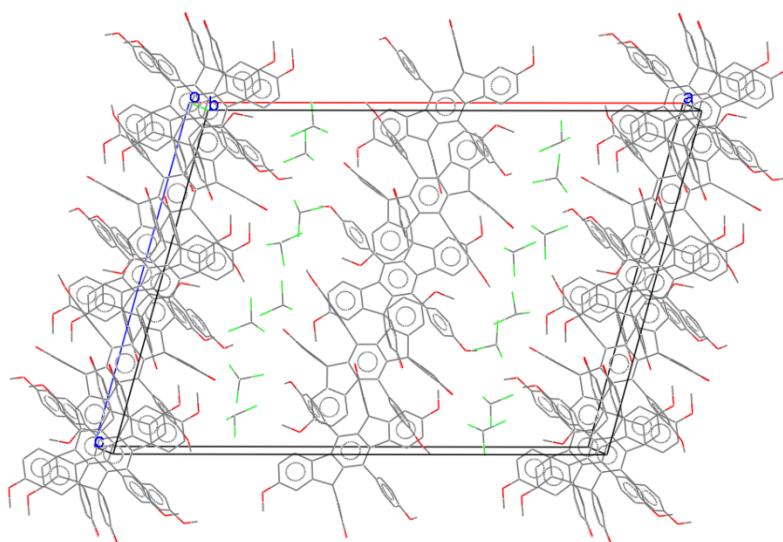
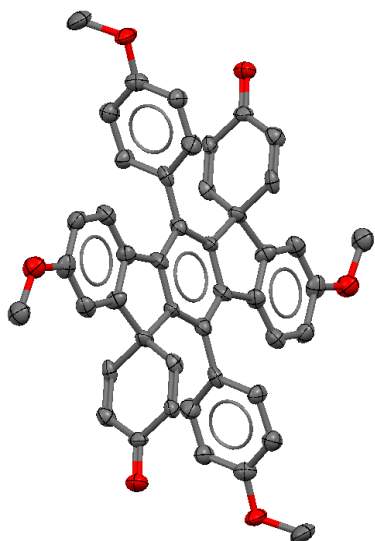
^1H NMR spectrum of hydrogenated indenofluorene 7b **^1H NMR spectrum of hydrogenated indenofluorene 7b**

Table 1. Crystal data and structure refinement for indenofluorene 7a (raj11g).

Identification code	raj11g	
Empirical formula	$C_{46}H_{34}O_6 \cdot 2CHCl_3$	
Formula weight	921.47	
Temperature	100(2) K	
Wavelength	1.54178 Å	
Crystal system	Monoclinic	
Space group	P 2/c	
Unit cell dimensions	a = 35.377(4) Å	$\alpha = 90^\circ$.
	b = 10.0059(12) Å	$\beta = 105.136(5)^\circ$.
	c = 25.216(3) Å	$\gamma = 90^\circ$.
Volume	8616.4(18) Å ³	
Z	8	
Density (calculated)	1.421 Mg/m ³	
Absorption coefficient	4.048 mm ⁻¹	
F(000)	3792	

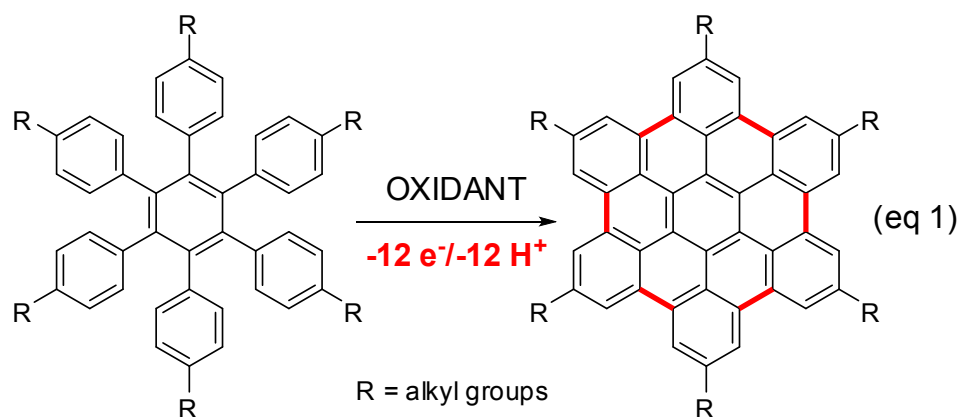
Crystal size	0.45 x 0.05 x 0.05 mm ³
Theta range for data collection	2.59 to 68.19°.
Index ranges	-41<=h<=40, 0<=k<=11, 0<=l<=30
Reflections collected	68170
Independent reflections	15243 [R(int) = 0.1535]
Completeness to theta = 68.19°	96.8 %
Absorption correction	Semi-empirical from equivalents
Max. and min. transmission	0.8232 and 0.2631
Refinement method	Full-matrix least-squares on F ²
Data / restraints / parameters	15243 / 0 / 1089
Goodness-of-fit on F ²	1.012
Final R indices [I>2sigma(I)]	R1 = 0.1474, wR2 = 0.3897
R indices (all data)	R1 = 0.2120, wR2 = 0.4204
Largest diff. peak and hole	0.923 and -0.801 e.Å ⁻³

CHAPTER 2B

Intramolecular Scholl Reactions of Alkoxy-Substituted hexaarylbenzenes Via Cation Radical (Electron Transfer) Mechanism

Introduction

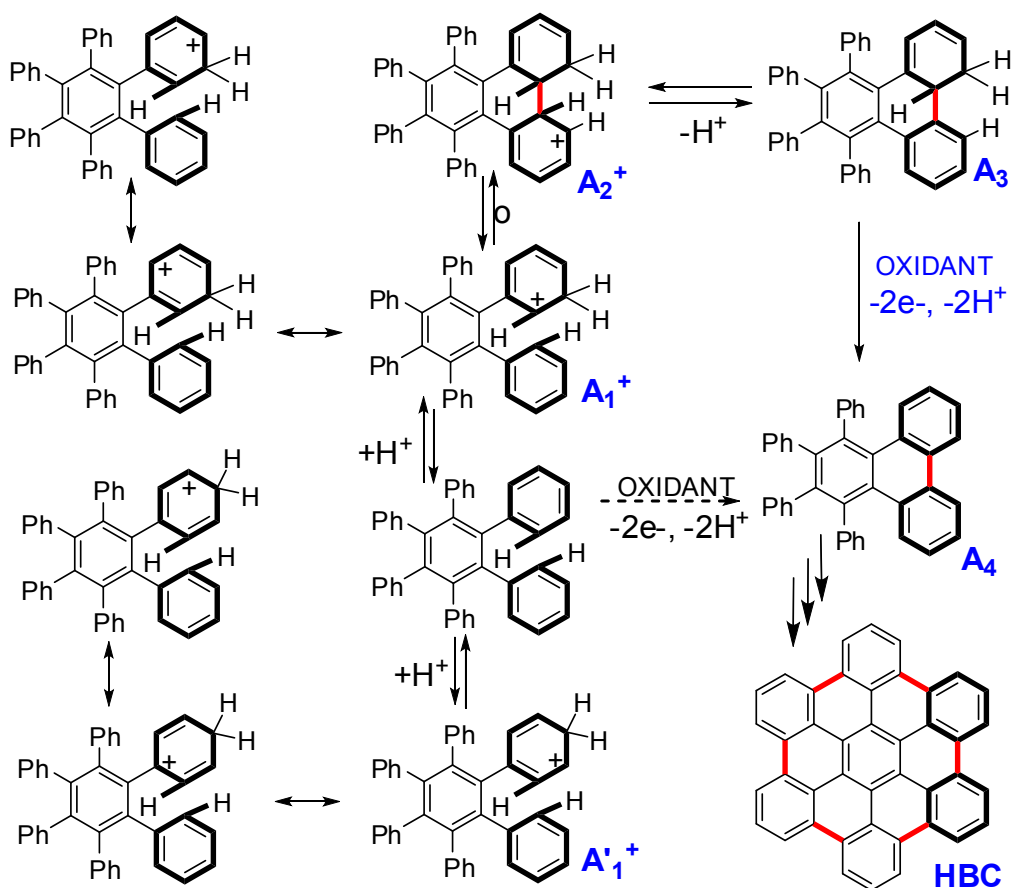
Intramolecular (oxidative) cyclodehydrogenation or Scholl reaction¹ is one of the oldest C-C bond forming reactions which has been extensively utilized for the transformation a variety of propeller-shaped hexaarylbenzenes into hexa-*peri*-hexabenzocoronenes,² i.e. eq 1.



The Scholl reaction in eq 1 can be accomplished with a variety of oxidants such as FeCl_3 ,³ CuCl_2 or $\text{Cu}(\text{OTf})_2$ and AlCl_3 ,⁴ $\text{Tl}(\text{O}_2\text{CCF}_3)_3$ in $\text{CF}_3\text{CO}_2\text{H}$ or $\text{BF}_3\text{-OEt}_2$,⁵ $\text{Pb}(\text{OAc})_4/\text{BF}_3\text{-Et}_2\text{O}$ in MeCN ,^{5,6} triethyloxonium hexachloroantimonate ($\text{Et}_3\text{O}^+ \text{SbCl}_6^-$),⁷ SbCl_5 ,⁸ MoCl_5 ,⁹ and dichlorodicyano-*p*-benzoquinone (DDQ, $E_{\text{red}} = +0.60 \text{ V vs. SCE}$).¹⁰ In a recent series of papers by King and coworkers¹¹ and Muellen and coworkers¹² have suggested largely based on theoretical calculations and a single experimental fact that oxidative cyclodehydrogenation of hexaarylbenzene including parent hexaphenylbenzene occur, exclusively, via diamagnetic arenium ion intermediates (\mathbf{A}_1^+), as detailed in

Scheme 1, owing to the presence of adventitious acids in the various oxidizing systems listed above.^{3,9}

Scheme 1. Arenium ion (or proton transfer) mechanism for the Scholl reactions proposed by King and coworkers.¹¹



The arenium ion mechanism for the formation **HBC** from **HPB** in Scheme 2, demands that C-C bond formation be accomplished only if the protonation occurs at a least preferred site, i.e. *meta* to an electron releasing phenyl substituent (A₁⁺) and thereby resulting into a non-aromatic cyclohexadiene-based intermediate (A₃) which undergoes a irreversible cyclodehydrogenation to A₄ with the aid of added oxidant.¹¹ The mechanism

of aromatization of the cyclohexadiene intermediate A_3 is completely overlooked in these studies, which supposedly is rapid and proceeds via an ECEC mechanism.¹³

Let us first consider the theoretical deliberations by King and coworkers concerning the arenium-ion mechanism in Scheme 1 as follows. As shown in Figure 1, these authors suggest, based on detailed theoretical analysis, that conversion of hexaphenylbenzene to HBC occurs in a continuous fashion where partially cyclized intermediates of hexaarylbenzene (see Figure 1) are far more reactive towards additional C-C bond formation as compared to the hexaarylbenzene, and they have termed this observation as a “slippery slope phenomenon”.

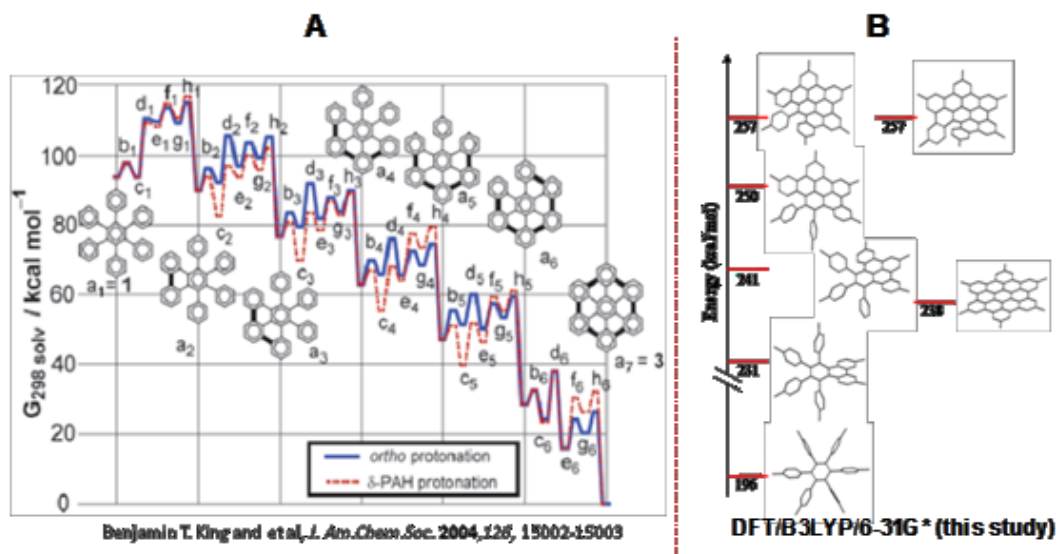


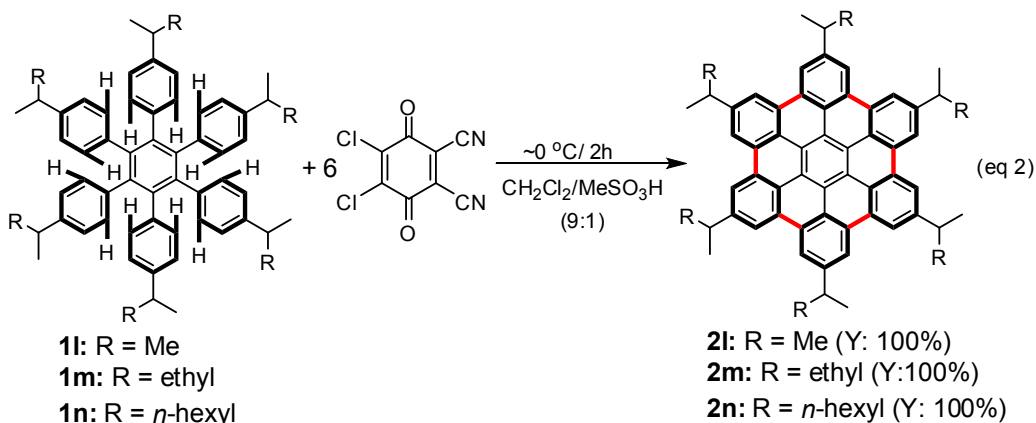
Figure 1. (A) Energies of various intermediates formed in the cyclodehydrogenation of hexaphenylbenzene by Benjamin King and coworkers. (B) Energies of various intermediates formed during cyclodehydrogenation of the HPB by DFT calculations at the B3LYP/6-31G* level.

Interestingly, however, our calculations of the energies of the different intermediates formed in the oxidative cyclodehydrogenation of hexaphenylbenzenes

using DFT at B3LYP/6-31G* level (see Figure 1B), suggested that (i) cyclized HBC is higher in energy than the starting hexaphenylbenzene and (ii) the energies of intermediates in comparison to HPB rise significantly (up to the formation of 5 C-C bonds) due to the expected increase in the strain energies caused by partial planarization of the HPB. It is further noted that the formation of final C-C bond leads to HBC which is significantly lower in energy as compared to the intermediates with 4 and 5 C-C bonds (see Figure 1B).

It is important to emphasize here that the only experimental evidence in support of theoretical calculations of these authors¹¹ in Figure 1A is the fact that when hexaphenylbenzene was subjected to the oxidative cyclodehydrogenation with less than required amounts of oxidant, the reaction produced only **HBC** and unreacted **HPB**. These authors further contended that a singular absence of the partially-cyclized intermediates in above experiment served as experimental evidence for the arenium mechanism proposed in Scheme 1 (Figure 1A).

We have recently introduced DDQ/H⁺ system which quantitatively transforms hexakis(4-alkylphenyl)benzenes to the corresponding HBC in the presence of 6 equivalent of DDQ, i.e. 1.



When the reaction of hexakis(4-isobutylphenyl)benzene (**1m**) was carried out with substoichiometric amounts of DDQ (e.g. 2 equivalent), it afforded 33% of HBC (**2m**) and 66% unreacted **1m** without the contamination from partially cyclized intermediates. The ^1H NMR spectra of the products obtained in reactions according to eq 2 with different amounts of DDQ are shown in Figure 2. As such, this finding confirms the prediction of King and coworkers¹¹ that partially cyclized intermediates of hexaarylbenzene derivatives (see Figure 1) are far more reactive towards additional C-C bond formation as compared to the corresponding hexaarylbenzene.

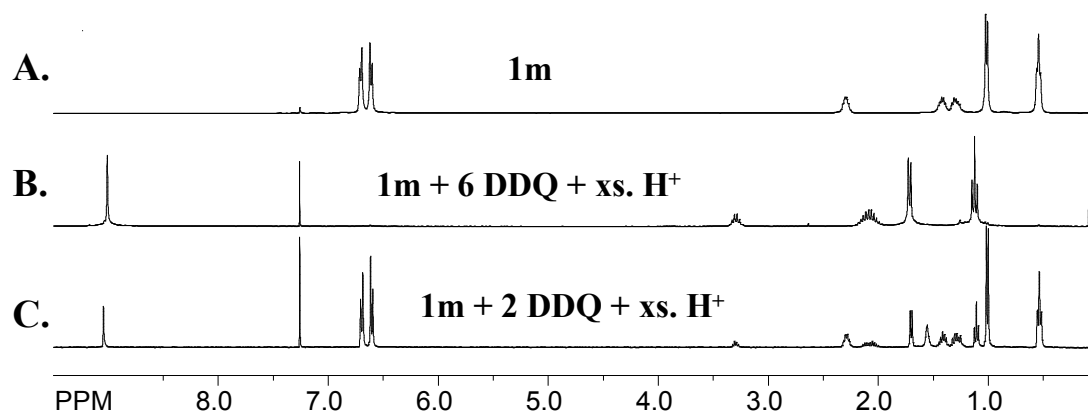
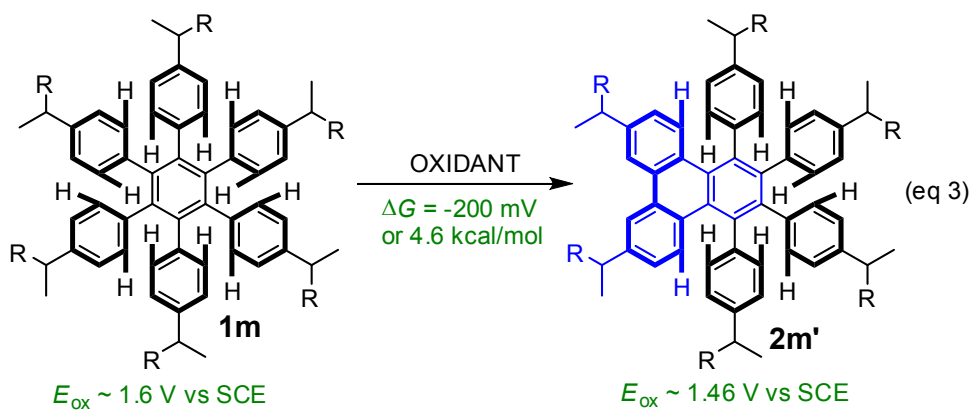


Figure 2. A. ^1H NMR spectrum of hexakis(4-isobutylphenyl)benzene (**1m**) in CDCl_3 . B. ^1H NMR spectrum of the crude product obtained after a reaction of **1m** with 6 equivalents of DDQ in CH_2Cl_2 in the presence of $\text{CH}_3\text{SO}_3\text{H}$ showing the quantitative formation of the corresponding HBC **2m**. C. ^1H NMR spectrum of the crude product obtained after a reaction of **1m** with 2 equivalents of DDQ in CH_2Cl_2 in the presence of $\text{CH}_3\text{SO}_3\text{H}$ showing that only $1/3$ of **1m** is transformed to corresponding HBC **2m**.

It can be readily envisioned that introduction of increasing number of C-C bonds in a hexaarylbenzene leads to planarized polyaromatic derivatives with increasing

aromaticity and thus decreasing redox potentials; and in turn leads to their increased reactivity towards the Scholl reaction, e.g. eq 3.



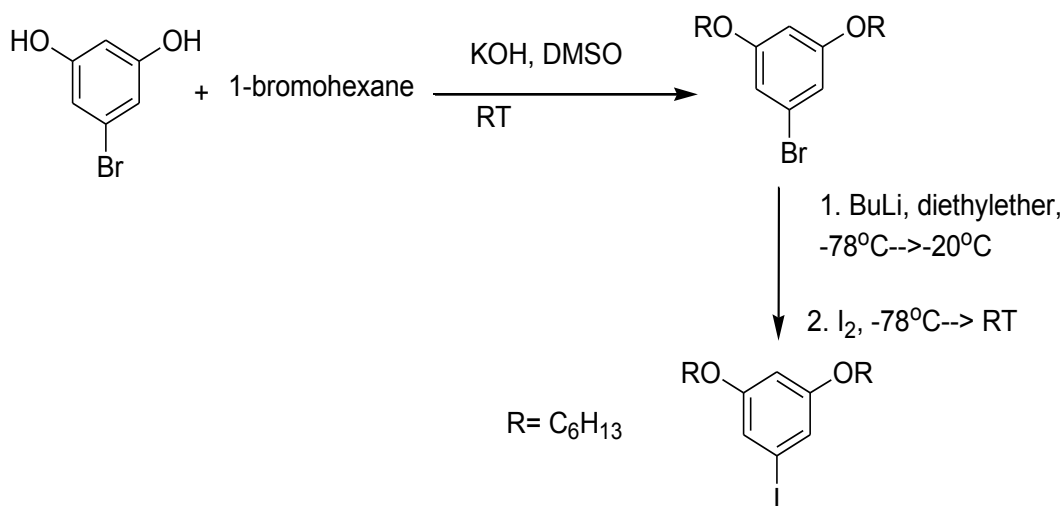
For example, based on the oxidation potential difference of 200 mV between hexaarylbenzene **1m** and the estimated potential of partially cyclized **2m'** (i.e. based on the oxidation potential of 3,6,10-tri-*tert*-butyltriphenylene, $E_{\text{ox}} = 1.39 \text{ V vs SCE}$) clearly suggests that even in a 1:1 mixture of **2m'**⁺⁺ and **1m**, the concentration of **1m**⁺⁺ will be negligible, and therefore the oxidative transformation of **1m** to corresponding HBC **2m** will not occur while **2m'** is present in the reaction mixture.

Results and Discussion

Synthesis of hexakis-3,5-dihexyloxyiodobenzene

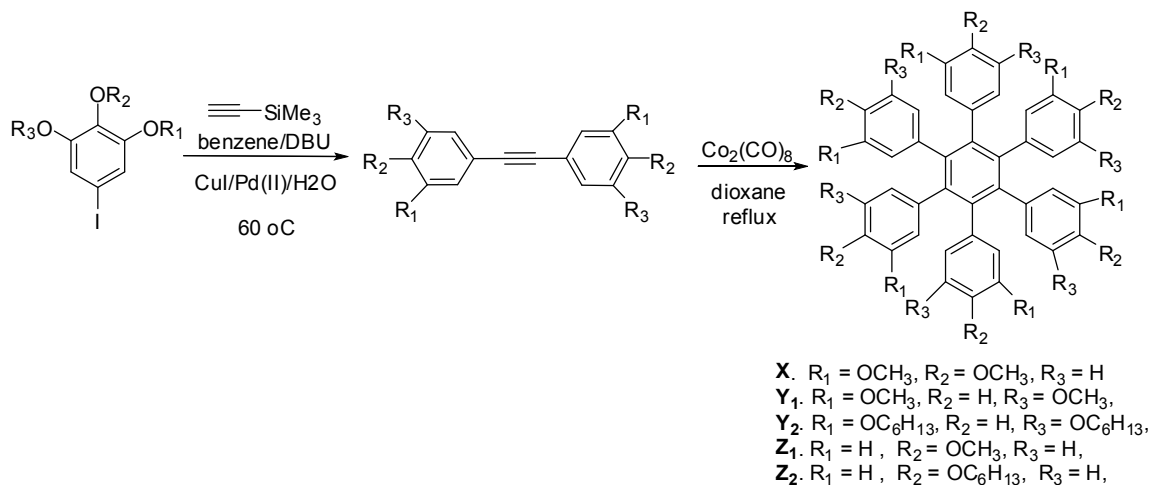
Commercially available 3,5-dihydroxybromobenzene was treated with two equivalents of 1-bromohexane in dimethylsulfoxide in the presence of potassium hydroxide as the base at room temperature to yield 3,5-dihexyloxybromobenzene in excellent yield. The bromo compound was converted to iodo compound by treating first with one equivalent of BuLi and then with excess iodine in anhydrous diethyl ether at -78°C (Scheme 3).

Scheme 3. Synthesis of 3,5-dihexyloxyiodobenzene.



Bis(dialkoxyphenyl)acetylene was synthesized by reacting one equivalent of alkoxyiodobenzene with half equivalent of trimethylsilylacetylene in the presence of DBU (1,8-diazobicyclo[5, 4, 0]undec-7-ene), CuI, Pd(PPh₃)₂Cl₂ and H₂O in anhydrous benzene using standard Sonogashira coupling conditions. Trimerization of bis(alkoxyphenyl)acetylene was done in anhydrous dioxane in the presence of Co(CO)₈ catalyst to yield hexakis(alkoxyphenyl)benzene in quantitative yield.

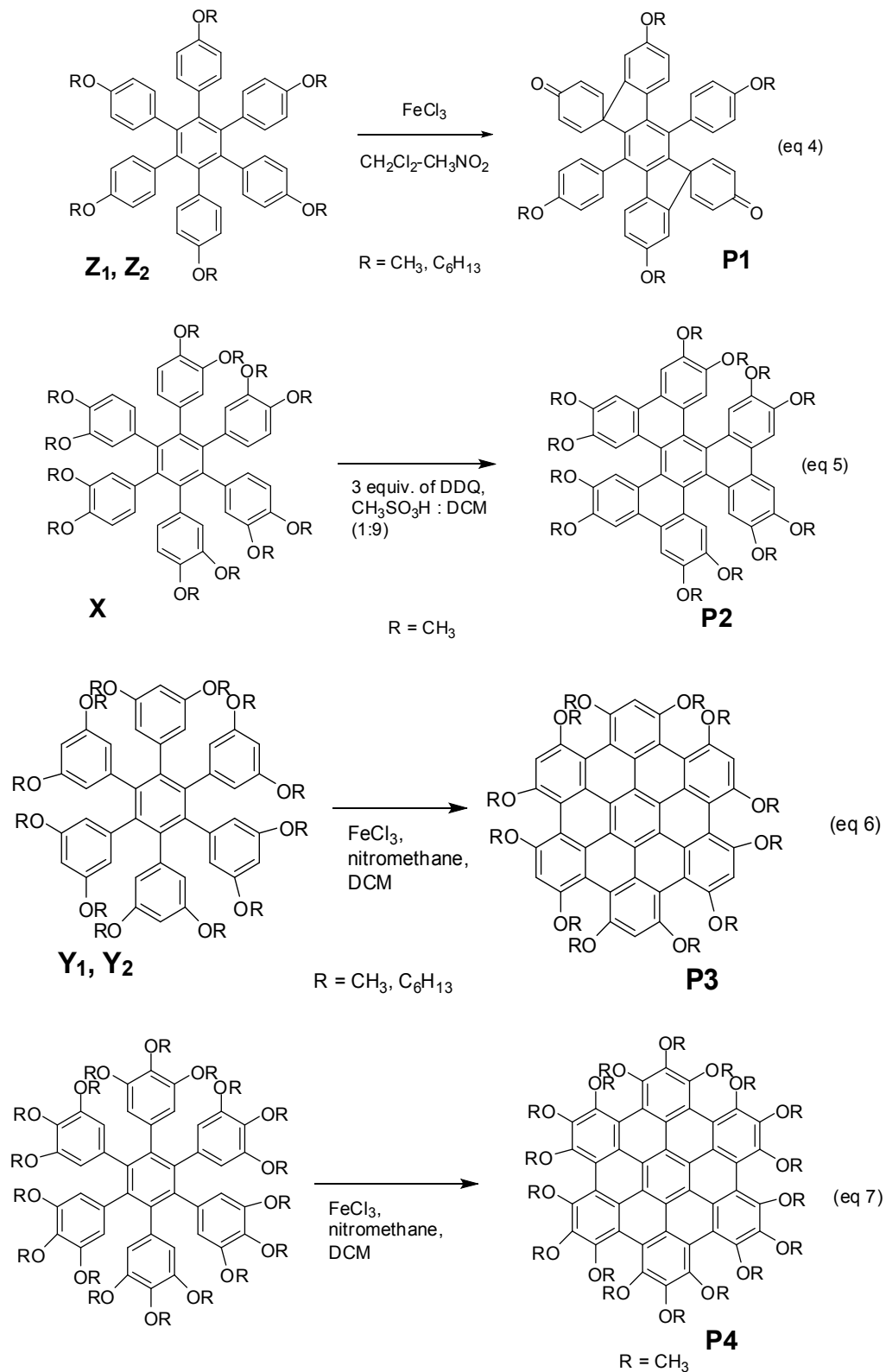
Scheme 4. Synthesis of hexakis(alkoxyphenyl)benzenes



Scholl reactions with various alkoxy-substituted hexaarylbenzenes.

The trimers Z_1, Z_2, Y_1, Y_2 were subjected to Scholl reaction conditions in the presence of excess ferric chloride as the oxidant and X was subjected to Scholl reaction in the presence of three equivalents of DDQ to yield different products as explained in Scheme 5. The obtained products were characterized by $^1\text{H}/^{13}\text{C}$ NMR spectroscopy and X-ray crystallography. The product in equation 4 has made by Mullen and coworkers by subjecting hexakis(trimethoxyphenyl)benzene to Scholl reaction in the presence of excess ferric chloride.

Scheme 5. Different products obtained from differently substituted hexaarylbenzenes



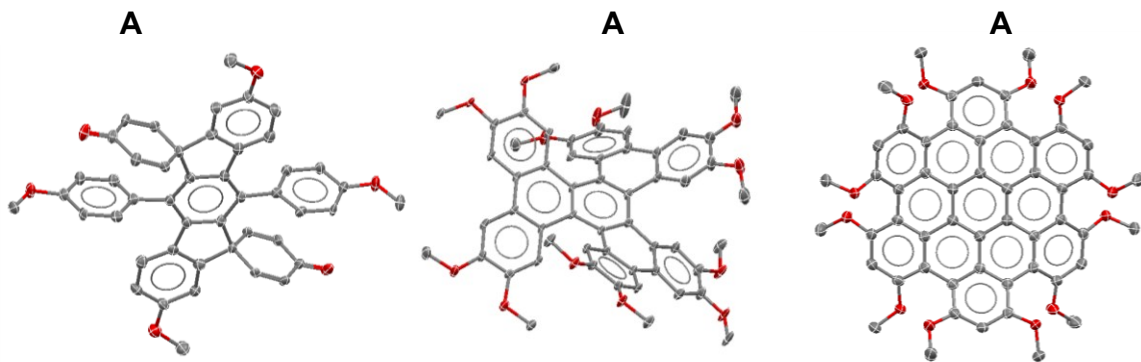


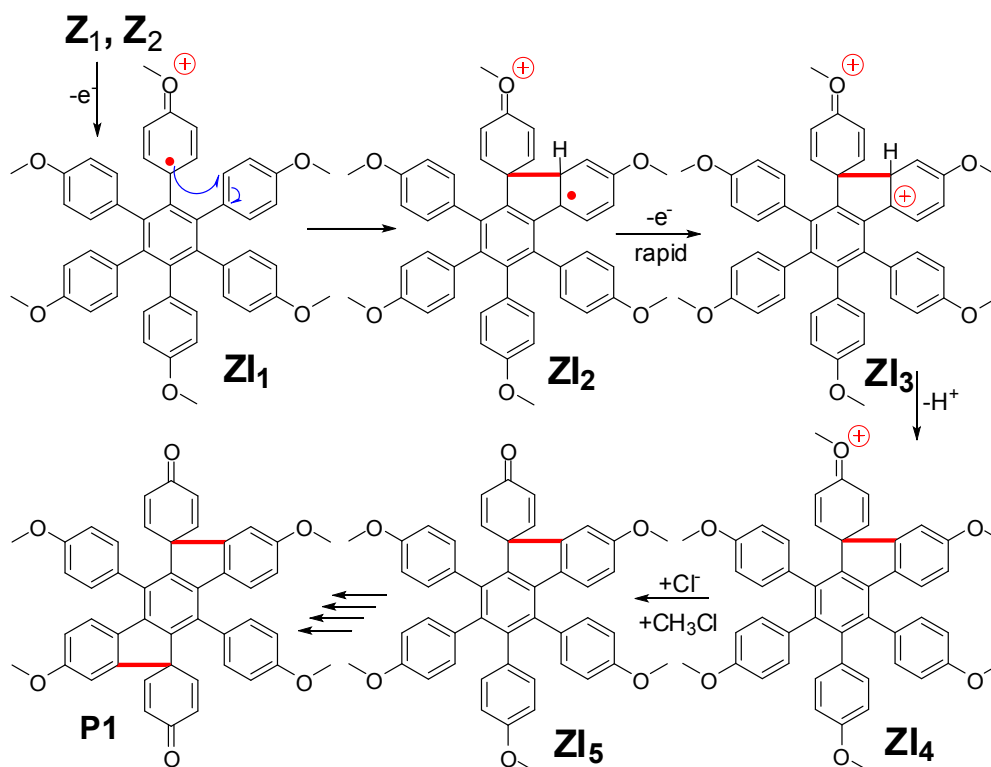
Figure 3. X-ray crystal structures of products obtained by oxidative cyclodehydrogenation of (A) 4-methoxy substituted, (B) 3,4-dimethoxy substituted, and (C) 3,5-dimethoxy substituted hexaarylbenzenes.

Mechanistic Rationale For the formation of different products from different alkoxy substituted hexaaryl benzenes.

Hexakis(4-alkoxyphenyl)benzene.

Upon oxidation cation radical (ZI_1) is formed and charge is stabilized by quinoidal distortion while the radical character concentrates on para carbon on anisyl group. This radical cation leads intramolecular cyclization to yield ZI_2 and rapid removal of electron produce dication ZI_3 . The removal of proton and an alkyl group produce ZI_5 which would have less oxidation potential than the initial hexaaryloxybenzene repeats the same series of steps to produce indenofluorene **P1**. Although excess of the oxidant is used, further cyclization would be controlled by the higher oxidation potential of **P1** and the large strain develops in the **P1** and expected products.

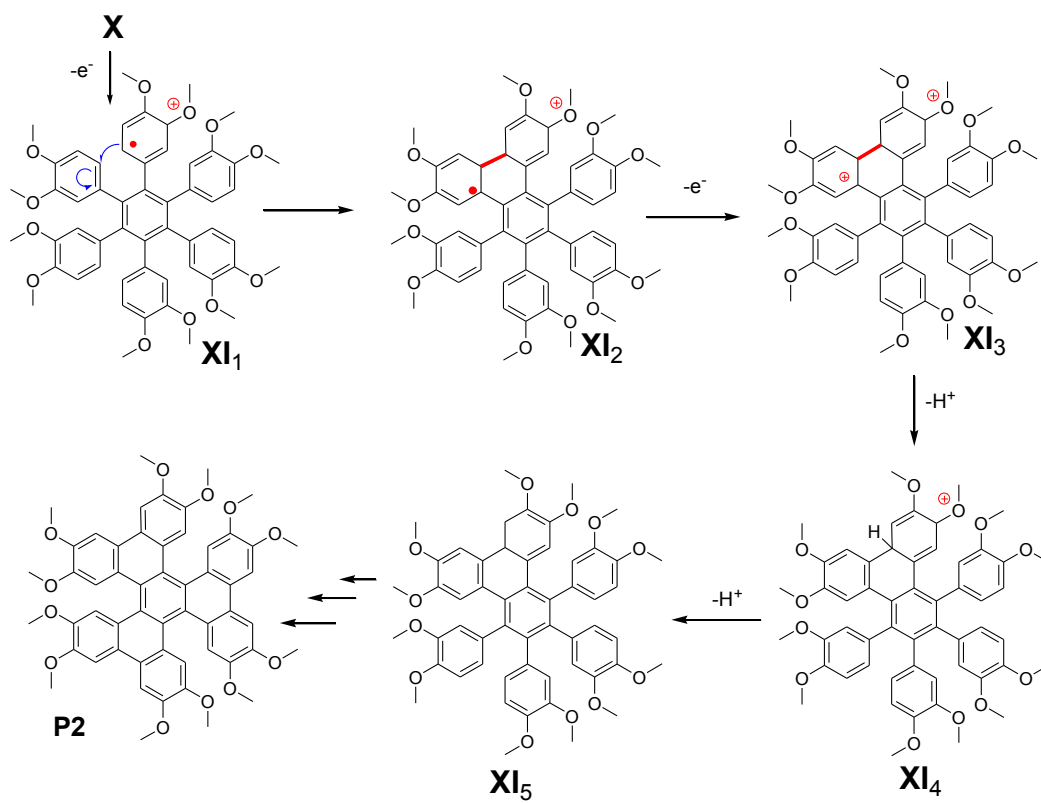
Scheme 6. The proposed cation radical mechanism for the cyclization of **Z₁** and **Z₂**.



Hexakis(3,4-dialkoxyphenyl)benzene.

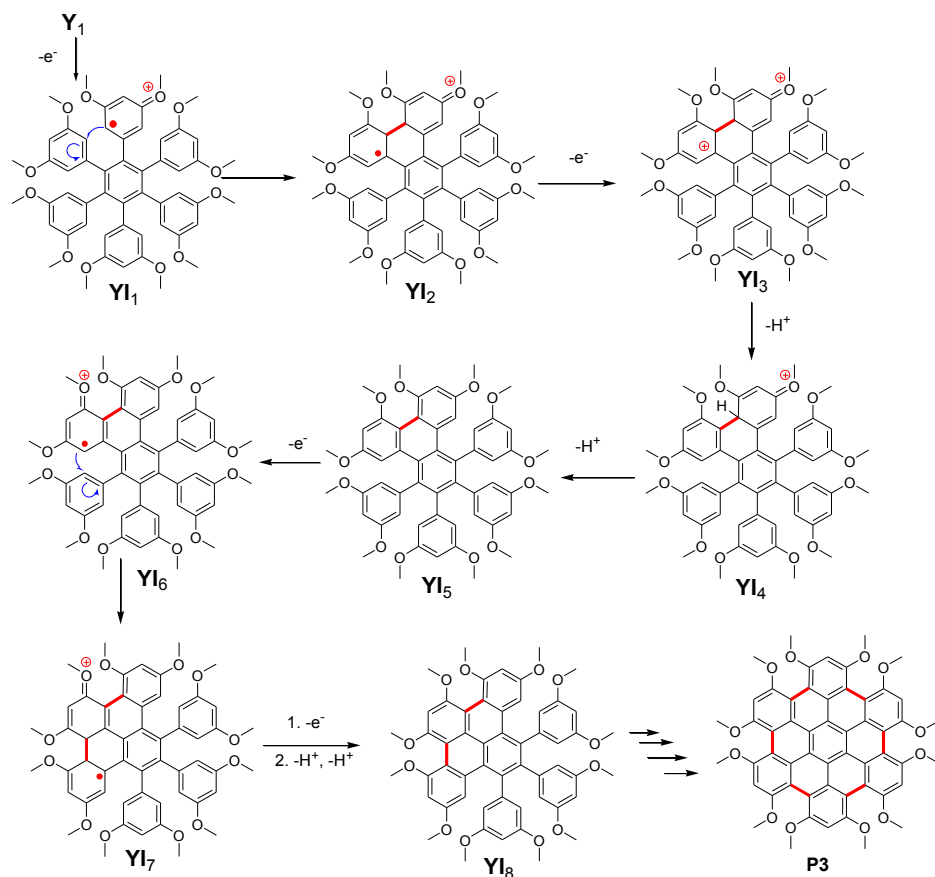
The oxidation of **X** produces **XI₁** and the cationic charge and the radical character is stabilized in the same way as in hexakis(4-alkoxyphenyl)benzene. Then intramolecular bond formation occurs leaving the radical character concentrated at a position para to the 4-methoxy group of the adjacent phenyl ring. Rapid removal of one more electron from **XI₂** form the dication (**XI₃**) and removal of two protons produces partially cyclized **XI₅** which leads to the formation of **P2** due to its lower oxidation potential than the uncyclized compound. Further cyclization of **P2** must be controlled by high oxidation potential of **P2** and three equivalents of the oxidant would produce only **P2** since the oxidation of **P2** is far away from that of intermediates **XI₂**, **XI₃**, **XI₄**.

Scheme 7. The proposed cation radical mechanism for the cyclization of **X**.



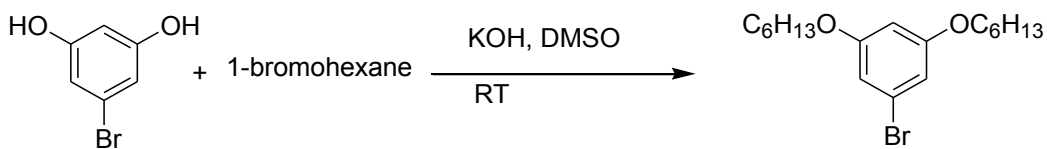
The oxidation of **Y₁** produces cation radical **YI₁** and the cationic charge and the radical character is stabilized by quinoidal distortion. Then intramolecular bond formation occurs leaving the radical character concentrated at a position meta to methoxy group of the adjacent phenyl ring. Due to the lower oxidation potential of the resulting species **YI₂** one more electron is removed to form the dication (**YI₃**) and removal of two protons produces partially cyclized **YI₅**. Due to the lower oxidation potential of **YI₅** it produces cation radical **YI₆** in the presence of an oxidant. **YI₆** follows the same series of steps to form **YI₈** which is having even lower oxidation potential and continue the cyclization till **P2** is obtained. In each cyclization step the bond formation is governed by the position where the radical character developed.

Scheme 8. The proposed cation radical mechanism for the cyclization of **Y**.



Experimental

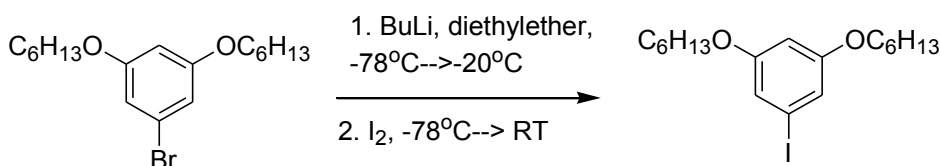
Synthesis of 3,5-dihexyloxybromobenzene



KOH (6.0 g, 109 mmol) was suspended in dimethylsulfoxide (50 mL) and 3,5-dihydroxybromobenzene (2.6 g, 13.75 mmol) was added into the above suspension and stirred for few minutes. 1-bromohexane (3.8 mL, 27.5 mmol) was added dropwise into the above solution and stirred for 30 minutes and water (50 mL) was added, extracted to

dichloromethane, dried over anhydrous MgSO_4 and evaporated to isolate colorless liquid which was used in the next step without further purification. Yield (70%) ; ^1H NMR (CDCl_3) δ : 0.92 (t, $J = 6.5, 13.4$ Hz, 6H), 1.33-1.53(m, 12H), 1.76 (qn, 4H), 3.90 (t, $J = 6.5, 13.1$ Hz, 4H), 6.37 (t, $J = 2.0, 4.1$ Hz, 1H), 6.64 (d, $J = 2.2$ Hz, 2H) . ^{13}C NMR (CDCl_3) δ : 14.22, 22.72, 25.87, 29.29, 31.74, 68.45, 100.73, 110.37, 123.00, 160.94.

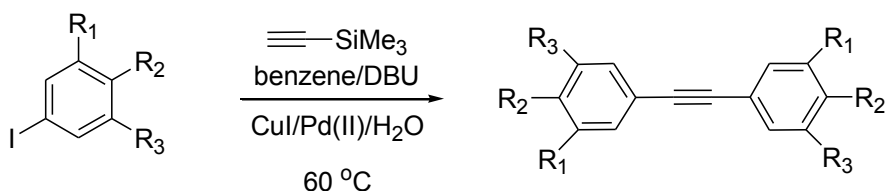
Synthesis of 3,5-dihexyloxyiodobenzene



3,5-Dihexyloxybromobenzene (3.3 g, 9.2 mmol) was dissolved in anhydrous diethylether (30 mL) and cooled it into -78°C under argon atmosphere. Then 2.5 M BuLi in hexane (4.4 mL, 11.08 mmol) was added dropwise to the above solution at -78°C under argon atmosphere. Then the temperature of the reaction mixture was brought to -20°C and stirred for one hour. The reaction mixture was cooled to -78°C under argon atmosphere and excess amount of iodine in anhydrous diethyl ether (10 mL) was added dropwise into it and then the temperature of the reaction mixture was brought to room temperature and stirred for 10 minutes. Aqueous NaHSO_3 solution was added and the product was extracted to ether, washed with brine solution, dried over anhydrous MgSO_4 and evaporated to isolate colorless liquid which was purified by column chromatography using hexane as the eluent. Yield (80%) ; ^1H NMR (CDCl_3) δ : 0.92 (t, $J = 6.8, 13.5$ Hz, 6H), 1.26-1.50 (m, 12H), 1.75 (qn, 4H), 3.89 (t, $J = 6.5, 13.0$ Hz, 4H), 6.40 (t, $J = 2.1,$

4.3 Hz, 1H), 6.84 (d, $J = 2.2$ Hz, 2H). ^{13}C NMR (CDCl_3) δ : 14.23, 22.81, 25.86, 29.30, 31.73, 68.41, 94.25, 101.59, 116.37, 160.80.

Synthesis of bis(alkoxyphenyl)acetylenes



- B.** $\text{R}_1 = \text{OCH}_3$, $\text{R}_2 = \text{OCH}_3$, $\text{R}_3 = \text{H}$
C₁. $\text{R}_1 = \text{OCH}_3$, $\text{R}_2 = \text{H}$, $\text{R}_3 = \text{OCH}_3$,
C₂. $\text{R}_1 = \text{OC}_6\text{H}_{13}$, $\text{R}_2 = \text{H}$, $\text{R}_3 = \text{OC}_6\text{H}_{13}$,

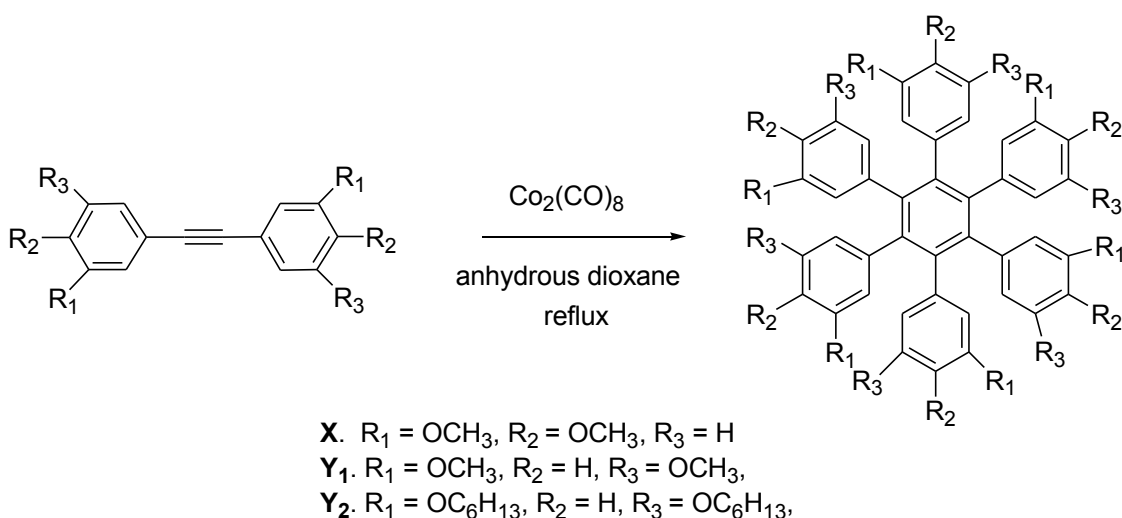
For an example 3,5-dihexyloxyiodobenzene (3.0 g, 7.43 mmol) was dissolved in anhydrous benzene (38 mL) in a Schlenk flask under argon atmosphere. DBU (6.8 mL, 45 mmol), CuI (70 mg, 0.37 mmol, 5% mol) and Pd(PPh_3) $_2\text{Cl}_2$ (0.158 g, 0.22 mmol, 3% mol) were added to the flask, and it was evacuated and refilled with argon three times. To this mixture was then added distilled water (0.053 mL, 2.97 mmol, 40 mol %) followed by trimethylsilylacetylene (0.52 mL, 3.72 mmol). The resulting mixture was first stirred for 1 hour at room temperature, and then at 60 °C for 24 hours. The solvent was evaporated under reduced pressure and the dark-colored residue was extracted with dichloromethane (2 x 25 mL). The dichloromethane layer was dried with anhydrous magnesium sulfate, filtered, and evaporated to afford a dark colored syrup. Purification of the product by column chromatography using hexanes:ethyl acetate (99:1) as eluent afforded **C₂** as a pale yellow solid.

C2 : Yield (1.7 g, 80 %); $^1\text{H NMR}$ (CDCl_3) δ : 0.91 (t, $J = 6.9, 14.0$ Hz, 12H), 1.26-1.51 (m, 24H), 1.77 (m, 8H), 3.94 (t, $J = 6.6, 13.1$ Hz, 8H), 6.45 (t, $J = 2.3, 4.6$ Hz, 2H), 6.66 (d, $J = 2.26$ Hz, 4H). $^{13}\text{C NMR}$ (CDCl_3) δ : 14.25, 22.82, 25.91, 29.38, 31.78, 68.37, 89.11, 102.99, 110.06, 124.49, 160.26.

B : Yield (80 %); $^1\text{H NMR}$ (CDCl_3) δ : 3.85 (s, 12H), 6.78 (d, $J = 8.24$ Hz, 2H), 7.00 (s, 2H) 7.09 (d, $J = 8.24$ Hz, 2H) . $^{13}\text{C NMR}$ (CDCl_3) δ : 55.90, 88.07, 111.07, 114.17, 115.64, 124.73, 148.64, 149.33.

C1 : Yield (80 %); $^1\text{H NMR}$ (CDCl_3) δ : 3.81 (s, 12H), 6.47 (t, $J = 2.35, 4.68$ Hz, 2H), 6.70 (d, $J = 2.35$ Hz, 2H). $^{13}\text{C NMR}$ (CDCl_3) δ : 55.63, 89.13, 102.13, 109.58, 124.55, 160.74.

Preparation of hexakis(3,5-hexyloxyphenyl)benzene

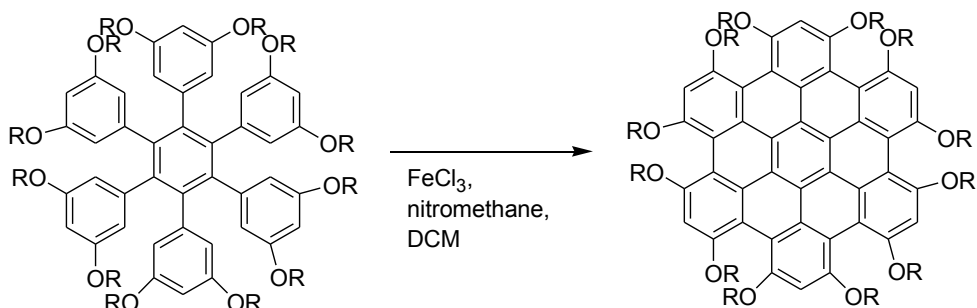


For an example *Bis*-(3,5-dihexyloxyphenyl)acetylene (1.4 g, 2.4 mmol) was dissolved in anhydrous dioxane (50 mL) in an oven dried Schlenk flask under an argon atmosphere and the flask was evacuated and filled with argon repeatedly (3x). Then, $\text{Co}_2(\text{CO})_8$ (80 mg) was added to the flask under an argon atmosphere and the flask was evacuated and filled with argon again (3 x). The resulting mixture was refluxed for 14 h

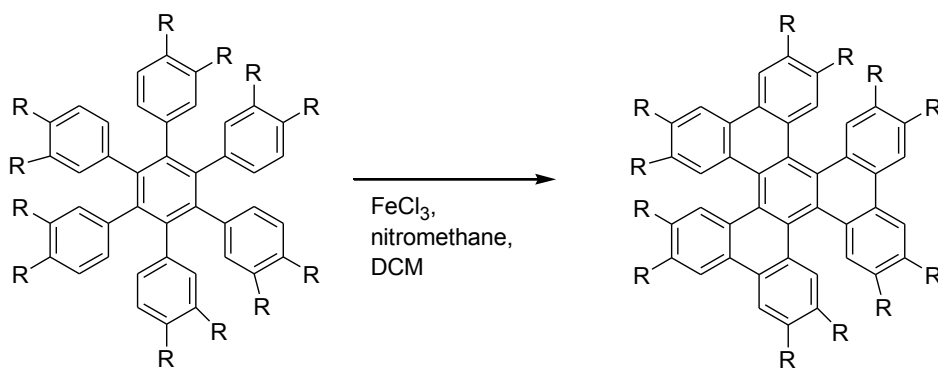
and the dioxane was evaporated. The resulting residue was dissolved in dichloromethane and filtered through a short pad of silica gel. Evaporation of the solvent afforded a dark colored solid which was purified by column chromatography using a mixture of hexane: ethyl acetate (99 : 1) as the eluent to yield **Y₂** as a yellow liquid.

Y₂: Yield (1.2 g, 85 %); ¹H NMR (CDCl₃) δ: 0.89 (t, *J* = 6.5, 13.6 Hz, 36H), 1.27 (m, 72H), 1.53 (m, 24H), 3.55 (t, *J* = 6.7, 13.4 Hz, 24H), 6.01 (t, *J* = 2.2, 4.4 Hz, 6H), 6.06 (d, *J* = 2.2 Hz, 12H). ¹³C NMR (CDCl₃) δ: 14.24, 22.83, 25.85, 29.28, 31.74, 68.34, 101.20, 110.44, 140.15, 142.34, 158.99. **Y₁**: Yield (85 %); ¹H NMR (CDCl₃) δ: 3.45 (s, 36H), 6.05 (t, *J* = 2.4, 5.0 Hz, 6H), 6.11 (d, *J* = 2.2 Hz, 12H). **X**: Yield (85 %); ¹H NMR (CDCl₃) δ: 3.41 (s, 18H), 3.69 (s, 18H), 6.36 (m, 18H). ¹³C NMR (CDCl₃) δ: 55.82, 109.97, 115.49, 124.19, 133.65, 140.45, 146.63, 147.67.

Oxidative cyclodehydrogenation of hexakis(3,5-dialkyloxyphenyl)benzene



Z₁. R = OCH₃
Z₂. R = OC₆H₁₃



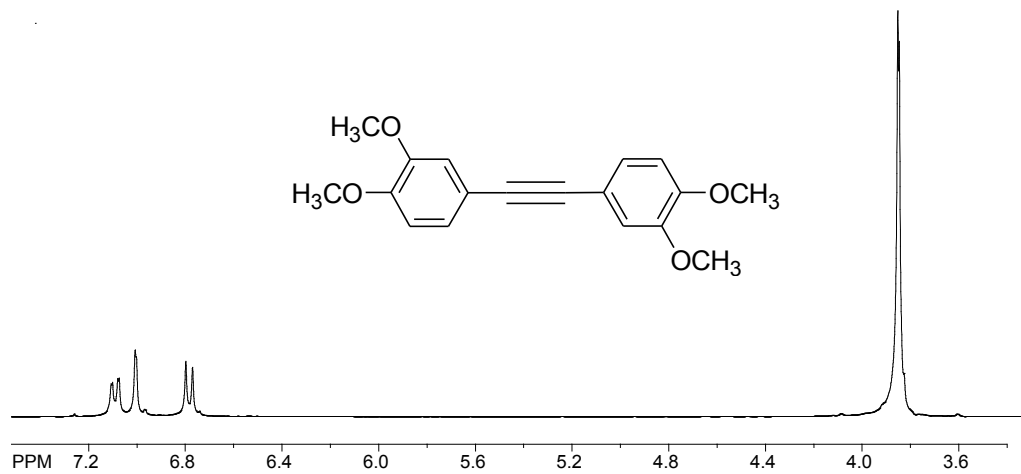
P. R = CH₃

For an example *hexakis*(3,5-dhexyloxyphenyl)benzene (0.5 g, 0.29 mmol) was dissolved in dry dichloromethane (30 mL) and cooled to ~ 0 °C in an ice bath under an argon atmosphere. A solution of ferric chloride (0.94 g, 5.76 mmol) in nitromethane (20 mL) was added dropwise into the above mixture. When the addition was completed, the ice bath was removed and the resulting mixture was stirred for 1 h at room temperature. [Note that throughout the reaction period, a slow stream of argon was passed through the reaction mixture to remove gaseous HCl formed in the reaction.] The reaction was quenched by addition of methanol (30 mL) and the formed dark orange product was filtered and recrystallized with dichloromethane: methanol (1:1) mixture.

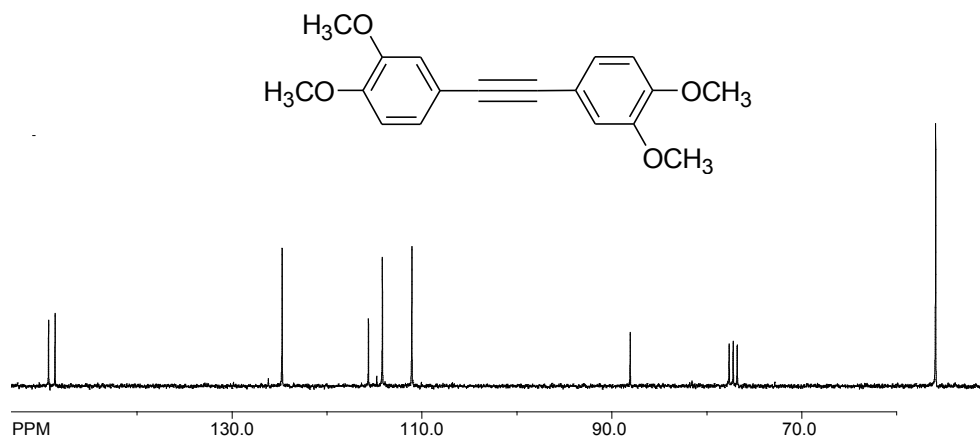
Z₂: Yield (90 %); ¹H NMR (CDCl₃) δ: 0.94 (m, 36H), 1.38 (m, 48H), 1.51 (m, 24H), 1.92 (m, 24H), 4.20 (dt, 24H) 7.13 (s, 6H). ¹³C NMR (CDCl₃) δ: 14.30, 22.89, 25.99, 30.03, 32.04, 69.78, 100.02, 109.49, 122.58, 129.42, 155.72. **Z₁**: Yield (90 %); ¹H NMR (CDCl₃) δ: 4.26 (s, 36H) 7.31 (s, 6H). **P**: Yield (90 %); ¹H NMR (CDCl₃) δ: 3.51 (s, 18H), 4.17 (s, 18H), 7.68 (s, 6H), 7.79 (s, 6H), ¹³C NMR (CDCl₃) δ: 55.87, 56.30, 104.08, 113.04, 124.07, 125.26, 126.51, 147.28, 148.94.

NMR Spectral data

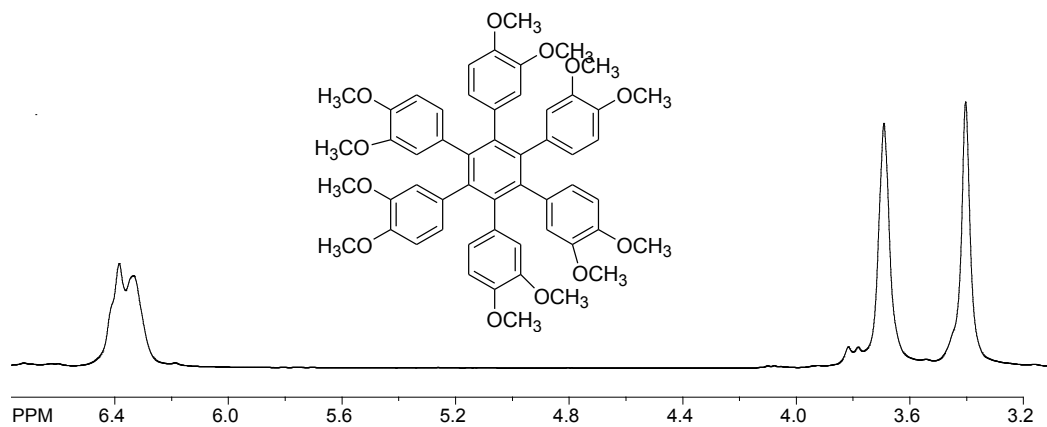
^1H NMR spectrum of bis-(3,4-dimethoxyphenyl)acetylene

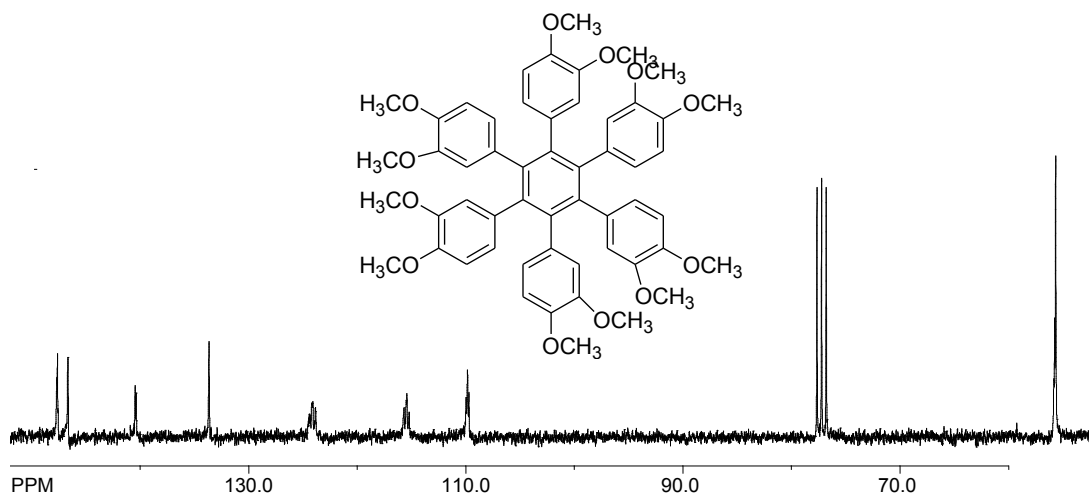
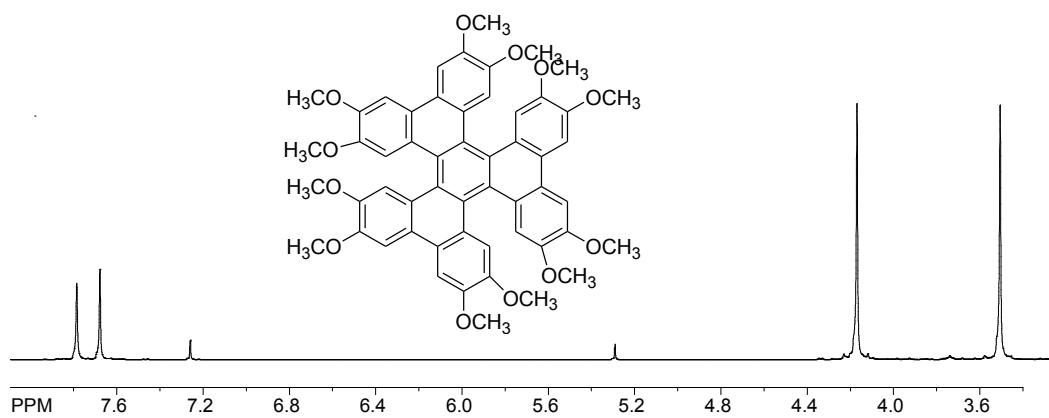
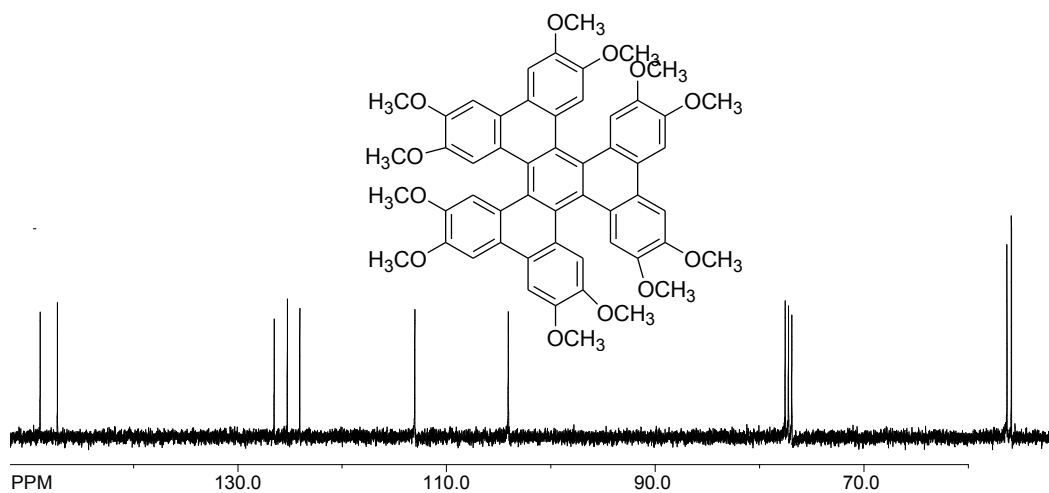


^{13}C NMR spectrum of bis-(3,4-dimethoxyphenyl)acetylene

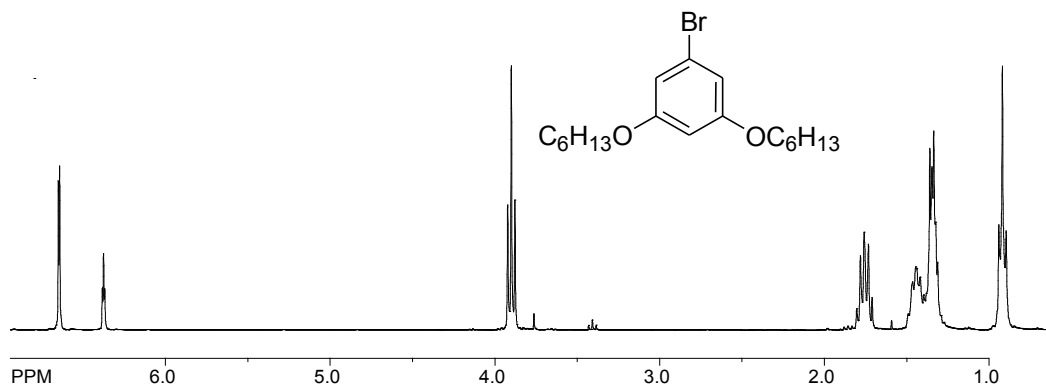


^1H NMR spectrum of hexakis-(3,4-dimethoxyphenyl)benzene

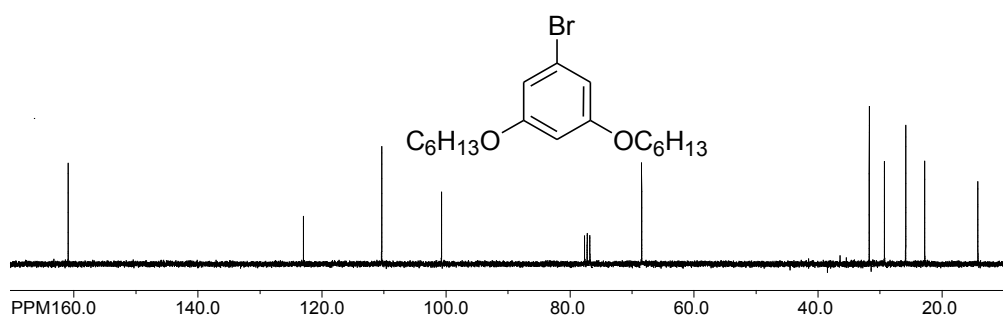


^{13}C NMR spectrum of hexakis-(3,4-dimethoxyphenyl)benzene ^1H NMR spectrum of cyclized hexakis-(3,4-dimethoxyphenyl)benzene ^{13}C NMR spectrum of cyclized hexakis-(3,4-dimethoxyphenyl)benzene

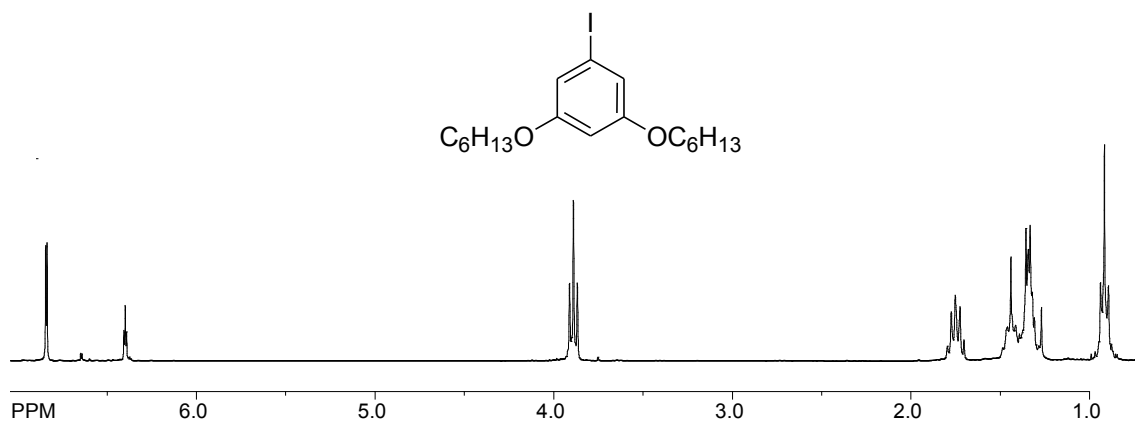
^1H NMR spectrum of 3,5-dihexyloxybromobenzene

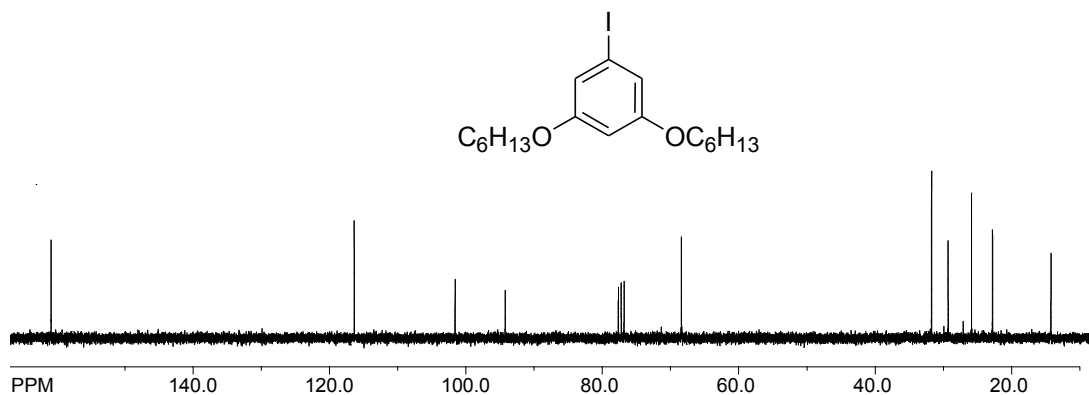
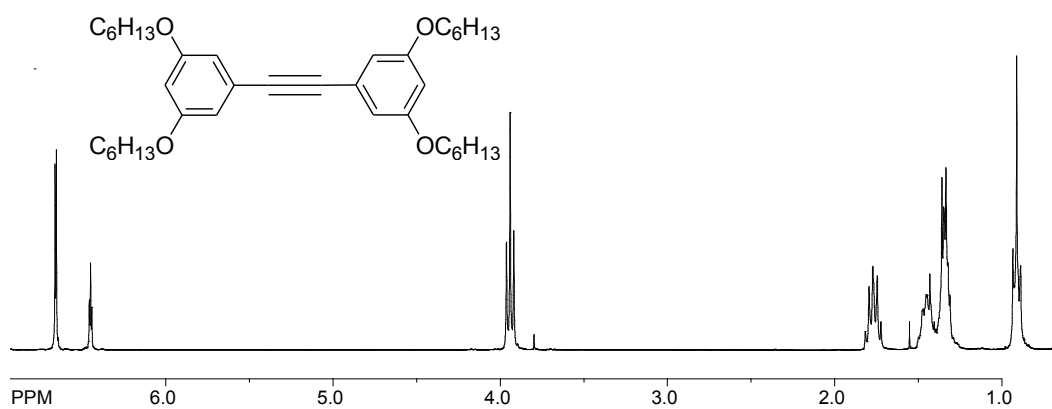
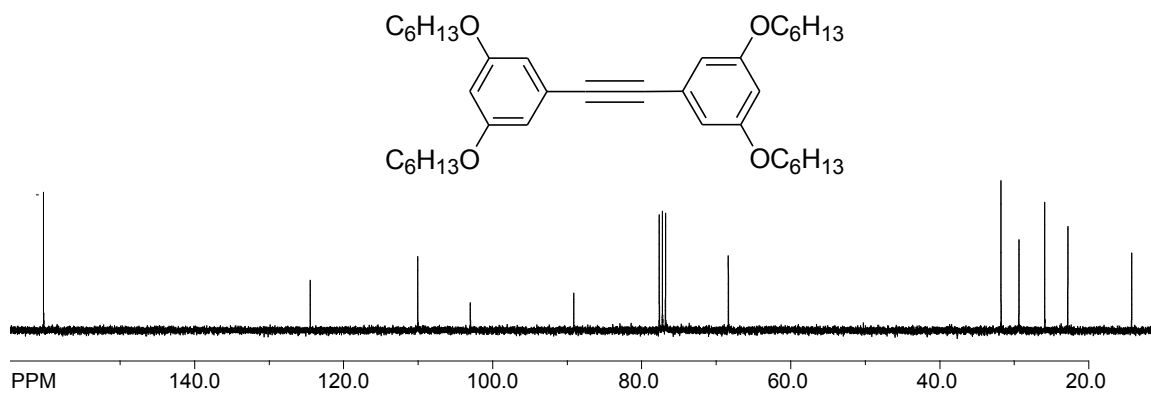


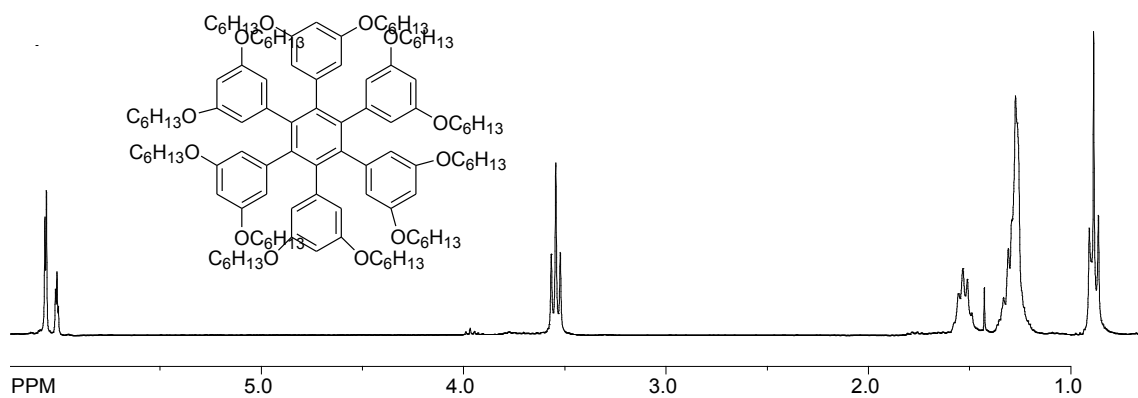
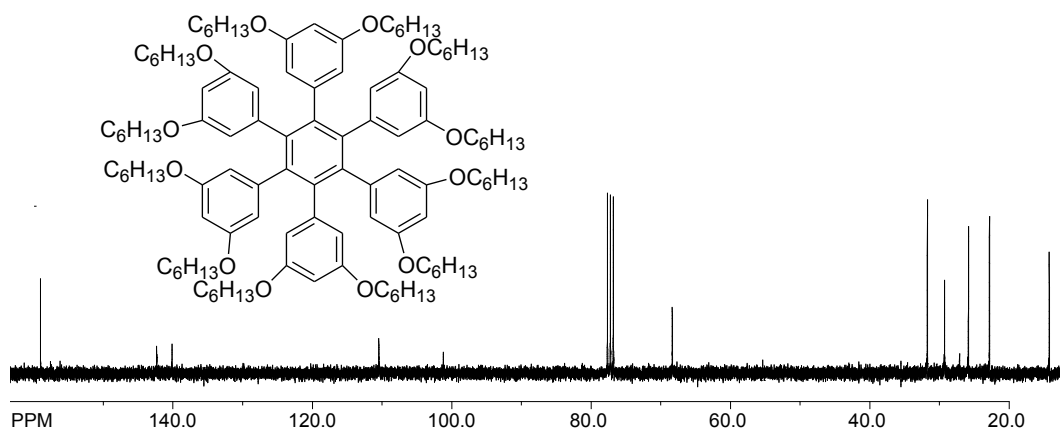
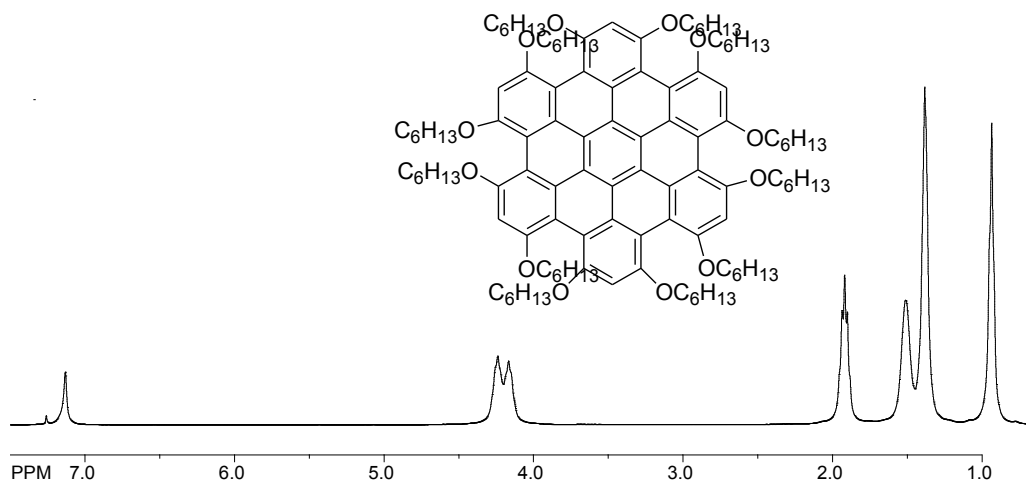
^{13}C NMR spectrum of 3,5-dihexyloxybromobenzene

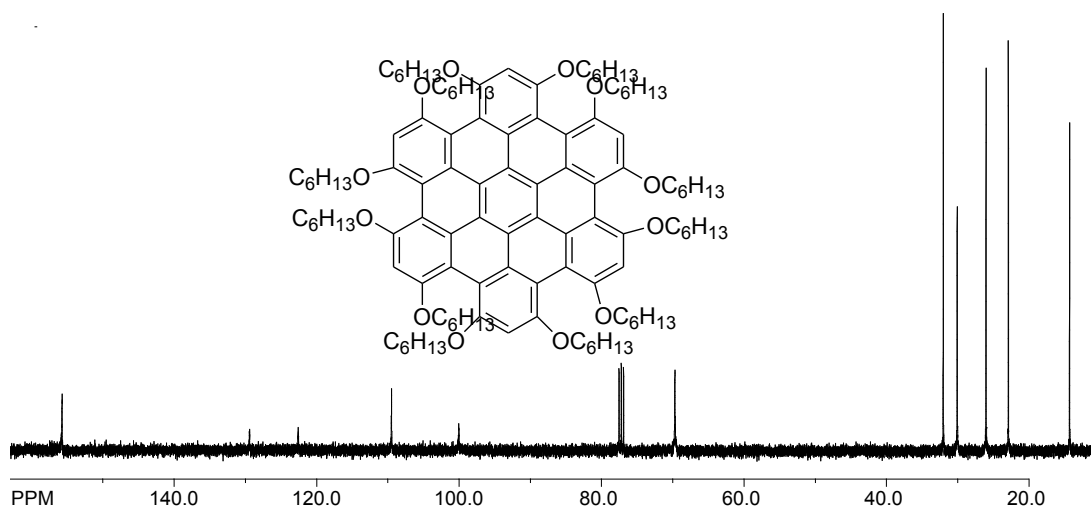
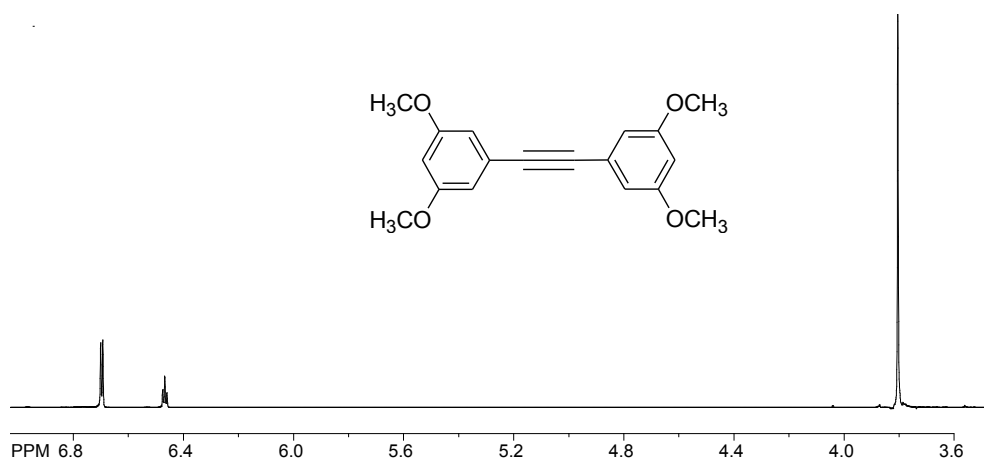
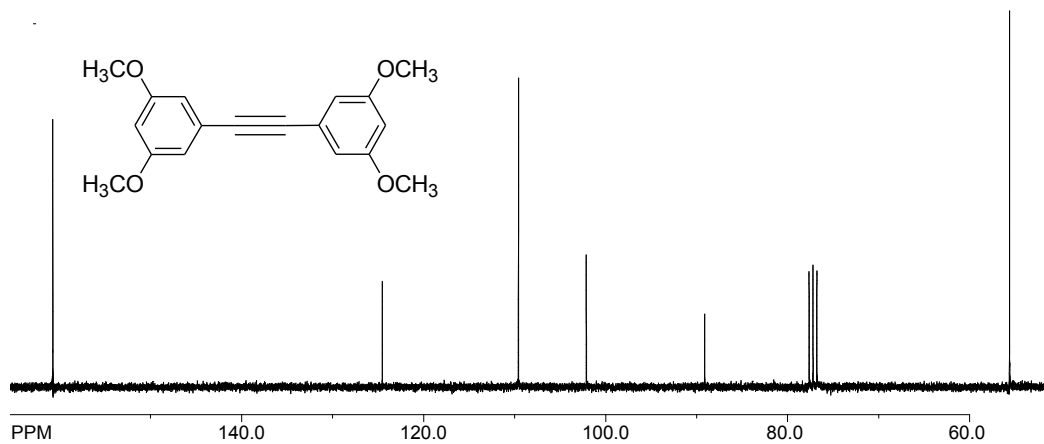


^1H NMR spectrum of 3,5-dihexyloxyiodobenzene

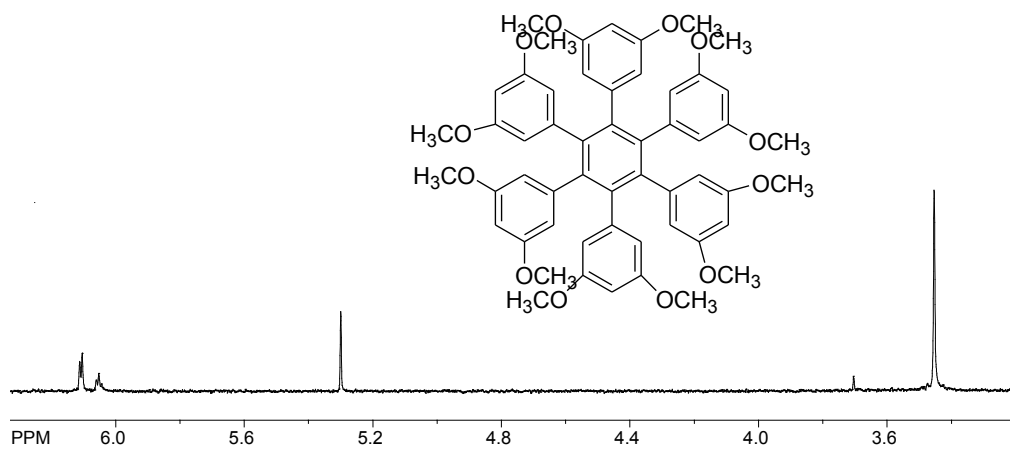


^{13}C NMR spectrum of 3,5-dihexyloxyiodobenzene ^1H NMR spectrum of bis-(3,5-dihexyloxyphenyl)acetylene ^{13}C NMR spectrum of bis-(3,5-dihexyloxyphenyl)acetylene

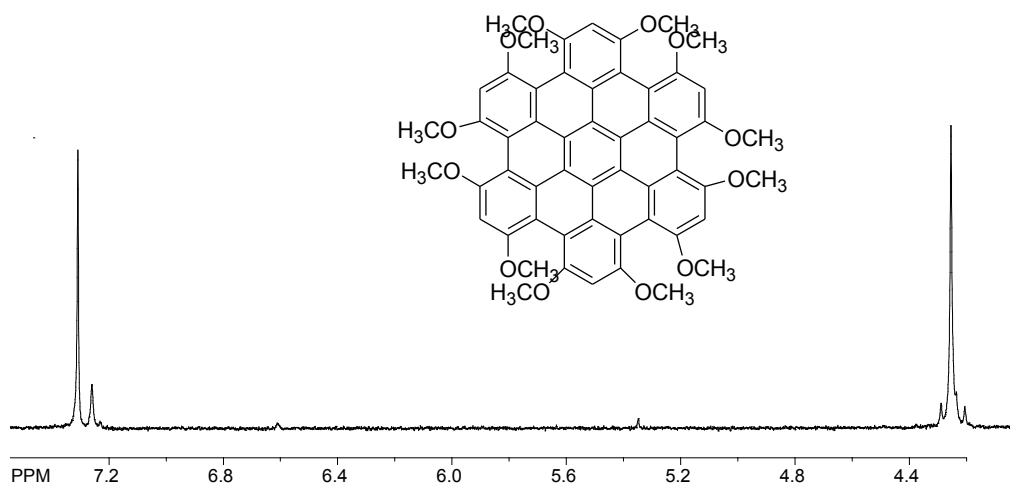
¹H NMR spectrum of hexakis(3,5-dihexyloxyphenyl)benzene¹³C NMR spectrum of hexakis(3,5-dihexyloxyphenyl)benzene¹H NMR spectrum of hexakis-3,5-dihexyloxy-hexa-peri-hexabenzocoronene

^{13}C NMR spectrum of hexakis-3,5-dihexyloxy-hexa-peri-hexabenzocoronene ^1H NMR spectrum of bis-(3,5-dimethoxyphenyl)acetylene ^{13}C NMR spectrum of bis-(3,5-dimethoxyphenyl)acetylene

^1H NMR spectrum of hexakis(3,5-dimethoxyphenyl)benzene



^1H NMR spectrum of hexakis-3,5-dimethoxy-hexa-peri-hexabenzocoronene



CHAPTER 2C

Dodecaalkoxy-hexa-*peri*-hexabenzocoronene: A Non-Planar PAH with Six Easily Accessible Oxidation States

Introduction

The design and synthesis of new and unique polycyclic aromatic hydrocarbons (PAHs)¹ have attracted increasing attention owing their unique electronic and optical properties and potential applications in the emerging areas of molecular electronics and nanotechnology. Among various PAHs, graphitic hexa-*peri*-hexabenzocoronenes (HBCs) and their derivatives are especially important because of their disc-shape structures which not only allows them to function as efficient charge carriers in bulk materials but also as liquid crystalline materials due to their efficient columnar packing.² Although, we and others^{3,4} continue to design and synthesize a variety of extended variants of parent HBC to hone their unique optoelectronic properties, the simplest of the alkoxy substituted derivatives of parent HBC are largely unexplored. It is noted that a decoration of the periphery of HBC core by alkoxy substituents is expected to lower its redox potential considerably as compared to the corresponding alkyl substituted HBCs,⁴ i.e. Structures **A** and **B**.

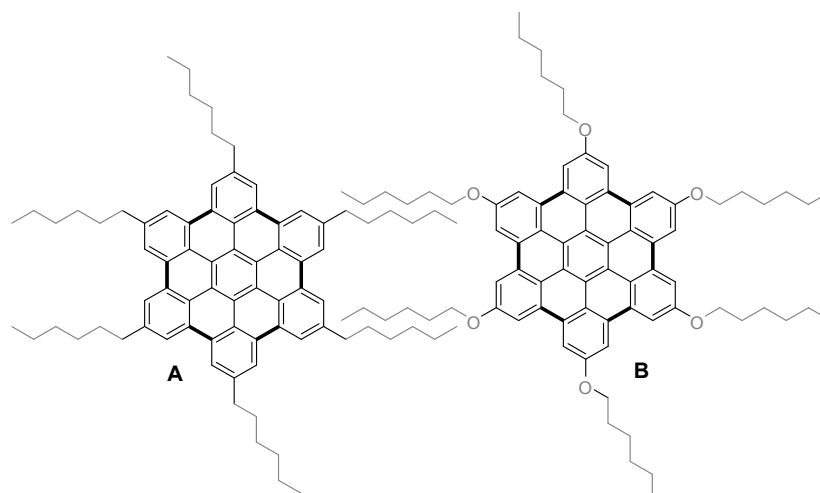


Figure 1A. Structures of **A** and **B**

As described in the previous chapter, we have recently synthesized hexaalkoxy-HBC (structure **B**) by an alternative route as it could not be accessed by a simple oxidative cyclodehydrogenation of the corresponding *hexakis*(4-alkoxyphenyl)benzene.^{4c} Interestingly, owing to the extensive aggregation of **B** in solution, its cyclic voltammogram was rather ill defined (see Experimental Section), however, these preliminary electrochemical data suggested that **B** undergoes an oxidation at relatively low potential ($E_{\text{ox}} \sim 0.6$ V vs SCE) as compared to the corresponding hexaalkyl-HBC (structure **A**, $E_{\text{ox}} \sim 1.0$ V vs SCE).^{4b}

Continued need for electron-rich organic donors for the preparation of conducting materials, often termed as organic metals,⁵ for the potential photovoltaic applications⁶ prompted us to search for an electrochemically well-behaved alkoxy-substituted HBCs, such as structures **C** and **D** (Figure 1). The molecular structures of **C** and **D** with methoxy substituents were calculated by DFT methods at B3LYP-6/31G* level and are also shown in Figure 1. As expected the structures of **C** and **D** are nonplanar due to the presence of *peri* substituents. Furthermore, a comparison of the structure of the

permethoxy derivative **C**, which has recently been prepared by Mullen and coworkers,⁷ with dodecamethoxy derivative **D** showed that (i) **C** is much more distorted from the planarity as compared to **D** and (ii) the methoxy groups in **C** lie above and below the aromatic plane while in **D** they lie in the aromatic plane (see Figure 1). It should be noted that out of plane methoxy groups do not stabilize a cationic hole on a aromatic ring as effectively as the methoxy groups which lie in aromatic plane, e.g. structures **E** and **F**.⁸

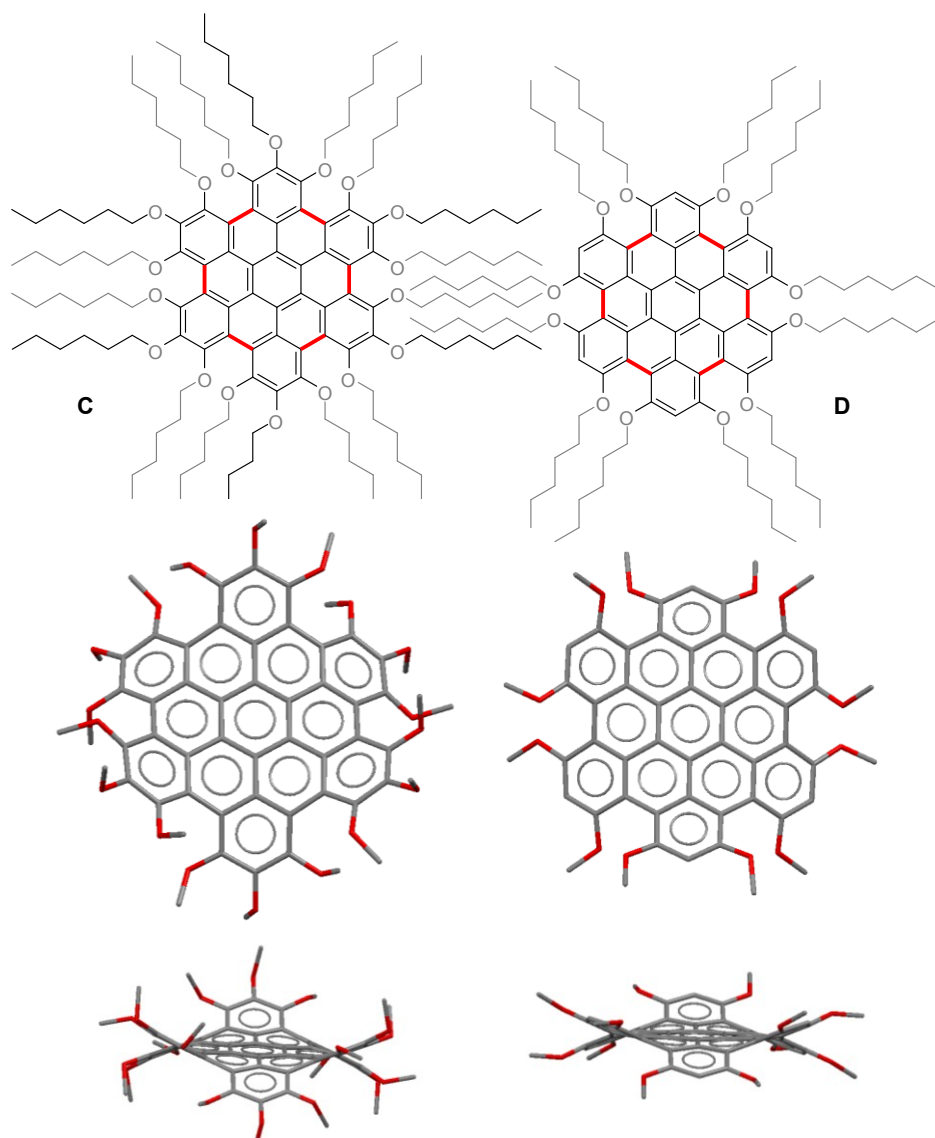
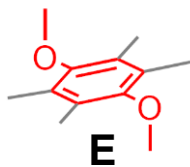
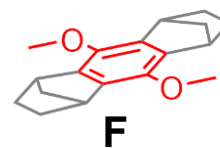


Figure 1B. The molecular structures of non-planar alkoxy substituted HBCs **C** and **D** obtained by DFT calculations at B3LYP/6-31G* level.



E_{ox} (vs SCE) 1.46 V



1.14 V

It is further noted that hydroquinone ether **F** not only undergoes a reversible electrochemical oxidation but forms a highly robust cation-radical salt which has been isolated and characterized crystallographically.⁹ In contrast, however, the hydroquinone ether **E** is irreversibly oxidized at relatively higher potential and its cation radical is highly transient even at $-90\text{ }^{\circ}\text{C}$.⁸

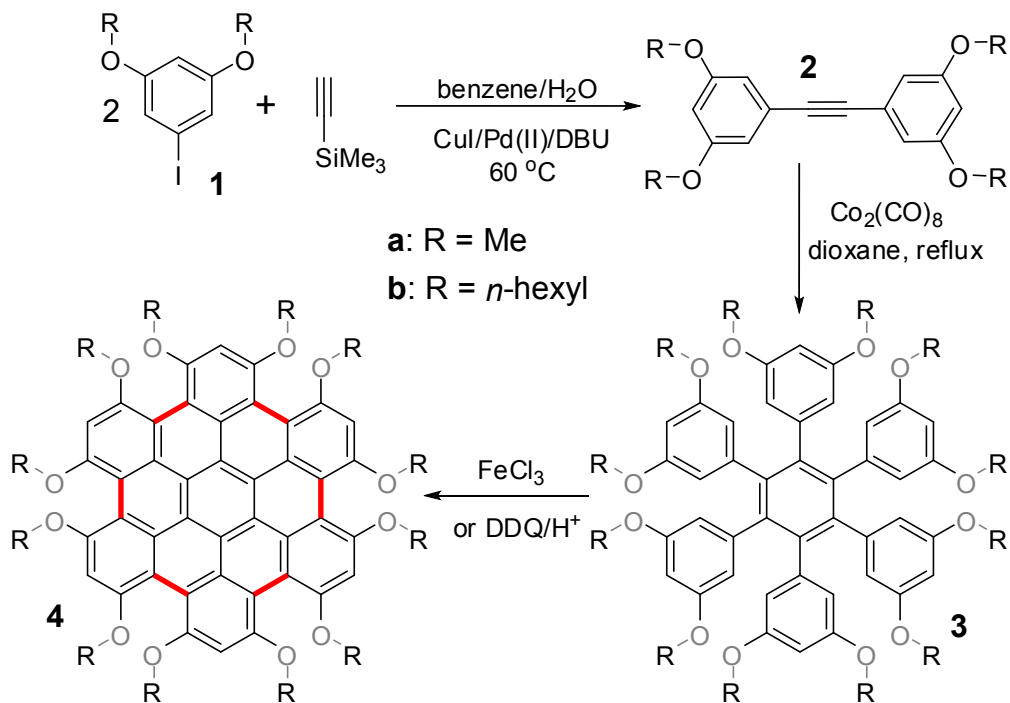
Taking in account the structural considerations discussed above, led us to synthesize the dodecalcoxy-HBC (**D**) and demonstrate with the aid of electrochemistry and optical spectroscopy that it undergoes six reversible electrochemical oxidations in a potential range that spans $\sim 0.9\text{ V}$ (i.e. 0.45 to 1.34 V). Approximately an equal separation ($\sim 195 \pm 35\text{ mV}$) between the oxidation potentials for the six oxidation states of dodecalcoxy-HBC (**D**) allows the generation of its mono, di, tri and tetracationic salts using readily available aromatic cation-radical salts as oxidants. Moreover, the remarkable lowering of the redox potential of dodecalcoxy-HBC in comparison to other alkyl-substituted HBCs, as well as the high stability of its (poly)cationic salts is attributed to its highly strained structure which was established by X-ray crystallography. The preliminary details of these findings are described herein.

Results and Discussion

Synthesis of Dodecalkoxy-HBCs.

Initially, we prepared bright orange-colored dodecamethoxy-HBC **4a** by a smooth oxidative cyclodehydrogenation of *hexakis*(3,5-dimethoxyphenyl)benzene (**3a**) using either FeCl₃ or DDQ/CH₃SO₃H in dichloromethane in nearly quantitative yield. The synthesis of required hexaarylbenzene derivative **3a** was accomplished via a standard three-step route (see Scheme 1). Thus, **3a** was obtained by a Co₂(CO)₈-catalyzed trimerization of bis(3,5-dimethoxyphenyl)acetylene (**2a**) in refluxing dioxane, which in turn was prepared from a modified Sonogashira coupling¹⁰ of the readily available 3,5-dimethoxyiodobenzene (**1a**).

Scheme 1. Synthesis of dodecamethoxy and dodecahexyloxy HBCs **4a** and **4b**.



The dodecamethoxy-HBC **4a** was sparingly soluble in dichloromethane and chloroform and therefore a readily soluble dodecahexyloxy-HBC **4b** was also prepared

using the similar procedures to those employed for the preparation of **4a** (see the Experimental section). Various hitherto unknown molecules in Scheme 1 were characterized by $^1\text{H}/^{13}\text{C}$ NMR spectroscopy and the structures of the methoxy-substituted hexaarylbenzene **3a** and HBC **4a** were further confirmed by X-ray crystallography as follows.

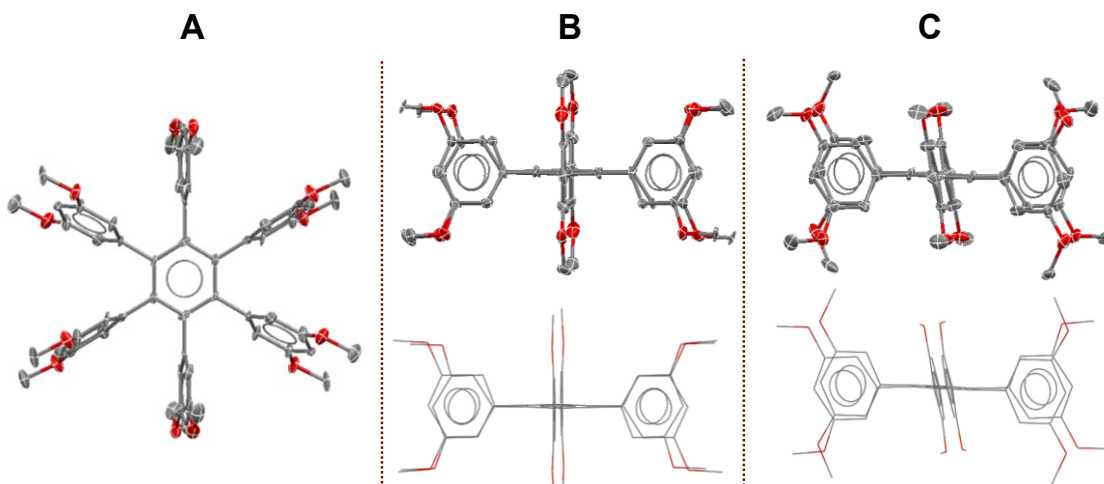


Figure 2. (A) The molecular structure of **3a** shown as ORTEP diagram (thermal ellipsoids drawn in 50% probability). (B)/(C) Two views showing that one pair of 3,5-dimethoxyphenyls (with syn oriented methoxy groups) lie at a dihedral angle of $\sim 89.4^\circ$ relative to central phenyl ring (middle) while the other two pairs of 3,5-dimethoxyphenyls (with anti oriented methoxy groups) lie at the dihedral angles of 74.6° and 72.7° .

X-ray Crystallography of Hexaarylbenzene **3a** and Dodecamethoxy-HBC **4a**.

The molecular structure of hexaarylbenzene **3a**, obtained by X-ray crystallography, is shown in Figure 2a. Generally, the aryl groups forming the propeller in various hexaarylbenzene derivatives are turned in the same direction with dihedral angles with central phenyl rings varying in the range of $60\text{--}80^\circ$. Interestingly, however, in **3a** a pair of 3,5-dimethoxyphenyl rings (with sin-oriented methoxy groups) at the para positions of central phenyl ring lie perpendicular relative the central phenyl ring (dihedral

angle 89.4°) while the two other pairs of 3,5-dimethoxyphenyl rings (with anti-oriented methoxy groups) form the expected dihedral angles of 74.6° and 72.7° with central phenyl ring. This unusual arrangement of the 3,5-dimethoxyphenyl rings around the central phenyl group in **3a**, i.e. one pair of rings are turned in one direction while another pair in the opposite direction and yet the remaining third pair of aryl rings lie perpendicular to the central phenyl ring, may, in part, arise due to the complex packing forces. The complex C-H \cdots O/C-H \cdots π networks indeed control the packing of **3a** in its crystals,¹¹ unfortunately; however, a single factor responsible for this unusual (intermediate) conformation could not be identified. One may be tempted to conjecture that the observed conformation of **3a** in its crystals represents an intermediate conformation as a transition state between the two propellers turned in opposite direction.

The molecular of highly crystalline dodecamethoxy-HBC **4a** was determined by X-ray crystallography and an ORTEP diagram of its structure is shown in Figure 3. The molecules of **4a** in the crystals found to be highly symmetric (crystallographic special position of symmetry -3) and are distorted from the planarity. Although the central benzene ring in **4a** is essentially planar, the outer rings are alternatively bent up and down from the mean plane by $\sim 21^\circ$ to avoid severe steric interactions between the meta-methoxy substituents. The significantly non-planar peripheral benzenoid rings in **4a** are arranged in a sofa-like conformation with deviation from planarity of $\sim 15^\circ$, i.e. atom C₁₁, indicated by an arrow in Figure 3A, deviates from the mean plane of the molecule by 15.3° . The obvious cause of the severe distortions from planarity in **4a** lies in the very short O \cdots O intramolecular contacts (2.57 \AA instead of 3.0 \AA). As a result, the oxygens deviate 0.16 and 0.19 \AA from the plane of the adjacent ring. One may conjecture that the

oxidation of **4a** to its cation radical or to another higher oxidation state may significantly relieve the strain energy associated with the distortion of **4a**, i.e. less pi-electrons in oxidized state and therefore less reduction in the conjugation energy).

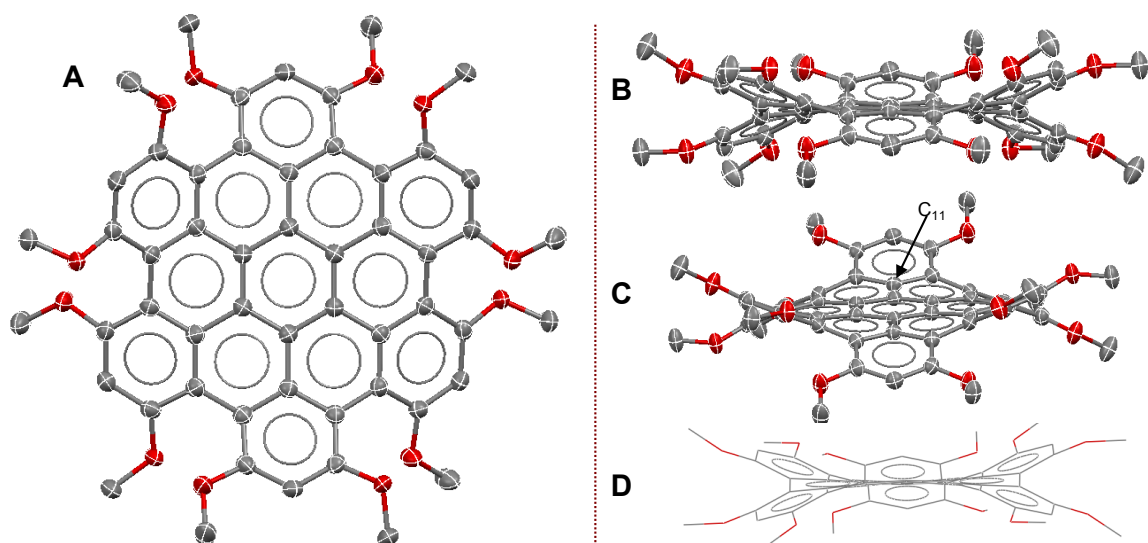


Figure 3. (A) The molecular structure of **4a** shown as ORTEP diagram (thermal ellipsoids drawn in 50% probability). (B)/(C)/(D) Three views showing the distortion of the HBC core from mean plane of the molecule.

Variable Temperature ¹H NMR Spectroscopy of Dodecaalkoxy-HBC **4b**.

Figure 4 shows the ¹H NMR spectra of **4b** at variable temperatures from 20-60 °C. At 20 °C temperature the ¹H NMR spectrum shows two signals at ~ 4.1 ppm due to the protons of the alkoxy methylenes and the splitting most likely occurs due to the slow flipping of the sofa like conformation of **4a** (see Figure 3). When the temperature increases the flipping rate becomes faster than the NMR detection time scale and the signals merge into one peak at 60 °C.

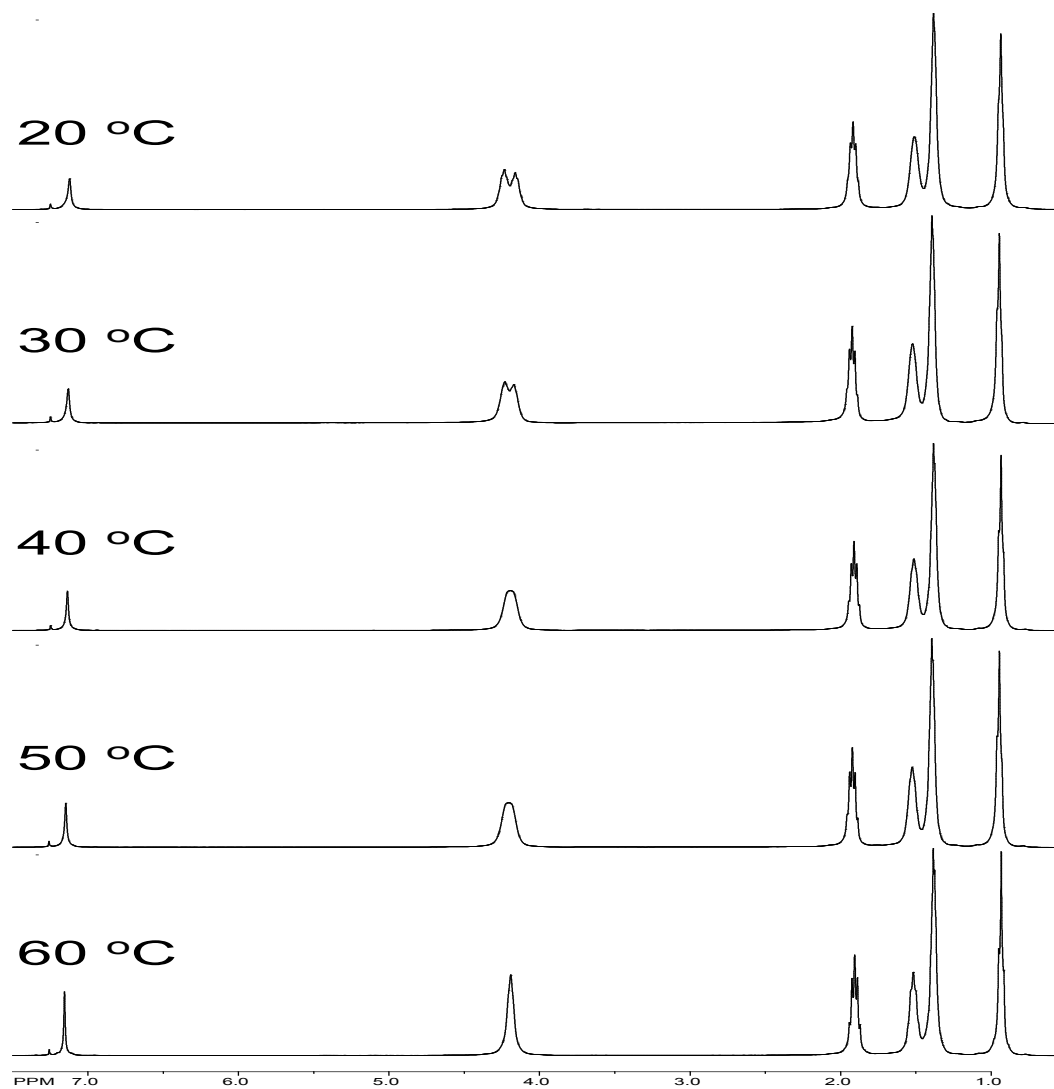


Figure 4. Comparison of variable temperature ^1H NMR spectra of **4a** in CDCl_3 recorded at 20, 30, 40, 50, and 60 °C. Temperatures are indicated on the spectra. Also, as shown in Figure 5, a number of ^{13}C signals (at δ : 14.30, 22.89, 25.99, 30.03, 32.04, 69.78, 100.02, 109.49, 155.72 ppm) sharpen considerably at 60 °C possibly due to increased rate of interconversion of between two alternate sofa conformations of HBC **4a**.

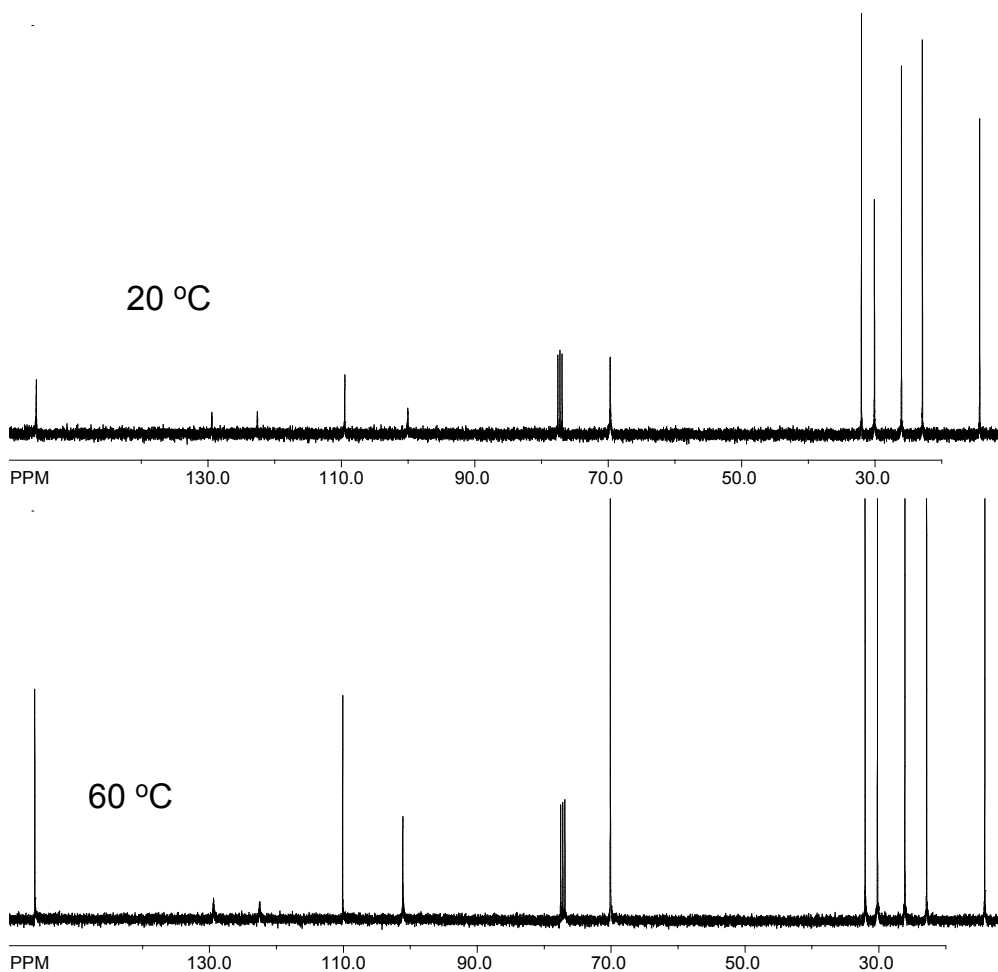


Figure 5. Comparison of the ¹³C NMR spectra of **4b** in CDCl₃ recorded at 20 and 60 °C. Temperatures are indicated on the spectra.

Electrochemical Oxidation (or Cyclic Voltammetry) of HBCs **4a and **4b**.**

The cyclic voltammogram of sparingly-soluble dodecamethoxy-HBC **4a** as a 0.1 mM solution in anhydrous dichloromethane containing 0.1 M tetra-*n*-butylammonium hexafluorophosphate (*n*-Bu₄NPF₆) as the supporting electrolyte was recorded in at a scan rate of 200 mV s⁻¹ and at 20 °C and is displayed in Figure 6. Although, **4a** showed

multiple oxidation waves, they were heavily distorted owing to the adsorption at the electrode.

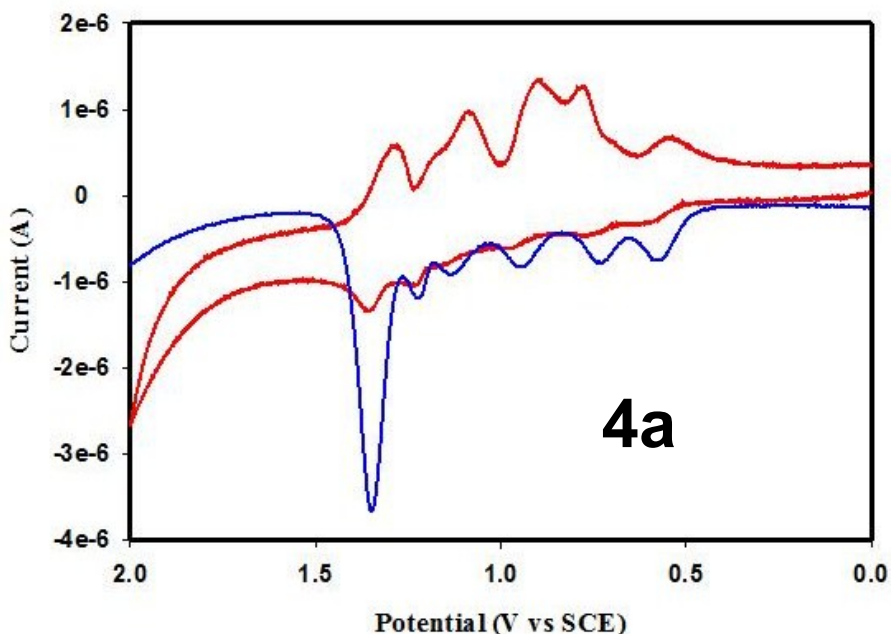


Figure 6. Cyclic (red curve) and square-wave (blue curve) voltamograms of a 0.18 mM solution of **4a** in CH_2Cl_2 containing 0.1 M $n\text{-Bu}_4\text{NPF}_6$ as the supporting electrolyte at a scan rate of 200 mV s^{-1} and at 20°C .

In contrast, however, the readily soluble hexahexyloxy-HBC **4b** in Figure 7, under otherwise identical conditions as **4a**, showed six well-defined reversible oxidation waves. The calibration of the CV peaks with added ferrocene as an internal standard showed that **4b** undergoes sequential ejection of six electron at the potentials of 0.45, 0.61, 0.84, 1.02, 1.18, 1.34 V vs SCE (Figure 7). Moreover, the ejection of each successive electron after the formation of $\mathbf{4b}^{+\bullet}$ (by loss of first electron at 0.45 V) occurs at potentials which increase by ~ 160 to 230 mV between various oxidation states (see Figure 7). The remarkable lowering of the first oxidation potential of **4b** and observation of six highly reversible oxidation waves suggests that removal of electrons from **4b** must provide efficient release of steric strain. For example, it is expected that loss of multiple

pi-electrons (i.e. up to 6 electrons) in hexacationic **4b** must make up to some extent for the loss of conjugation energy due to its heavy distortion from planarity.

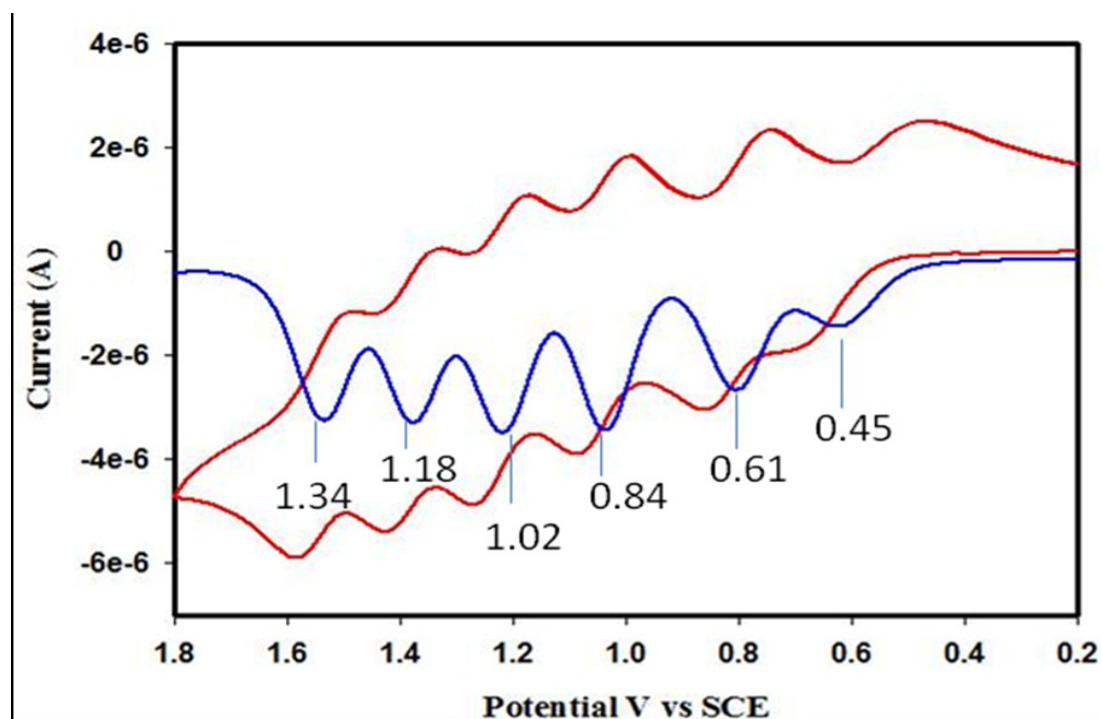


Figure 7. Cyclic (red curve) and square-wave (blue curve) voltammograms of a 1 mM solution of **4b** in CH_2Cl_2 containing 0.1 M $n\text{-Bu}_4\text{NPF}_6$ as the supporting electrolyte at a scan rate of 200 mV s^{-1} and at 20°C . The E_{ox} values of **4b** were referenced to ferrocene ($E_{\text{ox}} = 0.45 \text{ V vs. SCE}$) as an added internal standard.

Chemical oxidation of hexhexyloxy-HBC **4b** with Magic blue (MB^{++}).

Thus, Figure 8 shows the spectral changes observed upon the reduction of $3.6 \times 10^{-5} \text{ M}$ solution of MB^{++} [*tris*(4-bromophenylamminium hexachloroantimonate)]¹² by an incremental addition of substoichiometric amounts of $5.3 \times 10^{-4} \text{ M}$ solution of **4b** in dichloromethane at 22°C . Upon the addition of 0.25 equivalents **4b** to the solution of MB^{++} , the absorbance due to MB^{++} (monitored at 728 nm) completely disappeared while

the new absorption bands at 513 and 813 nm grew in. As such the observed 1:0.25 stoichiometry of $\text{MB}^{+\bullet}$: **4b** suggests that **4b** is oxidized to its tetracation (i.e. 4b^{+4}), i.e. eq 1 in Scheme 2.

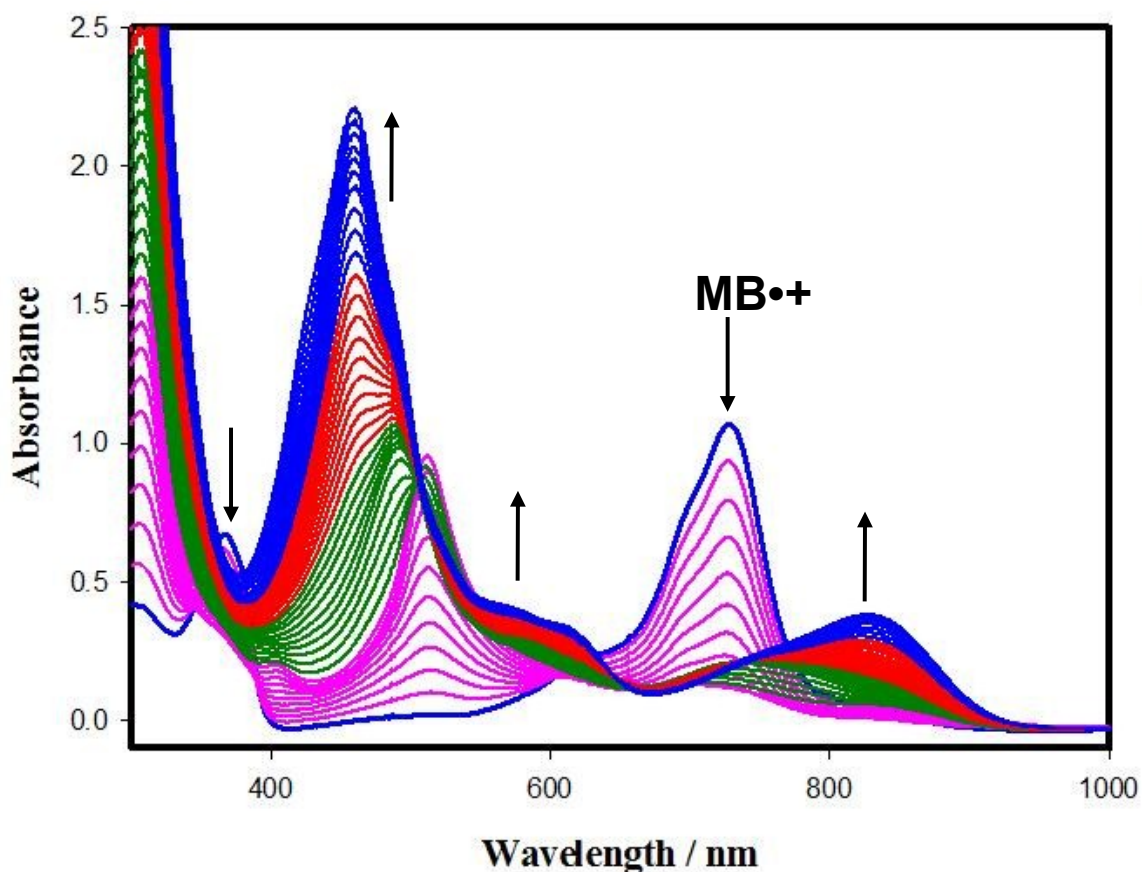
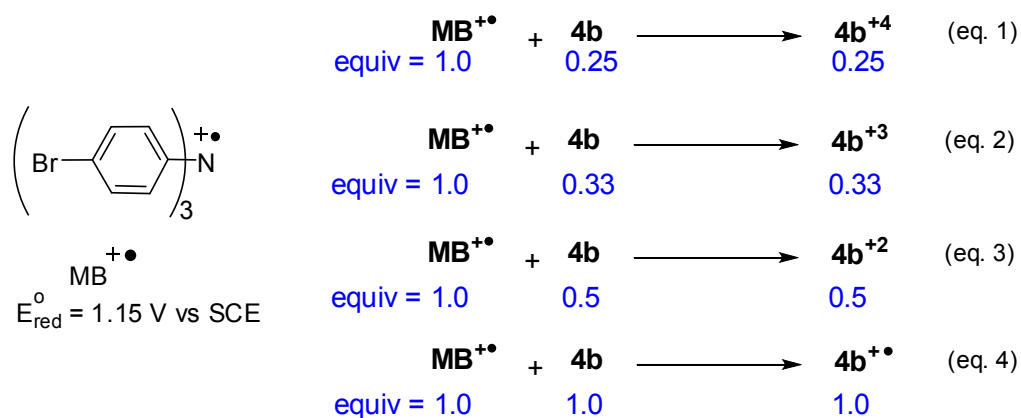


Figure 8: Spectral changes upon the reduction of 3.6×10^{-5} M $\text{MB}^{+\bullet}$ by an incremental addition of 5.3×10^{-4} M **4b** in CH_2Cl_2 at 22 °C. The coloring scheme in the above Figure is as follows: addition of 0 to 0.25 equiv of **4b** (pink spectra); addition of 0.25 to 0.5 equiv of **4b** (green spectra); addition of 0.5 to 0.75 equiv of **4b** (red spectra); addition of 0.75 to 1.0 equiv of **4b** (blue spectra)

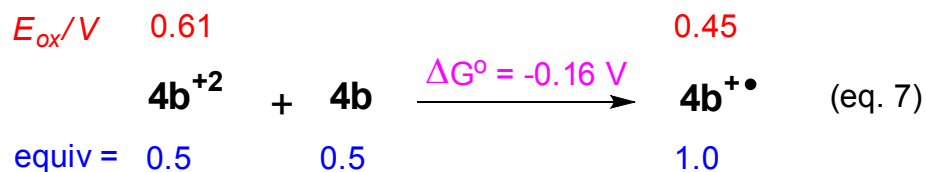
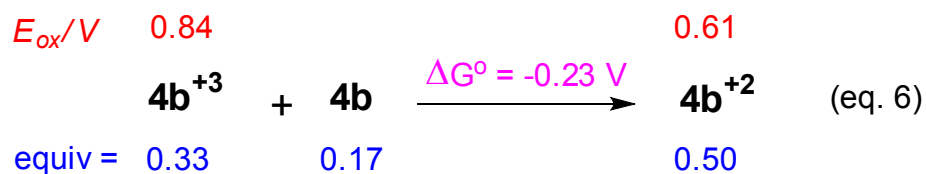
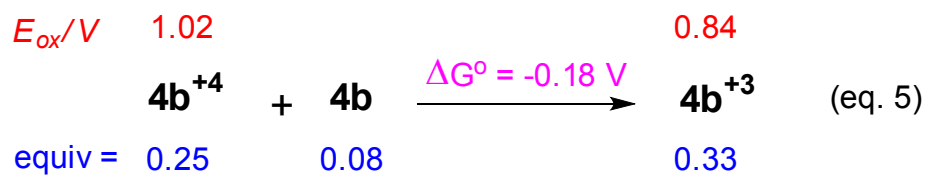
Interestingly, the continued addition of HBC **4b**, beyond 0.25 equivalent, i.e. up to 1 full equivalent, led to a series of spectral changes with well-defined isosbestic points and thereby suggesting that initially formed tetracationic 4b^{+4} is being converted to

tricationic $4b^{+3}$, dicationic $4b^{+2}$, and finally to cation radical $4b^{+\bullet}$ via disproportionation as depicted below in Scheme 2.

Scheme 2. Disproportionation of $4b^{+4}$ to tricationic $4b^{+3}$, dicationic $4b^{+2}$, and finally to cation radical $4b^{+\bullet}$ upon continued incremental addition of neutral $4b$ to a solution of $MB^{+\bullet}$ (see Figure 8).



According to Scheme 2, after the addition of 0.25, 0.33, 0.5, and 1.0 equivalent of $4b$ to a solution of oxidant $MB^{+\bullet}$ should produce the tetracationic $4b^{+4}$, tricationic $4b^{+3}$, dicationic $4b^{+2}$, and finally the cation radical $4b^{+\bullet}$, owing to fact that difference between the oxidation potentials of various oxidation states of $4b$ are ≥ 160 mV. Such a large difference potential of various oxidation states ensures that the disproportionation equilibria lie completely to right, i.e. eqs 5-7.



Indeed, the spectra extracted after the addition of 0.25, 0.33, 0.5, and 1.0 equiv of **4b** to a solution of oxidant **MB⁺** produces the characteristic absorption spectra shown in Figure 9 and are tentatively assigned to the tetracationic **4b⁺⁴**, tricationic **4b⁺³**, dicationic **4b⁺²**, and finally the cation radical **4b^{+•}**, respectively. It is noted that we have not yet attempted the generation of penta- and hexacation of **4b** which should be possible using a more potent oxidant such as $\text{NO}^+ \text{SbCl}_6^-$. We are in the process of growing crystals of cation radical **4b^{+•}** as well as various polycationic salts for X-ray crystallographic characterization.

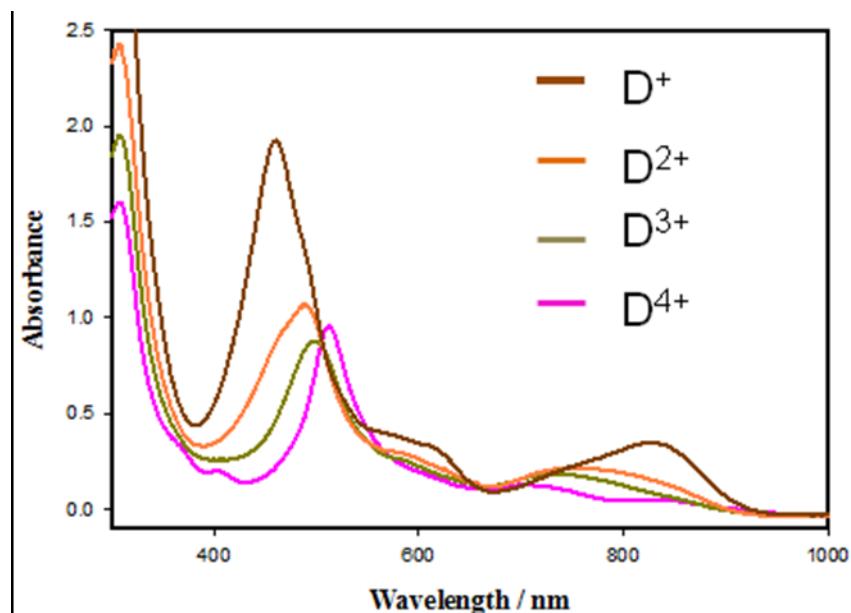


Figure 9. The UV-vis absorption spectra of tetracationic $4b^{+4}$, tricationic $4b^{+3}$, dicationic $4b^{+2}$, and finally the cation radical $4b^{+\bullet}$, produced upon treatment of a solution of MB^{+} to 0.25, 0.33, 0.50, and 1.00 equivalents of $4b$, respectively, in CH_2Cl_2 at 22 °C.

Optical Properties of of hexhexyloxy-HBC $4b$.

The UV-vis absorption spectrum of the neutral $4b$ in Figure 10A showed that it contained a highly structured absorption bands with various absorption bands centered at 285, 315, 425, 464, and 495 nm. A quantitative measure of the absorption spectra of $4b$ showed that it had a very high molar absorptivity, i.e. $\epsilon_{425} = 1.38 \times 10^5 \text{ M}^{-1} \text{ cm}^{-1}$ in CH_2Cl_2 . Figure 10B shows the emission spectrum of the $4b$ which was characteristically similar to other alkyl-substituted HBCs.

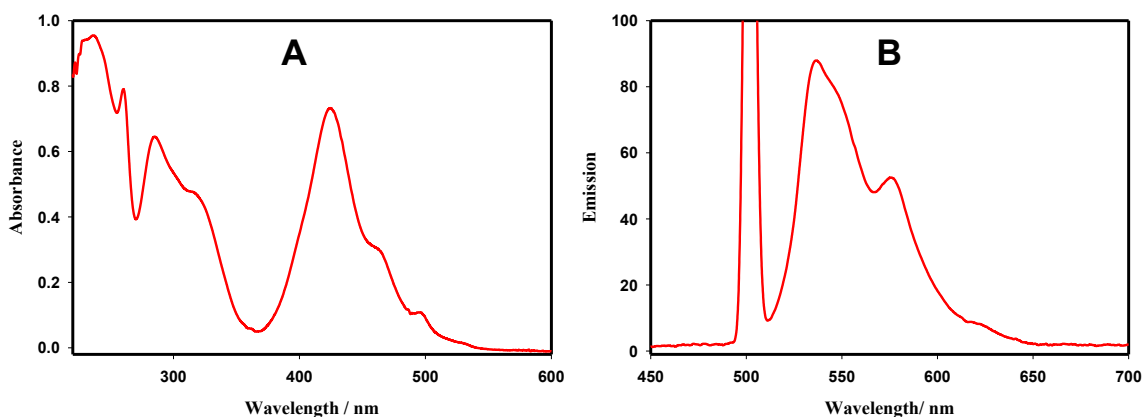


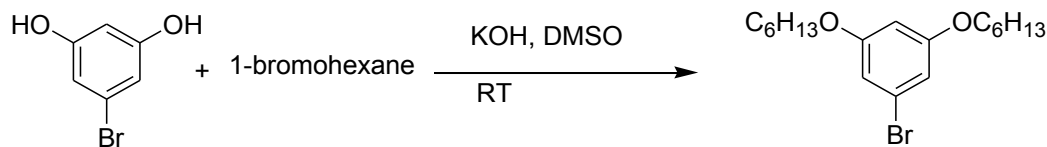
Figure 10. **A.** UV-vis absorption spectrum of neutral **4b** ($\lambda_{\text{max}} = 285, 315, 425, 464,$ and 495 nm; $\epsilon_{425} = 4.1 \times 10^5 \text{ M}^{-1} \text{ cm}^{-1}$) in CH_2Cl_2 . **B.** Emission spectrum of the **4b** in dichloromethane at 22°C .

Summery and Conclusion.

We have successfully synthesized a highly soluble derivative of dodecaloxy-HBC **4b** and demonstrated with the aid of cyclic voltammetry that it ejects up to six electrons reversibly. Moreover, owing the large potential difference (≥ 160 mV) between various oxidation states of **4b**, it allows the preparation of each oxidation state in pure form, as demonstrated by spectral characterization of the tetracationic **4b**⁺⁴, tricationic **4b**⁺³, dicationic **4b**⁺², and finally the cation radical **4b**^{+•}. We are actively pursuing the isolation and crystallization of cation radical **4b**^{+•} as well as its polycationic salts for X-ray crystallographic characterization.

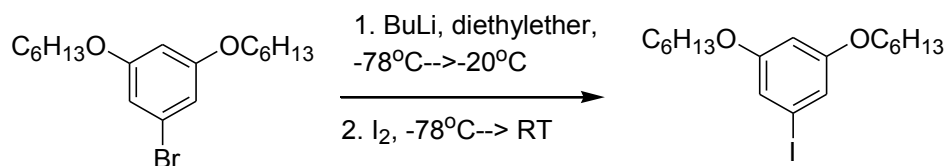
Experimental

Synthesis of 3,5-dihexyloxybromobenzene



KOH (6.0 g, 109 mmol) was suspended in dimethylsulfoxide (50 mL) and 3,5-dihydroxybromobenzene (2.6 g, 13.75 mmol) was added into it and stirred for few minutes. 1-bromohexane (3.8 mL, 27.5 mmol) was added dropwise into the above solution and stirred for 30 minutes and water (50 mL) was added, extracted to dichloromethane, dried over anhydrous MgSO_4 and evaporated to isolate colorless liquid which was used in the next step without further purification. Yield (83%); ^1H NMR (CDCl_3) δ : 0.92 (t, $J = 6.5, 13.4$ Hz, 6H), 1.33-1.53 (m, 12H), 1.76 (qn, 4H), 3.90 (t, $J = 6.5, 13.1$ Hz, 4H), 6.37 (t, $J = 2.0, 4.1$ Hz, 1H), 6.64 (d, $J = 2.2$ Hz, 2H). ^{13}C NMR (CDCl_3) δ : 14.22, 22.72, 25.87, 29.29, 31.74, 68.45, 100.73, 110.37, 123.00, 160.94.

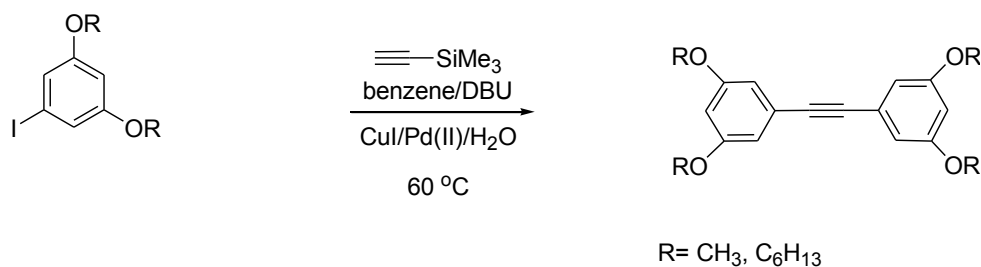
Synthesis of 3,5-dihexyloxyiodobenzene (1b)



3,5-Dihexyloxybromobenzene (3.3 g, 9.2 mmol) was dissolved in anhydrous diethyl ether (30 mL) and cooled it into -78°C under argon atmosphere. Then 2.5 M solution of BuLi in hexane (4.4 mL, 11.08 mmol) was added dropwise to the above solution at -78°C under argon atmosphere. Then the temperature of the reaction mixture

was brought to $-20\text{ }^{\circ}\text{C}$ and stirred for one hour. The reaction mixture was cooled to $-78\text{ }^{\circ}\text{C}$ under argon atmosphere and excess amount of iodine in anhydrous diethyl ether (10 mL) was added dropwise into it and then the temperature of the reaction mixture was brought to room temperature and stirred for 10 minutes. Aqueous NaHSO_3 solution was added and the product was extracted to ether, washed with brine solution, dried over anhydrous MgSO_4 and evaporated to isolate colorless liquid which was purified by column chromatography using hexanes as the eluent. Yield (80%); $^1\text{H NMR}$ (CDCl_3) δ : 0.92 (t, $J = 6.8, 13.5$ Hz, 6H), 1.26-1.50 (m, 12H), 1.75 (qn, 4H), 3.89 (t, $J = 6.5, 13.0$ Hz, 4H), 6.40 (t, $J = 2.1, 4.3$ Hz, 1H), 6.84 (d, $J = 2.2$ Hz, 2H). $^{13}\text{C NMR}$ (CDCl_3) δ : 14.23, 22.81, 25.86, 29.30, 31.73, 68.41, 94.25, 101.59, 116.37, 160.80.

Synthesis of bis(3,5-dialkoxyphenyl)acetylene (2b)

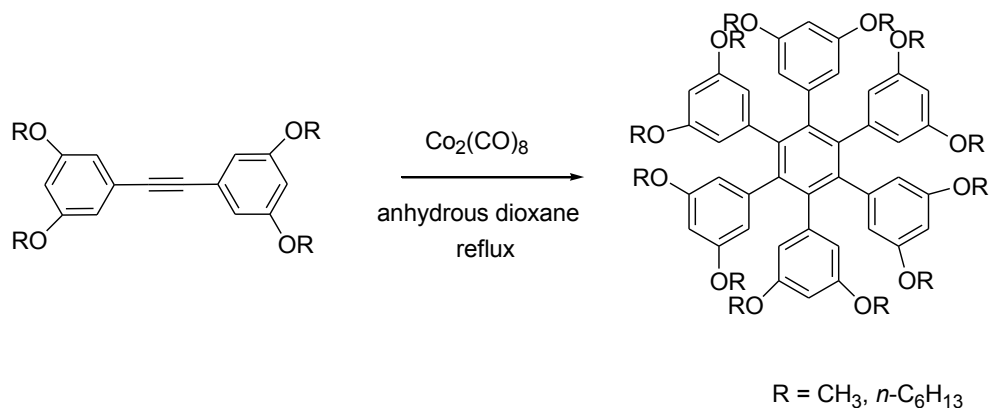


For example, 3,5-dihexyloxyiodobenzene (3.0 g, 7.43 mmol) was dissolved in anhydrous benzene (38 mL) in a Schlenk flask under argon atmosphere. DBU (6.8 mL, 45 mmol), CuI (70 mg, 0.37 mmol, 5% mol) and $\text{Pd}(\text{PPh}_3)_2\text{Cl}_2$ (0.158 g, 0.22 mmol, 3% mol) were added to the flask, and it was evacuated and refilled with argon three times. To this mixture was then added distilled water (0.053 mL, 2.97 mmol, 40 mol %) followed by trimethylsilylacetylene (0.52 mL, 3.72 mmol). The resulting mixture was first stirred for 1 hour at room temperature, and then at $60\text{ }^{\circ}\text{C}$ for 24 hours. The solvent was evaporated under reduced pressure and the dark-colored residue was extracted with

dichloromethane (2 x 25 mL). The dichloromethane layer was dried with anhydrous magnesium sulfate, filtered, and evaporated to afford dark colored syrup. Purification of the product by column chromatography using a 99:1 mixture of hexanes/ethyl acetate as eluent afforded bis(3,5-dihexyloxyphenyl)acetylene (**2b**) as a pale yellow solid. Yield (1.7 g, 71 %); $^1\text{H NMR}$ (CDCl_3) δ : 0.91 (t, 6H), 1.34 (m, 8H), 1.45 (m, 4H), 1.78 (qn, 4H), 3.95 (t, 4H), 6.85 (d, $J = 9.1$ Hz, 4H), 7.42 (d, $J = 9.1$ Hz, 4H). $^{13}\text{C NMR}$ (CDCl_3) δ : 14.26, 22.82, 25.92, 29.39, 31.79, 68.27, 88.15, 114.69, 115.69, 133.04, 159.17.

Using the same procedure as above the methoxy substituted bis(3,5-dimethoxyphenyl)acetylene (**2a**) was prepared from 3,5-dimethoxyiodobenzene. Yield (80 %); $^1\text{H NMR}$ (CDCl_3) δ : 3.81 (s, 12H), 6.47 (t, $J = 2.35, 4.68$ Hz, 2H), 6.70 (d, $J = 2.35$ Hz, 2H). $^{13}\text{C NMR}$ (CDCl_3) δ : 55.63, 89.13, 102.13, 109.58, 124.55, 160.74.

Preparation of hexakis(3,5-dialkoxyphenyl)benzene (**3a** and **3b**)



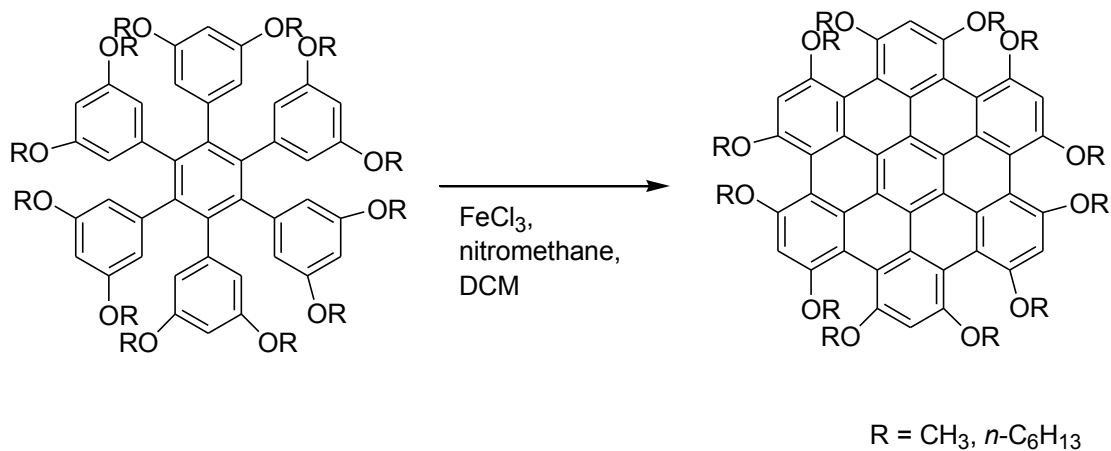
For example, bis(3,5-dihexyloxyphenyl)acetylene (1.4 g, 2.4 mmol) was dissolved in anhydrous dioxane (50 mL) in an oven dried Schlenk flask under an argon atmosphere and the flask was evacuated and filled with argon repeatedly (3x). Then, $\text{Co}_2(\text{CO})_8$ (80 mg) was added to the flask under an argon atmosphere and the flask was

evacuated and filled with argon again (3x). The resulting mixture was refluxed for 14 h and the dioxane was evaporated. The resulting residue was dissolved in dichloromethane and filtered through a short pad of silica gel. Evaporation of the solvent afforded a dark colored solid which was purified by column chromatography using a mixture of hexane: ethyl acetate (99 : 1) as the eluent to yield *hexakis(3,5-dihexyloxyphenyl)benzene* (**3b**) as a yellow liquid.

Hexakis(3,5-dihexyloxyphenyl)benzene (3b): Yield (1.2 g, 85 %); $^1\text{H NMR}$ (CDCl_3) δ : 0.89 (t, $J = 6.5$, 13.6 Hz, 36H), 1.27 (m, 72H), 1.53 (m, 24H), 3.55 (t, $J = 6.7$, 13.4 Hz, 24H), 6.01 (t, $J = 2.2$, 4.4 Hz, 6H), 6.06 (d, $J = 2.2$ Hz, 12H). $^{13}\text{C NMR}$ (CDCl_3) δ : 14.23, 22.79, 25.83, 29.30, 31.73, 68.32, 101.18, 110.45, 140.14, 142.34, 158.99.

Hexakis(3,5-dimethoxyphenyl)benzene (3a): Yield (85 %); $^1\text{H NMR}$ (CDCl_3) δ : 3.45 (s, 36H), 6.05 (t, $J = 2.4$, 5.0 Hz, 6H), 6.11 (d, $J = 2.2$ Hz, 12H). $^{13}\text{C NMR}$ (CD_2Cl_2) δ : 55.47, 98.69, 109.75, 139.97, 142.46, 159.50.

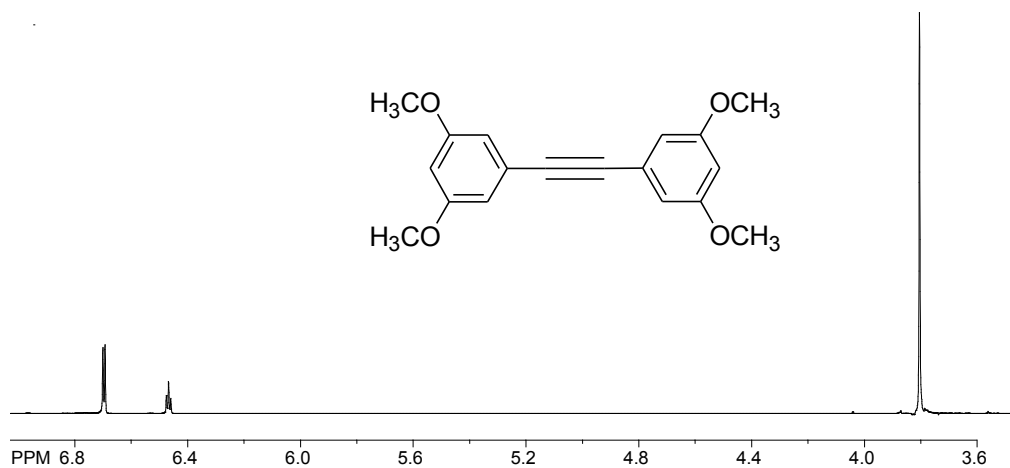
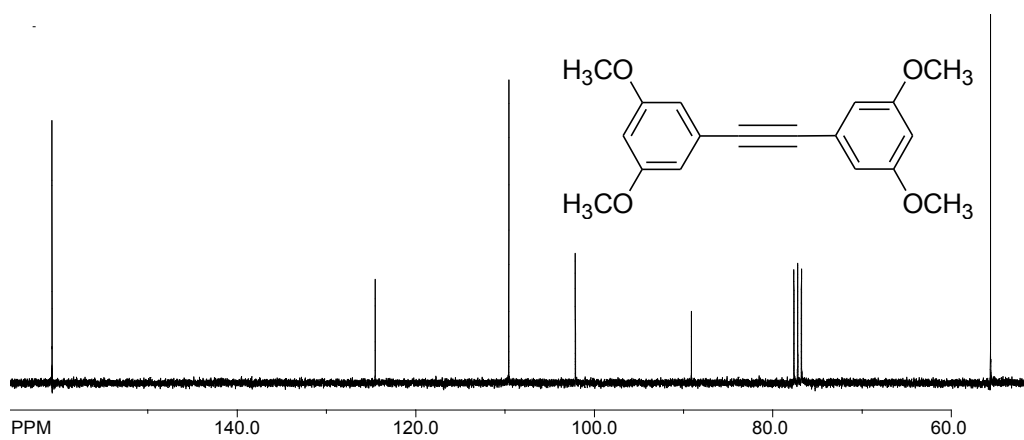
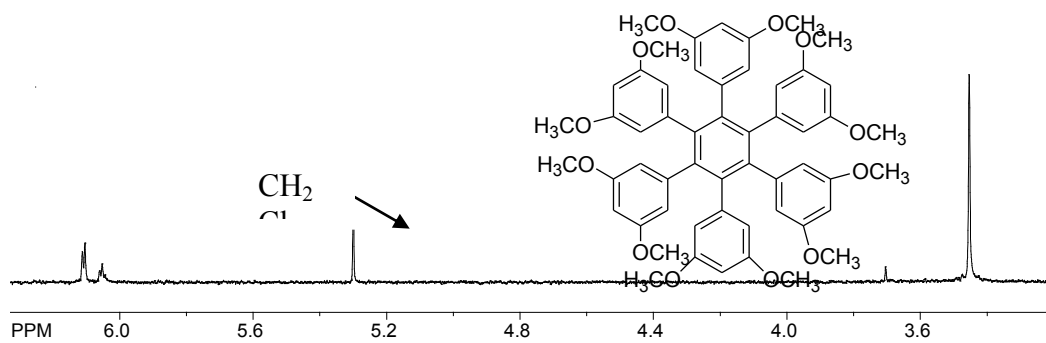
Oxidative cyclodehydrogenation of hexakis(3,5-dialkyloxyphenyl)benzenes.



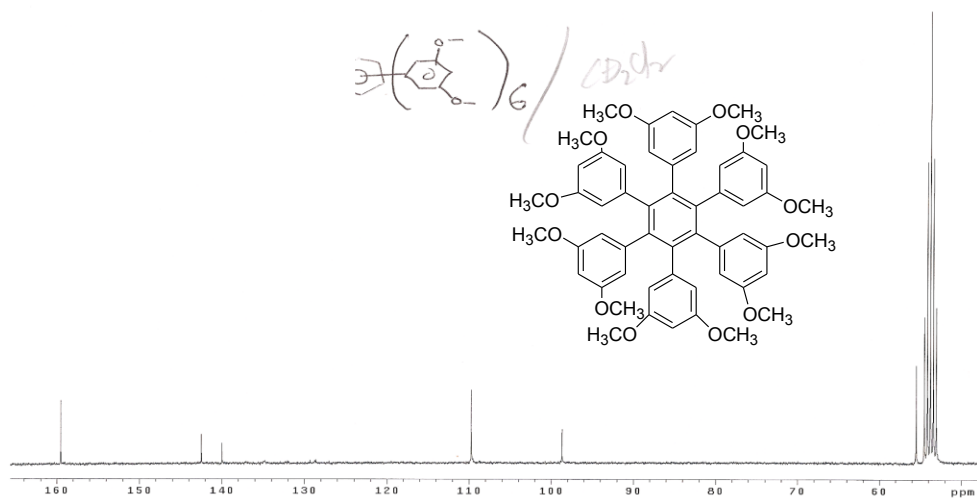
For an example *hexakis*(3,5-dihexyloxyphenyl)benzene (0.5 g, 0.29 mmol) was dissolved in dry dichloromethane (30 mL) and cooled to ~ 0 °C in an ice bath under an argon atmosphere. A solution of ferric chloride (0.94 g, 5.76 mmol) in nitromethane (20 mL) was added dropwise into the above mixture. When the addition was completed, the ice bath was removed and the resulting mixture was stirred for 1 h at room temperature. [Note that throughout the reaction period, a slow stream of argon was passed through the reaction mixture to remove gaseous HCl formed in the reaction.] The reaction was quenched by addition of methanol (30 mL) and the formed dark orange product was purified by recrystallization. Using the same method *hexa-peri*-(3,5-dimethoxybenzo)coronene (**4a**) was prepared

Hexa-peri-(3,5-dihexyloxybenzo)coronene (4b): Yield (90 %); ^1H NMR (CDCl_3) δ : 0.94 (m, 36H), 1.38 (m, 48H), 1.51 (m, 24H), 1.92 (m, 24H), 4.20 (dt, 24H) 7.13 (s, 6H). ^{13}C NMR (CDCl_3) δ : 14.30, 22.89, 25.99, 30.03, 32.04, 69.78, 100.02, 109.49, 122.58, 129.42, 155.72.

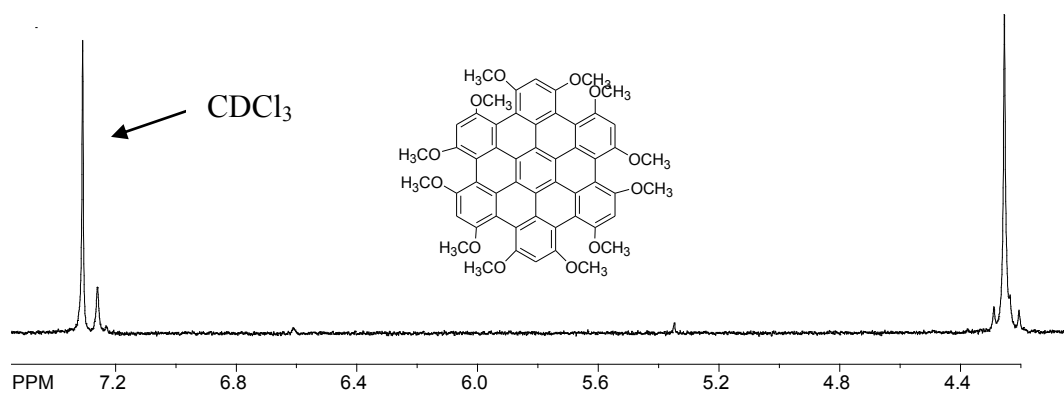
Hexa-peri-(3,5-dimethoxybenzo)coronene (4a): Yield (90 %); ^1H NMR (CDCl_3) δ : 4.26 (s, 36H) 7.31 (s, 6H). Due to poor solubility of **4a** we could not record its ^{13}C NMR spectrum.

^1H NMR spectrum of bis-(3,5-dimethoxyphenyl)acetylene **^{13}C NMR spectrum of bis-(3,5-dimethoxyphenyl)acetylene** **^1H NMR spectrum of hexakis(3,5-dimethoxyphenyl)benzene**

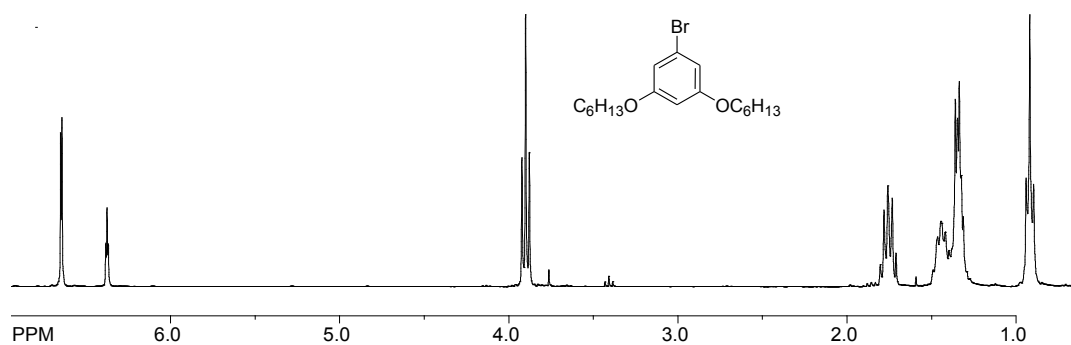
^{13}C NMR spectrum of hexakis(3,5-dimethoxyphenyl)benzene

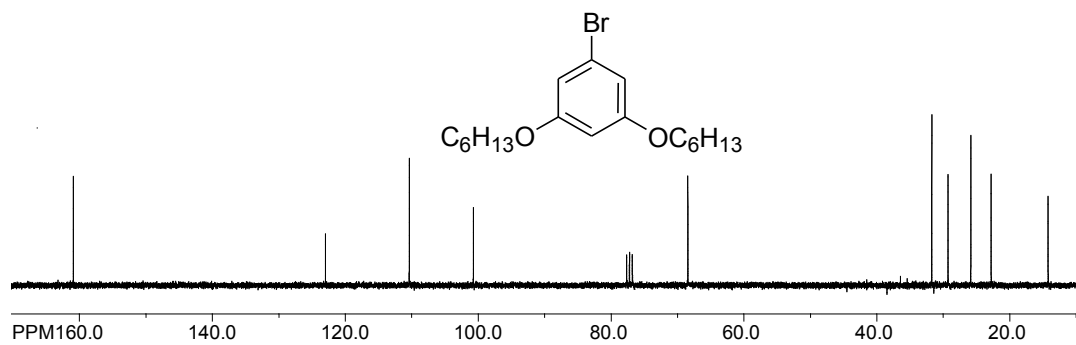
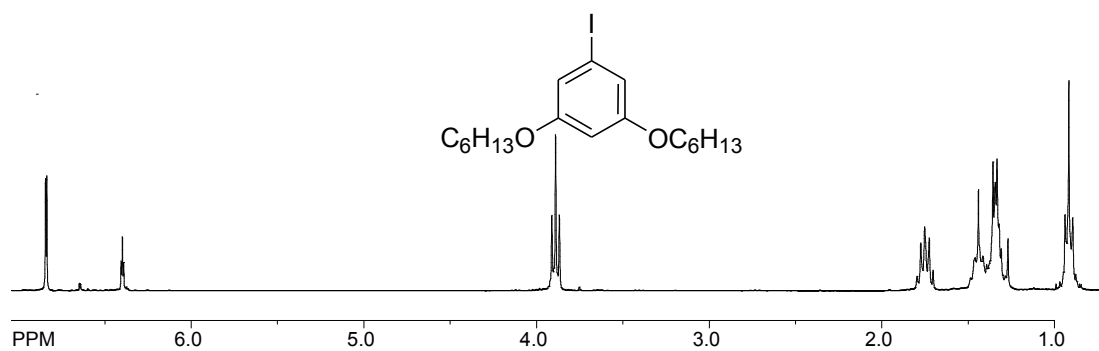
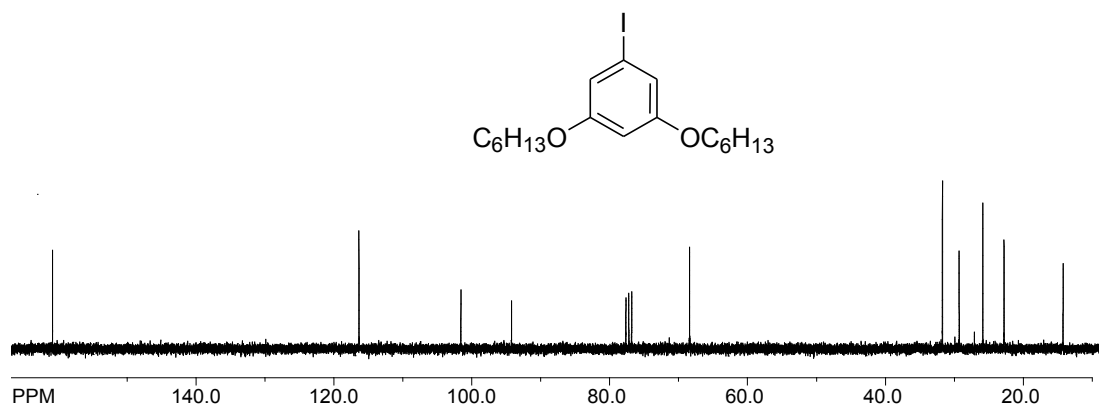


^1H NMR spectrum of hexakis-3,5-dimethoxy-hexa-peri-hexabenzocoronene

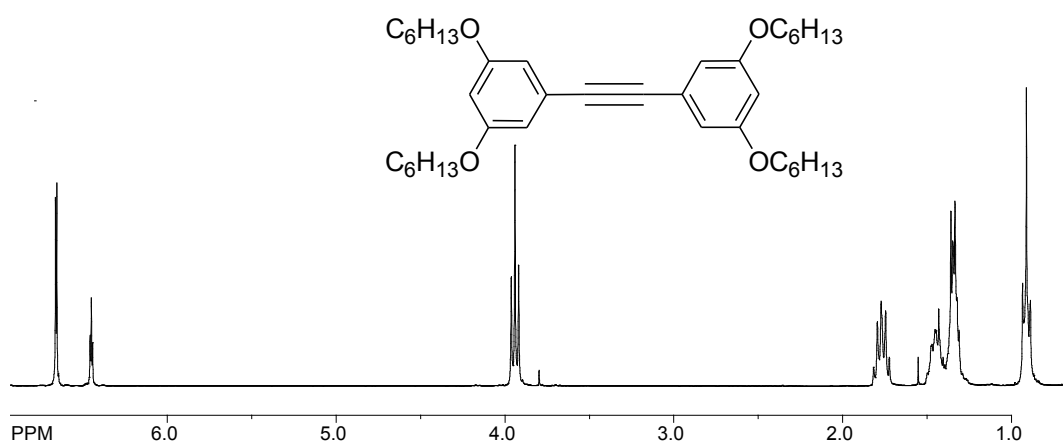


^1H NMR spectrum of 3,5-dihexyloxybromobenzene

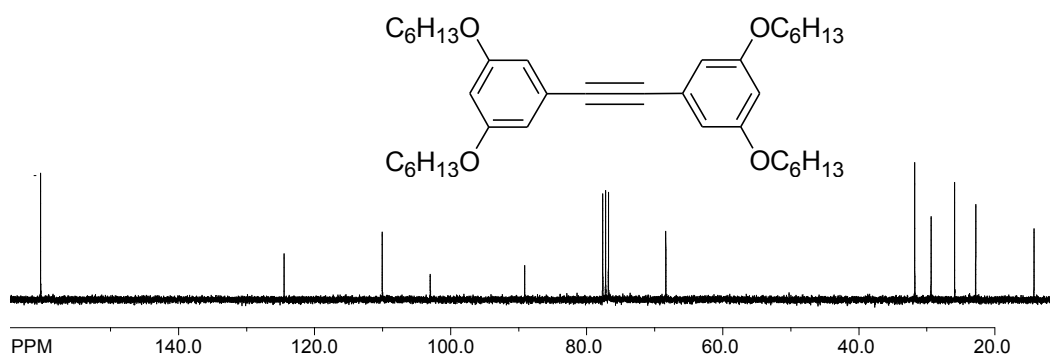


^{13}C NMR spectrum of 3,5-dihexyloxybromobenzene **^1H NMR spectrum of 3,5-dihexyloxyiodobenzene** **^{13}C NMR spectrum of 3,5-dihexyloxyiodobenzene**

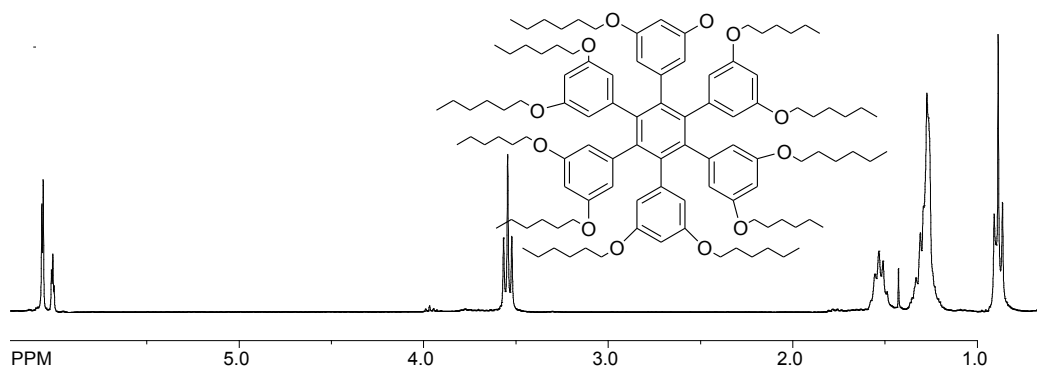
^1H NMR spectrum of bis-(3,5-dihexyloxyphenyl)acetylene

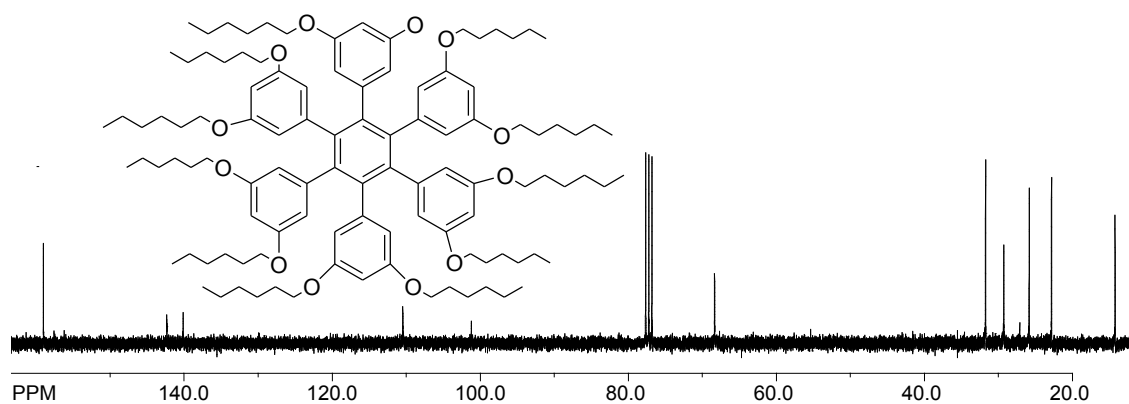
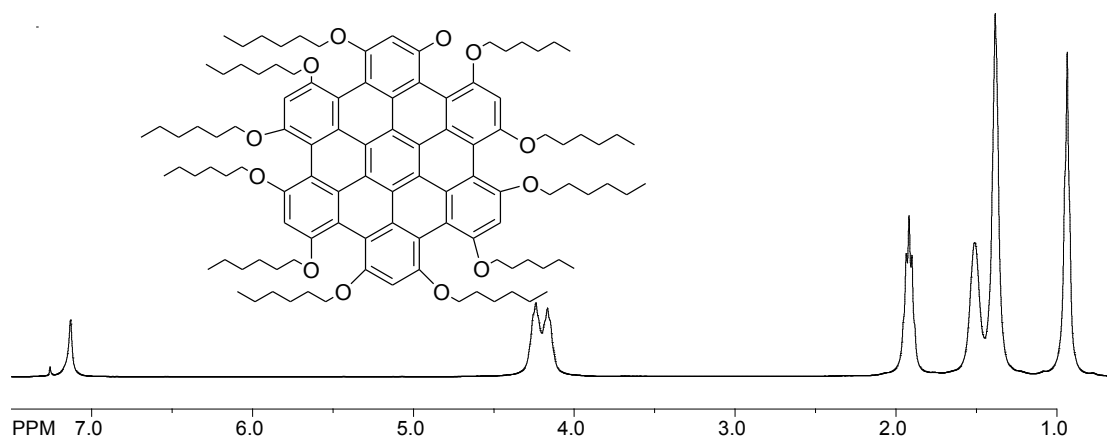
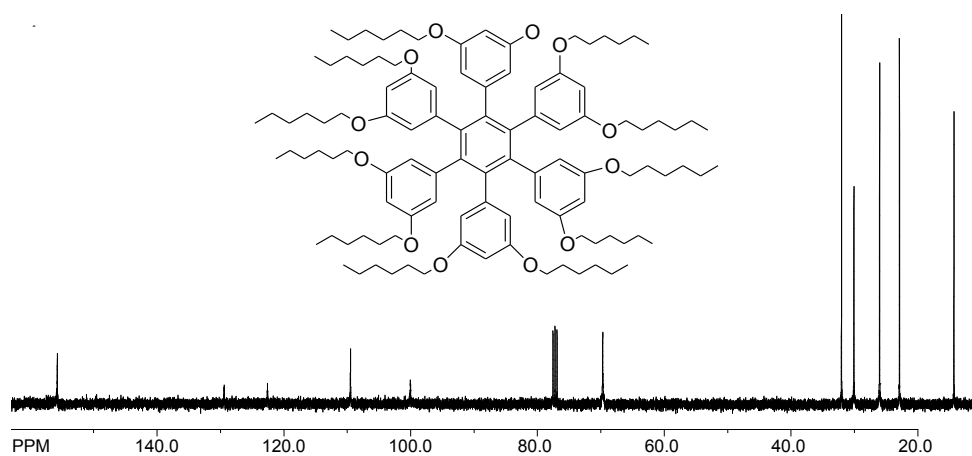


^{13}C NMR spectrum of bis-(3,5-dihexyloxyphenyl)acetylene



^1H NMR spectrum of hexakis(3,5-dihexyloxyphenyl)benzene



^{13}C NMR spectrum of hexakis(3,5-dihexyloxyphenyl)benzene **^1H NMR spectrum of hexakis-3,5-dihexyloxy-hexa-peri-hexabenzocoronene** **^{13}C NMR spectrum of hexakis-3,5-dihexyloxy-hexa-peri-hexabenzocoronene**

CHAPTER 3A

Substitution on Tetraphenylethylene towards electroactive Tetraphenylethylene-core dendrimers

Introduction

Dendrimers have attracted considerable attention owing to their well-defined, three dimensional frameworks in which various functional groups can be attached at desired positions to impart specific properties in the molecule.¹ Redox active core-dendrimers have been proposed as promising materials for miniaturized information storage circuits.² Various redox-active core dendrimers have been synthesized to study their electron transfer and energy transport properties. Although organometallic redox active units³ are common in those dendrimers as the core, organic redox active units⁴ are very rare as the core. Tetraphenylethylene has rich electrochemical⁵ and excited state properties⁶ as well as potential for incorporation into various optoelectronic and optomechanical switching and storage devices.⁷⁻⁹ We have recently demonstrated that the non-emitting tetraphenylethylene core could be made to emit by the introduction of dendritic pentaphenylphenyl group in the highly hindered *tetrakis*(pentaphenylphenyl)ethylene.¹⁰

Our continuing pursuit of developing dendritic structures based on TPE core led us to investigate the effect of introducing aryloxy linkage that could later be extended to more complex dendritic structures. In order to probe the effect of the directive influence of the substituted groups on TAE core upon the optoelectronic properties of resulting tetraaryloxyphenylethylenes (TAEs), we undertook a systematic study of the structure-

property relationship of a series of electron donating/withdrawing groups attached to the aryloxy units. Having established that aryloxy substitution of tetraphenylethylene does not significantly alter its redox properties and thus can serve as an excellent electro active core for dendrimers based on robust diphenyl ether linkages. Accordingly, we undertook the preparation of macromolecular dendritic structures extending from the electro active tetraphenylethylene core. The resulting dendrimers could be decorated with a variety of donor groups such as duryl(tetramethylbenzene), pentamethylbenzene, mesityl, xylyl, substituted pyrenes, coronenes, triaryl and diaryl amines, substituted fluorene at the periphery to study the electron transfer process from the periphery to the core – a fundamental requirement for potential materials' applications.

Accordingly, herein we describe an efficient synthesis of a well-defined series of tetraaryloxyphenylethylenes (**A-D**), with *p*-chlorophenoxy, phenoxy, *p*-methylphenoxy and *p*-methoxyphenoxy substituents, respectively and the synthesis of the two generations (**G1**, **G2**) of dendrimers with TAE core. The availability of a series of TAEs and the dendrimers allows us to evaluate their optical and electrochemical properties. The details of these preliminary findings are presented herein.

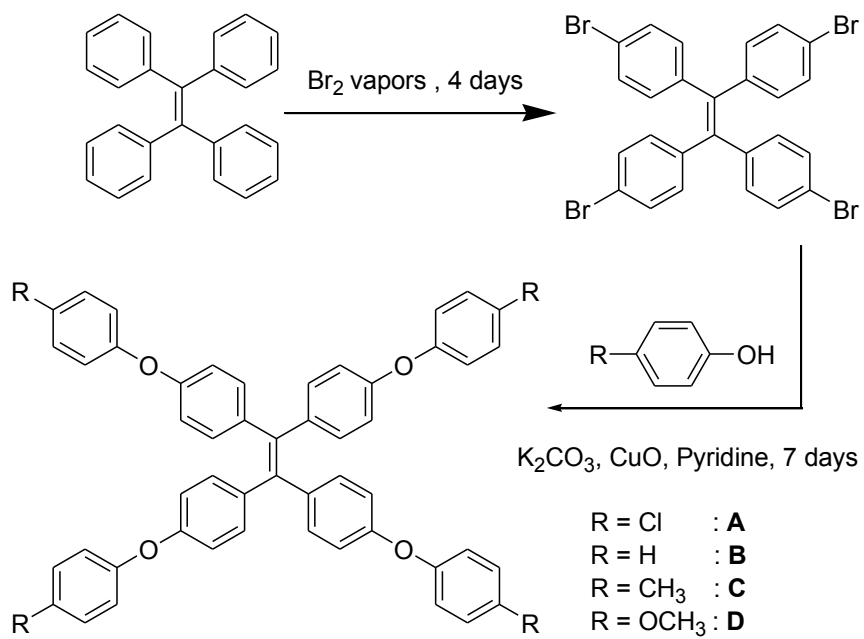
Results and Discussion

Synthesis

The tetraaryloxyphenylethylenes (**A-D**) were synthesized in excellent yields by Ullmann coupling between *p*-chlorophenol, phenol, *p*-methylphenol and *p*-cresol, and *tetrakis*(4-bromophenyl)ethylene (Scheme 1). The desired *tetrakis*(*p*-bromophenyl)ethylene¹¹ was easily prepared from tetraphenylethylene via a solid-phase

reaction with gaseous bromine. The structures of **A-D** were easily established by $^1\text{H}/^{13}\text{C}$ NMR spectroscopy and were further confirmed by X-ray crystallography.

Scheme 1. Synthesis of tetraaryloxyphenylethylenes (**A-D**).



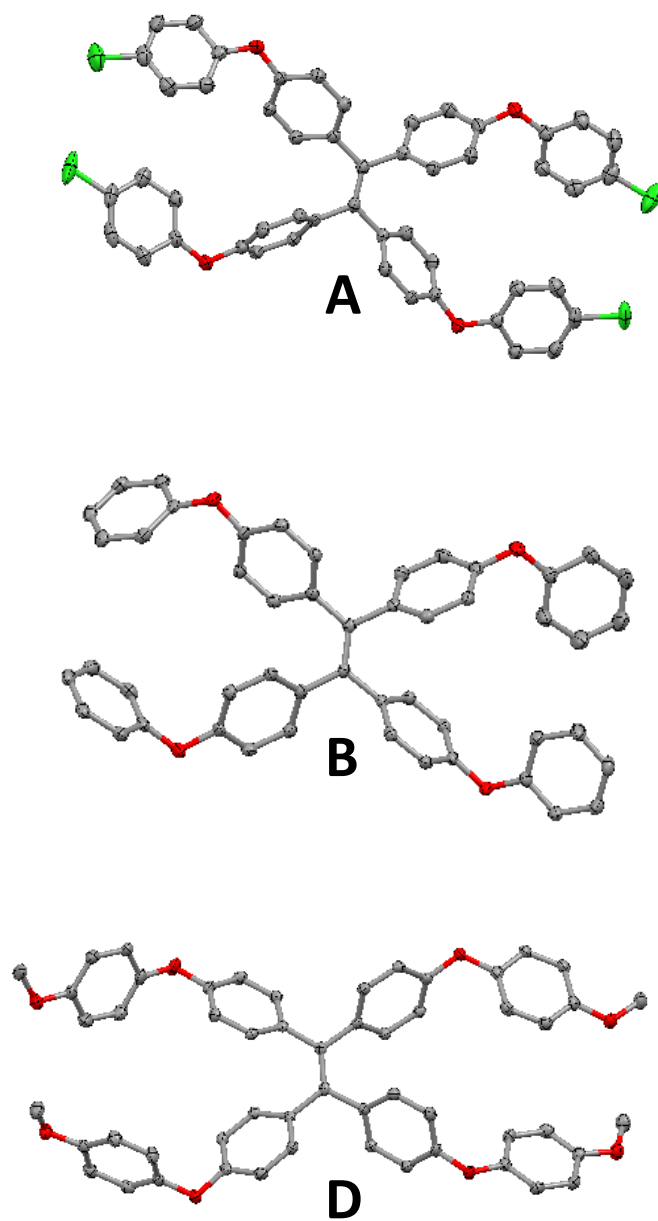
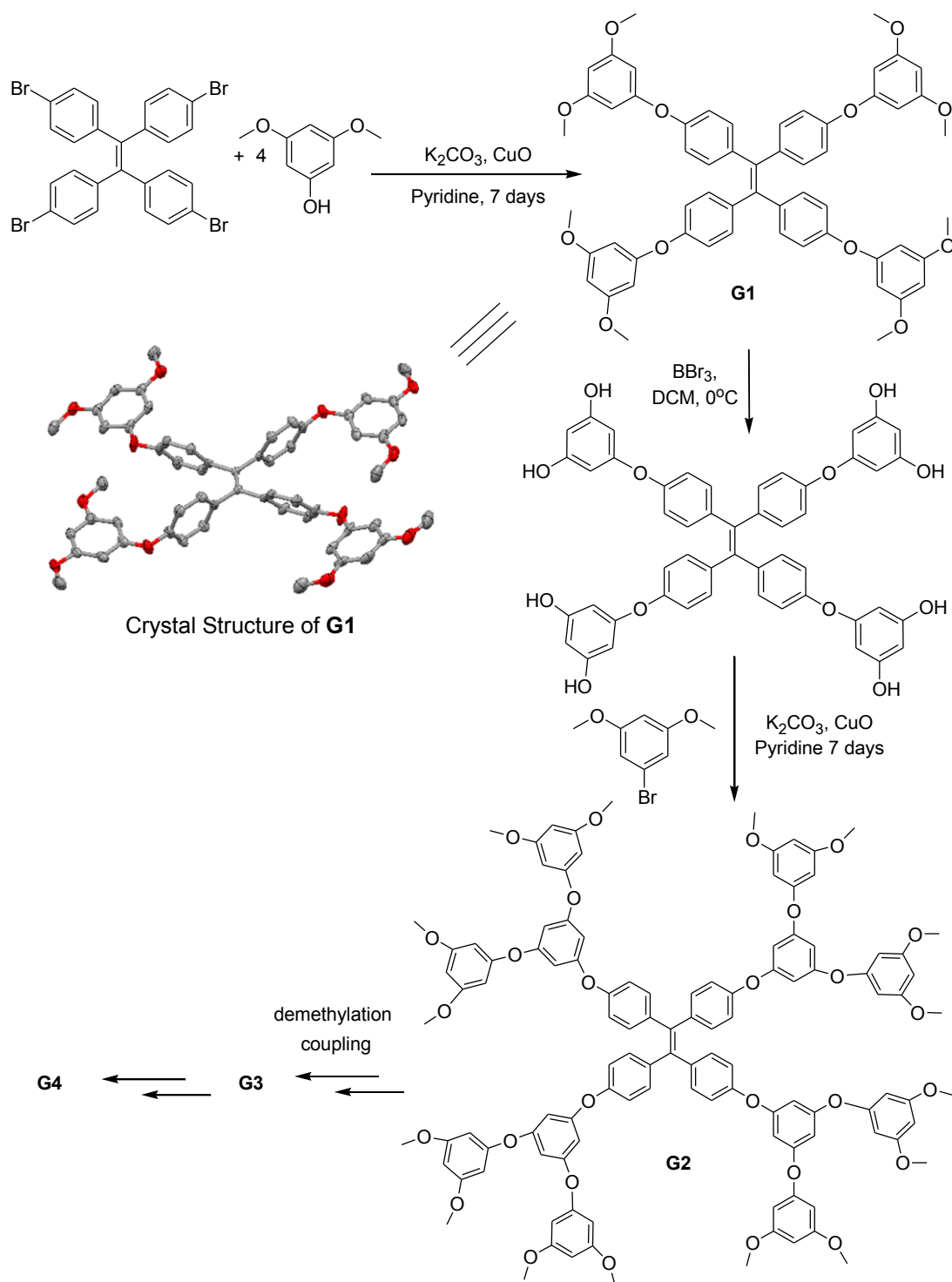


Figure 1. The molecular structure of **A**, **B** and **D** shown as ORTEP diagram.

The first (**G1**) and second (**G2**) generation of dendrimers were synthesized with phloroglucinol as the branching aryloxy unit using the synthetic strategy shown in Scheme 2. Thus a fourfold Ullmann reaction between *tetrakis*(4-bromophenyl)ethylene and 3,5-dimethoxyphenol resulted in first generation dendrimer (**G1**), the structure of which was established by ^1H and ^{13}C NMR spectroscopy and further confirmed by X-ray crystallography. A subsequent BBr_3 mediated demethylation of the peripheral methoxy groups of G1 followed by an Ullmann reaction with excess of 3,5-dimethoxybromobenzene yielded the second generation dendrimer **G2** (see Scheme 2 and the structure below). Efforts are underway to prepare next two generations of dendrimers in the similar fashion as depicted in Scheme 2.

Scheme 2. Synthesis of dendrimers (G1-G4)

Electronic Properties

The redox properties of **A-D** were evaluated by electrochemical oxidation at a platinum electrode as a 1.25×10^{-3} M solution in dichloromethane containing 0.2 M tetra-*n*-butylammonium hexafluorophosphate (*n*-Bu₄NPF₆) as the supporting electrolyte. All four compounds (**A-D**) shows two reversible 1-electron oxidations in their cyclic voltammograms. The first and second oxidation waves of **A** and **B** are completely superimposed thereby indicating simultaneous ejection of two electrons, while the two waves of **C** and **D** are separated enough to distinguish. The oxidation potentials of **A-D** were referenced to added ferrocene, as an internal standard ($E_{\text{ox}} = 0.45$ V vs. SCE),¹² and the E_{ox} values are compiled in Table 1. As expected, with the increasing electron donar ability of substituents in **A** to **D**, a decrease in their oxidation potential was observed. Thus, while a change from electron withdrawing chloro substituent in **A** to hydrogen in **B** decreased the E_{ox} by 50 mV, a substitution by electron donating methyl group in **C** brought the E_{ox} further down by another 50 mV. A further decrease of 30 mV was observed upon the substitution of methoxy group in **D**.

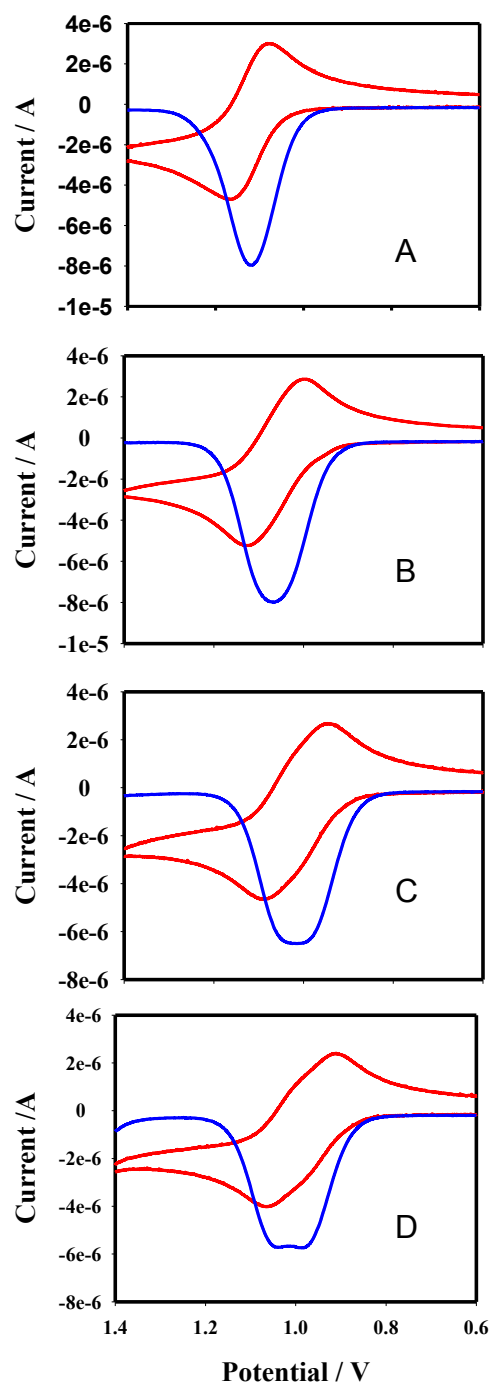


Figure 2. Cyclic voltammograms of 1.25×10^{-3} M **A-D** in CH_2Cl_2 containing 0.2 M $(n\text{-Bu})_4\text{NPF}_6$ at 22 °C at scan rate of 100 mV s^{-1} .

A plot of first oxidation potentials of **A-D** against the substituent constants (σ) satisfies the Hammett correlation (Table 1, Figure 3). Use of Hammett correlation can be helpful for rapid estimation and accurate calculation of oxidation potentials of other substituted or polysubstituted tetraaryloxyphenylethylenes. This predictability in turn would greatly assist in designing macromolecular structures for usage in molecular electronics and nanotechnology.

Table 1. Electrochemical Oxidation Potentials and substituent constant σ of tetraaryloxyphenylethylenes.

Compound	Substituent	σ value	E_{ox}^0 (I) (V vs. SCE)
A	Cl	0.227	1.12
B	H	0.000	1.07
C	CH ₃	0.170	1.02
D	OCH ₃	0.268	0.99

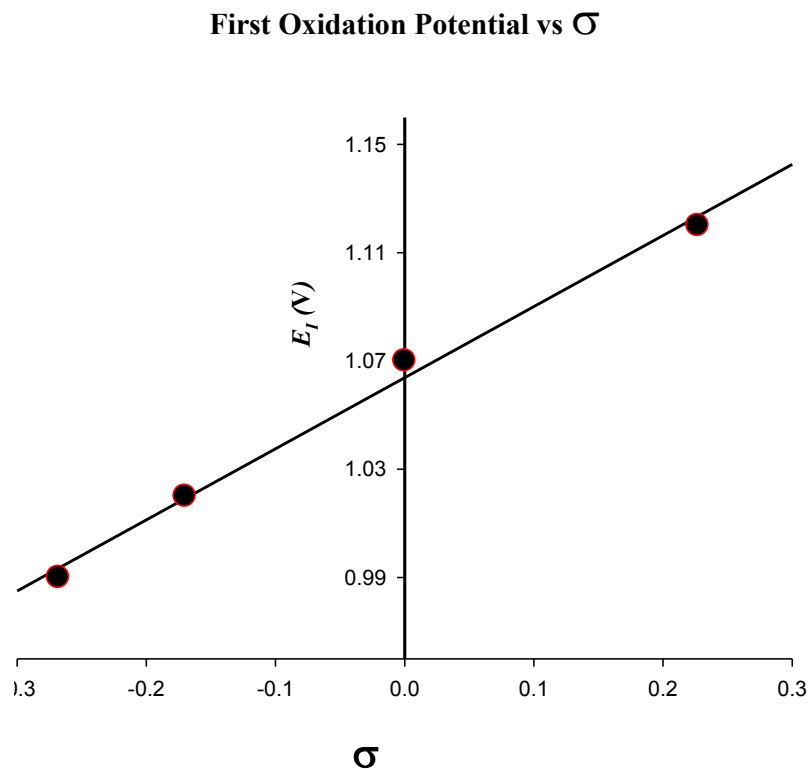
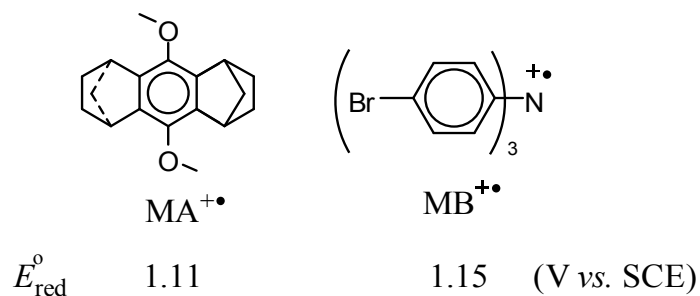


Figure 3. The Hammett plot of the oxidation potentials of various tetraaryloxyphenylethylenes in dichloromethane solutions at 22 °C vs substituent constant σ (regression coefficient = 0.99).

The reversibility of 1-electron oxidation in cyclic voltammetry of various TAEs prompted us to evaluate the stability of their cation radical salts using stable triarylamine (**MB**)¹³ and/or a hydroquinone ether (**MA**)¹⁴ cation-radical salts as robust 1-electron oxidants.



Thus, Figure 5 shows the spectral changes attendant upon the reduction of MB^{++} SbCl_6^- [$\lambda_{\text{max}} (\log \epsilon) = 728 \text{ nm} (4.45)$] by an incremental addition of D to MB (and corresponding oxidation of D to its cation radical D^{++}) in dichloromethane at 22°C . The presence of well-defined isosbestic points at $\lambda_{\text{max}} = 662$ and 766 nm in Figure 5 established the uncluttered character of the electron transfer.

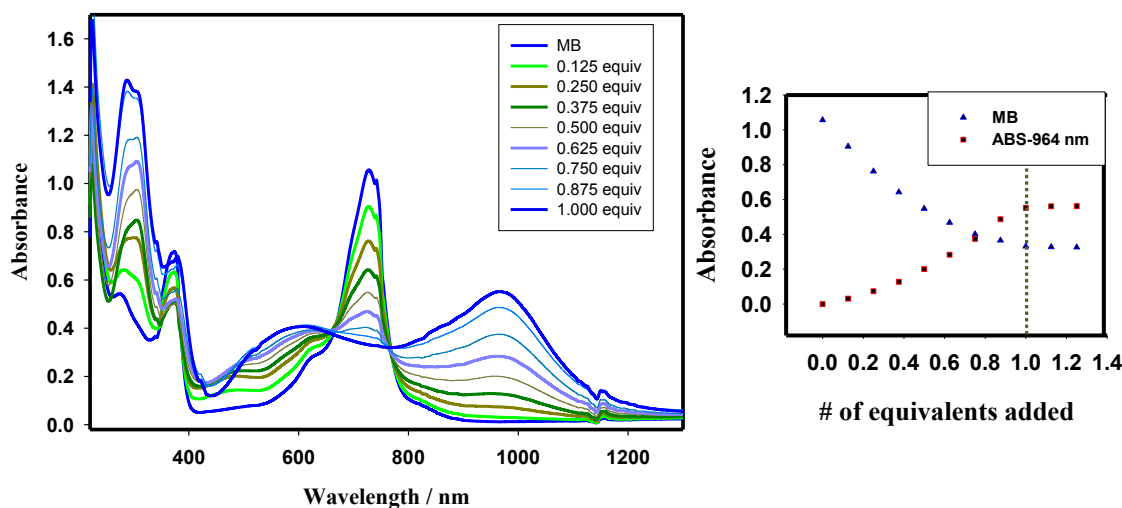


Figure 4. **Left.** Spectral changes upon the reduction of $4.1 \times 10^{-5} \text{ M } \text{MB}^{++}$ by incremental addition of $2.0 \times 10^{-3} \text{ M } \text{D}$ to its radical cation in CH_2Cl_2 at 22°C **Right.** A plot of depletion of absorbance of MB^{++} (blue triangles, at 728 nm) and an increase of the absorbance of D^{++} (red squares, at 964 nm) against the equivalent of added neutral D .

Furthermore, a plot of the depletion of MB^{++} and formation of D^{++} against the increments of added neutral D established that D^{++} was completely consumed after the addition of 1 equiv of D ; the resulting absorption spectrum of D^{++} remained unchanged upon further addition of neutral D (i.e., eq. 1). Although D shows two one-electron oxidations at 0.99 and 1.04 V vs SCE respectively, the spectrum of dication D^{++} can't be distinguished in Figure 4 since D^{0+} and D^{++} are in equilibrium (I.e., eq. 2, $K_{\text{eq}} = 0.122$).



Similar radical-cation absorption spectra were obtained for **A-D**, upon oxidation with hindered hydroquinone ether (CRET). All cation radicals were intense blue in color and were significantly stable at room temperature. They all showed twin absorption bands in the region 600-610 nm and 956-966 nm (figure 5) characteristic of parent TPE cation radical [$\lambda_{\text{max}} (\log \varepsilon) = 490, 842 (3.72)$]¹⁵.

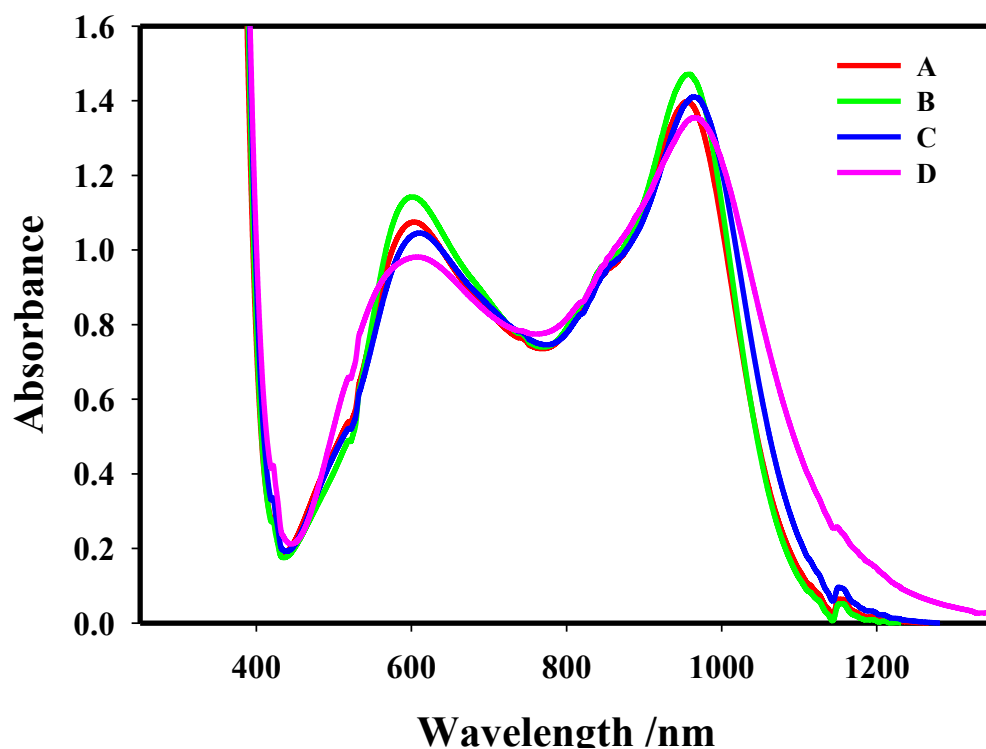


Figure 5. Comparison of the absorption spectra of radical cation of **A-D** obtained upon reduction of 6.85×10^{-5} M **CRET**^{•+} by one equivalent of TAEs in CH_2Cl_2 at 22 °C.

The absence of any significant change in the absorption wavelength of the cation radicals of **A-D** is due to the fact that the HOMO in tetraaryloxyphenylethylenes largely lies on the tetraphenylethylene core (Figure 6).

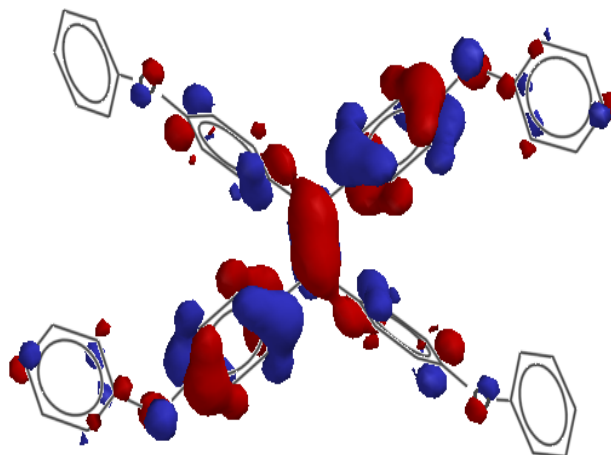


Figure 6. Showing HOMOs of **B** obtained by AM1 calculations.

The stability of cation radical solution of **A-D** prompted us to isolate the crystals of their cation radical salts. The blue-colored dichloromethane solution of $\mathbf{D}^{+\bullet}\text{SbCl}_6^-$, obtained in eq 1, was carefully layered with toluene and stored in a refrigerator at $-10\text{ }^\circ\text{C}$ for 2 days. However, the attempted crystallization of cation-radical salt of **D** [i.e. $\mathbf{D}^{+\bullet}\text{SbCl}_6^-$ salt] as a representative example, led to the isolation of a dication, i.e. $\mathbf{D}^{+2}(\text{SbCl}_6^-)_2$ salt which was characterized by X-ray crystallography (Figure 7) and by UV-vis spectroscopy (Figure 8). We^{15, 16} have earlier shown that a stepwise one-electron oxidation of various tetraarylethylene donors (**T**) can be carried out by electron exchange with stable aromatic cation radicals as oxidants to selectively afford the cation radicals ($\mathbf{T}^{+\bullet}$) and the dications (\mathbf{T}^{2+}) according to their disproportionation constants (K_{disp}) which can be easily estimated from the cyclic voltammetric data. Interestingly, despite the low

values of disproportionation constants for various tetraarylethylene cation radicals, they all undergo crystallization induced disproportionation to form the corresponding crystalline dicationic salts.^{15, 16}

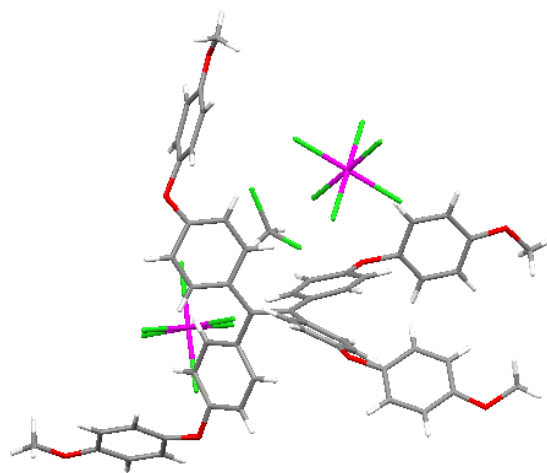


Figure 7. The crystal structure of \mathbf{D}^{2+} (SbCl_6^-)₂ shown as ORTEP diagram.

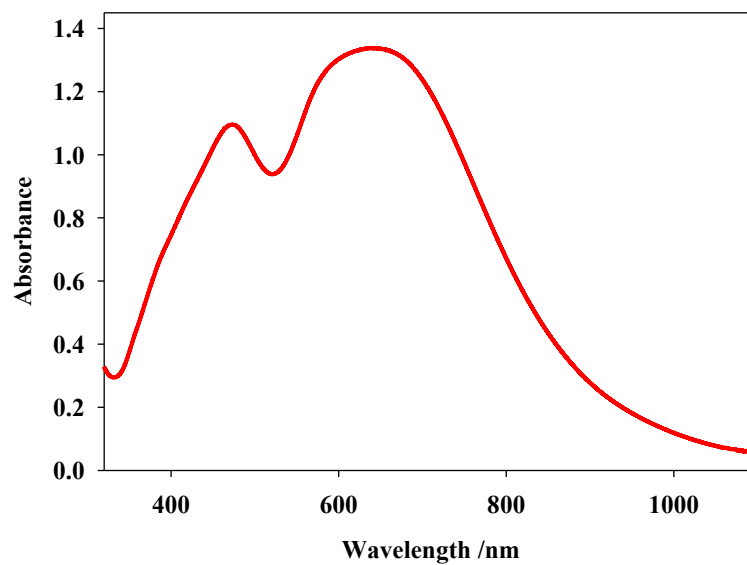


Figure 8. UV-vis absorption spectrum of a solution of \mathbf{D}^{2+} obtained by dissolving the dicationic crystals isolated for X-ray diffraction in dichloromethane.

The X-ray crystallographic analysis of the dicationic salts of various tetraarylethylenes (with H, Me, and OMe substituents) showed that the central ethylenic bond undergoes a twist of $\sim 60^\circ$ around the central C=C bond.¹⁴ Interestingly, the dicationic salt of **D** undergoes a twist of $\sim 90^\circ$ possibly due to the steric crowding caused by the bulky aryloxy groups.

Electronic Properties of Dendrimers

The redox properties of **G1** and **G2** dendrimers were evaluated by electrochemical oxidation at a platinum electrode as a 2.5 mM solution in dichloromethane containing 0.2 M tetra-*n*-butylammonium hexafluorophosphate (*n*-Bu₄NPF₆) as the supporting electrolyte. Both dendrimers **G1** and **G2** show two reversible and simultaneous one electron oxidations at 1.06 V vs SCE and 1.13 V vs SCE respectively in their cyclic voltammograms (Figure 9). The oxidation potential values of dendrimers are little higher than that of parent TPE (E_{ox} = V vs SCE) due to the meta substitution of methoxy groups. The reversible oxidation of **G1** and **G2** dendrimers allows us to evaluate the properties of their cation radical in solution which is stable at room temperature. The cation radicals of **G1** and **G2** were generated in dichloromethane using the oxidants MA^{+o} and MB^{+o} respectively. Both **G1**^{+o} and **G2**^{+o} show cation radical spectra (Figure 10) which are similar to the spectra of A-D derivatives and the parent TPE indicating that the oxidation occurs in TPE core and the redox properties are well retained in bulky dendritic structure. As shown in figure 11 dendrimers show attractive emission properties compared to the properties of **D** when all three compounds were excited at 270 nm. **G2** shows less emission than **G1** unexpectedly. This might be due to self-quenching by the crowdedness of end groups.

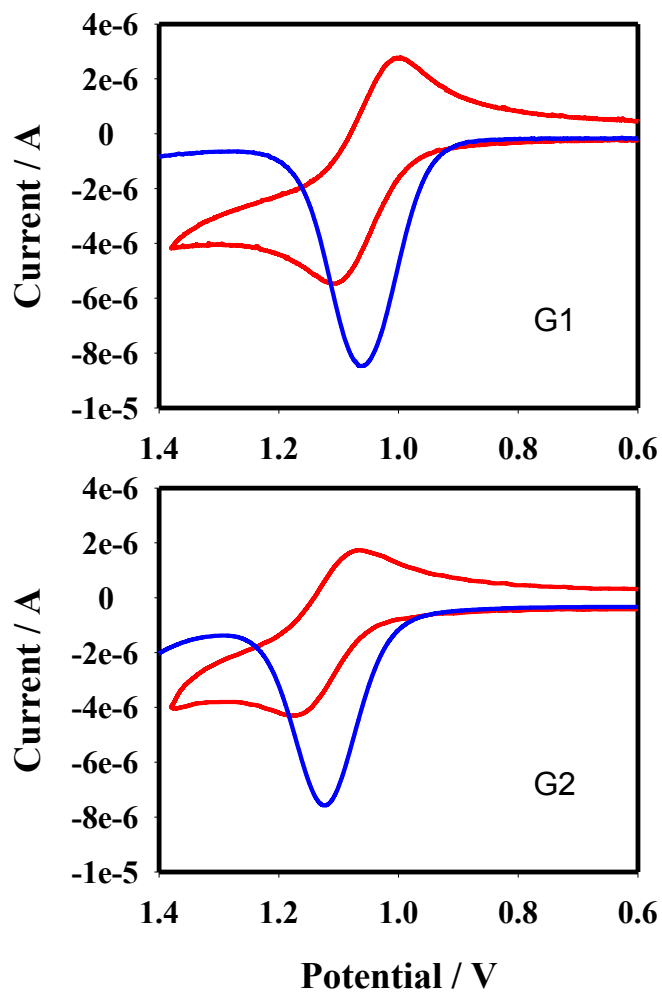


Figure 9. Cyclic voltammograms of 2.5 mM **G1** and **G2** in CH_2Cl_2 containing 0.2 M $(n\text{-Bu})_4\text{NPF}_6$ at 22 °C at scan rate of 100 mV s^{-1} .

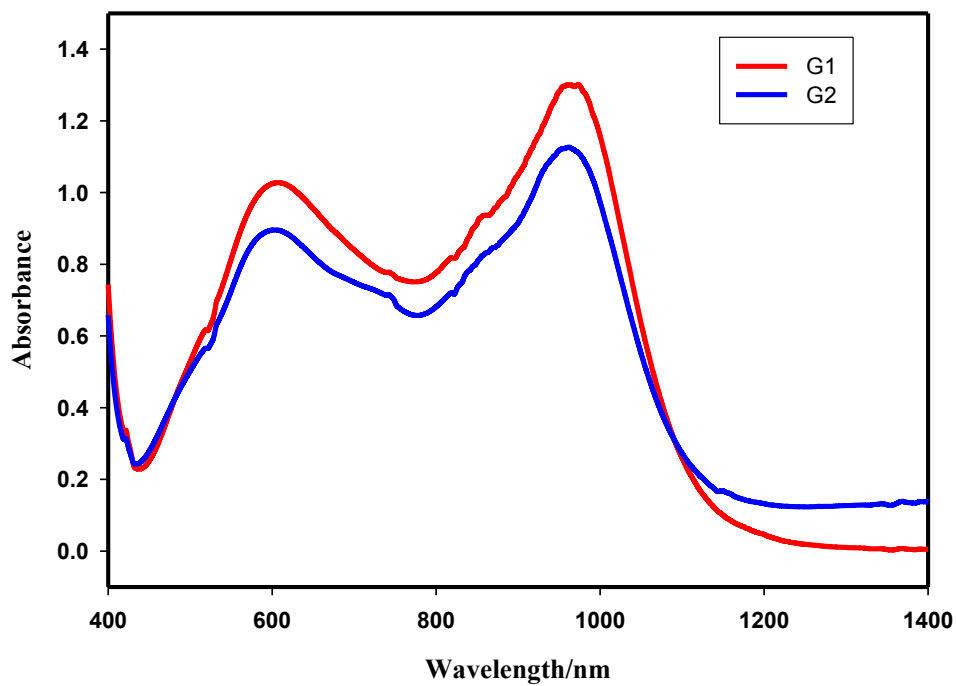


Figure 10. Comparison of the absorption spectra of radical cation of **G1** and **G2** obtained upon reduction of 6.85×10^{-5} M **CRET⁺** and 7.10×10^{-5} M **MB⁺** by one equivalent of G1 and G2 respectively in CH_2Cl_2 at 22 °C.

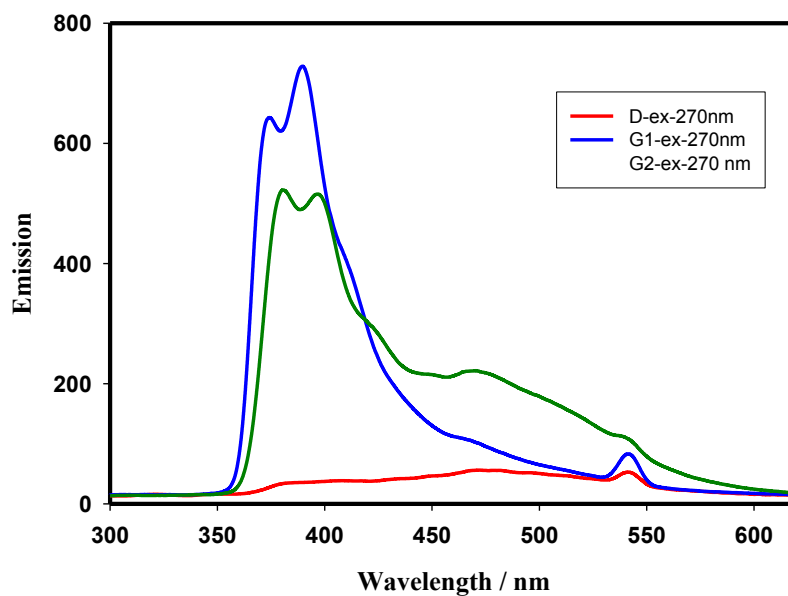


Figure 11. Comparison of Emission properties of dendrimers (**G1**, **G2**) with **D**

In summary, we did a systematic study of the structure-property relationship of a series of electron donating/withdrawing groups attached to the aryloxy units in order to probe the effect of the directive influence of the substituted groups on the aryloxy units upon the optoelectronic properties of resulting TPEs (**A-D**). Although the oxidation potential values of **A-D** are not dramatically changed due to weak coupling between substituent and TPE core through the aryloxy linkage, they show a linear dependence on the electron donating/withdrawing ability of the substituents at para position of the phenoxy group and very well follow Hammett correlation. Further, two generations of dendrimers extending from the highly electro active tetraphenylethylene core using phloroglucinol as branching aryloxy units were synthesized which are able to retain the redox properties of TPE core. Efforts are in progress to prepare higher generation dendrimers and study the electron transfer processes in the resulting dendrimers. The dramatic decrease in melting point of from G1 (mp: 174-176 °C) to G2 (mp: 54-56 °C) suggest the increasing liquid crystalline behavior in higher generations of this TPE dendrimers.

EXPERIMENTAL

General Experimental Methods and Materials. Dicobaltoctacarbonyl, trimethylsilylacetylene, potassium hydroxide, DMSO, *p*-iodophenol, 1-bromohexane, ferric chloride, nitromethane, anhydrous benzene 1,8-diazobicyclo[5,4,0]undec-7-ene (DBU), CuI, trimethylsilylacetylene, BuLi, trimethylborate, toluene, ethanol, sodium carbonate, tetrakis(triphenylphosphine)palladium, acetonitrile, *N*-bromosuccinamide, *bis*(triphenylphosphine)palladium dichloride and anhydrous dioxane were commercially available and were used without further purification.

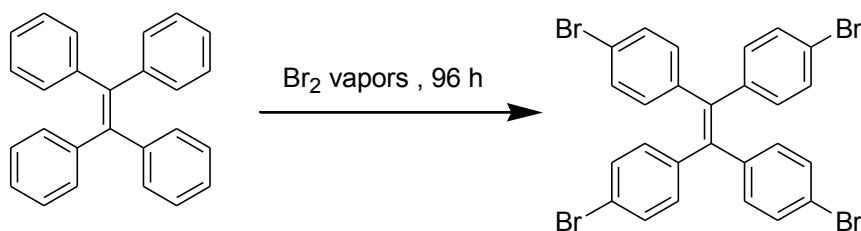
Anhydrous tetrahydrofuran (THF) was prepared by refluxing the commercial tetrahydrofuran over lithium tetrahydroaluminate under an argon atmosphere for 24 hours followed by distillation. It was stored under an argon atmosphere in a Schlenk flask equipped with a Teflon valve fitted with Viton O-rings. Dichloromethane was repeatedly stirred with fresh aliquots of conc. sulfuric acid (~10 % by volume) until the acid layer remained colorless. After separation it was washed successively with water, aqueous sodium bicarbonate, water, and saturated aqueous sodium chloride and dried over anhydrous calcium chloride. The dichloromethane was distilled twice from P₂O₅ under an argon atmosphere and stored in a Schlenk flask equipped with a Teflon valve fitted with Viton O-rings. The hexanes and toluene were distilled from P₂O₅ under an argon atmosphere and then refluxed over calcium hydride (~12 hrs). After distillation from CaH₂, the solvents were stored in Schlenk flasks under argon atmosphere.

Cyclic Voltammetry. Cyclic voltammetry (CV) was performed on an Electrochemical Analyser. The CV cell was of an air-tight design with high vacuum Teflon valves and Viton O-rings seals to allow an inert atmosphere to be maintained without contamination by grease. The working electrode consisted of an adjustable platinum disk embedded in a glass seal to allow periodic polishing (with a fine emery cloth) without changing the surface area (~1 mm²) significantly. The reference SCE electrode (saturated calomel electrode) and its salt bridge were separated from the catholyte by a sintered glass frit. The counter electrode consisted of platinum gauze that was separated from the working electrode by ~3 mm. The CV measurements were carried out in a solution of 0.1M supporting electrolyte (tetra-*n*-butylammonium hexafluorophosphate, TBAH) and 0.24 –

2.5 mmol substrate in 97:3 dichloromethane –acetonitrile mixtures under an argon atmosphere. All cyclic voltammograms were recorded at the sweep rate of 100 mV sec⁻¹, unless otherwise specified and were IR compensated. The oxidation potentials ($E_{1/2}$) were referenced to SCE which was calibrated with added (equimolar) ferrocene ($E_{1/2} = 0.45$ V vs. SCE). The $E_{1/2}$ values were calculated by taking the average of anodic and cathodic peak potentials in the reversible cyclic voltammograms.

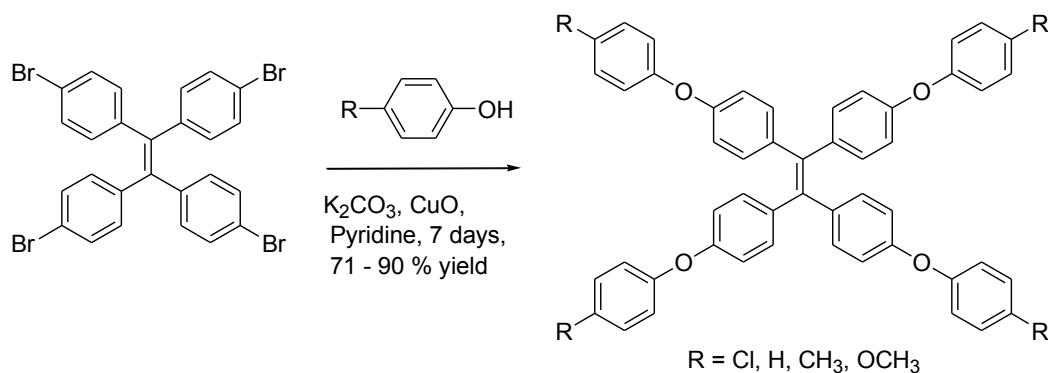
Synthesis and Spectral data

Synthesis of tetra(4- bromophenyl)ethylene



An open vessel containing liquid bromine (11.58 mL, 217.16 mmol) was placed in the lower part of the desiccator. A evaporating dish containing finely powdered tetraphenylethylene (10.3 g, 31.02 mmol) was placed on the rack above the bromine. The lid of the desiccator was not completely closed since hydrogen bromide was often given off. After four days the formed reddish brown solid was allowed to stand until constant weight was obtained. The crude product was dissolved in dichloromethane (250 mL) and stirred for 20 minutes, filtered and recrystallized with dichloromethane/methanol (2:1) mixture to produce white crystals Yield (18.0 g, 90 %) ; ¹H NMR (CDCl₃) δ:6.85 (d, $J = 8.56$ Hz, 8H), 7.26 (d, $J = 8.56$ Hz, 8H) . ¹³C NMR (CDCl₃) δ : 121.50, 131.52, 132.98, 139.82, 141.69.

Synthesis of substituted tetraphenyl ethylene derivatives



For example, tetra(4-bromophenyl)ethylene (0.58 g, 0.89 mmol), *p*-methoxyphenol (0.69 g, 5.34 mmol, 6 equiv), K₂CO₃ (2.3 g, 16.6 mmol), pyridine (15 mL) were placed in a 100 mL Schlenk flask under Ar atmosphere and evacuated and backfilled the flask with Ar three times. Then CuO (1.3 g, 16.6 mmol) was added into the flask under Ar atmosphere and refluxed for 7 days. The reaction mixture was cooled, dissolved in dichloromethane (100 mL) and filtered through short Silica Gel column. The obtained dark red solution was then treated with dil. HCl (25 x 2 mL), treated with dil. NaOH (25 x 2 mL), dried over anhydrous MgSO₄ and evaporated to isolate dark red crude product which was recrystallized with dichloromethane/ methanol (1:1) mixture to isolate pale yellow crystals. Using the same procedure derivatives B, C and D were prepared.

Chloro derivative(A): Yield (0.70 g, 93 %) mp: 184-186 °C ; ¹H NMR (CDCl₃) δ: 6.78 (d, *J* = 8.82 Hz, 8H), 6.91 (d, *J* = 9.00 Hz, 8H), 7.02 (d, *J* = 8.82 Hz, 8H), 7.27 (d, *J* =

9.00 Hz, 8H). ^{13}C NMR (CDCl_3) δ : 118.29, 120.25, 120.27, 128.54, 129.89, 129.92, 132.99, 139.05, 139.52, 155.67, 155.81.

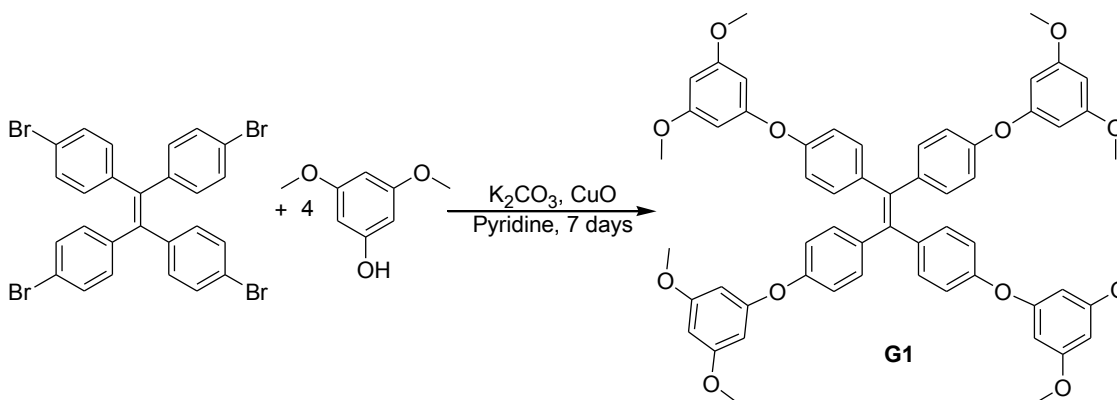
H derivative(B): Yield (1.00 g, 92 %) mp: 199-200 °C ; ^1H NMR (CDCl_3) δ : 6.80 (d, J = 8.69 Hz, 8H), 6.99 (d, J = 8.42 Hz, 8H), 7.03 (d, J = 8.69 Hz, 8H), 7.10 (t, J = 7.7, 14.93 Hz, 4H), 7.32 (t, J = 8.33, 15.86 Hz, 8H), ^{13}C NMR (CDCl_3) δ : 118.25, 119.06, 123.44, 129.91, 132.93, 138.88, 139.48, 155.91, 157.22.

Methyl derivative(C): Yield (1.00 g, 86 %) mp: 192-193 °C ; ^1H NMR (CDCl_3) δ : 2.33 (s, 12H), 6.74 (d, J = 8.72 Hz, 8H), 6.88 (d, J = 8.35 Hz, 8H), 6.98 (d, J = 8.72 Hz, 8H), 7.12 (d, J = 8.35 Hz, 8H). ^{13}C NMR (CDCl_3) δ : 20.93, 117.74, 119.22, 119.24, 130.40, 132.87, 133.05, 138.62, 139.36, 154.78, 156.39.

Methoxy derivative(D): Yield (0.90 g, 71 %) mp: 155-156 °C ; ^1H NMR (CDCl_3) δ : 3.80 (s, 12H), 6.71 (d, J = 8.95 Hz, 8H), 6.87 (d, J = 8.95 Hz, 8H), 6.96 (m, 16H). ^{13}C NMR (CDCl_3) δ : 55.83, 114.98, 117.01, 120.91, 132.84, 138.35, 139.19, 150.22, 156.02, 157.03.

Synthesis of dendrimers

Synthesis of G1



Tetra(4-bromophenyl)ethylene (1 equiv.), 3,5-dimethoxyphenol (6 equiv), K_2CO_3 (6 equiv.), pyridine (15 mL) were placed in a 100 mL Schlenk flask under Ar atmosphere and evacuated and backfilled the flask with Ar three times. Then CuO (6 equiv.) was added into the flask under Ar atmosphere and refluxed for 7 days. The reaction mixture was cooled, dissolved in dichloromethane (100 mL) and filtered through short Silica Gel column. The obtained dark red solution was then treated with dil. HCl (25 x 2 mL), treated with dil. NaOH (25 x 2 mL), dried over anhydrous $MgSO_4$ and evaporated to isolate dark red crude product which was recrystallized with dichloromethane/ methanol (1:1) mixture to isolate pale yellow crystals. Yield (80 %); 1H NMR ($CDCl_3$) δ : 3.73 (s, 24H), 6.13(d, $J = 2.19$ Hz, 8H), 6.20 (t, $J = 2.2, 4.4$ Hz, 4H), 6.82 (d, $J = 8.73$ Hz, 8H), 7.04(d, $J = 8.73$ Hz, 8H), ^{13}C NMR ($CDCl_3$) δ : 55.50, 95.46, 97.23, 118.78, 132.88, 139.12, 139.57, 155.30, 159.29, 161.68.

Demethylation of G1

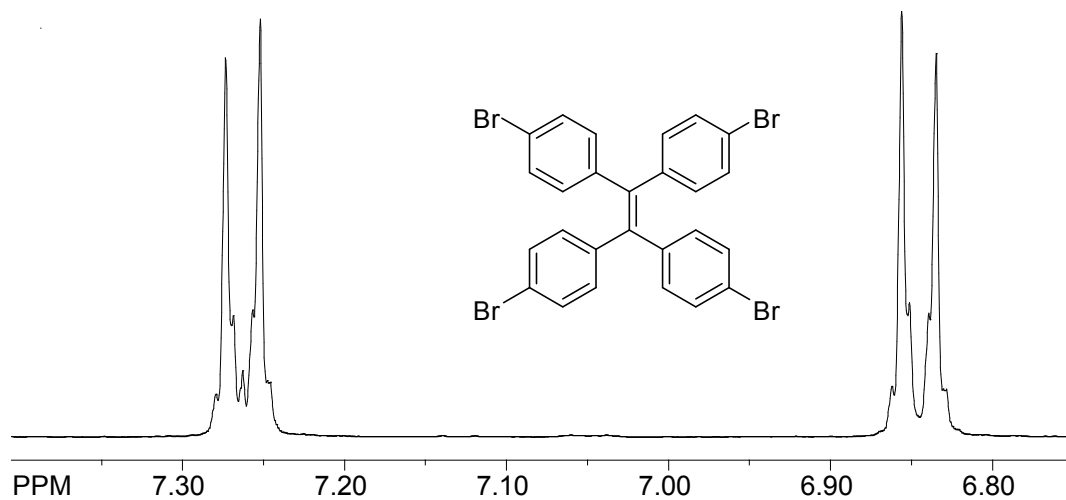
For an example G1(1.46 g, 1.55mmol) was dissolved in anhydrous dichloromethane (40 mL) and cooled to 0°C. Then BBr₃ (3.52 mL, 37.27 mmol) in anhydrous dichloromethane(10 mL) was added drop-wise to the cold solution of G1, the temperature was brought to room temperature gradually and stirred for two hours. The reaction mixture was Cooled to 0°C and water was added dropwise to quench excess BBr₃ and filtered to isolate pure demethylated G1 as a brown solid. Yield (1.2 g, 94 %) ; ¹H NMR (CD₃OD) δ: 5.88 (m, 8H), 5.99 (m, 4H), 6.74 (d, *J* = 8.17 Hz, 8H), 6.97 (d, *J* = 8.17 Hz, 8H) . ¹³C NMR (CD₃OD) δ : 99.47, 99.70, 120.22, 134.58, 134.62, 141.03, 141.51, 157.87, 161.16, 161.29.

Synthesis of G2

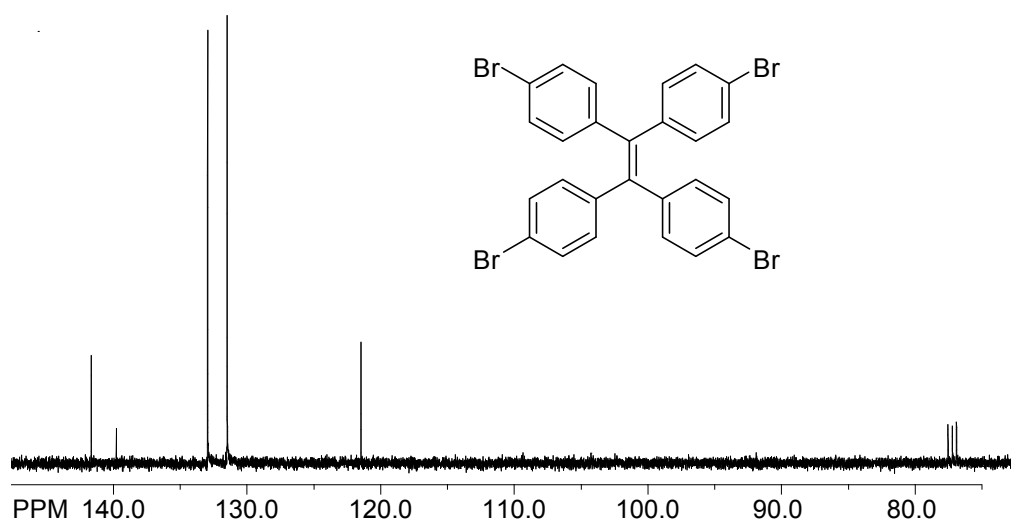
Demethylated G1 (1.2 g, 1.45 mmol), 3,5-dimethoxybromobenzene (3.1 g, 14.5 mmol), K₂CO₃ (2.0 g,14.5 mmol), pyridine (15 mL) were placed in a 100 mL Schlenk flask under Ar atmosphere and evacuated and backfilled the flask with Ar three times. Then CuO (1.15 g, 14.5 mmol) was added into the flask under Ar atmosphere and refluxed for 7 days. The reaction mixture was cooled, dissolved in dichloromethane (100 mL) and filtered through short Silica Gel column. The obtained dark red solution was then treated with dil. HCl (25 x 2 mL), treated with dil. NaOH (25 x 2 mL), dried over anhydrous MgSO₄ and evaporated to isolate dark red crude product which was recrystallized with dichloromethane/ methanol (1:1) mixture to isolate pale yellow crystals.Yield (2.2 g, 76 %) ; ¹H NMR (CDCl₃) δ: 3.73 (s, 48H), 6.21(m, 24H), 6.38 (m, 12H), 6.79 (d, *J* = 8.74 Hz, 8H), 6.98(d, *J* = 8.74 Hz, 8H), . ¹³C NMR (CDCl₃) δ : 55.53,

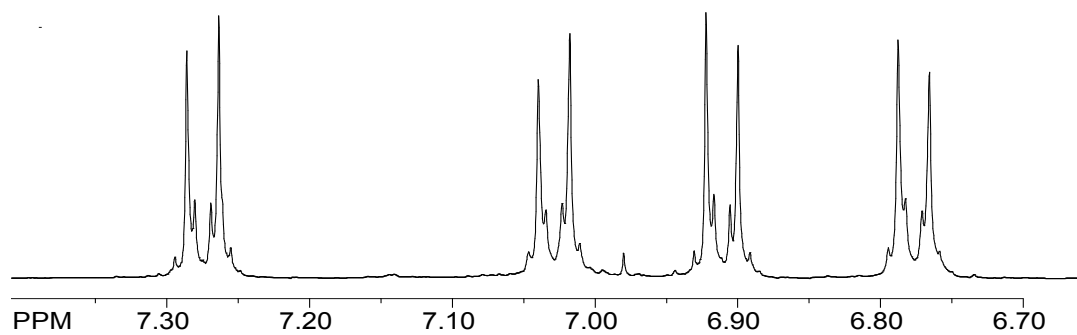
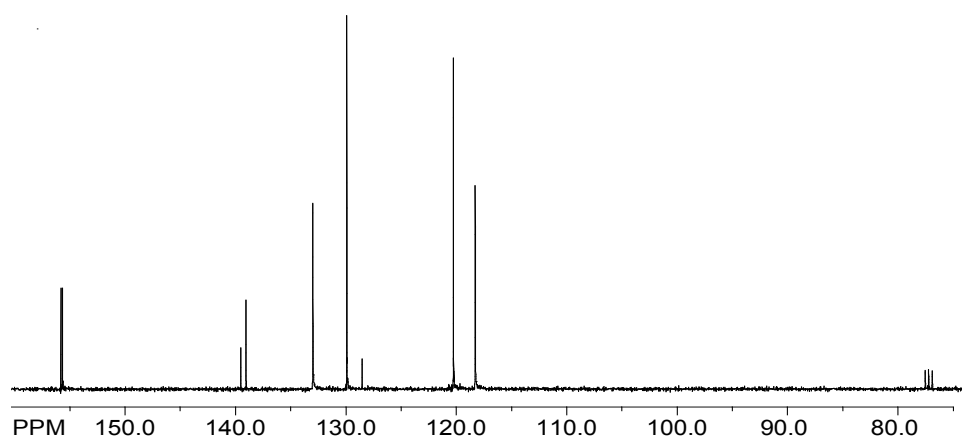
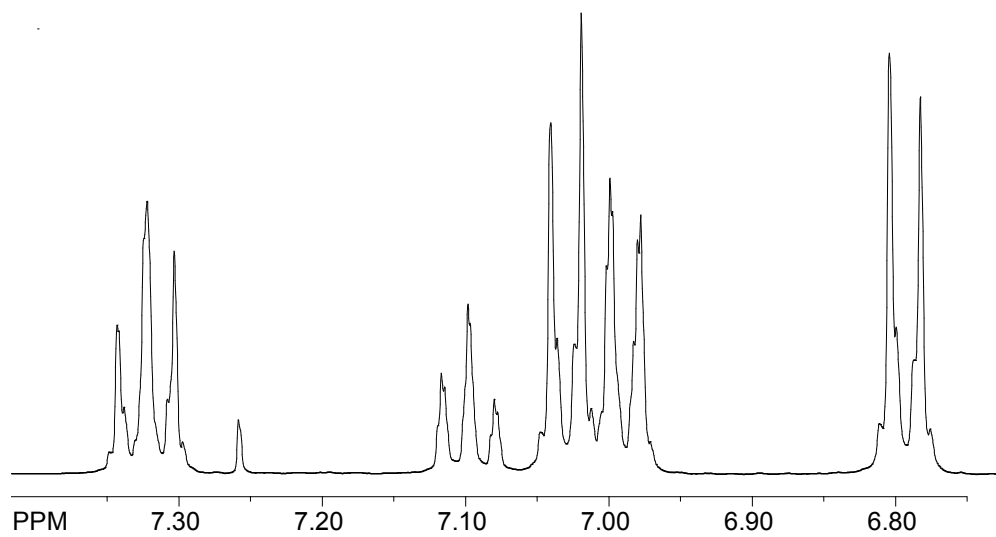
96.25, 97.83, 103.98, 119.08, 132.95, 139.34, 139.52, 154.90, 158.18, 159.00, 159.58, 161.72, 161.73.

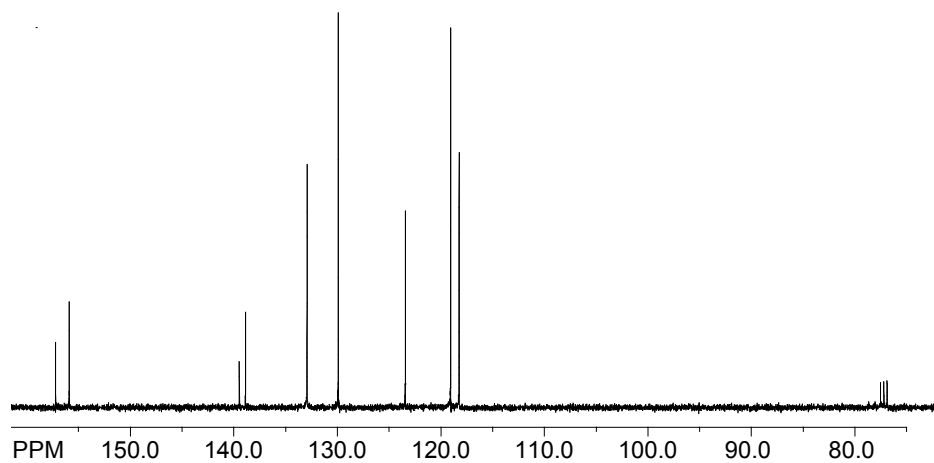
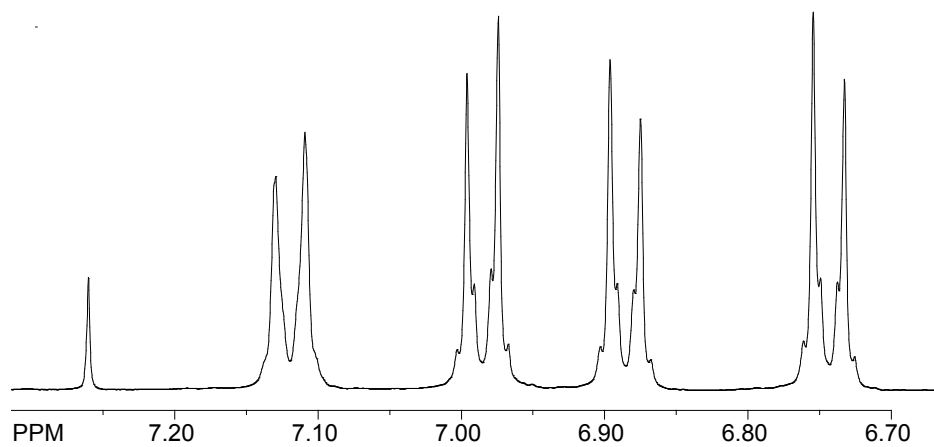
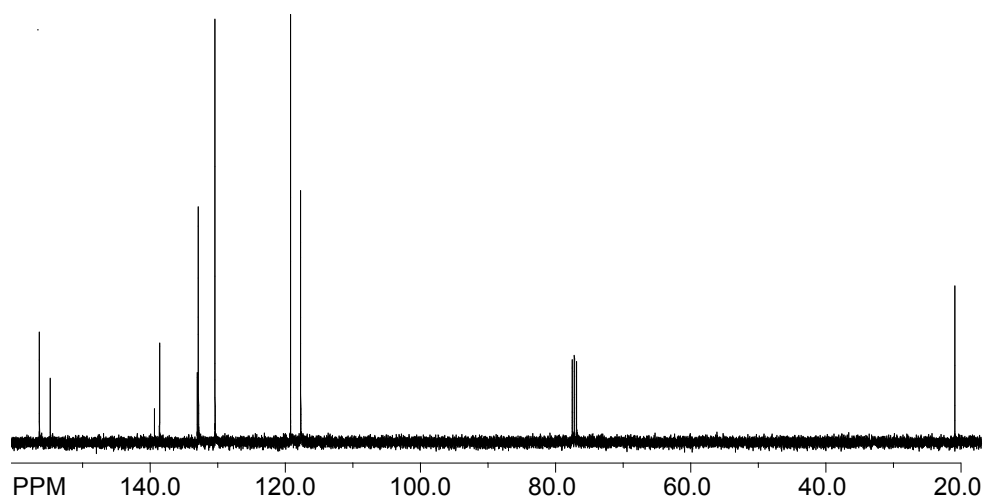
¹H NMR spectrum of tetrakis(4-bromophenyl)ethylene

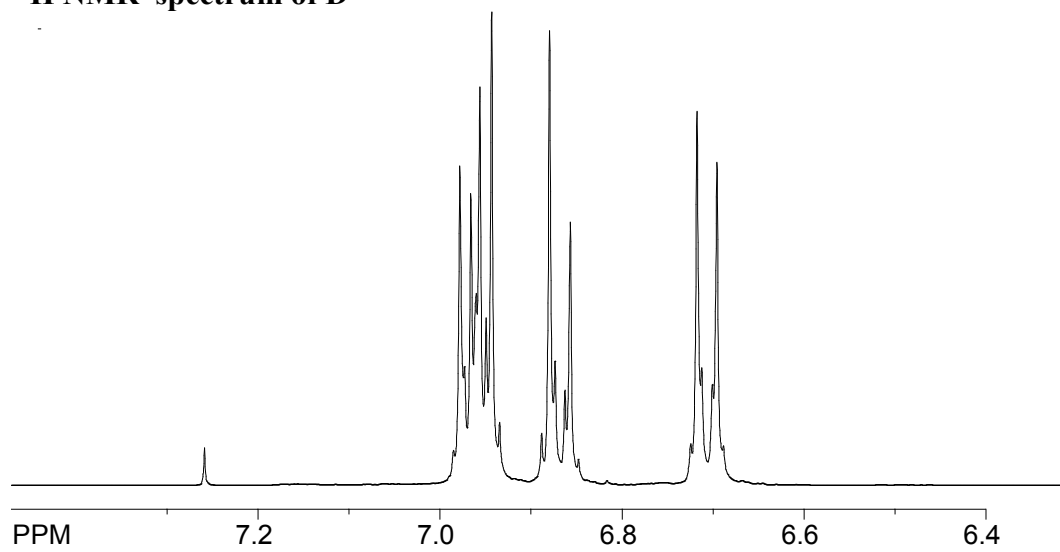
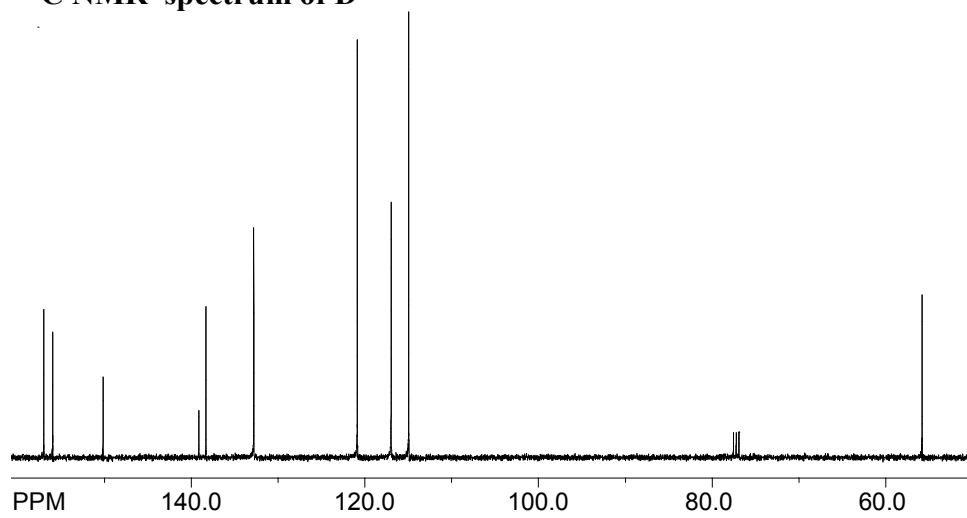
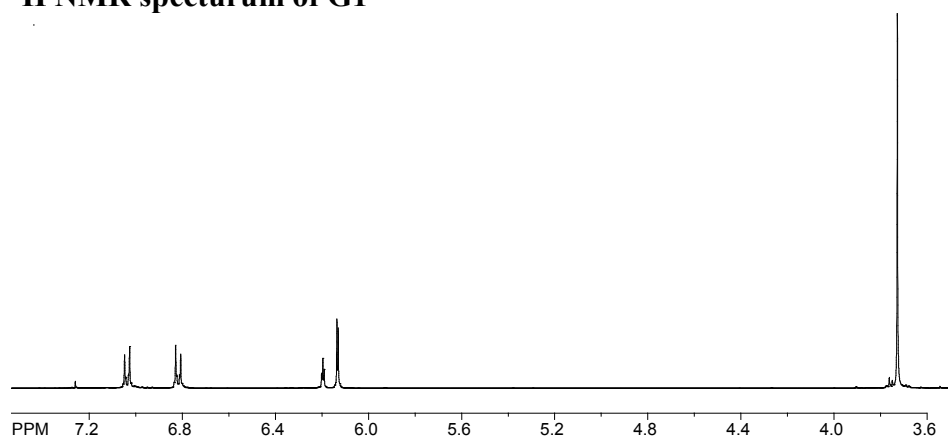


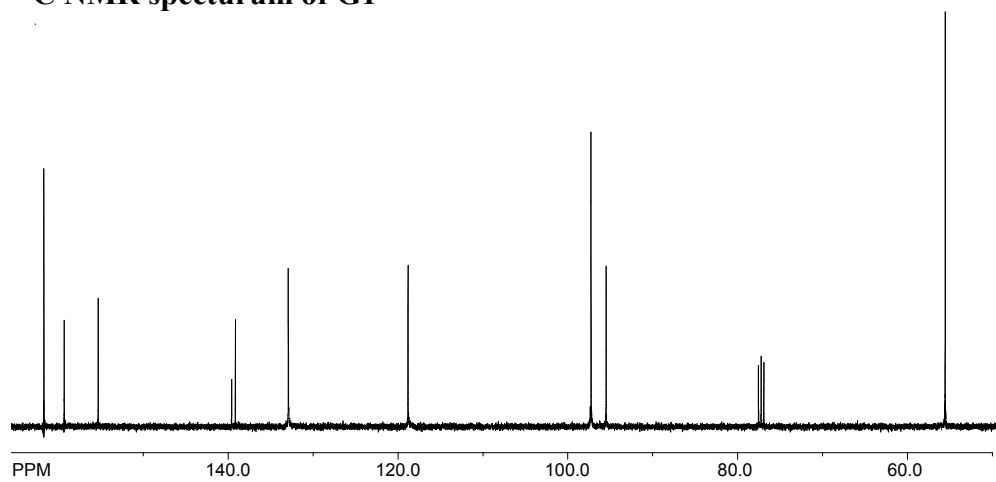
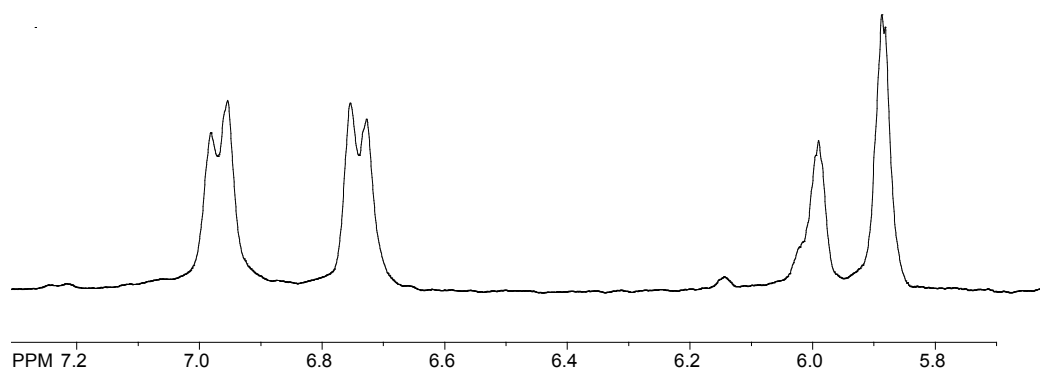
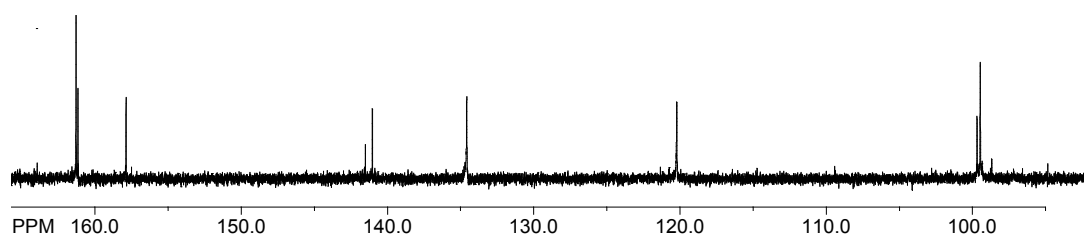
¹³C NMR spectrum of tetrakis(4-bromophenyl)ethylene

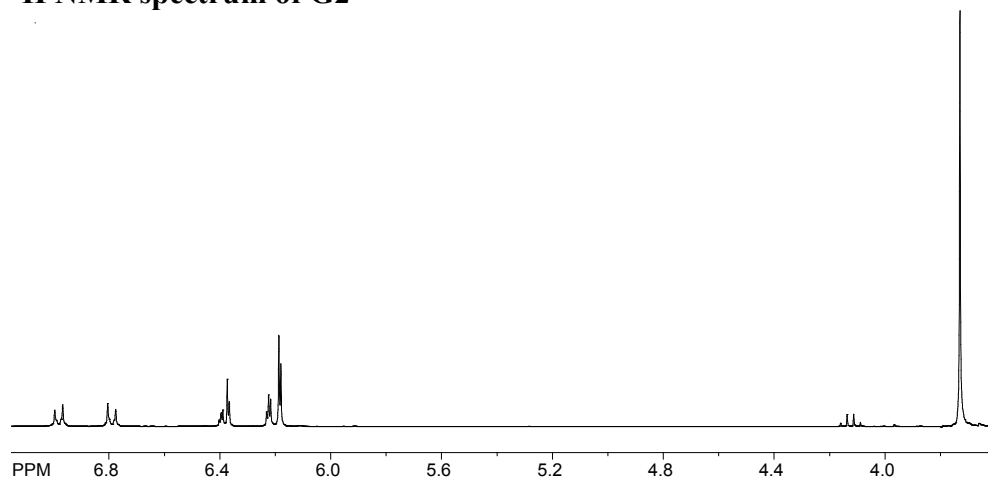
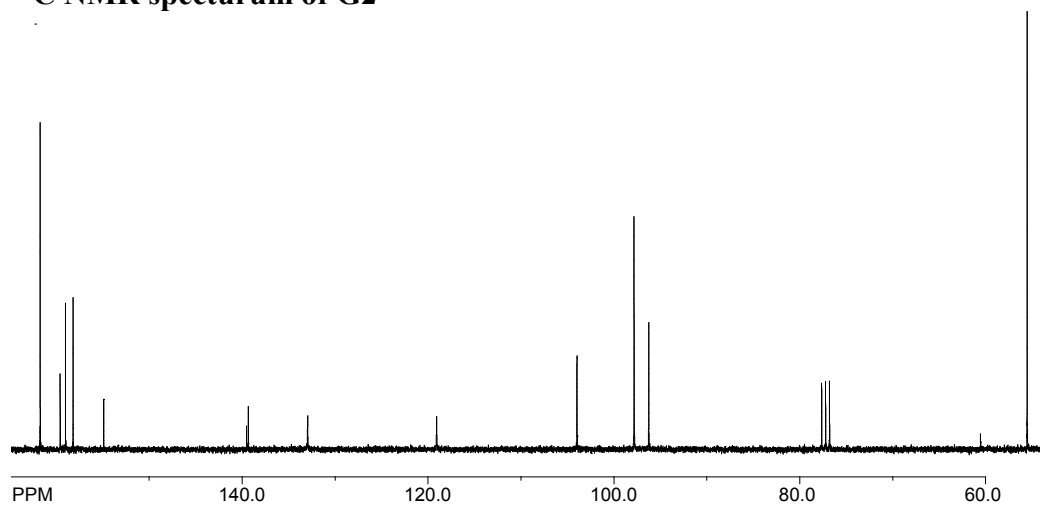


^1H NMR spectrum of A **^{13}C NMR spectrum of A** **^1H NMR spectrum of B**

^1H NMR spectrum of B **^1H NMR spectrum of C** **^{13}C NMR spectrum of C**

^1H NMR spectrum of D **^{13}C NMR spectrum of D** **^1H NMR spectrum of G1**

^{13}C NMR spectrum of G1 **^1H NMR spectrum of demethylated G1** **^{13}C NMR spectrum of demethylated G1**

^1H NMR spectrum of G2 **^{13}C NMR spectrum of G2**

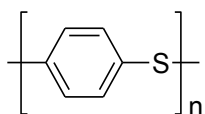
CHAPTER 3B

Structure and Optoelectronic Properties of Acyclic and Cyclic Polyphenyl Ether (PPE) Oligomers

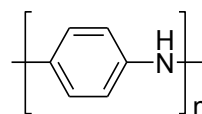
Introduction

The discovery of conducting polyacetylene in 1977¹ opened many doors to study conducting polymers. Among conducting polymers heteroatom containing polymers such as polyphenylene sulfide² and polyaniline³ are known to have unique properties.

Polyphenylene sulfides possess high chemical and thermal stability⁴ and widely used for thermal and chemical resists⁵, while polyanilines show ability to form electrically conducting films⁶ and used for applications in electromagnetic shielding and corrosion inhibition.⁷

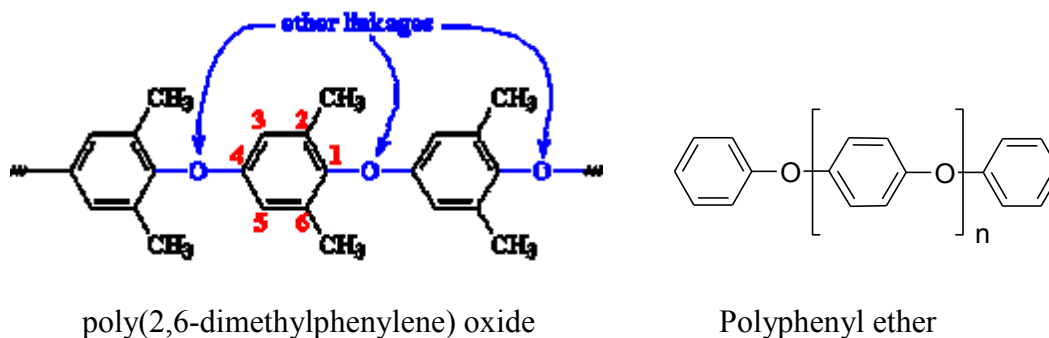


Polyphenylene sulfide



Polyaniline

Polyphenyl ether (PPE) is one of the most important engineering plastics with high strength, excellent heat resistance, high glass transition temperature and good dimensional stability.⁸ Poly(2,6-dimethylphenylene)oxide is commercially available, linear and noncrystalline. Modified PPE is widely used for electrical housings and structural components since it has excellent insulating properties, flame resistance, and dimensional stability over a wide range of service temperatures.



Although some physical and mechanical properties of PPEs such as melting point, boiling point, glass transition temperature, mixing behavior, hardness, tensile strength and elasticity are known, their usage as charge transport materials have been largely unexplored. Our continued interest in charge transport materials prompted us to study a series of polyphenylether oligomers E1-E6 and cyclic phenyl ether E_{cyclic} in which two aryl groups are connected with various number of phenylene oxide units. Electrochemical and optoelectronic analysis of E1-E6 and E_{cyclic} suggests their significant electronic coupling between two end aryl groups connected via phenylene oxide units and the extent of coupling decreases with the chain length for the linear compounds while the cyclic compound shows the most effective coupling. Preliminary details of these findings are described herein.

Results and Discussion

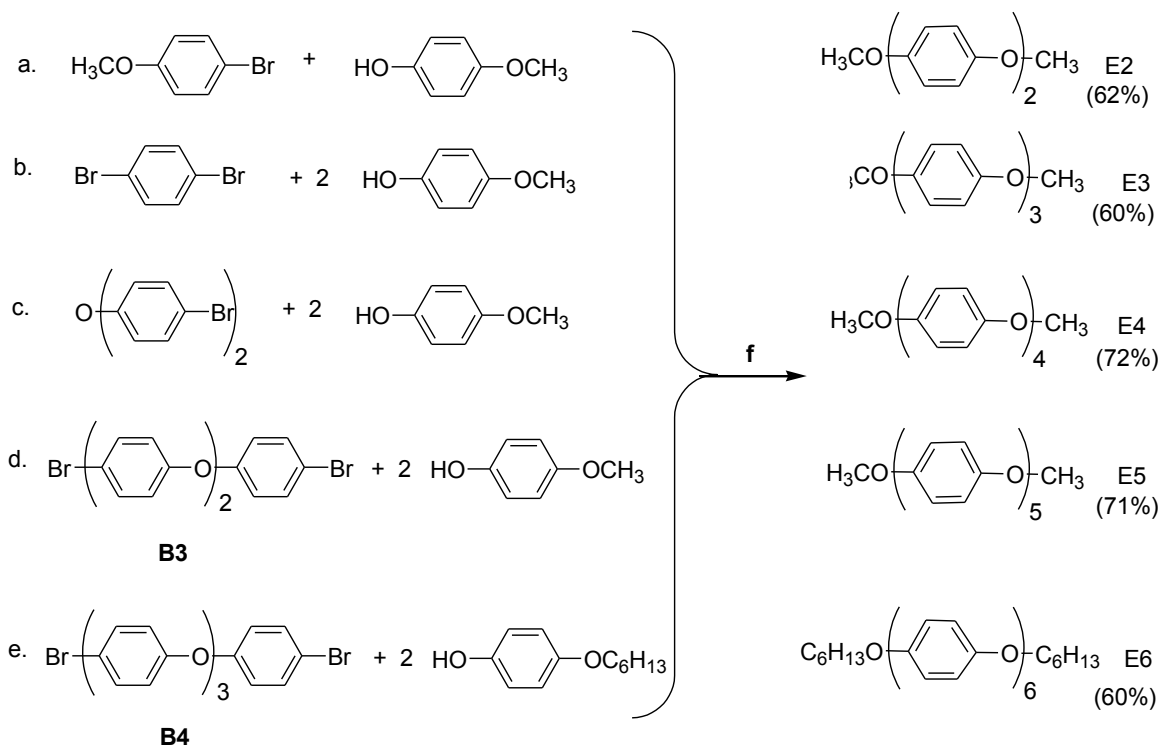
Synthesis of linear and cyclic PPE oligomers (E1- E_{cyclic})

E2 was synthesized from the coupling between one equivalent of each commercially available 4-methoxyphenol and 4-bromoanisole in the presence of equivalent amount of CuO and anhydrous K_2CO_3 at reflux conditions in pyridine. **E3** was prepared by using one equivalent of 1,4 -dibromobenzene and two equivalents of 4-

methoxyphenol using the same reaction conditions. **E4** was prepared by using one equivalent of 4,4'-dibromobiphenylether and two equivalents of 4-methoxyphenol using the same reaction conditions (Scheme 1). The precursors PE₃ and PE₄ for the preparation of B3 and B4 were prepared by using one equivalent of 1,4-dibromobenzene and two equivalents of phenol and one equivalent of 4,4'-dibromobiphenylether and two equivalents of phenol respectively using the same reaction conditions. The B3 and B4 were obtained by bromination of PE₃ and PE₄ with bromine in dichloromethane at room temperature (scheme 2). **E5** was synthesized using one equivalent of B3 and two equivalents of 4-methoxyphenol while one equivalent of B4 and two equivalents of 4-hydroxyphenol were used for **E6** in the said Ullmann reaction conditions (Scheme 1).

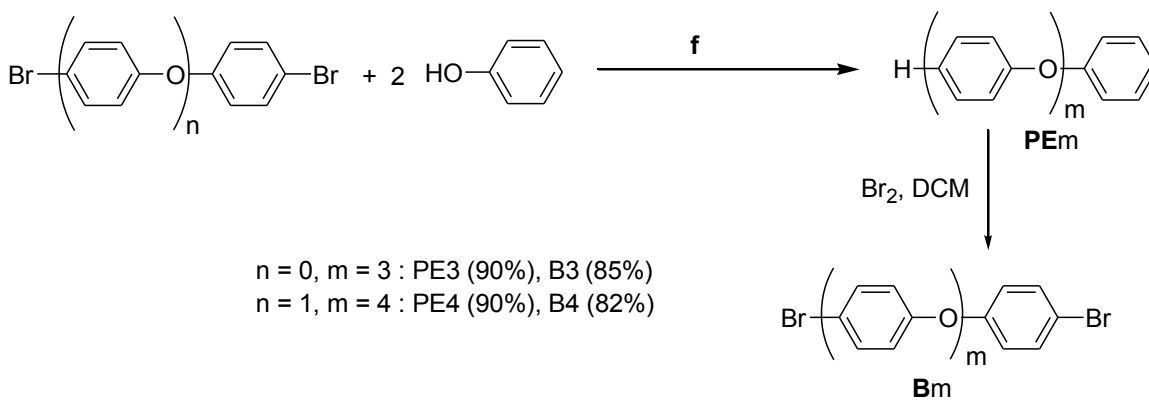
The cyclic ether was prepared by heating one equivalent of 4,4'-(4-hydroxyphenoxy)diphenylether and one equivalent of 4,4'-diiododiphenylether in the presence of N,N-DMG, catalytic amount of CuI and four equivalents of CsCO₃ in DMF under argon atmosphere at 100 °C for 48 h (Scheme 3). Poly *p*-phenylether oligomers were characterized by ¹H/¹³C NMR spectroscopy as well as X-ray crystallography (see Experimental). The X-ray crystal structures show that the angles between adjacent phenyleneoxide moieties are 60.25°, 59.46° and 58.94° for **E2**, **E3**, **E4** respectively. As well as the terminal methoxy group is coplanar with adjacent phenylene oxide moiety (Figure 1).

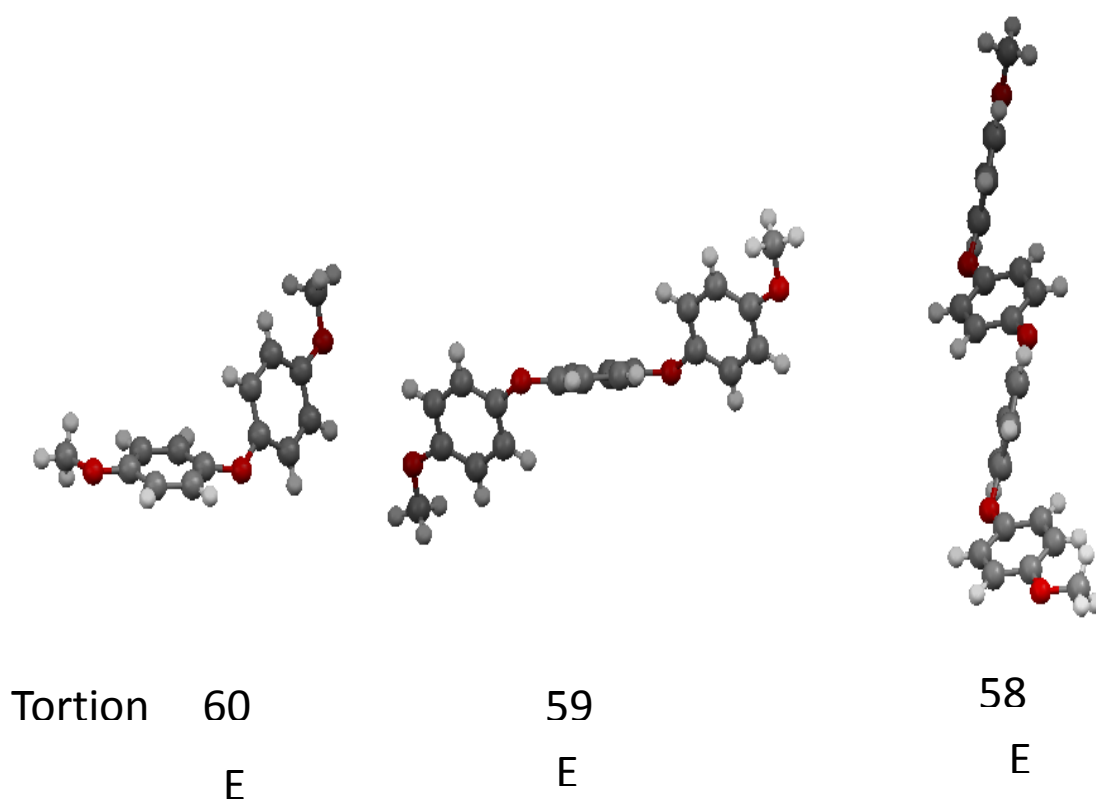
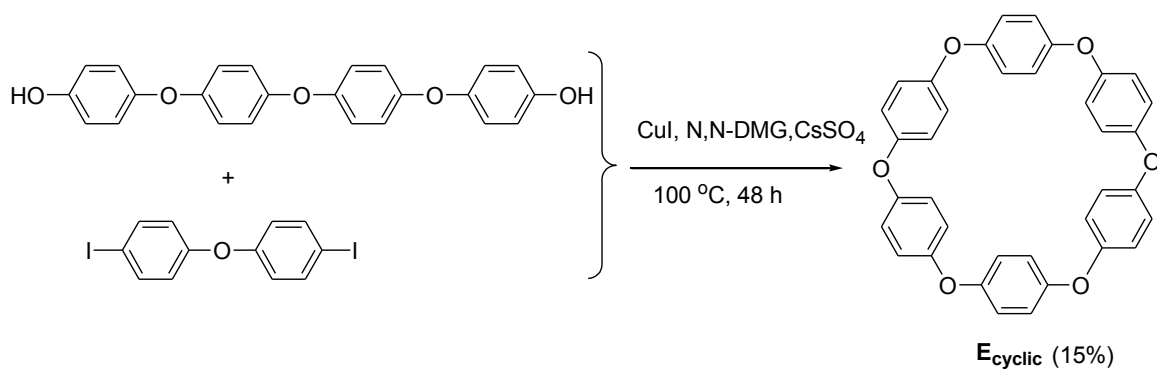
Scheme 1. Synthesis of **E1-E6** by using Ullman coupling.



f: K_2CO_3 , pyridine, CuO , 4-7 days

Scheme 2. Synthesis of precursors **PE3**, **PE4**, **B3**, **B4**



Scheme 3. Synthesis of the cyclic ether oligomer**Figure 1.** The ball and stick display of X-ray crystal structures of E2, E3 and E4 respectively.

Electrochemical Analysis of cyclic and acyclic p-PPEOs (E1-E_{cyclic}, PE3,PE4, DHB)

The redox properties of oligomers were evaluated by electrochemical oxidation of poly-*p*-phenyl ether oligomers at platinum electrode as a 2.5×10^{-3} mM solution in dichloromethane in the presence of 0.2 M tetra-*n*-butylammoniumhexafluorophosphate as the supporting electrolyte at 22 °C. All the potential values were calibrated with ferrocene ($E_{\text{red}} = 0.45$ V). As the Figure 2 shown **E1** shows only one reversible oxidation at 1.34 V vs SCE since it has only one hydroquinone moiety. **E2** shows one reversible (1.40 V vs SCE) and one irreversible (1.85 V vs SCE) while **E3** shows three consecutive quasi-reversible oxidations (1.43, 1.60, 1.71 V vs SCE). **E4**, and **E5** show three oxidations as **E4** (two oxidations at 1.46, 1.90 V vs SCE), **E5** (two oxidations at 1.45, 1.72 V vs SCE). **E6** shows four oxidations (two oxidations at 1.42, 1.63, 1.95 V vs SCE). The cyclic ether shows three oxidations (1.53, 1.78, 1.83 V vs SCE).

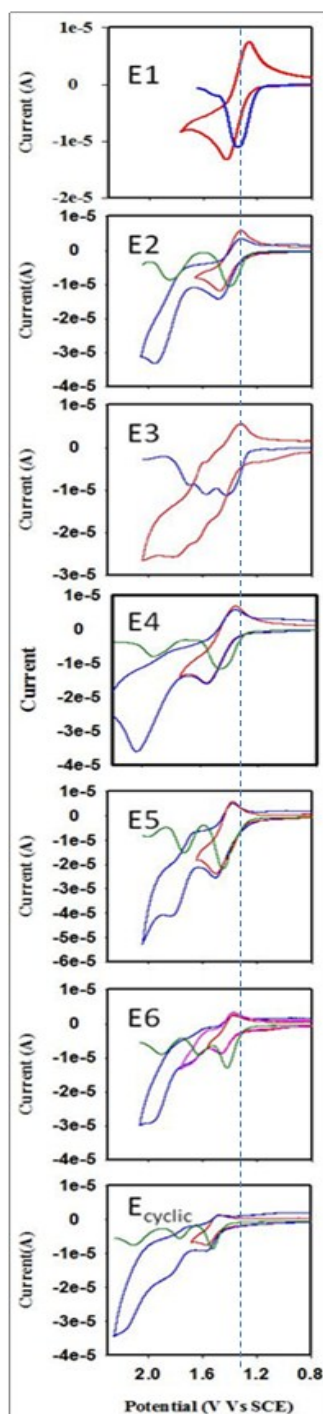


Figure 2. Cyclic voltammograms and square wave voltammograms of the *p*-PPEOs obtained from 2.5×10^{-3} mM solution in dichloromethane in the presence of 0.2 M Tetra-*n*-butylammoniumhexafluorophosphate as the supporting electrolyte at 22°C

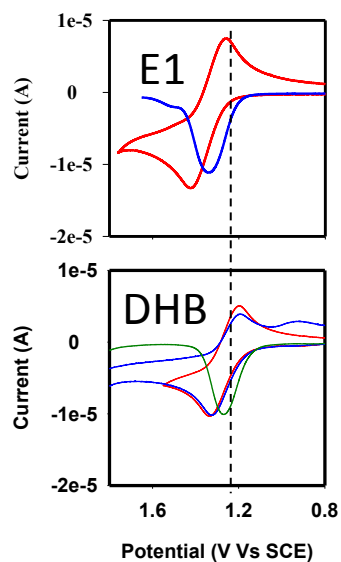


Figure 3. Comparison of Cyclic voltammograms of E1 and 1,4-dihexyloxybenzene obtained from 2.5×10^{-3} mM solution in dichloromethane in the presence of 0.2 M Tetra-n-butylammoniumhexafluorophosphate as the supporting electrolyte at 22°C

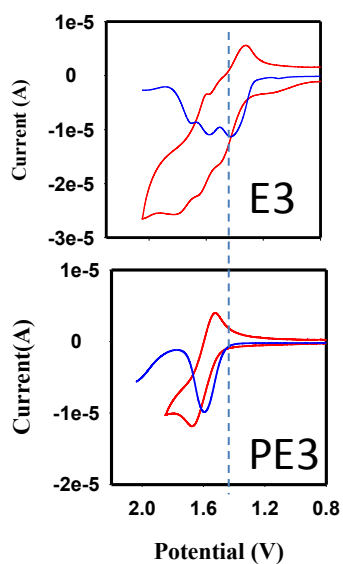


Figure 4. Comparison of Cyclic voltammograms of E3 with PE3 obtained from 2.5×10^{-3} mM solution in dichloromethane in the presence of 0.2 M Tetra-n-butylammoniumhexafluorophosphate as the supporting electrolyte at 22°C.

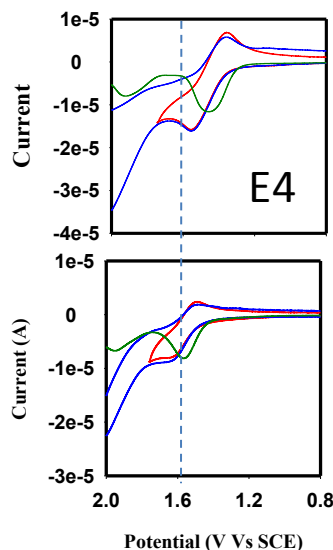


Figure 5. Cyclic voltammograms of **E4** and **PE4** obtained from 2.5×10^{-3} mM solution in dichloromethane in the presence of 0.2 M Tetra-*n*-butylammoniumhexafluorophosphate as the supporting electrolyte at 22°C.

As shown in Figure 3, 1,4-dihexyloxybenzene shows lower potential than that of methoxy substituted compound due to the higher donor ability of hexyloxy than methoxy group. The effect of methoxy substituent can be explained by the higher oxidation potentials shown by **PE3** and **PE4** than that of **E3** and **E4** respectively (Figure 4 and Figure 5). According to these cyclic voltammograms the first oxidation potential of linear ether oligomers is increasing upto **E4** as 1.34, 1.40, 1.43, 1.46 V vs SCE and then become constant ~1.45-1.46 V vs SCE (Table 2). As explained above the cycloannulated biaryl ethers (**1-5**) which can be used as model compound for these polyphenyl ether oligomers show charge delocalization at end aryl groups. Similarly in the poly phenyl ether oligomers the charge delocalization occur on the end aryloxy groups. Thus, this oxidation potential increase is attributed to the decrease in the extent of conjugation as the length of the ether linkage which connects the end aromatic groups increases. The unexpected decrease in the first oxidation potential in **E6** is due to the higher donor

ability of hexyloxy substituents. As the Table 2 shows the second oxidation potential decreases from **E1** to **E6** and the difference between first and second oxidation potentials decreases when the length of the aryl ether bridge increases and become constant. This trend in difference between first and second oxidation potential is explained by the decreasing coupling of the two end aryloxy groups as the length of the ether linkage increases as the HOMO(High Occupied Molecular Orbital) lies at the end aryl groups of the PPE oligomers as shown in Figure 6.

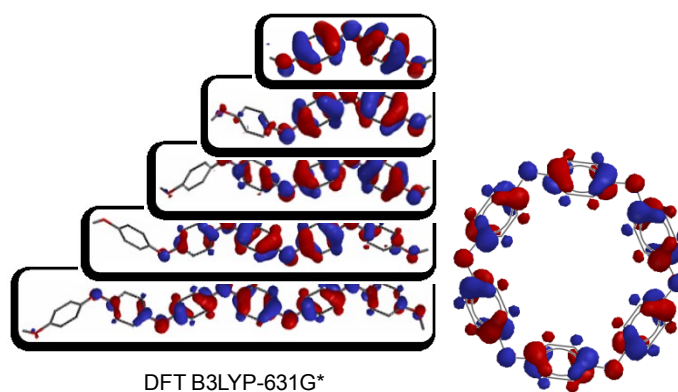


Figure 6. The HOMO Pictures of linear and cyclic ether oligomers.

Table 1. Oxidation potential values of E1-E_{cyclic}, PE3, PE4, DHB

Compound	E^{ox}_1 / V vs SCE	E^{ox}_2 / V vs SCE	E^{ox}_3 / V vs SCE	$E^{ox}_2 - E^{ox}_1$
E1	1.34			1.34
E2	1.40	1.85		0.45
E3	1.43	1.60	1.71	0.17
E4	1.46	1.46	1.90	0.00
E5	1.45	1.45	1.72	0.00
E6	1.42	1.42	1.63	0.00
E _{cyclic}	1.53	1.78	1.83	0.25
DHB	1.27	1.90		
PE3	1.60			
PE4	1.56			

Optical properties of Poly p-phenyl ether oligomers.

The electronic absorption spectra and emission spectra of 4.5×10^{-5} M solutions of (E1-Ecyclic, PE3, PE4, DHB and model 2) in dichloromethane were recorded at 22 °C. The UV-vis spectra of linear ethers show two characteristic bands around 230-240 nm and 283 nm as listed below. The cyclic ether and precursors **E3** and **E4** show four characteristic bands.

Table 2. λ_{\max} values for the bands observed for linear and cyclic poly p-phenyl ethers.

Compound	$\lambda_{\max}/ \text{nm}$		Compound	$\lambda_{\max}/ \text{nm}$	
E1	230	292			
E2	234	283	E _{cyclic}	237	278, 290, 300
E3	240	282	PE3	234	271, 279, 320
E4	242	282	PE4	241	271, 279, 321
E5	245	283			
E6	245	283			

The high energy band around 240 nm which is attributed to $\pi\text{-}\pi^*$ transitions in the phenyl moieties show a slight bathochromic shift with increasing the number of phenylene oxide units indicating that the phenyl rings in the linear phenyl ether oligomers (**E1-E6**) are slightly conjugated and the similar values for the **E5** and **E6** reveals that the conjugation is effective up to five phenylene oxide moities. The $\pi\text{-}\pi^*$ transitions in the phenyl moieties of **PE3** and **PE4** are higher in energy (lower λ_{\max}) than that of **E3** and **E4** respectively and this observation indicates that the donor methoxy groups facilitate the conjugation among phenylene oxide units. The low energy band around 283 nm which is attributed to $n\text{-}\pi^*$ transitions is invariant for linear polyphenyl ether oligomers

(E2-E6). As the Figure 7 (e) shows the emission wave length is invariant for all the poly *p*- phenyl ether oligomers.

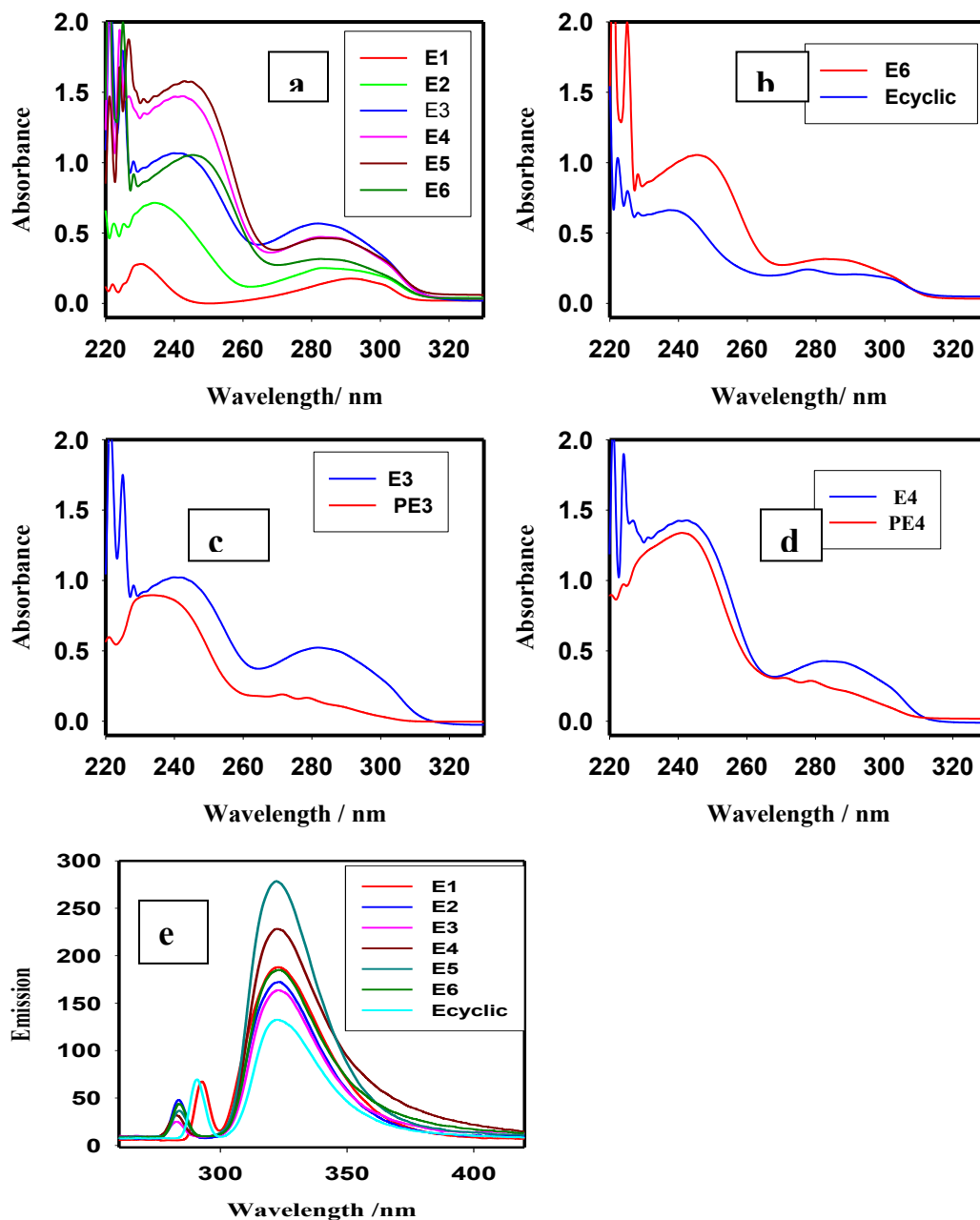


Figure 7. (a) Comparison of the UV-Vis spectra of neutral ethers E1-E6, (b) E6- Eyclic (c) PE3 and E3 (d) PE4 and E4 (e) Emission spectra of E1-E_{yclic} in 4.5×10^{-5} M in dichloromethane at 22 °C.

Electronic absorption spectra of Cation radicals of p-PPEOs

Cation radical of each ether oligomers except **E1** was generated by using one equivalent of $\text{NO}^+\text{SbCl}_6^-$ in anhydrous dichloromethane at 22 °C (Figure 8, 9) as well as by using Laser flash photolysis(Figure 10, 11). The electronic absorption spectra were recorded in UV-vis and near-IR region. As shown in Figure z. the $\text{E}2^{+0} - \text{E}6^{+0}$ spectra contain additional characteristic broad band in the near-IR region centered at ~1300 nm and the intensity of the bands decreases with length of the aryl ether. The cyclic ether shows a band with bathochromic shift (1600 nm) due to having most coupling among aryl groups(Figure 8). The presence of the NIR transitions for the cation radicals of the phenyl ether oligomers suggest that the long range coupling of the end aryloxy groups occurs via hopping mechanism. The decrease in the intensity of the band is also due to the decrease in the extent of coupling between end aryloxy groups.

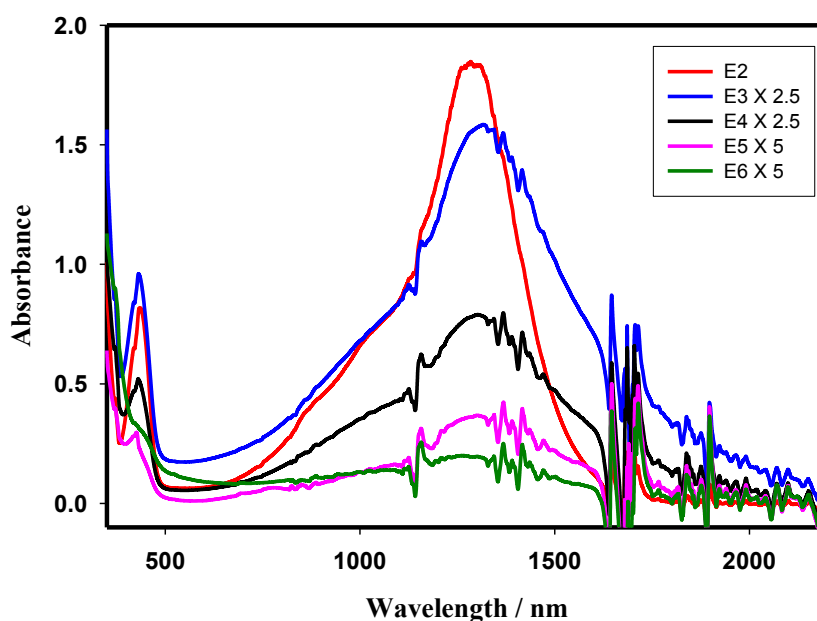


Figure 8. The absorption spectra of 3.02×10^{-4} M Cation radical of linear poly - phenylether oligomers generated by using $\text{NO}^+\text{SbCl}_6^-$.

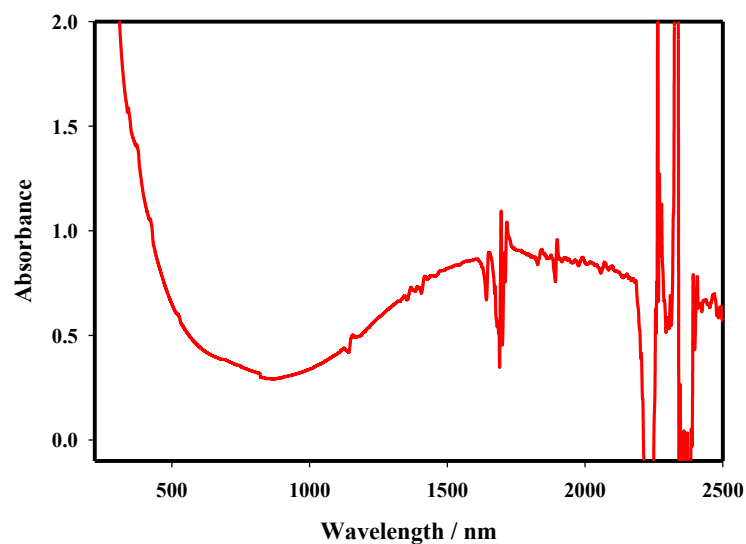


Figure 9. The absorption spectra of Cation radical of cyclic poly-*p*-phenylether oligomers generated by using $\text{NO}^+\text{SbCl}_6^-$.

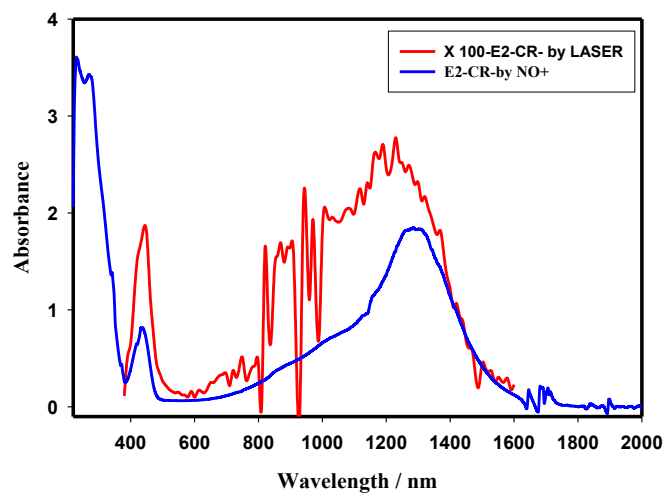


Figure 10. Comparison of The absorption spectra of Cation radical of poly-*p*-phenylether oligomers generated by using $\text{NO}^+\text{SbCl}_6^-$ and Laser flash photolysis.

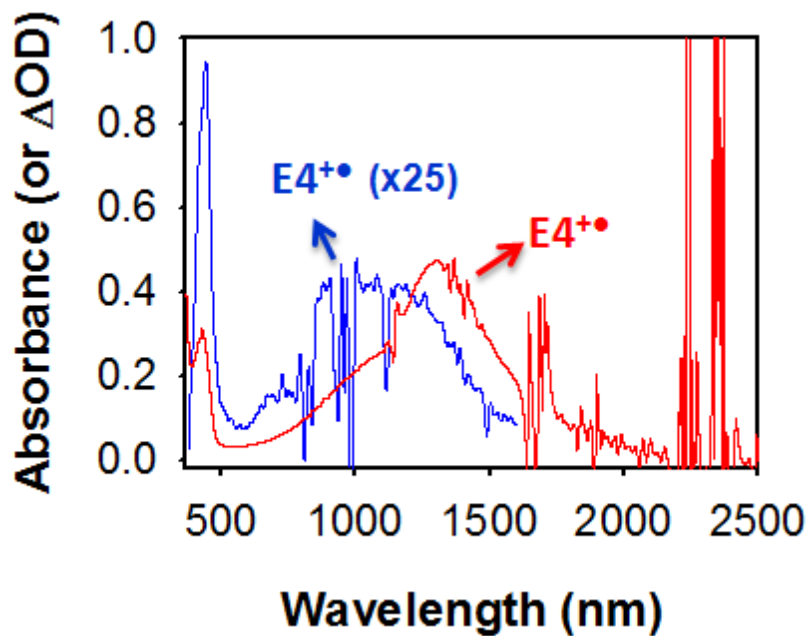
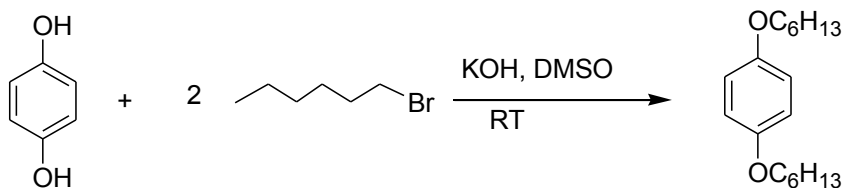


Figure 11. Comparison of the absorption spectra of Cation radical of poly-*p*-phenylether oligomers generated by using $\text{NO}^+\text{SbCl}_6^-$ (red) and Laser flash photolysis (blue).

Experimental

Synthesis of 1,4 – dihexyloxybenzene



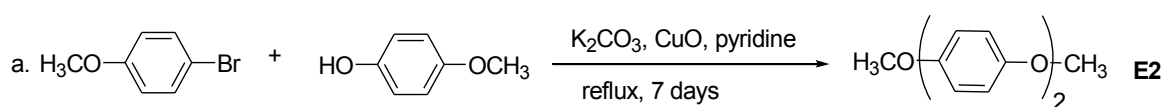
KOH (2.24 g, 40 mmol) was suspended in DMSO (40 mL) and then Hydroquinone (1.10 g, 10 mmol) was added and stirred for few minutes. 1-Bromohexane (3.30 g, 20 mmol) was added drop wise to the resulting mixture and stirred for 30 minutes. Cold water (30 mL) was added to the reaction mixture and the crude product

was extracted to dichloromethane (25 mL x 2) and purified by column chromatography using hexane as the eluent.

Yield (95%) ; $^1\text{H NMR}$ (CDCl_3) δ : 0.92 (t, $J = 6.7, 13.3$ Hz, 6H), 1.35 (m, 8H), 1.46 (m, 4H), 1.76 (qn, 4H), 3.91 (t, 4H), 6.83 (s, 4H). $^{13}\text{C NMR}$ (CDCl_3)

δ : 14.25, 22.83, 25.95, 29.57, 31.83, 68.84, 115.57, 153.39.

Synthesis of E2



p-methoxybromobenzene (4.6 g, 25 mmol), *p*-methoxyphenol (3.72 g, 30 mmol),

K_2CO_3 (3.8 g, 28 mmol), pyridine (15 mL) were placed in a 100 mL Schlenk flask under argon atmosphere and evacuated and backfilled the flask with argon three times. Then

CuO (2.23 g, 28 mmol) was added into the flask under argon atmosphere and refluxed for 7 days. The reaction mixture was cooled, dissolved in dichloromethane (100 mL) and

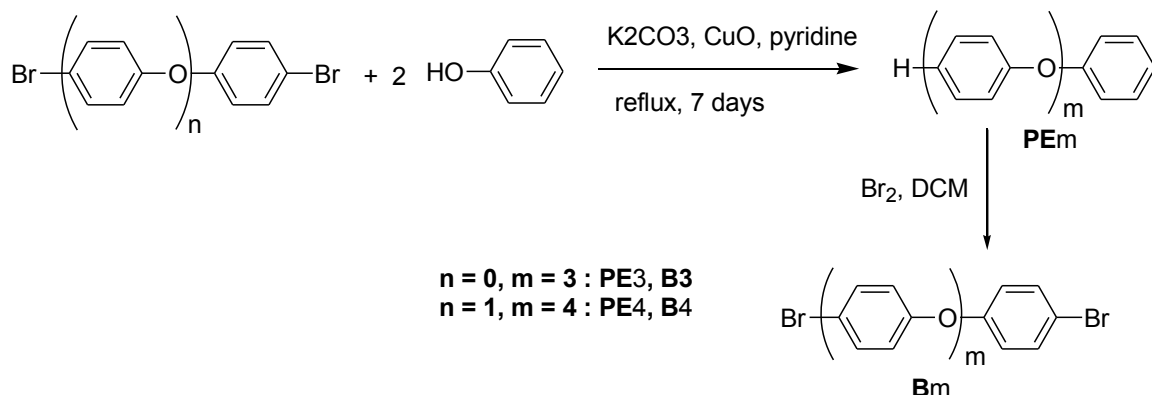
filtered through short Silica Gel column. The obtained dark red solution was treated with dil. HCl (25 x 2 mL), and then with dil. NaOH (25 x 2 mL), dried over anhydrous

MgSO_4 and evaporated to isolate dark red crude product which was recrystallized with dichloromethane/ methanol (1:1) mixture to afford white solid.

E2: Yield (62%) ; mp: 101-102 °C. $^1\text{H NMR}$ (CDCl_3) δ : 3.79 (s, 6H), 6.88 (m, 8H). ^{13}C

NMR (CDCl_3) δ : 55.88, 114.95, 119.74, 151.79, 155.53.

General Procedure for the synthesis of PE3, PE4 intermediate compounds



Dibromocompound (1 mmol), phenol (3 mmol), K_2CO_3 (2.8 mmol), pyridine (15 mL) were placed in a 100 mL Schlenk flask under argon atmosphere and evacuated and backfilled the flask with argon three times. Then CuO (2.8 mmol) was added into the flask under argon atmosphere and refluxed for 7 days. The reaction mixture was cooled, dissolved in dichloromethane (100 mL) and filtered through short Silica Gel column. The obtained dark red solution was treated with dil. HCl (25 x 2 mL), and then with dil. NaOH (25 x 2 mL), dried over anhydrous MgSO_4 and evaporated to isolate dark red crude product which was recrystallized with dichloromethane/ methanol (1:1) mixture afforded white solid.

PE3 Yield (90 %) ; ^1H NMR (CDCl_3) δ : 6.99 – 7.03 (m, 8H), 7.10 (t, $J = 7.3, 14.8$ Hz, 2H), 7.34 (d, $J = 8.68$ Hz, 4H) . ^{13}C NMR (CDCl_3) δ : 118.45, 118.46, 120.66, 123.19, 129.93, 152.85, 157.94.

PE4 Yield (90 %) ; ^1H NMR (CDCl_3) δ : 6.97 – 7.03 (m, 12H), 7.09 (t, $J = 7.3, 14.8$ Hz, 2H), 7.33 (dd, $J = 8.68$ Hz, 4H) . ^{13}C NMR (CDCl_3) δ : 118.42, 120.05, 120.71, 120.72, 123.18, 129.94, 152.65, 153.44, 157.97.

General Procedure for the synthesis of B3, B4 intermediate compounds

Bromine liquid (2 equiv.) in dichloromethane was added dropwise to a solution of the white solid products PE3(or PE4) (1 equiv.) in a round bottomed flask at room temperature, stirred for 5 minutes, aqueous NaHSO₃ solution was added and stirred for few minutes, extracted with dichloromethane, dried over anhydrous MgSO₄ and evaporated to isolate pale brown solid which was recrystallized with dichloromethane/methanol(1:1) to yield white solid products B3 (or B4) respectively.

B3 Yield (85%) ; ¹H NMR (CDCl₃) δ : 6.88 (d, *J* = 8.99 Hz, 4H), 6.99 (s, 4H), 7.43 (d, *J* = 8.99 Hz, 4H) ¹³C NMR(CDCl₃) δ : 115.71, 120.15, 120.80, 132.89, 152.70, 157.04.

B4 Yield (82%) ; ¹H NMR (CDCl₃) δ : 6.89 (d, *J* = 8.99 Hz, 4H), 6.99 (s, 8H), 7.42 (d, *J* = 8.99 Hz, 4H), ¹³C NMR (CDCl₃) δ : 115.57, 120.02, 120.18, 120.85, 132.86, 152.20, 153.68, 157.22.

As the above Scheme 1 explains dibromocompound (1 mmol), *p*- alkyloxyphenol (3 mmol), K₂CO₃ (2.8 mmol), pyridine (15 mL) were placed in a 100 mL Schlenk flask under argon atmosphere and evacuated and backfilled the flask with argon three times. Then CuO (2.8 mmol) was added into the flask under argon atmosphere and refluxed for 7 days. The reaction mixture was cooled, dissolved in dichloromethane (100 mL) and filtered through short Silica Gel column. The obtained dark red solution was treated with dil. HCl (25 x 2 mL), treated with dil. NaOH (25 x 2 mL), dried over anhydrous MgSO₄ and evaporated to isolate dark red crude product which was recrystallized with dichloromethane/ methanol (1:1) mixture white solids.

E3: Yield (60%) ; mp: 139-140 °C; ¹H NMR (CDCl₃) δ: 3.79 (s, 6H), 6.84-6.99 (m, 12H). ¹³C NMR (CDCl₃) δ : 55.84, 114.99, 119.33, 120.26, 151.09, 155.60, 155.79.

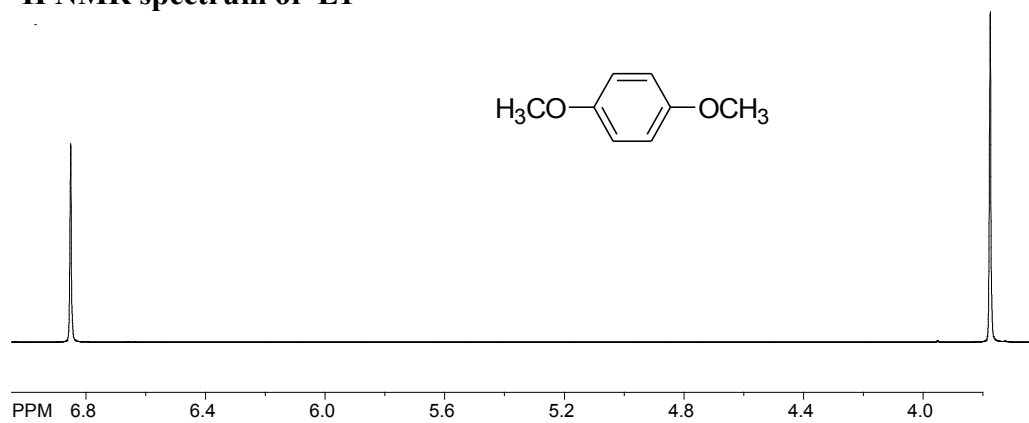
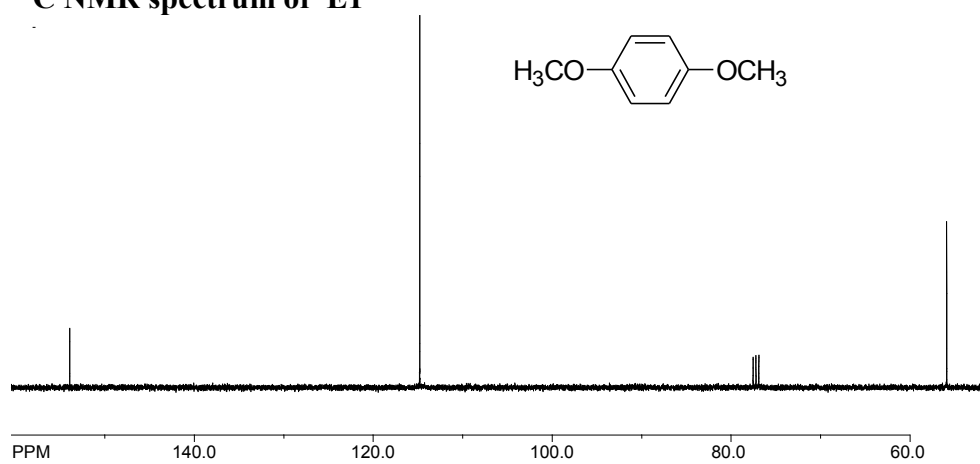
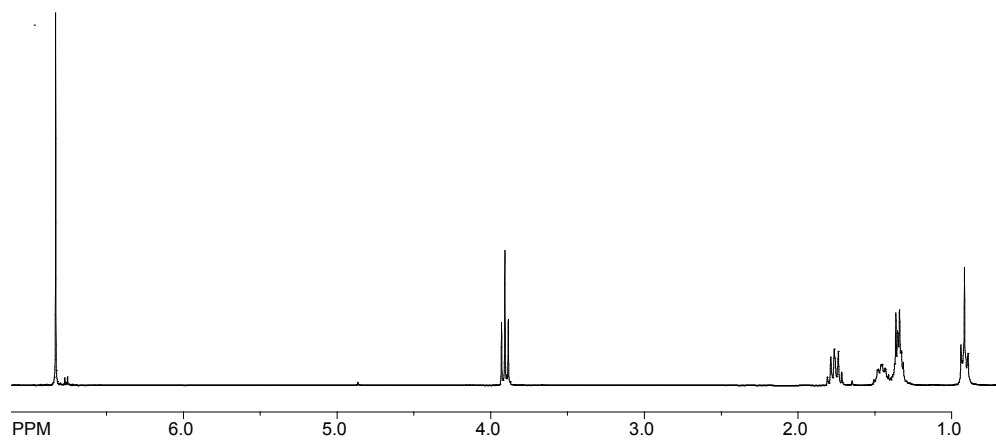
E4: Yield (72%) ; mp: 171-172 °C; ¹H NMR (CDCl₃) δ: 3.80 (s, 6H), 6.85-6.96 (m, 16H). ¹³C NMR (CDCl₃) δ : 55.89, 115.06, 119.34, 120.42, 150.98, 152.96, 154.04, 155.92.

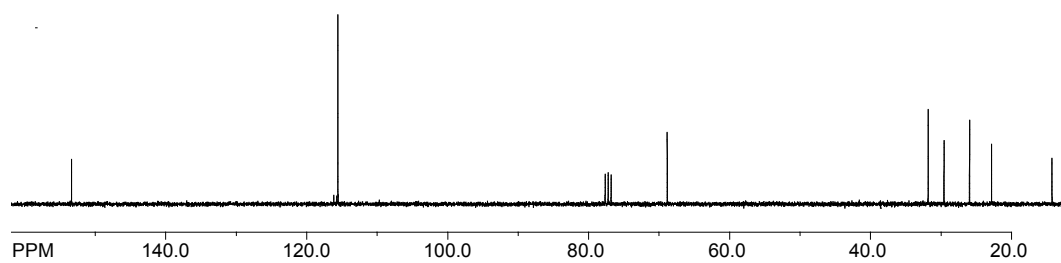
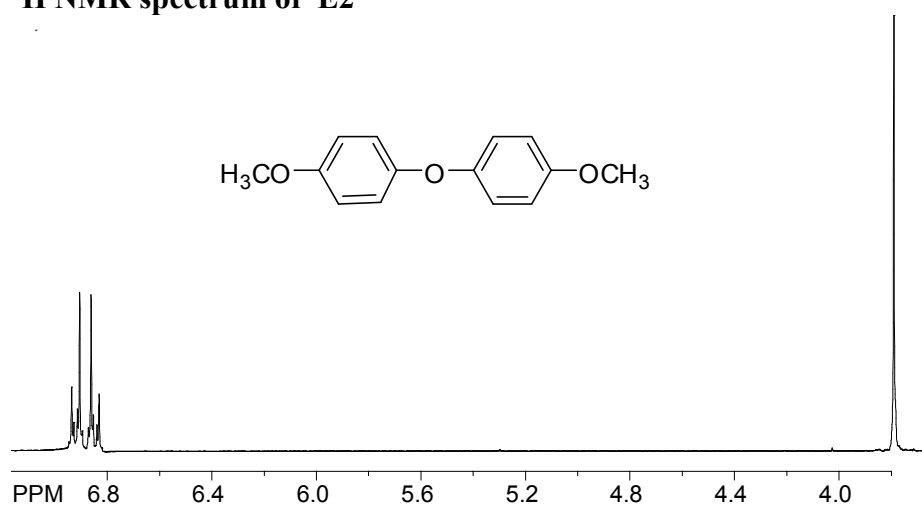
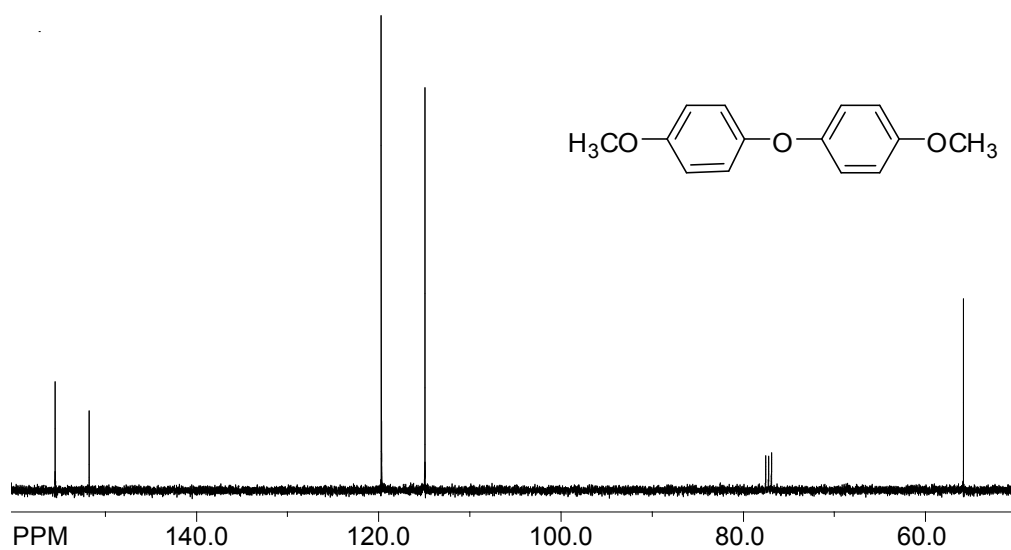
E5: Yield (71%) ; mp: 184-185 °C; ¹H NMR (CDCl₃) δ: 3.80 (s, 6H), 6.84-7.05 (m, 20H). ¹³C NMR(CDCl₃) δ: 55.97, 115.26, 119.47, 119.97, 120.10, 120.43, 151.24, 153.03, 153.55, 154.27, 156.14.

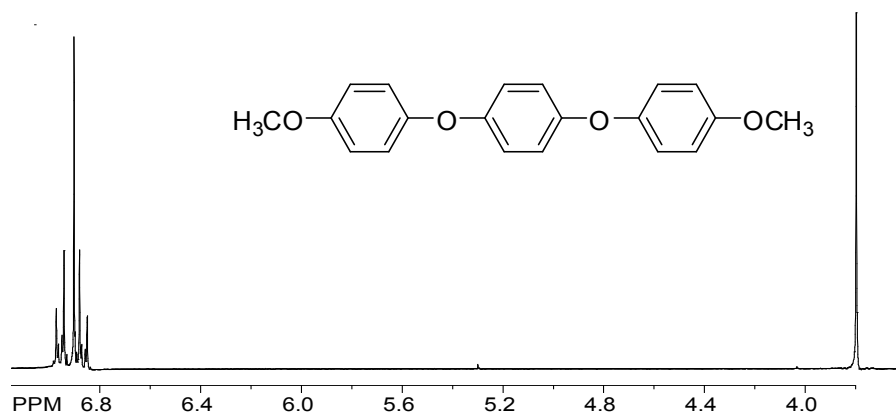
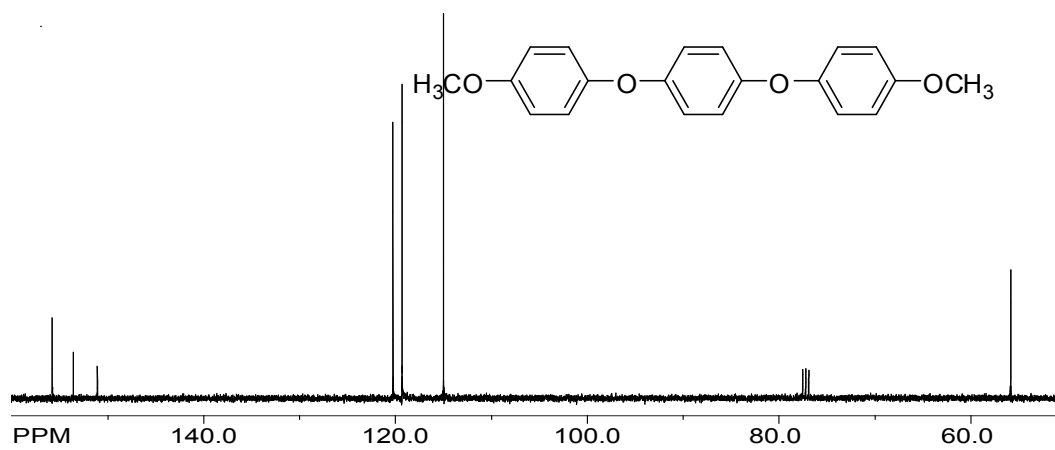
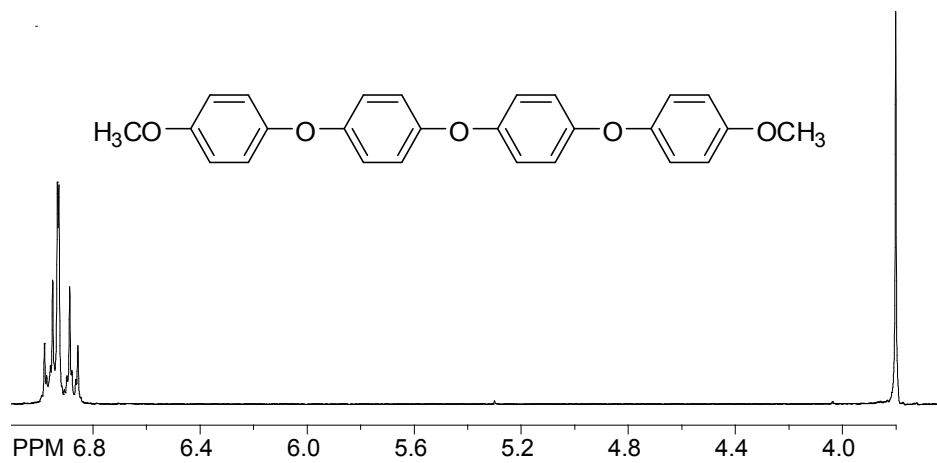
E6: Yield (60%) ; ¹H NMR (CDCl₃) δ: 0.92 (t, *J* = 7.17, 14.16 Hz, 6H), 1.33-1.53(m, 12H), 1.78 (qn, 4H), 3.94 (t, *J* = 6.42, 13.08 Hz, 4H), 6.84-7.03 (m, 24H). ¹³C NMR (CDCl₃) δ : 14.18, 22.82, 25.99, 29.60, 31.85, 68.98, 115.96, 119.43, 119.95, 120.08, 120.13, 120.43, 151.04, 152.94, 153.40, 153.67, 154.37.

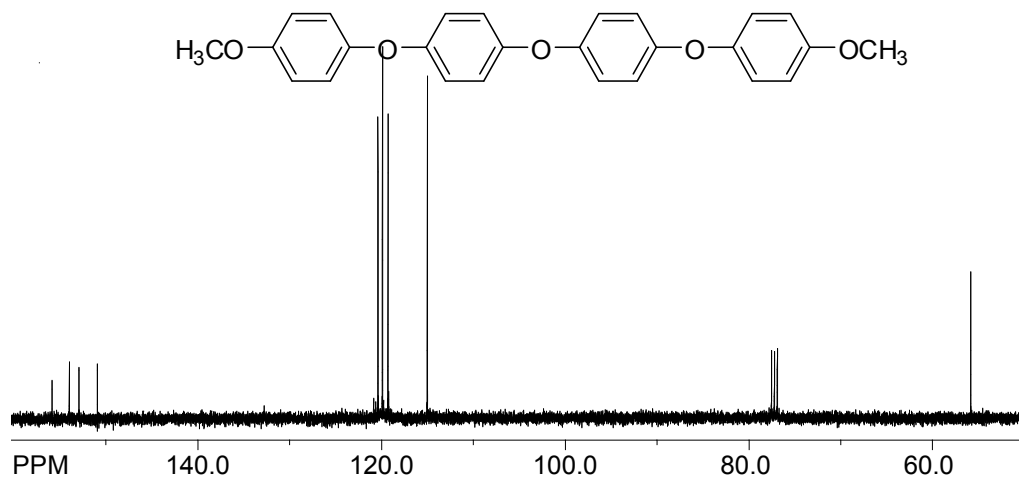
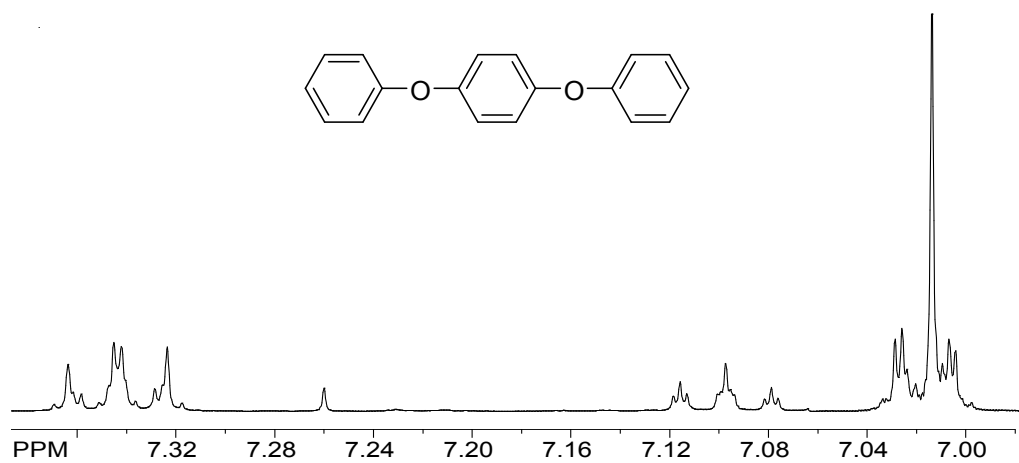
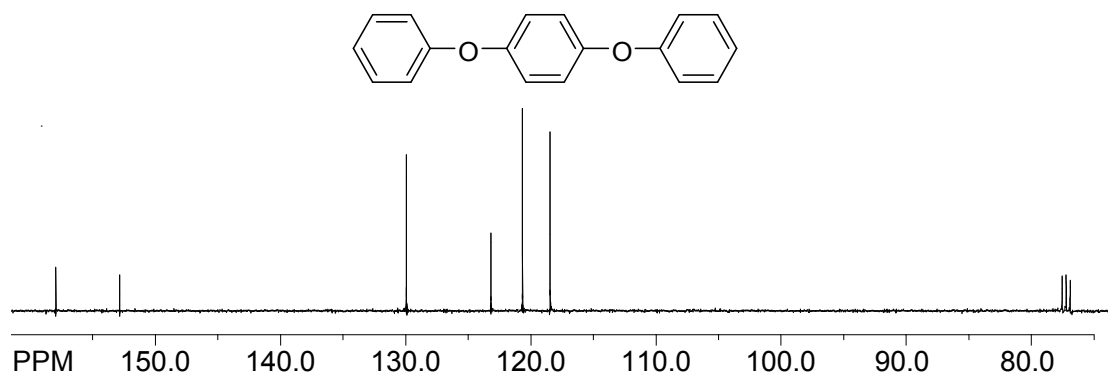
To a 100 mL Schlenk flask were added 4,4'-(4-hydroxyphenoxy)diphenylether (1.80 g, 4.66 mmol), 4,4'-diiododiphenylether (1.96 g, 4.66 mmol), CuI (0.11 g, 0.58 mmol), N,N-DMG (0.19 g, 1.86 mmol), CsCO₃ (6.07 g, 18.6 mmol) and DMF (100 mL) under argon atmosphere and heated at 100 °C for 48 h. The reaction mixture was cooled to room temperature and water (100 mL) was added into it , extracted with dichloromethane (50 mL x 2) and dried over anhydrous MgSO₄ and evaporated to isolate dark colored crude product which was purified by column chromatography using hexane: ethylacetate (95:5) as the eluent.

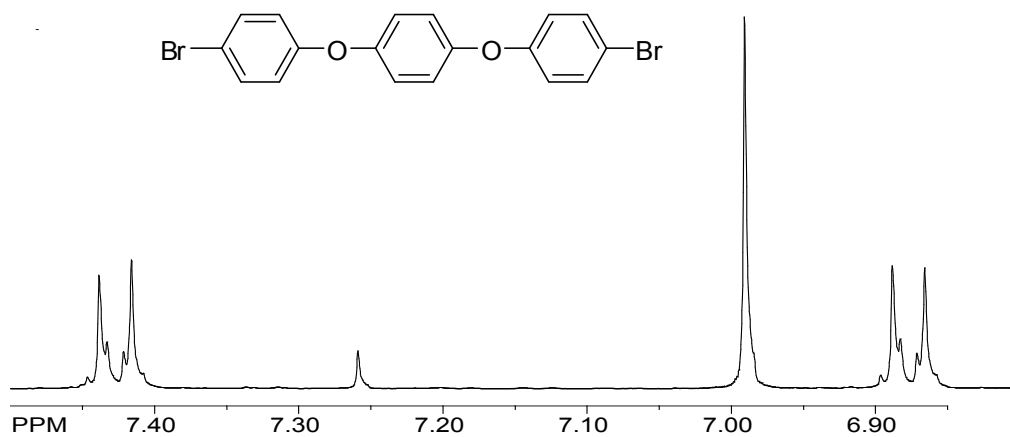
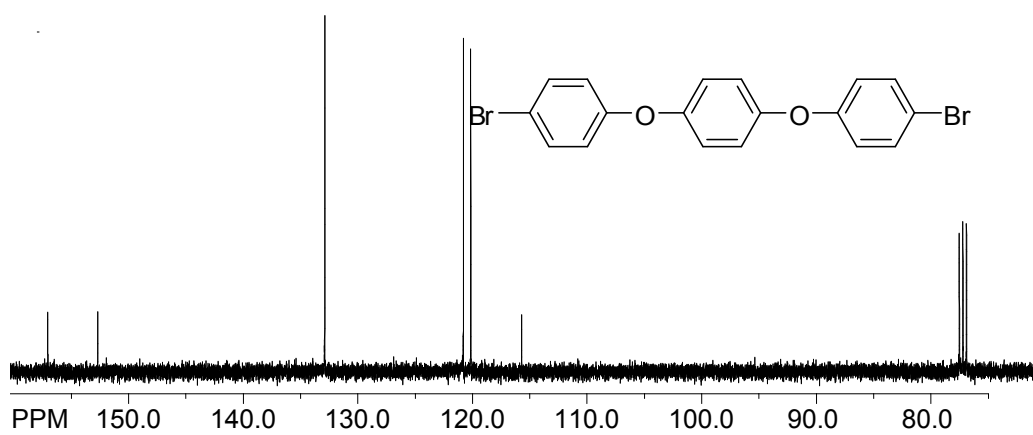
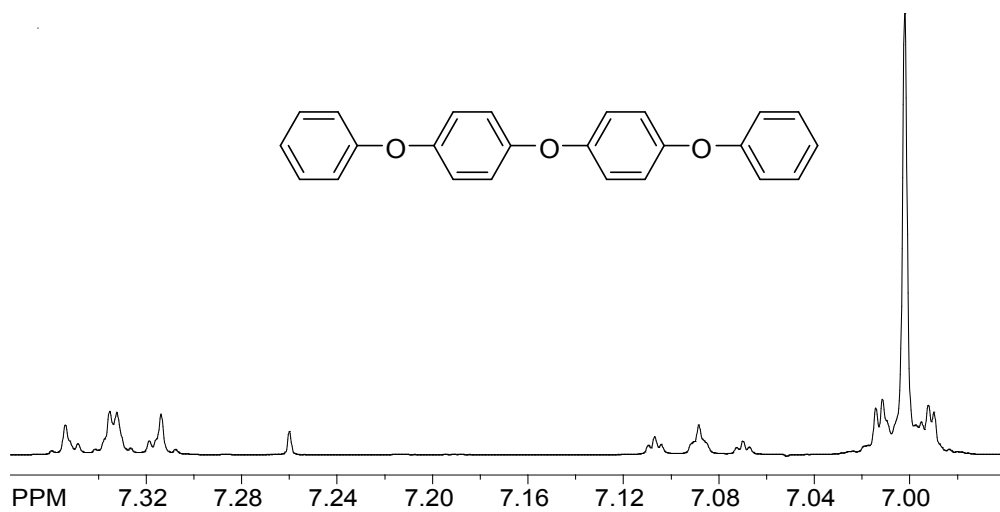
E_{cyclic}: Yield (15%); ¹H NMR (CDCl₃) δ: 6.85 (s, 24H). ¹³C NMR (CDCl₃) δ : 120.55, 154.33.

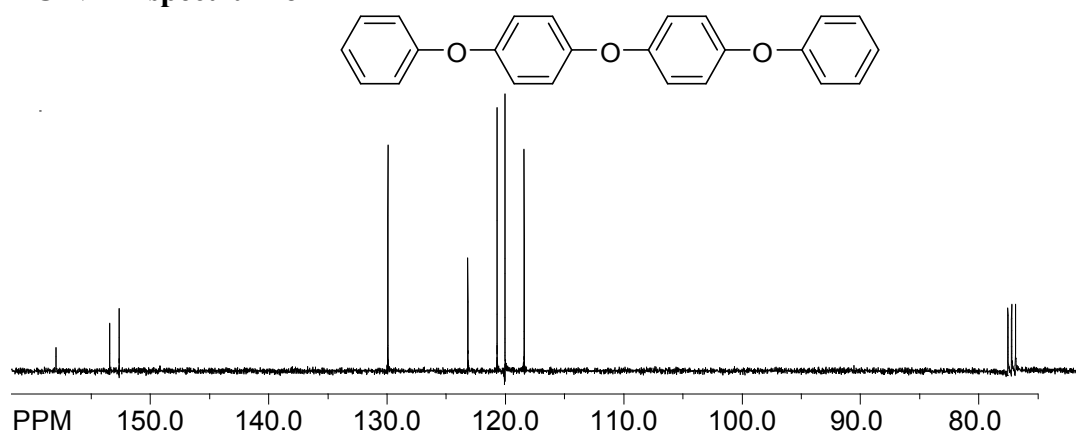
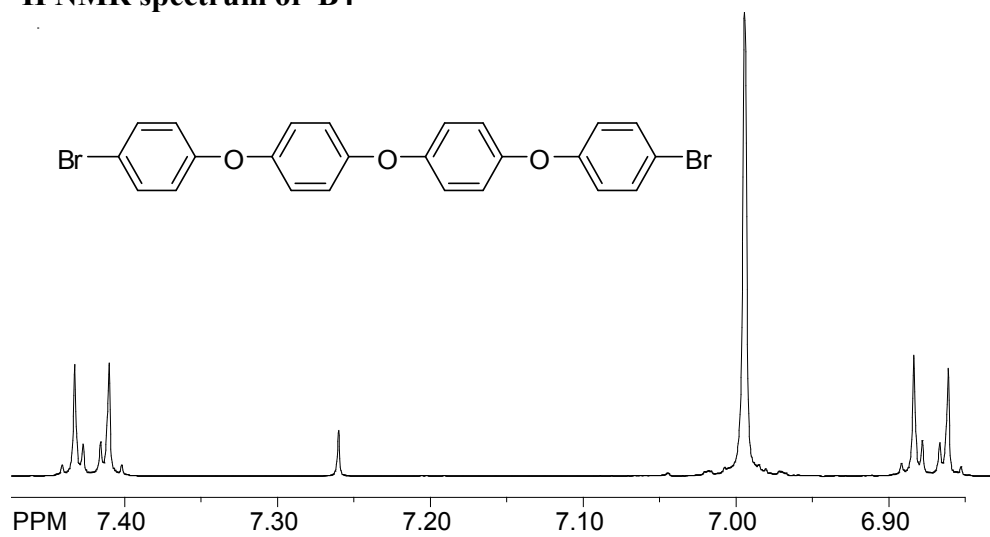
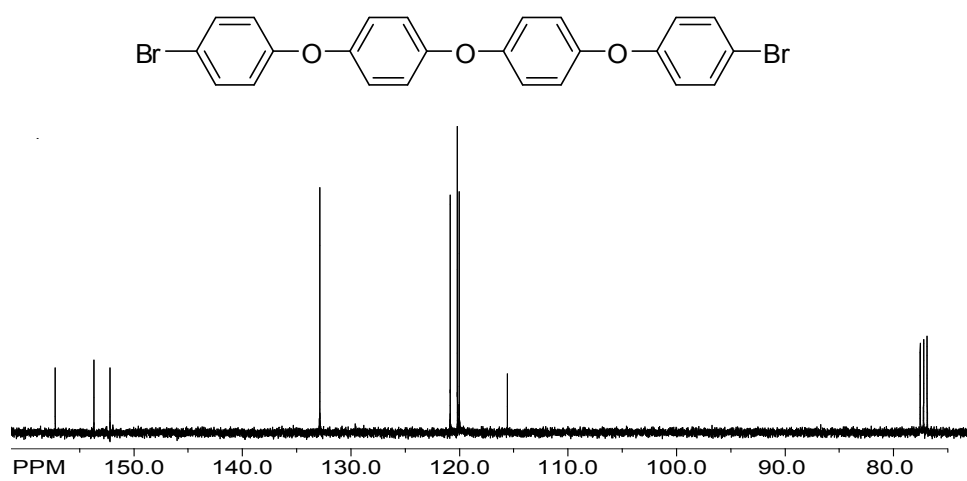
¹H NMR spectrum of E1**¹³C NMR spectrum of E1****¹H NMR spectrum of 1,4-dihexyloxybenzene**

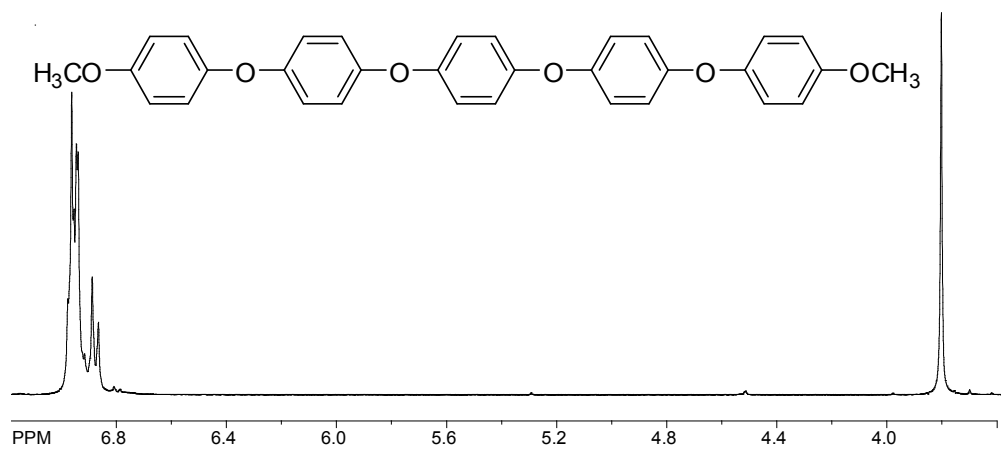
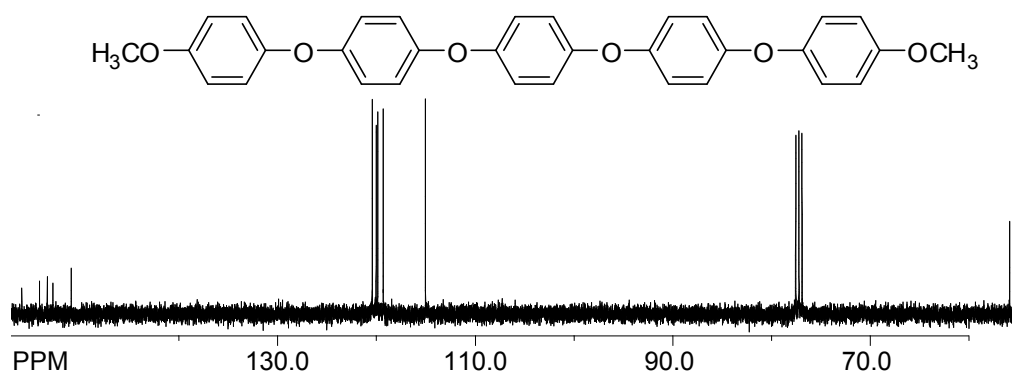
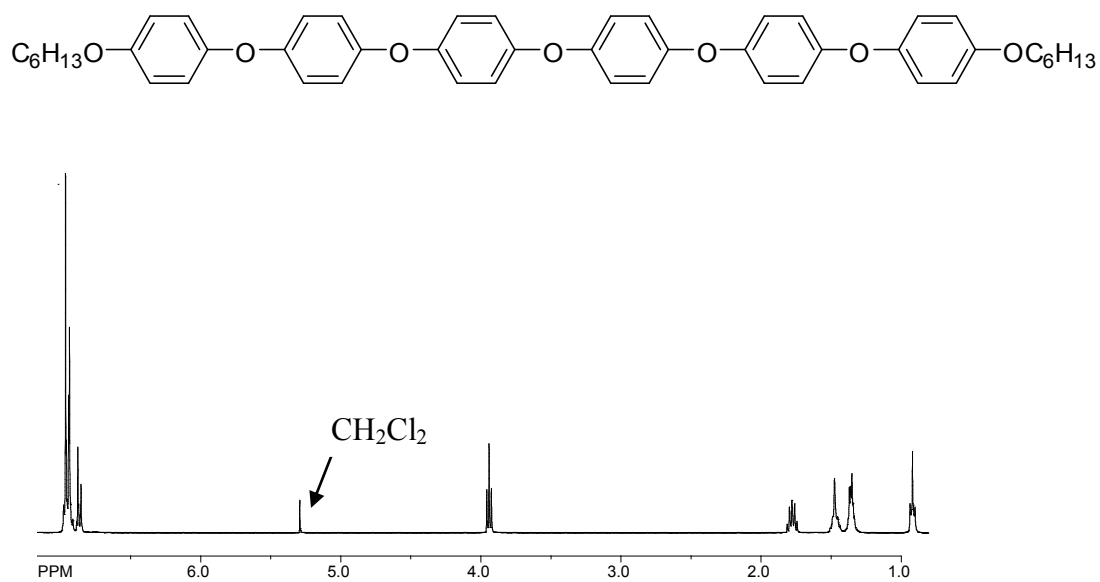
^1H NMR spectrum of 1,4-dihexyloxybenzene **^1H NMR spectrum of E2** **^{13}C NMR spectrum of E2**

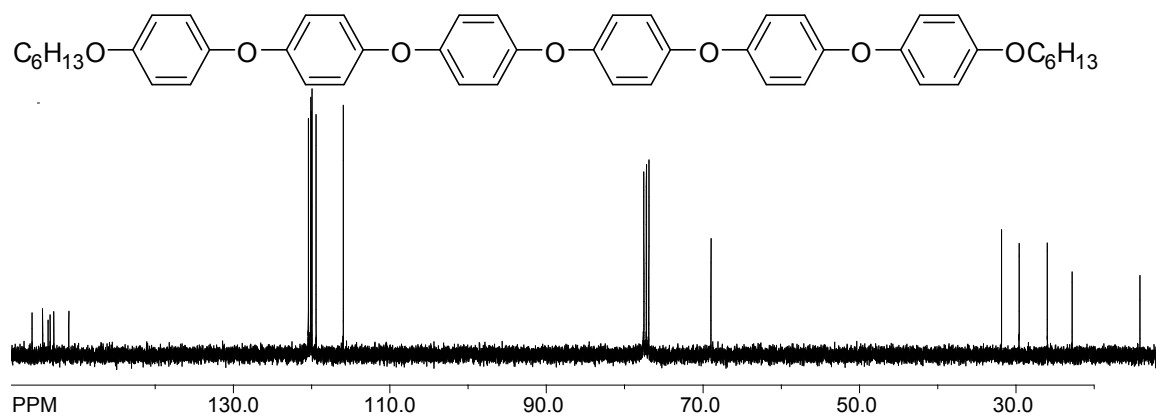
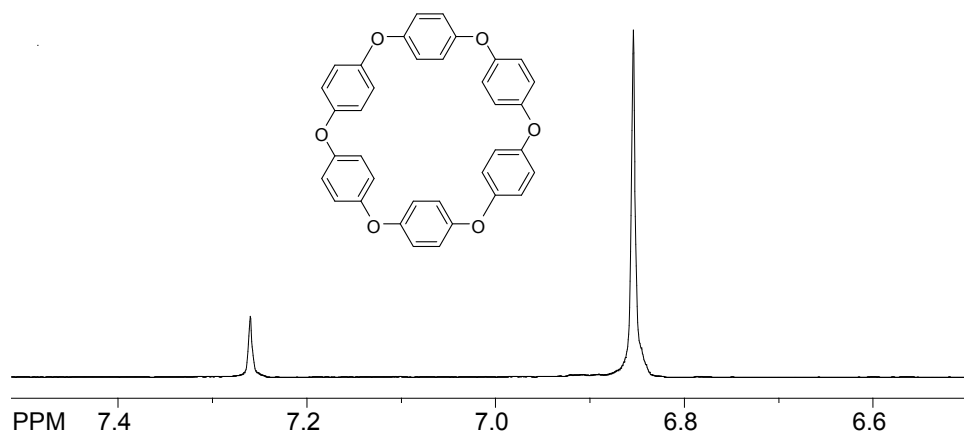
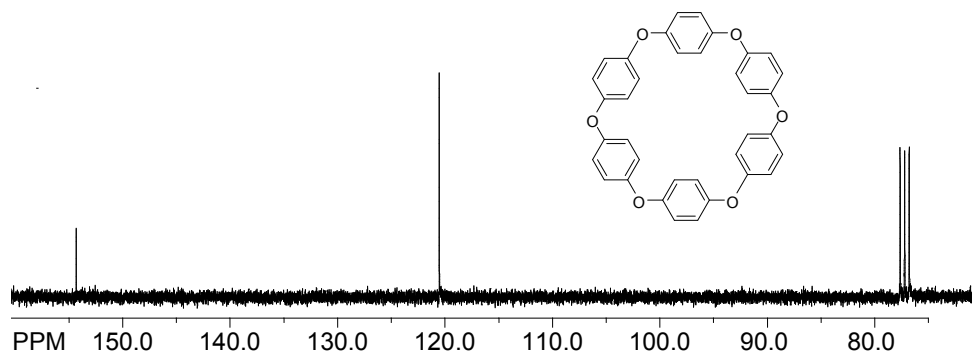
¹H NMR spectrum of E3**¹³C NMR spectrum of E3****¹H NMR spectrum of E4**

¹³C NMR spectrum of E4**¹H NMR spectrum of PE3****¹³C NMR spectrum of PE3**

¹H NMR spectrum of B3**¹³C NMR spectrum of B3****¹H NMR spectrum of PE4**

¹³C NMR spectrum of PE4**¹H NMR spectrum of B4****¹³C NMR spectrum of B4**

^1H NMR spectrum of E5 **^{13}C NMR spectrum of E5** **^1H NMR spectrum of E6**

^{13}C NMR spectrum of E6 **^1H NMR spectrum of cyclic ether** **^{13}C NMR spectrum of cyclic ether**

CHAPTER 4

Cycloannulated Aromatic Donors and Their Highly Robust Cation Radical Salts as Redox Tunable Oxidants

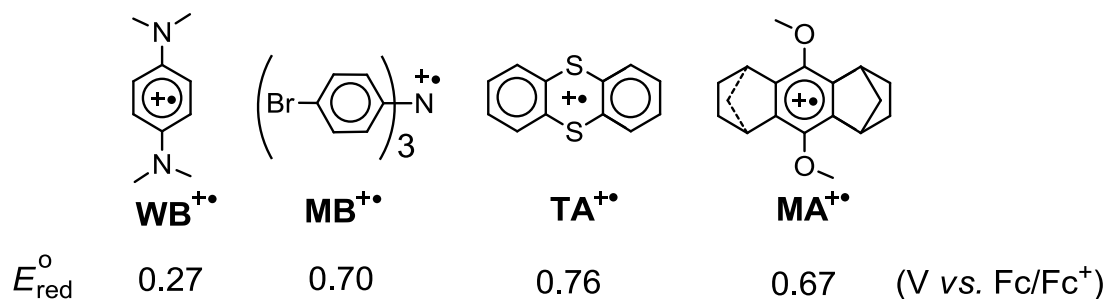
Introduction

One-electron oxidation of neutral molecules generates paramagnetic cation radicals which are of fundamental importance not only in the traditional areas of chemistry but also in material science and in modern area of photovoltaics. Although, cation radicals [such as Wurster's Blue ($\mathbf{WB}^{+\bullet}$) and Red ($\mathbf{WR}^{+\bullet}$)]¹ were first isolated in 1879 and named by Weitz in 1926,² they have not gained much prominence as the reactive intermediates in Organic textbooks except as transient species in mass spectrometry.³ The cation radicals are expected to be highly reactive intermediates because they possess both a cationic charge and an unpaired electron. The cation radicals in solution can be formed by chemical oxidation (using SbCl_5 , NO^+ salts, Et_3O^+ SbCl_6^- , FeCl_3 , quinones/ $\text{CH}_3\text{SO}_3\text{H}$, etc.), electrochemical oxidation, radiolytic oxidation, and most commonly employed photochemical methods.⁴ The cation radicals in solution have been extensively probed both by transient time-resolved laser spectroscopy and by EPR methods.⁵

The high reactivity of the cation radicals is attested by the fact that they undergo a variety of homolytic and electrophilic transformations such as nucleophilic attack, deprotonation, self-dimerization, rearrangement, fragmentation, polymerization, etc.⁶ Unlike the carbocation intermediates, a number of highly stable heteroatom-centered cation radicals (see Chart 1)⁷ have been isolated, as early as 1960s, and utilized as 1-electron oxidants in

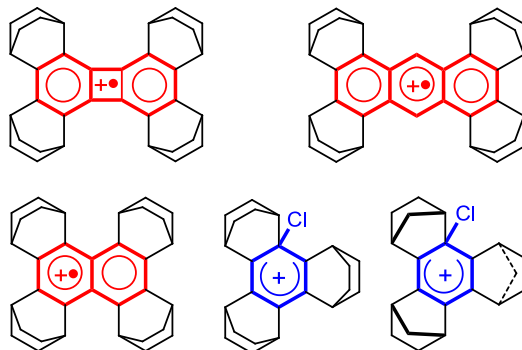
a plethora of chemical transformations including cycloadditions, C-C bond forming reactions, epoxidations, etc.^{4,6,7}

Chart 1. Structures of highly robust heteroatom centered and a bicycloheptan-annulated hydroquinone ether cation radical.



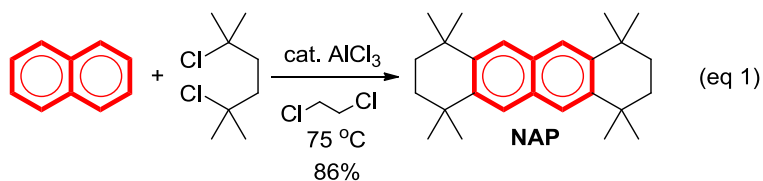
Amongst the highly robust cation radicals in Chart 1, the bicycloheptane-annulated hydroquinone ether cation radical (**MA^{+•}**), with comparable redox potential to that of commonly employed Magic Blue (**MB^{+•}**), is noteworthy because it can be easily prepared in multi-gram scale by a 4-step synthesis, presented in recent *Organic Syntheses* article,⁸ and can be stored indefinitely at ambient temperatures. The observed high-stability of **MA^{+•}** arises due to the lack of the labile C-H bonds directly connected to the benzene ring, owing to the Bredt's rule protection, and facial steric bulk that prevents the commonly observed dimerization process.^{9,10} Note that self-dimerization of cation radicals produces stabilized dimeric cation radicals which have been extensively probed both by spectroscopic methods and by X-ray crystallography.¹⁰ Dimeric cation radicals are also implicated as intermediates in Scholl reaction.⁴

Chart 2. Bicycloalkane-annulated aromatic hydrocarbons for the isolation of cation radicals and Wheland intermediates.



Indeed, the bicycloheptane- and bicyclooctane-annulation of aromatic hydrocarbons (such as benzene, naphthalene, anthracene, and biphenylene)^{8,11} allowed the isolation and X-ray crystallographic characterization of their cation radical salts^{8,11} as well as highly reactive Wheland intermediates (Chart 2).¹² Although, bicyclooctane-annulated polyaromatic hydrocarbons produce stable cation-radical salts, their precursors are obtained via laborious syntheses¹¹ and they possess relatively low redox potentials which span in a narrow range of 0.17-0.33 vs Fc/Fc^+ .¹¹

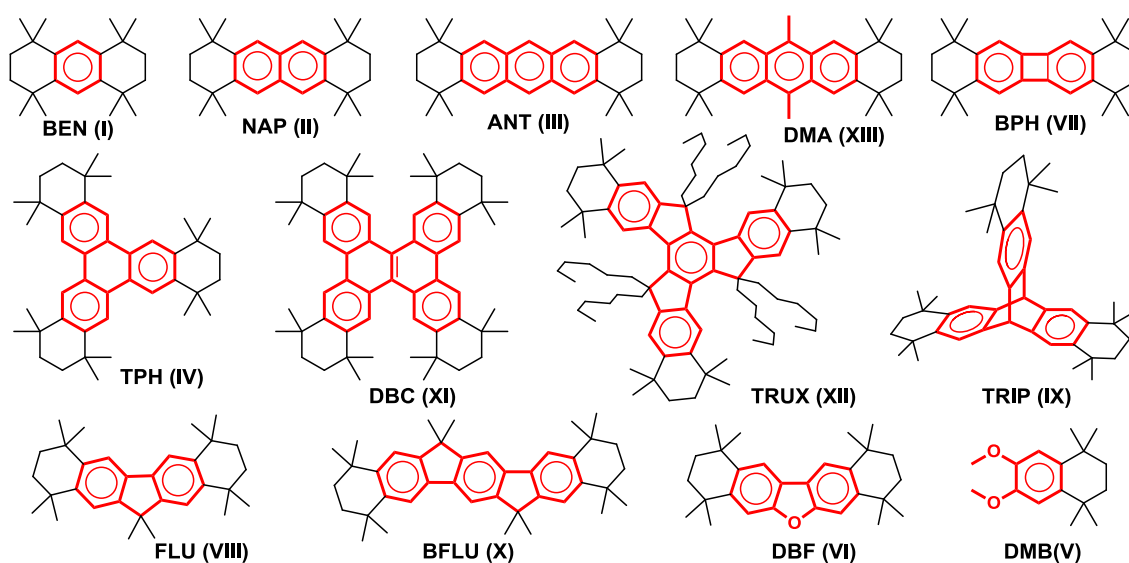
Interestingly, we have noted earlier¹³ that a well-known,¹⁴ one-step, Friedel-Crafts cycloannulation of naphthalene, using inexpensive 2,5-dichloro-2,5-dimethylhexane, produces a hindered naphthalene derivative (eq 1) that undergoes a highly reversible electrochemical oxidation and produces a stable cation-radical salt.



Over the last decade, we have made extensive use of this $\text{NAP}^{+\bullet}$ as a versatile 1-electron oxidant for the generation and study of a variety of aromatic and olefinic

cation radicals¹⁰ as well as its usage in mechanistic investigations of C-C bond forming reactions.⁴ Indeed, the simplicity of the cycloannulation reaction in eq 1 was exploited to prepare a variety of cycloannulated polyaromatic hydrocarbons which are derived from benzene, naphthalene, anthracene, biphenylene, triphenylene, truxene, triptycene, fluorene, dibenzofuran, veratrole, etc., and they all undergo reversible electrochemical oxidations and form stable cation-radical salts (see Chart 3).

Chart 3. Structures and naming scheme for various cycloannulated aromatic hydrocarbons for the generation of robust cation radical salts.



Accordingly, this manuscript will present a detailed systematic study of the preparation and spectroscopic characterization of a library of cycloannulated aromatic electron donors and their stable cation radicals with redox potentials that span from 0.5-1.1 V vs Fc/Fc⁺. The structures of representative cycloannulated cation radicals will also be probed with the aid of X-ray crystallography in order to establish that the facial steric

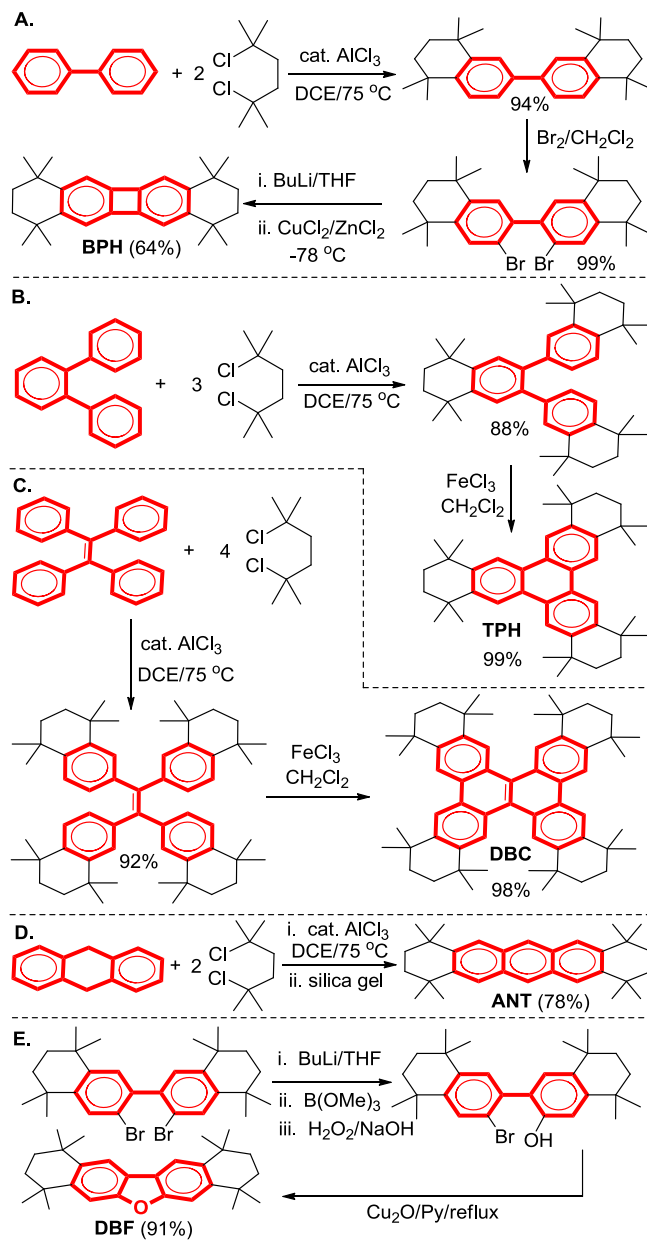
bulk imposed by cycloannulation prevents the dimerization of these cation radicals even in solid state. More importantly, we will illustrate, with the aid of electronic spectroscopy that these cation radicals with varying colors and spectroscopic features can be successfully employed as tunable aromatic oxidants to carry out stoichiometric 1-electron oxidation of a variety of organic and inorganic electron donors. We will also demonstrate that ready availability of a series of redox-tunable aromatic oxidants will facilitate the exploration of mechanisms of reactions that involve single electron transfer steps. The details of these findings are described herein.

Results and Discussion

Synthesis of cycloannulated aromatic Donors. A Friedel-Craft cycloannulation of simple aromatic compounds with readily-available and rather inexpensive 2,5-dichloro-2,5-dimethylhexane¹⁴ in the presence of a catalytic amounts of aluminum chloride has been known since 1955 (i.e. eq 1).¹⁴ After some experimentation, we have developed a slightly modified general procedure for the cycloannulation of various aromatic hydrocarbons in Chart 3 as follows. Thus, to a solution of naphthalene (10 mmol) in 1,2-dichloroethane (10 mL), cooled to 0 °C, was added a catalytic amount of anhydrous AlCl₃ under argon atmosphere. To this mixture, a solution of 2,5-dichloro-2,5-dimethylhexane (25 mmol) in 1,2-dichloroethane (25 mL) was added dropwise and the resulting mixture was warmed to room temperature and then heated to 60-70 °C for 4h. An aqueous work-up and crystallization of the resulting crude material from methanol afforded doubly-cycloannulated naphthalene as colorless needles in excellent yield (9.2 mmol). This general cycloannulation procedure was applicable for the preparation of most

cycloannulated aromatic compounds in Chart 3. Interestingly, a number of cycloannulated aromatic hydrocarbons derived from biphenylene (**BPH**), triphenylene (**TPH**), dibenzochrysenes (**DBC**), anthracene (**ANT**) and dibenzofuran (**DBF**) can be prepared much more easily and cost effectively via indirect routes rather than direct cycloannulation of the corresponding aromatic hydrocarbons (i.e. Scheme 1).

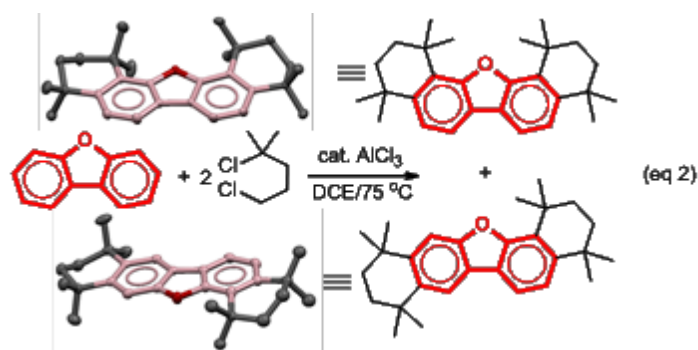
Scheme 1. Indirect routes for the syntheses of selected cycloannulated polycyclic aromatic hydrocarbons.



For example, the parent biphenylene¹⁵ needed for the preparation of annulated **BPH** is obtained from 2,2'-dibromobiphenyl which in turn is prepared from biphenyl in three steps.¹⁶ In an indirect route, shown in Scheme 1A, an efficient cycloannulation of biphenyl followed by bromination and conversion to **BPH** is accomplished in simple 3-step synthesis. Similarly, a cycloannulation of ortho-terphenyl followed by oxidative cyclodehydrogenation using FeCl₃ afforded annulated triphenylene **TPH** in nearly quantitative yield (Scheme 1B). Parent dibenzochrysenes are available via a multi-step synthesis¹⁷ and has rather poor solubility. In the indirect route, a simple cycloannulation of tetraphenylethylene followed by a reaction with FeCl₃ afforded annulated dibenzochrysenes **DBC** in excellent yield (Scheme 1C). Direct annulation of anthracene was found to be rather unclear due to highly reactive 9,10 positions. A cycloannulation of dihydroanthracene and chromatography on silica gel produced the annulated anthracene **ANT** in good yield (Scheme 1D). Note that annulated dihydroanthracene underwent smooth aromatization during chromatography. The annulated dimethylantracene **DMA** was obtained from **ANT** via bromomethylation followed by a hydrodehalogenation reaction using LAH.

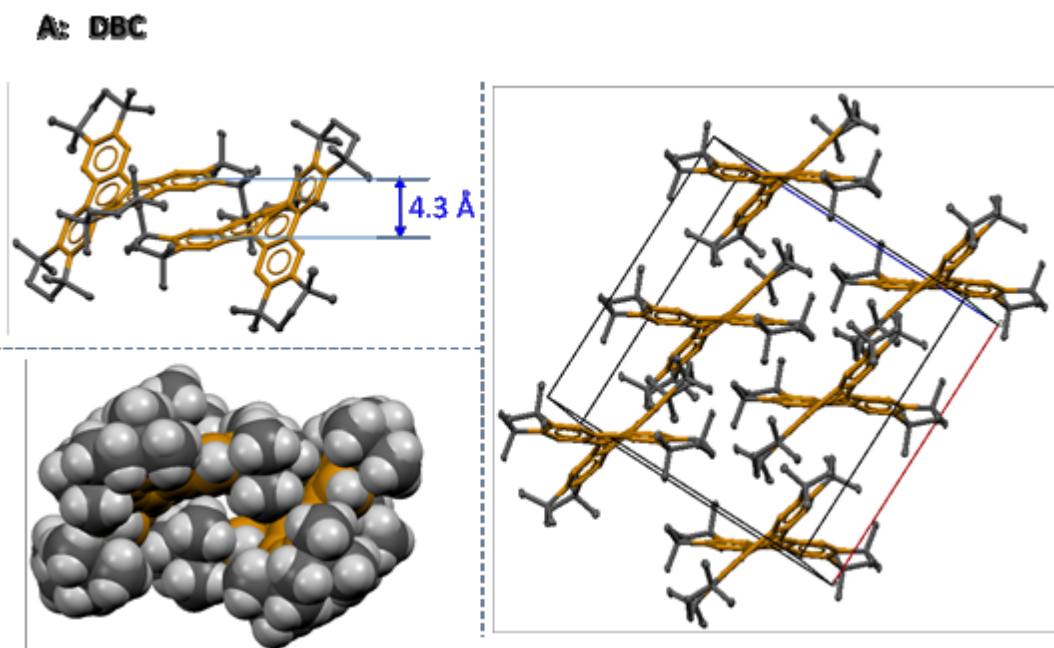
Interestingly, attempted cycloannulation of dibenzofuran produced a mixture of undesired

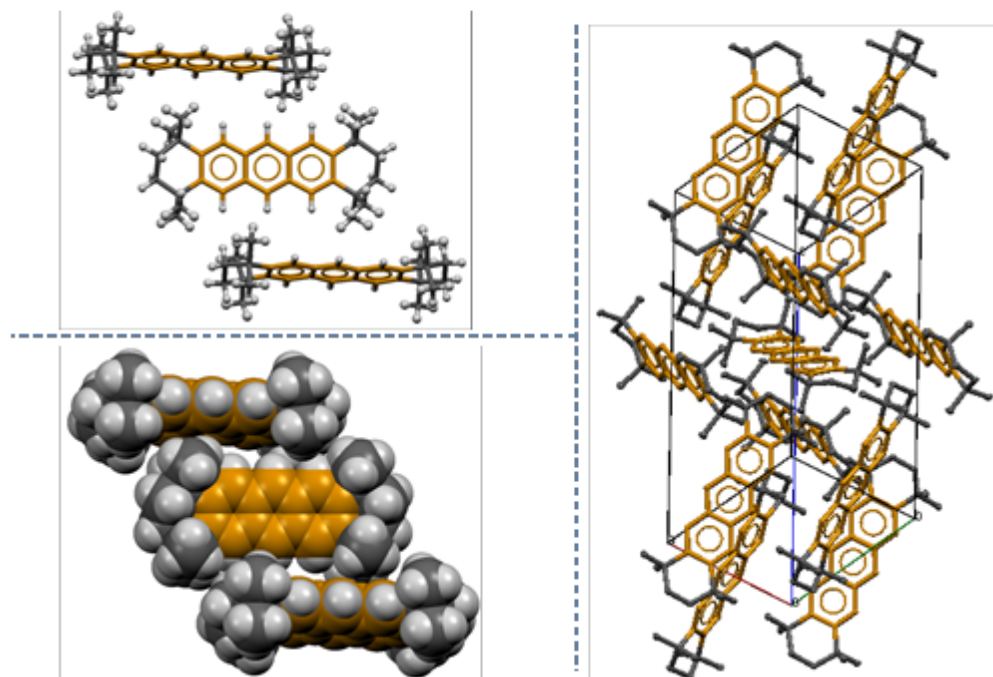
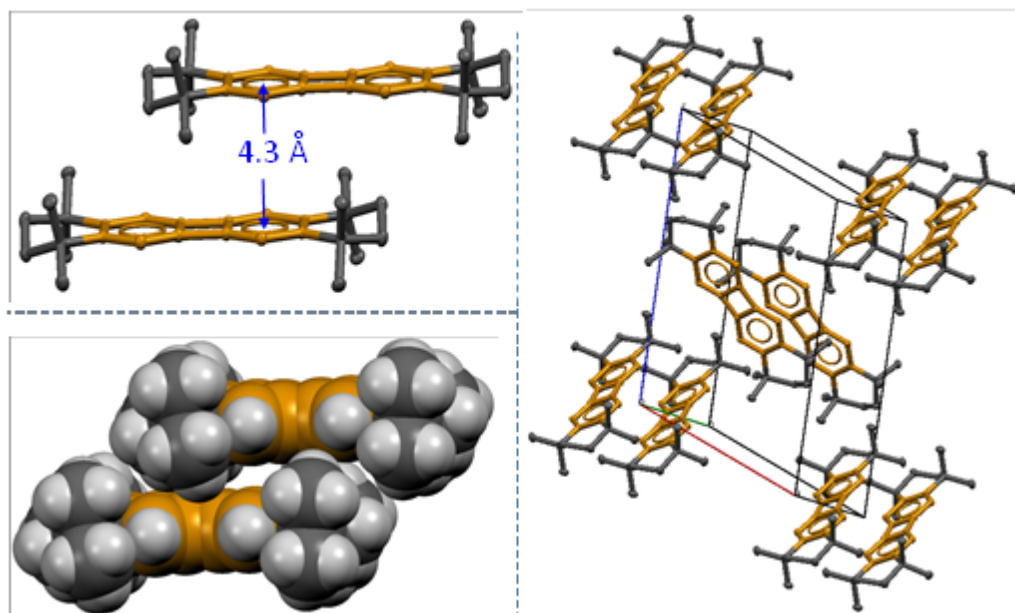
isomers in quantitative yield, i.e. eq 2.



The structures of isomeric products in eq 2 were established by NMR spectroscopy and by X-ray crystallography (see eq 2). However, an indirect route in Scheme 1E in which a transformation of a bromo to a phenolic substituent in cycloannulated dibromobiphenyl (see Scheme 1A) using standard procedure followed by Cu-catalyzed cyclization afforded the annulated **DBF** in excellent yield.

The molecular structures of various annulated hydrocarbons in Chart 1 were confirmed by $^1\text{H}/^{13}\text{C}$ NMR spectroscopy and mass spectrometry (see Experimental section). X-ray crystallography of a number of annulated hydrocarbons further established their structures and showed that steric hindrance imposed by cycloannulation prevents face-face contact in most annulated aromatic hydrocarbons (e.g. see Figure 1A-D).



B: ANT**C: BPH**

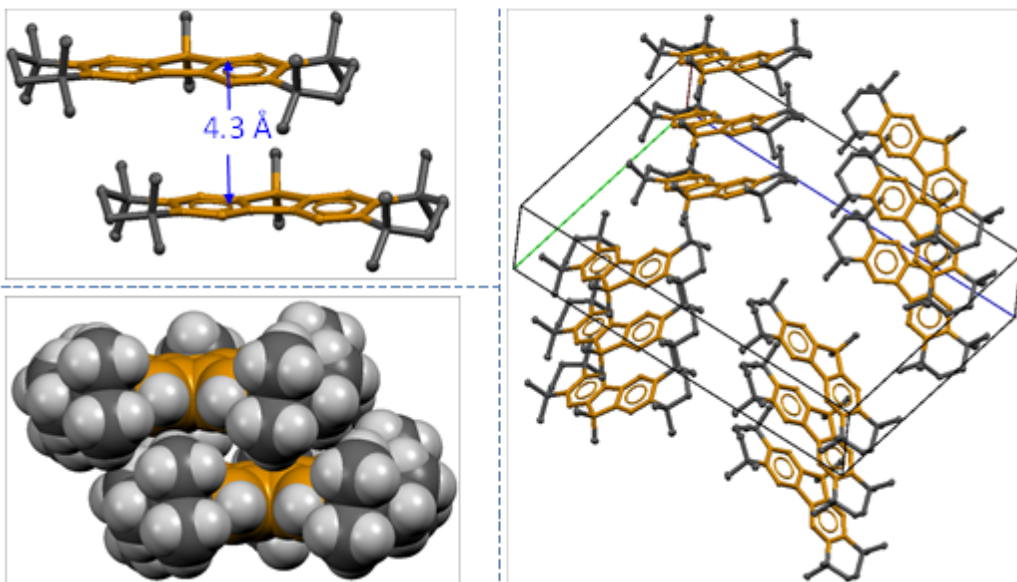
D: FLU

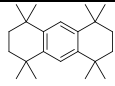
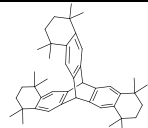
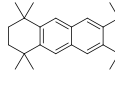
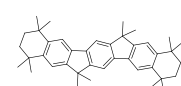
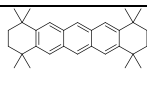
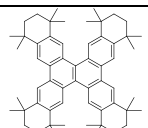
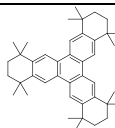
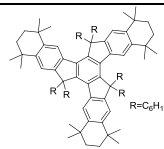
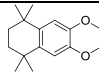
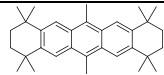
Figure 1. A-D. Representative X-ray crystal structures of cycloannulated hydrocarbons showing that steric hindrance prevents face-face contact of aromatic moieties.

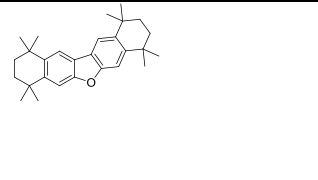
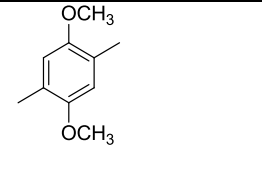
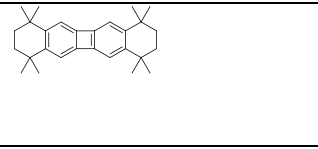
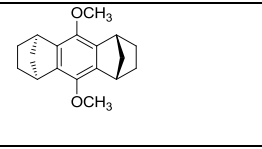
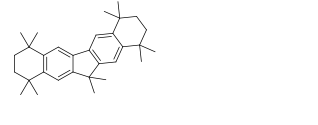
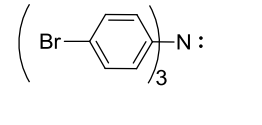
Electrochemical Oxidation of Cycloannulated Aromatic Donors

The redox properties of the cycloannulated compounds **I-XIII** (Table 1) were evaluated by electrochemical oxidation at a platinum electrode as a 2.5×10^{-3} M solution in dichloromethane containing 0.2 M tetra-*n*-butylammonium hexafluorophosphate (*n*-Bu₄NPF₆) as the supporting electrolyte. The oxidation potential values of **I-XIII** lie in a wide range of 0.82-1.85 V vs SCE and the values were referenced to added ferrocene, as an internal standard ($E_{\text{ox}} = 0.45$ V vs SCE). The first oxidation was reversible for all the cycloannulated aromatic donors (Figure 2A) as gauged by the consistently obtained cyclic voltammograms with anodic/cathodic current ratio of $i_a/i_c = 1$ at various scan rates $\nu = 50$ -1000 mVs⁻¹ (few examples given in Figure 2B). Although an oxidant is not

available for donors such as compound **I** (1.85 V vs SCE) the cation radical can be studied by using LASER flash photolysis since the cation radical is stable as predicted by the cyclicvoltammogram (Figure 1A). The availability of redox potentials (0.82-1.85 V vs SCE) for the cycloannulated aromatic donors with significant difference among the values provide large window of oxidation for variety of donors. The oxidation potentials in Table 1 can be converted to Fc/Fc^+ potential by subtracting a value of 450 mV from the potential that are referenced to SCE.

Table 1. Electrochemical Oxidation Potentials of the cycloannulated aromatic donos **I-XIII**.

Compound	Structure	$E_1/$ vs SCE	Compound	Structure	$E_1/$ vs SCE
I		1.85	IX		1.57
II		1.39	X		1.13
III		0.98	XI		1.00
IV		1.44	XII		1.23
V		1.27	XIII		0.82

VI		1.51			1.11
VII		1.03	MA		1.12
VIII		1.36	MB		1.15

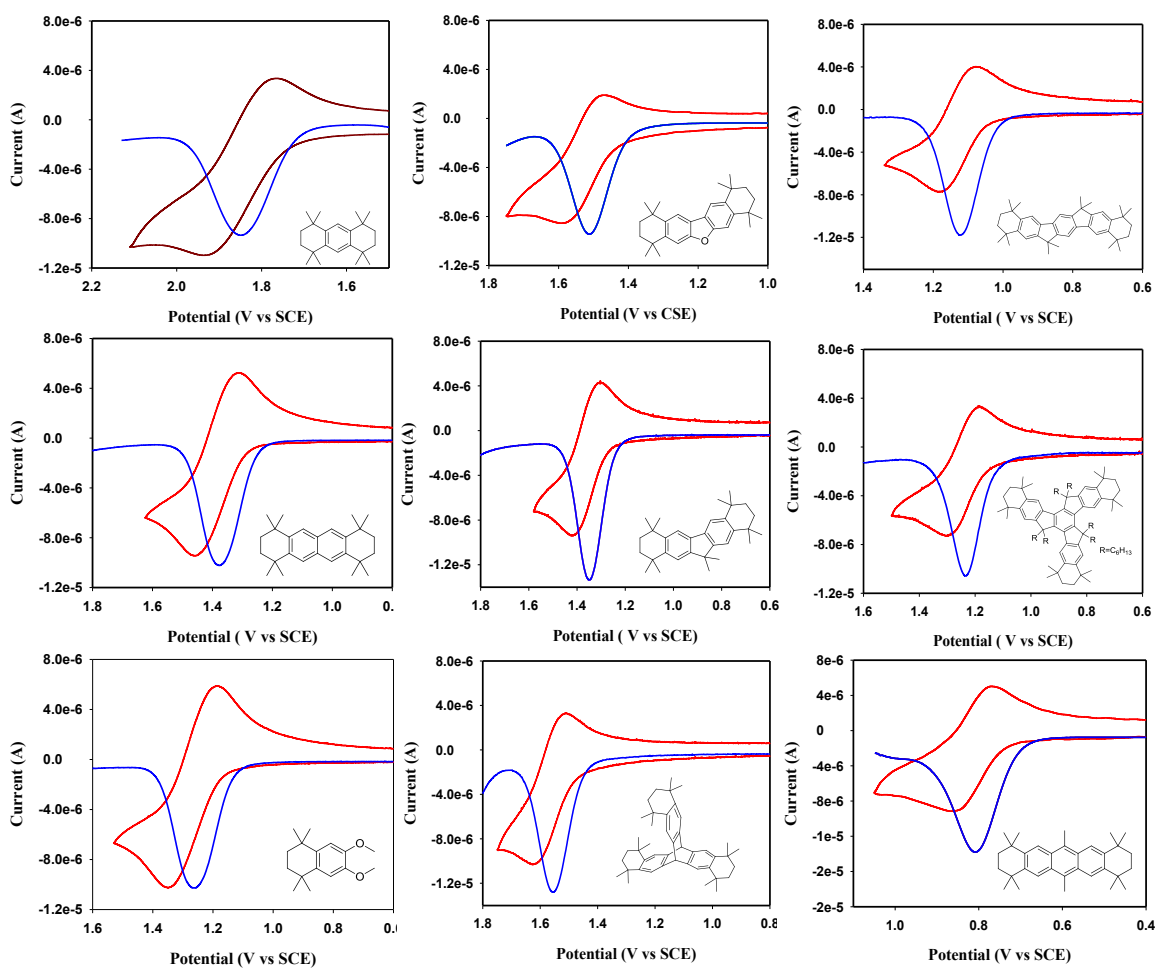


Figure 2A. Cyclic voltammograms and square wave voltammograms of **I**, **II**, **V**, **VII**, **VIII-X**, **XII**, and **XIII** as a 2.5×10^{-3} M solution in dichloromethane containing 0.2 M tetra-*n*-butylammonium hexafluorophosphate (*n*-Bu₄NPF₆) as the supporting electrolyte at sweep rate of 200 mV s^{-1} .

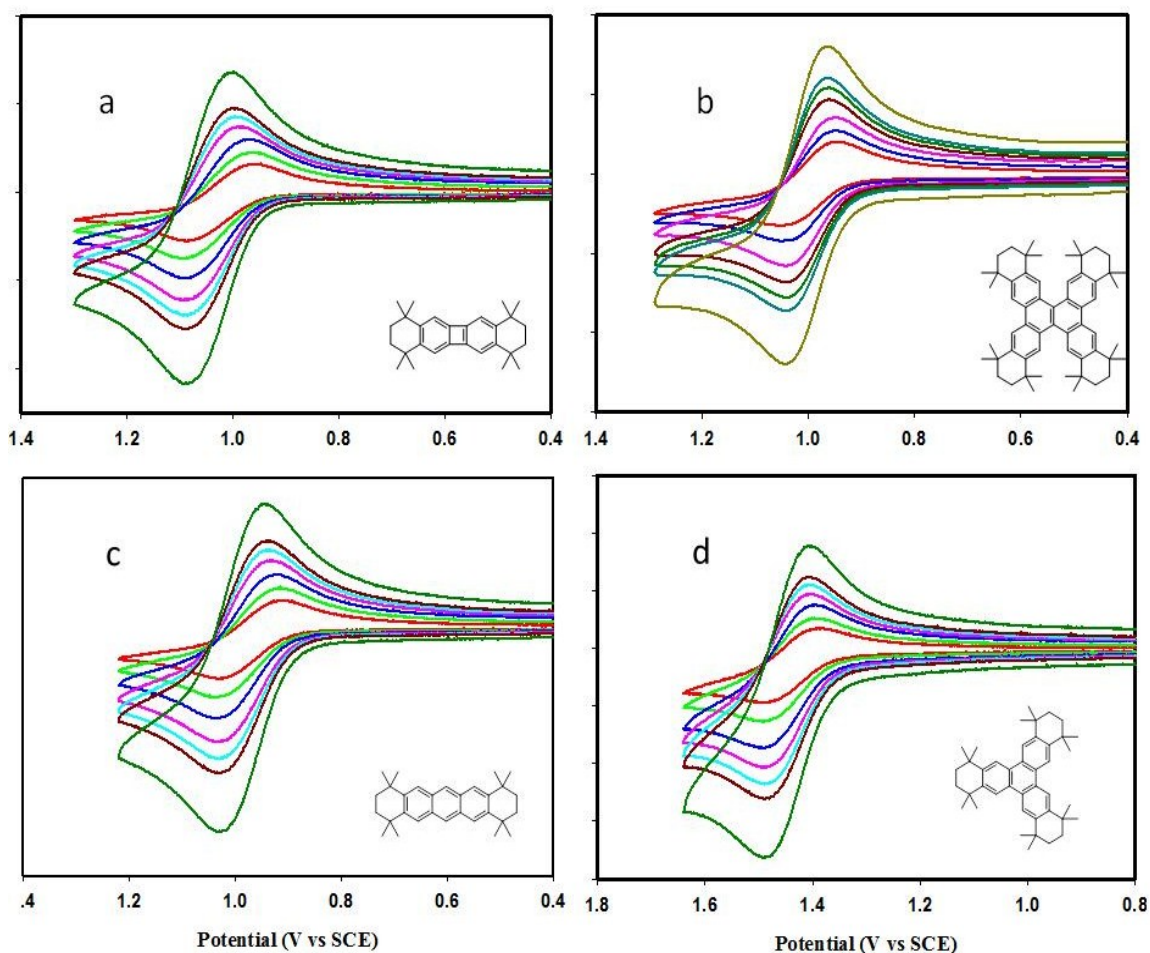


Figure 2B. Cyclic voltammograms of (a) VII (b) XI (c) III and (d) IV as a 2.5×10^{-3} M solution in dichloromethane containing 0.2 M tetra-*n*-butylammonium hexafluorophosphate ($n\text{-Bu}_4\text{NPF}_6$) as the supporting electrolyte at sweep rates 50-1000 mV s^{-1} .

Preparation of Cation radicals of the cycloannulated aromatic donors I-XIII as hexachloroantimonate salts in dichloromethane.

Oxidation with $\text{MA}^{+\text{o}}\text{SbCl}_6^-$ or $\text{MB}^{+\text{o}}\text{SbCl}_6^-$: A colorless solution of aromatic donors in dichloromethane was treated with one equivalent of $\text{MA}^{+\text{o}}\text{SbCl}_6^-$ or $\text{MB}^{+\text{o}}\text{SbCl}_6^-$ under

argon atmosphere at 22 °C. The obtained deeply colored solutions were used for further studies (Table 2).

Oxidation with $\text{NO}^+\text{SbCl}_6^-$: Known amount of $\text{NO}^+\text{SbCl}_6^-$ was dissolved in in dichloromethane under argon atmosphere at 22 °C. The resulting solution was cooled to ~0 °C and one equivalent of the donor was added and stirred. The producing NO gas was removed by repeating the process of evacuating and refilling with argon few times. The obtained deeply colored solutions were used for further studies (Table 2).

Table 2. Radical cation data of various cycloannulated aromatic donors.

Compound	λ_{max}	ϵ	color
II	672	9300	blue
III	744	27113	Yellowish green
IV	748	6211	green
V	465	3838	yellow
VI	713	1300	green
VII	634	27261	blue
VIII	712	15230	Blue-green
IX	1648	3375	brown
X	1038	24932	yellow
XI	740	20664	purple
XII	1400	9216	Blue-green
XIII	699	15288	Yellowish green

Spectral Properties of Radical Cations of Cycloannulated Aromatic Donors.

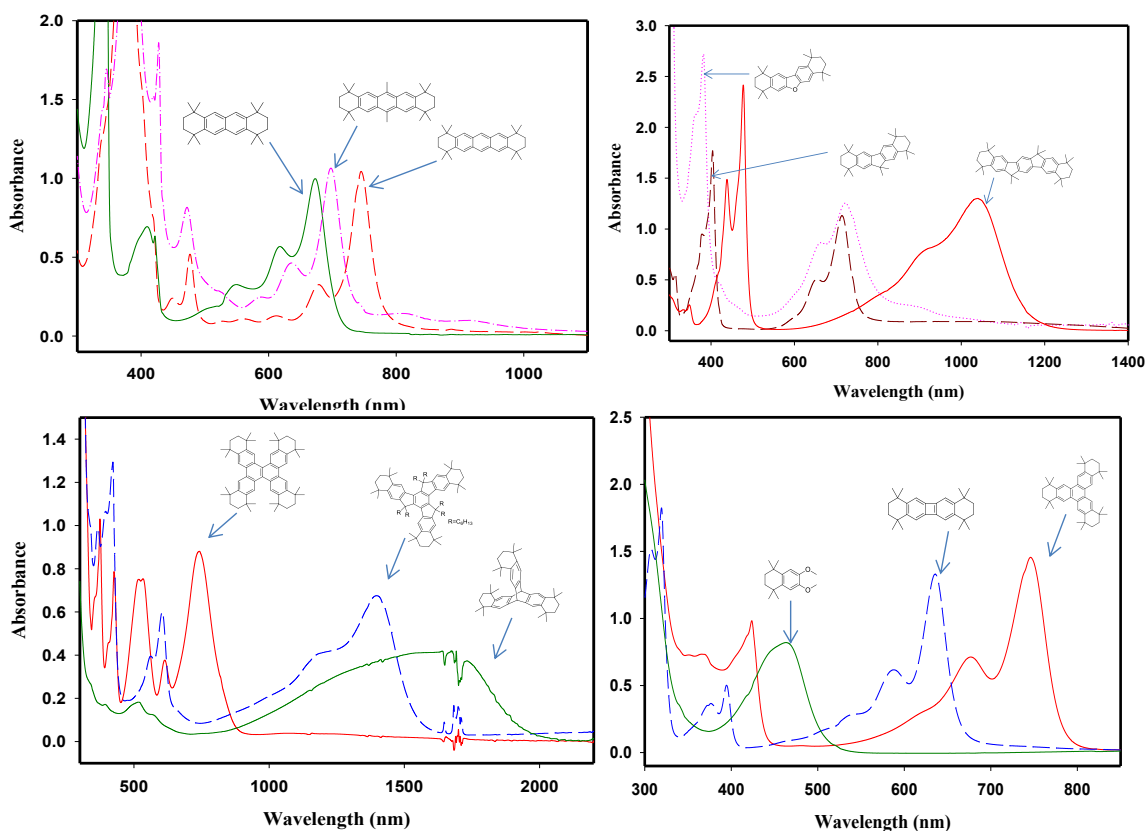


Figure 3. The electronic absorption spectra of radical cations of (II- XIII) obtained by oxidizing with or $\text{NO}^+\text{SbCl}_6^-$ under argon atmosphere at 22 °C.

Isolation of crystalline radical cations and X-ray crystal structures of V and VII.

[V] SbCl_6 : A solution of $\text{NO}^+\text{SbCl}_6^-$ in anhydrous dichloromethane at 0°C was treated with one equivalent of **V** under argon atmosphere and stirred for few minutes. The obtained colored solution was evacuated and refilled with argon to remove produced NO gas and was carefully layered with anhydrous toluene and kept in dark at -20°C under argon atmosphere. After 12-14 h X-ray quality pale yellow crystals were obtained (Figure 4).

[VII]SbCl₆: A solution of **VII** in anhydrous dichloromethane was treated with one equivalent of **MA**⁺ under argon atmosphere and stirred for few minutes. The obtained deep blue solution was carefully layered with anhydrous toluene and kept in dark at -20°C. After 12-14 h X-ray quality dark colored crystals were obtained (Figure 4).

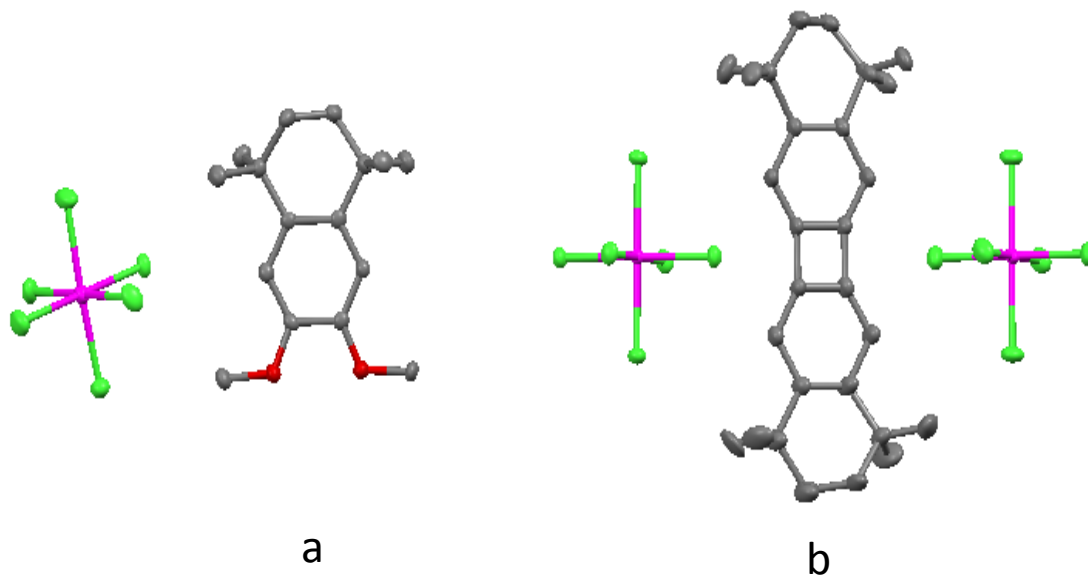


Figure 4. X-ray crystal structures of (a) **[V]**⁺ **SbCl₆**⁻ and (b) **[VII]**⁺ **SbCl₆**⁻

Applications of the Cation Radicals of the aromatic donors as Oxidants

A. Use of Napthalene cation radical [II]⁺ SbCl₆⁻ (NAP⁺) as an oxidant in some of the spectroscopic determinations in our laboratory.

Determination of number of electrons ejecting upon oxidation

It has been found that tetraarylmethane (TAM) and hexaarylbenzene (HAB) oxidize at the same potential (1.11 V vs SCE) under electrochemical oxidation. Due to the differences in size and the shape and hence the differences in diffusion coefficients of the donors they do not allow us to determine the number of ejecting electrons easily using an added

internal standard. Therefore in this situation the number of electrons, which is ejected upon oxidation, was determined using a titrimetric method using NAP^{+0} as the oxidant as follows. As the Figure 5 (left) shows the depletion of the band of NAP^{+0} at 672 nm and increase of the band (1000 nm) due to the cation radical formation upon oxidation of the TAM. The Figure F (right) explains the stoichiometry of NAP^{+0} and TAM in the oxidation process where all the NAP^{+0} is consumed after the addition of 0.25 equivalent of TAM to one equivalent of NAP^{+0} showing that TAM ejects four electrons at 1.11V vs SCE. Similarly Figure 6 (right) shows one equivalent of NAP^{+0} consumed after the addition of one sixth equivalent of HAB indicating that HAB ejects six electrons at 1.11 V vs SCE.

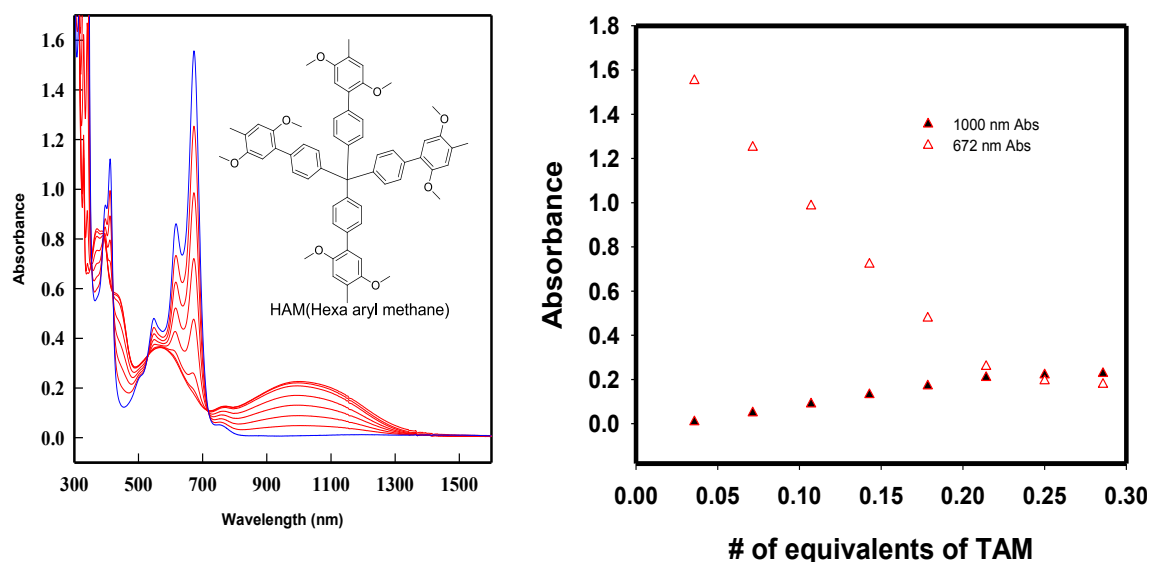


Figure 5. (left) Spectral changes attendant upon the reduction of 1.5×10^{-4} M naphthalene cation radical (NAP^{+0}) by incremental addition of 1.2×10^{-3} M TAM to its tetracation radical TAM^{4+} in dichloromethane at 22°C . (right) A plot of depletion of absorbance of NAP^{+0} (open triangles), monitored at 672 nm) and an increase of the absorbance of TAM^{4+} (filled triangles, monitored at 1000 nm) against the equivalent of added TAM.

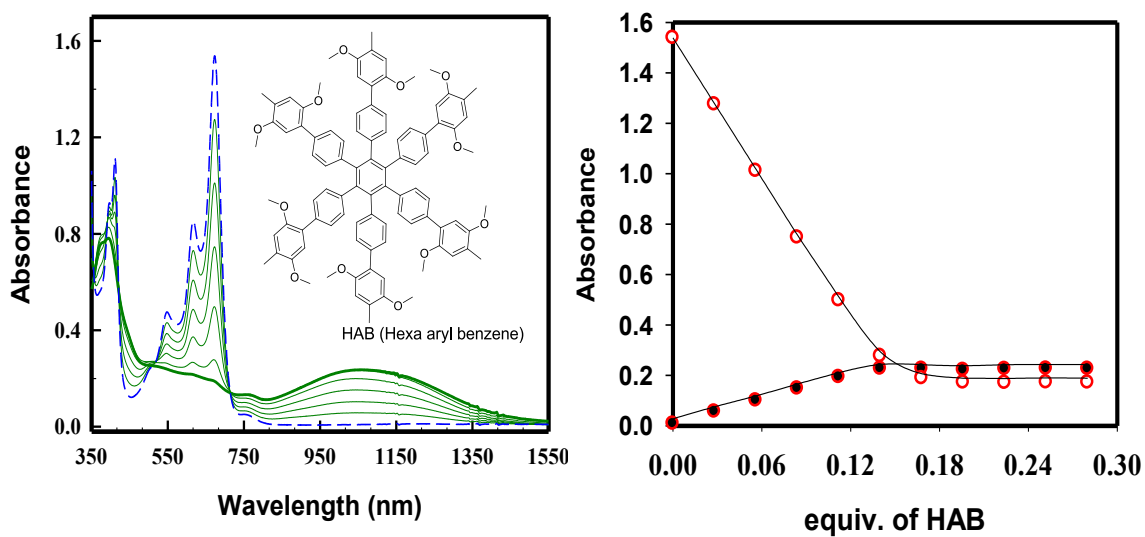


Figure 6. (left) Spectral changes attendant upon the reduction of 1.5×10^{-4} M naphthalene cation radical ($\text{NAP}^{+\bullet}$) by incremental addition of 1.2×10^{-3} M HAB to its hexacation radical $\text{HAB}^{6+\bullet}$ in dichloromethane at 22°C . (right) A plot of depletion of absorbance of $\text{NAP}^{+\bullet}$ (open circles), monitored at 672 nm and an increase of the absorbance of $\text{TAM}^{6+\bullet}$ (filled circles, monitored at 1000 nm) against the equivalent of added HAB.

Determination of formation and disappearance of charge transfer complex upon oxidation in a biaryl compound.

As the figure 7 (left) shows the band at 464 nm continue to increase upon the addition of $\text{NAP}^{+\bullet}$ to a solution of biaryl compound in dichloromethane at 22°C while the band at 1530 nm which is due to the formation of charge transfer complex increases upto one equivalent of the added oxidant and then disappears due to the formation of separate cation radicals at the linked aromatic groups (Scheme 2).

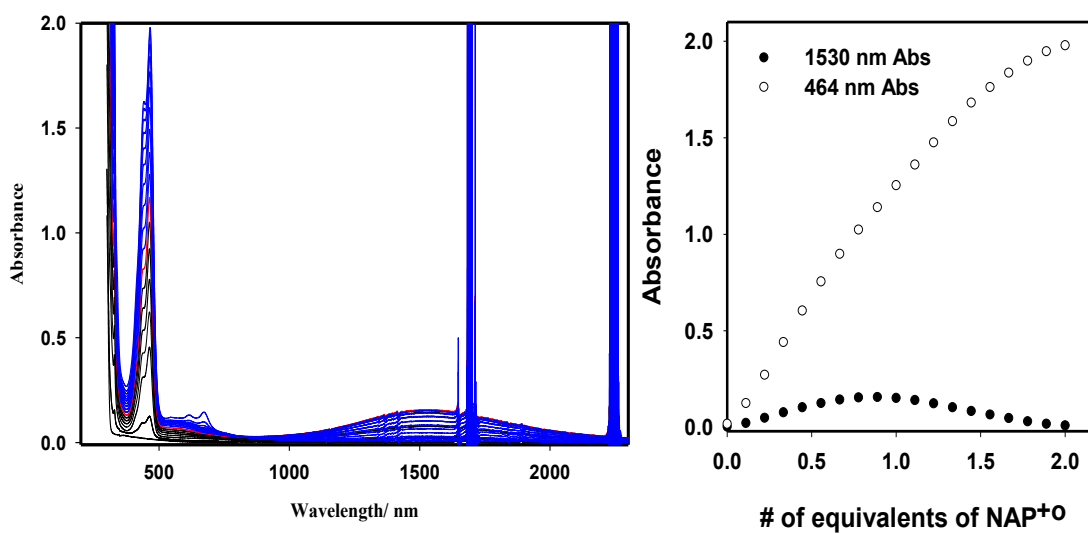
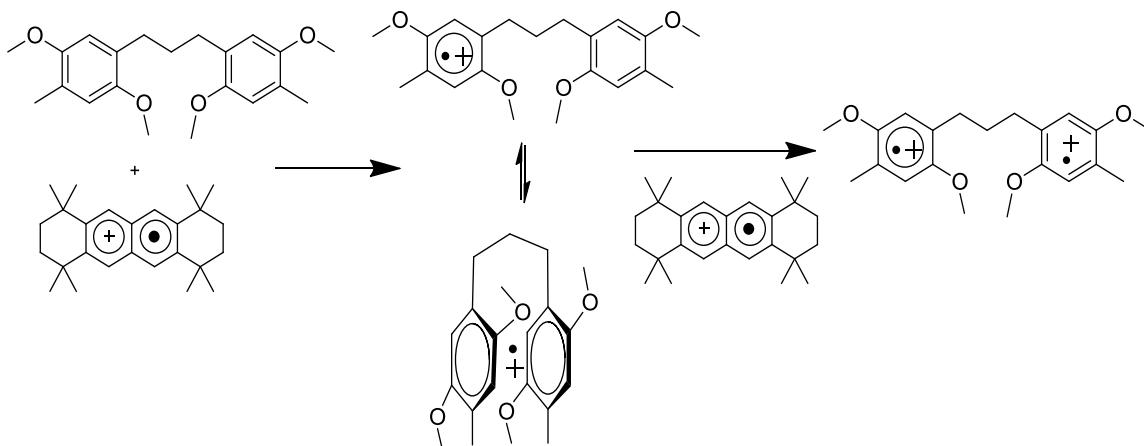


Figure 7. (left) Spectral change upon the addition of NAP⁺0 to a solution of biaryl compound in dichloromethane at 22 °C. (right) The appearance of the band (464 nm) due to monocation (open circles) and appearance and disappearance of the band (1530 nm) due to the charge transfer complex formation (filled circles).

Scheme 2. The formation and disappearance of charge transfer complex upon oxidation of the biaryl compound.



B. Determination of the dication formation of octamethoxytetraphenylene(OMTP) using cation radical $\text{VIII}^{0+} \text{SbCl}_6^-$ as the oxidant

Magic blue (MB^{+0}) is commercially available oxidant ($E_1 = 1.15 \text{ V vs SCE}$). MA^{+0} ($E_1 = 1.12 \text{ V vs SCE}$) is another widely used oxidant which was made by Rathore and coworkers. But their oxidation potential is limited to the mentioned values and Magic blue is having additional band in NIR region which interferes with cation radical bands in most of the cases. As an example, the two electron process, C-C bond formation, of octamethoxy tetraphenylene upon oxidation ($E_1 = 1.25 \text{ V vs SCE}$) can't be studied with either Magic blue or CRET because of the higher oxidation potential involves in this process. This can easily solved by using the oxidant $\text{VIII}^{0+} \text{SbCl}_6^-$ as shown in figure 8. The Figure 8 (right) shows that all the $\text{VIII}^{0+} \text{SbCl}_6^-$ has been consumed after the addition of 0.5 equivalents OMTP indicating that it is a two electron proces (Scheme 3).

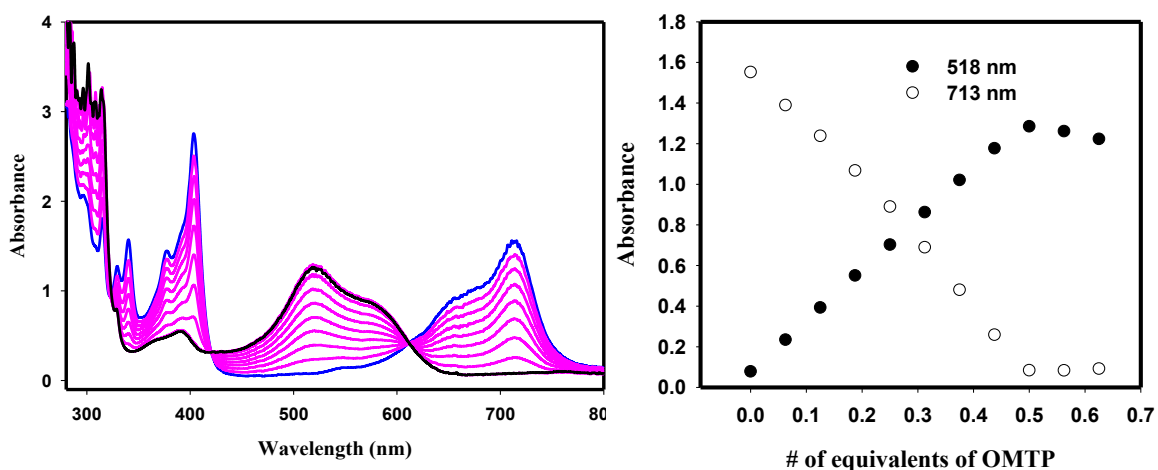
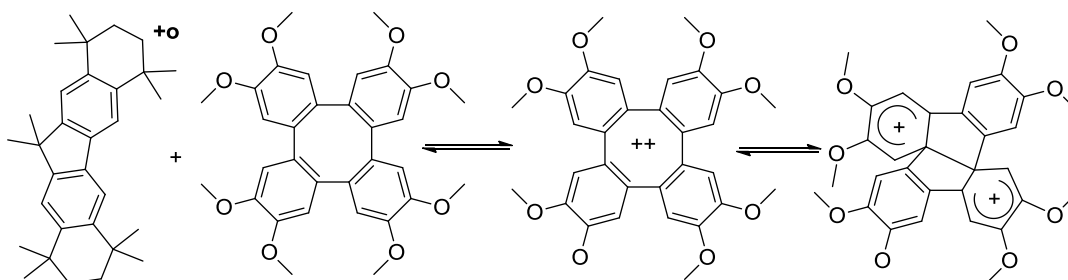


Figure 8. (left) Spectral changes attendant upon an incremental addition of neutral octamethoxytetraphenylene ($1.61 \times 10^{-3} \text{ M}$) to a solution of $\text{VIII}^{0+} \text{SbCl}_6^-$ ($1.08 \times 10^{-4} \text{ M}$) in dichloromethane at 25°C . (right) The depletion of $\text{VIII}^{0+} \text{SbCl}_6^-$ (open circle) and increase in the absorption at 518 nm (dark circle) in dichloromethane at 25°C .

Scheme 3. Reversible C-C bond formation in octamethoxytetraphenylene upon oxidation

C. Formation of octamethylbiphenylene cation radical using $X^{0+}SbCl_6^-$ as an oxidant.

Figure 8 shows the use of cation radical $X^{0+}SbCl_6^-$ as an oxidant for the determination of the chemical oxidation process of octamethylbiphenylene (OMBP). The Figure 9 (right) shows that the bands (1038 nm and 475 nm) due to the $X^{0+}SbCl_6^-$ completely disappear at one equivalent addition of OMBP and the band at 602 nm due to the cation radical of OMBP comes to a maximum indicating that OMBP oxidation (Scheme 4) is a one electron process.

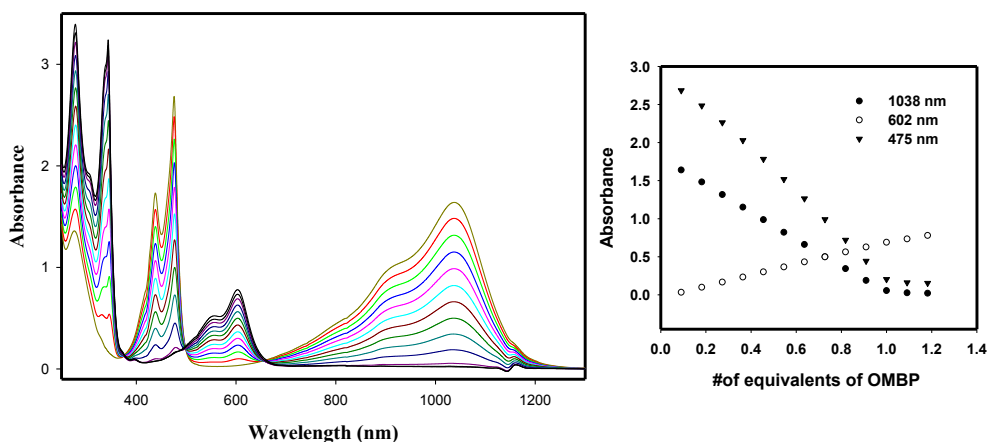
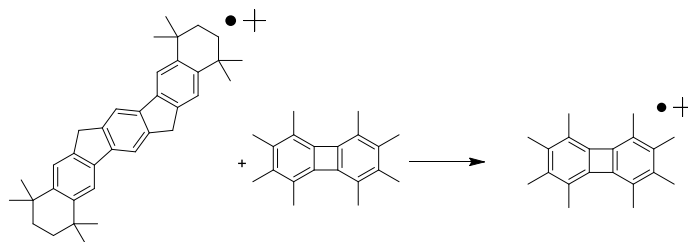


Figure 9. Spectral changes attendant upon an incremental addition of neutral octamethylbiphenylene (3.22×10^{-3} M) to a solution of $X^{0+}SbCl_6^-$ (5.38×10^{-5} M) in dichloromethane at 25°C.

Scheme 4. Formation of octamethylbiphenylene cation radical



D. Usage of $\text{VII}^{\text{O}^+} \text{SbCl}_6^-$ as an oxidant for the determination of octamethoxy dibenzochrysenene (OMBC) cation radical

Octamethoxy dibenzochrysenene has oxidation potential of 0.91 V vs SCE.

Although $\text{MA}^{\text{+O}}$ is able to oxidize OMBC, it cannot be used to study the oxidation process of OMBC due to the overlap of cation radical bands with the bands of $\text{MA}^{\text{+O}}$.

$\text{VII}^{\text{O}^+} \text{SbCl}_6^-$ can be used to resolve the overlapping of bands as follows. Figure 10 (right) shows that OMBC cation radical absorption becomes a constant after the addition of one equivalent of OMBC indicating that oxidation of octamethoxy dibenzochrysenene at 0.91 is one electron process (Scheme 5).

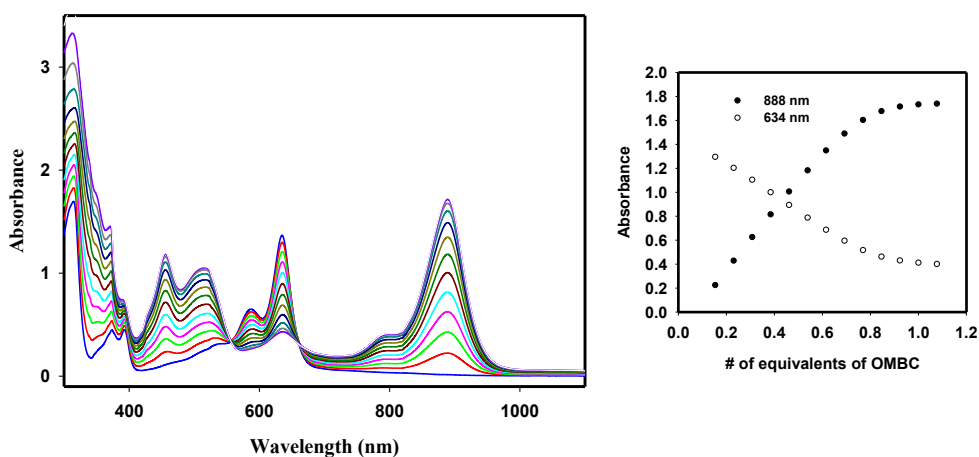
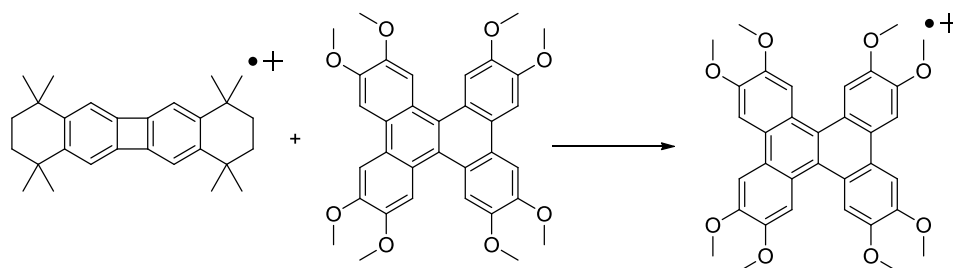


Figure 10. Spectral changes attendant upon an incremental addition of neutral octamethoxychrysenene ($8.22 \times 10^{-4} \text{ M}$) to a $6.85 \times 10^{-5} \text{ M}$ solution of $\text{VII}^{\text{O}^+} \text{SbCl}_6^-$ in dichloromethane at 25°C .

Scheme 5. Formation of octamethoxychrysene cation radical using $V^{0+}SbCl_6^-$ as the oxidant



E. Use of $V^{0+}SbCl_6^-$ as an oxidant in the spectroscopic determination of tetramethylbiphenylene(TMBP).

Figure 11 (left) shows that the absorbance of $V^{0+}SbCl_6^-$ (465 nm) decreases while the absorbance of the band at 594 nm increases due to the formation of tetramethylbiphenylene(TMBP) cation radical in dichloromethane. As shown in the Figure 11 (right) all the $V^{0+}SbCl_6^-$ consumed after the addition of one equivalent of TMBP indicating that a one electron oxidation process (Scheme 6).

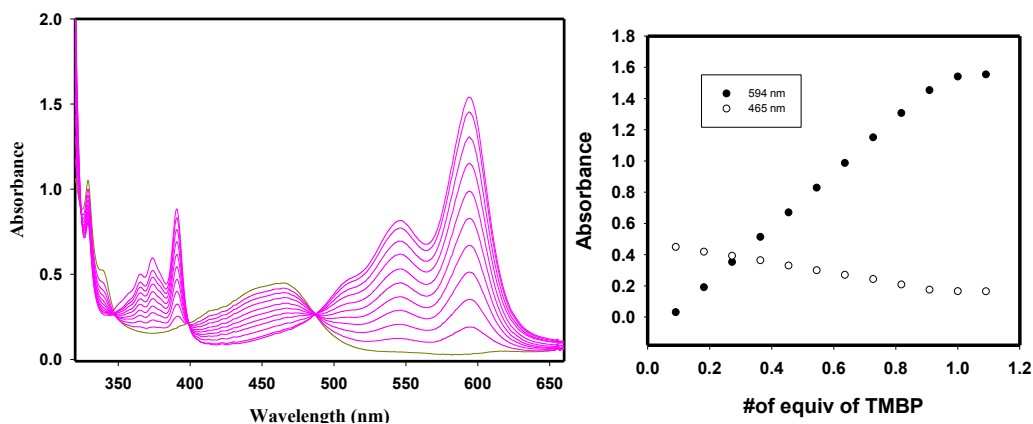
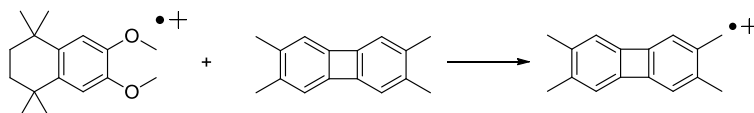


Figure 11. Spectral changes attendant upon an incremental addition of neutral tetramethylbiphenylene($3.22 \times 10^{-3} M$) to a M solution of $V^{0+}SbCl_6^-$ ($1.08 \times 10^{-4} M$) in dichloromethane at $25^\circ C$.

Scheme 6. Formation of tetramethylbiphenylene cation radical using $V^{0+} SbCl_6^-$ as the oxidant.



Summary and Conclusions

Cycloannulated aromatic donors (**I-XIII**) have been synthesized and characterized by NMR spectroscopy as well as X-ray crystallography. Since the synthesis of such cycloannulated aromatic donors is easier compared to the donors reported in literature, large scale preparation can be accomplished easily.

Cycloannulated aromatic donors (**I-XIII**) are good electron donors as indicated by their reversible oxidations (0.88 -1.85 V vs SCE). Upon oxidation by CRET, MB or $NO^+SbCl_6^-$ the cycloannulated aromatic donors (**I-XIII**) produce cation radical salts with various bright colors which are stable in dichloromethane solutions for several hours even at room temperature as judged by their electronic absorption spectra. Cation radical salts of some cycloannulated aromatic donors were isolated in crystalline form such as $V^{0+} SbCl_6^-$ and $VII^{0+} SbCl_6^-$.

Limited number of available oxidants limits the spectroscopic determinations due to having specific oxidation potentials and spectroscopic features which results band overlapping, uncontrolled oxidations, unavailability of proper oxidants .etc. Since the cation radicals of cycloannulated aromatic donors (**I-XIII**) provide wide range of oxidation potential values and long term stability of their cation radicals. Furthermore they have various λ_{max} values of their cation radical bands by which variety of the spectroscopic determinations can be accomplished.

Experimental

General Experimental Methods and Materials.

Dichloromethane, dichloroethane, anhydrous benzene, ZnCl_2 , CuCl_2 , bromine, 1-bromohexane, ferric chloride, BuLi , aluminum chloride, hydrochloric acid, naphthalene, 9,10-dihydroanthracene, triphenylene, 1,2-dimethoxybenzene, dibenzofuran, 9,9-Dimethylfluorene, anhydrous toluene, trypticene, tetraphenylethylene, 1-indanone, biphenyl, glacial acetic acid, HBr in acetic acid, formaldehyde, ethanol, sodium carbonate, tetrakis(triphenylphosphine)palladium, *N*-bromosuccinamide, were commercially available and were used without further purification.

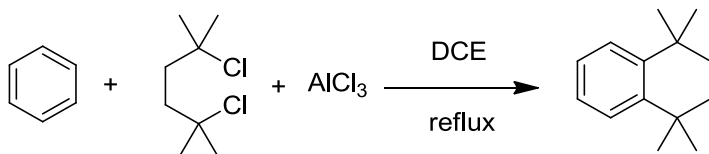
Anhydrous tetrahydrofuran (THF) was prepared by refluxing the commercial tetrahydrofuran over lithium tetrahydroaluminate under an argon atmosphere for 24 hours followed by distillation. It was stored under an argon atmosphere in a Schlenk flask equipped with a Teflon valve fitted with Viton *O*-rings. Dichloromethane was repeatedly stirred with fresh aliquots of conc. sulfuric acid (~10 % by volume) until the acid layer remained colorless. After separation it was washed successively with water, aqueous sodium bicarbonate, water, and saturated aqueous sodium chloride and dried over anhydrous calcium chloride. The dichloromethane was distilled twice from P_2O_5 under an argon atmosphere and stored in a Schlenk flask equipped with a Teflon valve fitted with Viton *O*-rings. The hexanes and toluene were distilled from P_2O_5 under an argon atmosphere and then refluxed over calcium hydride (~12 hrs). After distillation from CaH_2 , the solvents were stored in Schlenk flasks under argon atmosphere.

Cyclic Voltammetry.

Cyclic voltammetry (CV) was performed on an Electrochemical Analyser. The CV cell was of an air-tight design with high vacuum Teflon valves and Viton O-rings seals to allow an inert atmosphere to be maintained without contamination by grease. The working electrode consisted of an adjustable platinum disk embedded in a glass seal to allow periodic polishing (with a fine emery cloth) without changing the surface area ($\sim 1 \text{ mm}^2$) significantly. The reference SCE electrode (saturated calomel electrode) and its salt bridge were separated from the catholyte by a sintered glass frit. The counter electrode consisted of platinum gauze that was separated from the working electrode by $\sim 3 \text{ mm}$. The CV measurements were carried out in a solution of 0.1M supporting electrolyte (tetra-*n*-butylammonium hexafluorophosphate, TBAH) and 0.24 – 2.5 mmol substrate in 97:3 dichloromethane –acetonitrile mixtures under an argon atmosphere. All cyclic voltammograms were recorded at the sweep rate of 100 mV sec^{-1} , unless otherwise specified and were IR compensated. The oxidation potentials ($E_{1/2}$) were referenced to SCE which was calibrated with added (equimolar) ferrocene ($E_{1/2} = 0.45 \text{ V vs. SCE}$). The $E_{1/2}$ values were calculated by taking the average of anodic and cathodic peak potentials in the reversible cyclic voltammograms.

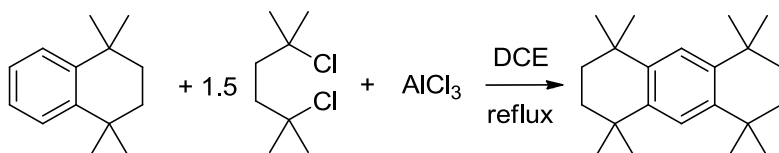
Synthesis and spectral data

Compound **Ia**



Anhydrous benzene (5 mL) was placed in a 100 mL schlenk flask and cooled to 0 °C at argon atmosphere. Catalytic amount of anhydrous AlCl_3 was added and 2,5-dichloro-2,5-dimethylhexane (1.8 g, 10 mmol) in anhydrous benzene (3 mL) was added drop-wise to the above solution and heated for reflux for 4 hours. The resulting mixture was cooled to room temperature and poured into ice-HCl mixture (ice 100 g : 10mL HCl) and stirred for 15 min. The crude product was extracted to dichloromethane, dried over anhydrous MgSO_4 , filtered through a short pad of silica and evaporated the solvents to isolate yellow oil which was purified by column chromatography to afford mono-substituted product as a colorless oil. Yield : (1.25 g, 86 %), $^1\text{H NMR}$ (CDCl_3) δ : 1.28 (s, 12 H), 1.68 (s, 4 H), 7.11 (s, 2 H), 7.30 (s, 2 H). $^{13}\text{C NMR}$ (CDCl_3) δ : 32.11, 34.41, 35.33, 125.74, 126.67, 144.96.

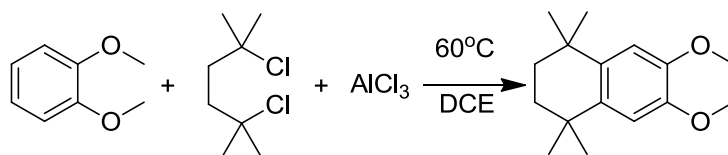
Compound **I**



Compound **Ia** (1.25 g, 6.64 mmol) was dissolved in dichloroethane (5 mL) and cooled to 0 oC at argon atmosphere. Catalytic amount of anhydrous AlCl_3 was added and 2,5-dichloro-2,5-dimethylhexane (1.8 g, 10 mmol) in dichloroethane was added drop-

wise to the above solution and heated for reflux for 2 hours. The resulting mixture was cooled to room temperature and poured into ice-HCl mixture (ice 100 g : 10mL HCl) and stirred for 15 min. The crude product was extracted to dichloromethane, dried over anhydrous MgSO_4 , filtered through a short pad of silica and evaporated the solvents to isolate dark yellow paste which was purified by recrystallization with dichloromethane : methanol (1:1) to afford di-substituted product as a colorless shiny plates. Yield : (1.32 g, 67 %), ^1H NMR (CDCl_3) δ : 1.27 (s, 24 H), 1.66 (s, 8 H), 7.19 (s, 2 H). ^{13}C NMR (CDCl_3) δ : 32.20, 34.17, 35.50, 124.22, 141.85.

Synthesis of compound V

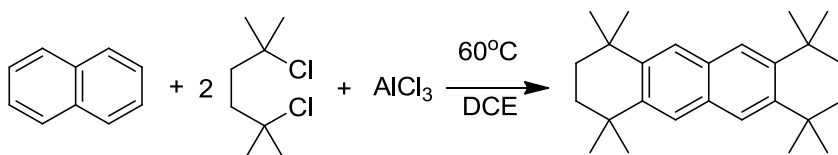


1,2-dimethoxybenzene(1 mmol) was dissolved in 10 mL of dichloroethane and cooled to 0 °C in an ice bath and catalytic amount of anhydrous AlCl_3 was added under argon atmosphere. Then 2,5-dichloro-2,5-dimethylhexane (1.2 mmol) in dichloroethane (10 mL) was added dropwise to the above mixture and heated to 60-80 °C under argon atmosphere for 2h while the reaction was monitored by NMR. Once the reaction was completed the reaction mixture was poured into a ice-.HCl mixture(ice 100g : 10 mLHCl), stirred for 15 min, and the product was extracted to dichloromethane. The organic layer was dried over anhydrous MgSO_4 , filtered through a short pad of silica and evaporated to isolate the crude product which was recrystallized with dichloromethane : methanol (1 :1) mixture to obtain pure product as colorless crystals.Yield : ^1H NMR

(CDCl₃) δ : 1.28 (s, 12 H), 1.69 (s, 4 H), 3.87 (s, 6H), 6.79 (s, 2 H). ¹³C NMR (CDCl₃)
 δ : 32.02, 34.16, 35.39, 55.96, 109.38, 137.20, 147.40.

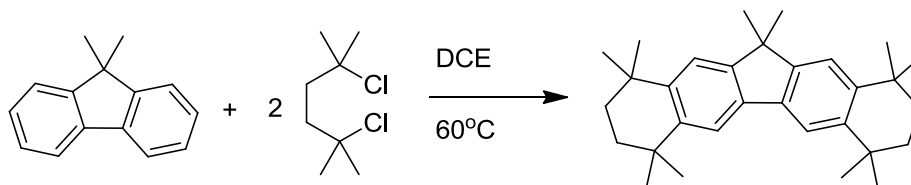
Using the same experimental procedure following cycloannulated aromatic compounds
II, VIII, IX, X, XII were prepared as indicated bellow.

Compound II



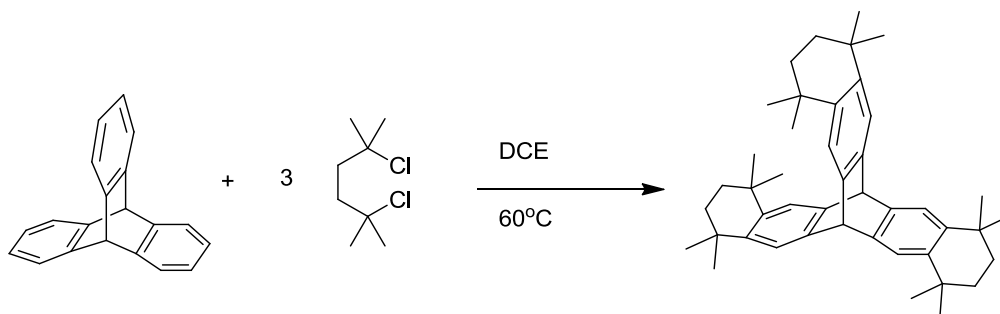
Yield : ¹H NMR (CDCl₃) δ : 1.40 (s, 24 H), 1.78 (s, 8 H), 7.19 (s, 4 H). ¹³C NMR
 (CDCl₃) δ : 32.79, 34.70, 35.41, 124.23, 130.51, 143.67.

Compound VIII



Yield : ¹H NMR (CDCl₃) δ : 1.32 (s, 12 H), 1.37 (s, 12 H), 1.44 (s, 4 H), 1.72 (s, 8 H),
 7.29 (s, 2 H), 7.58 (s, 2 H). ¹³C NMR (CDCl₃) δ : 27.97, 32.44, 34.72, 34.89, 35.54,
 35.56, 46.32, 117.32, 120.32, 137.09, 143.43, 143.69, 151.22.

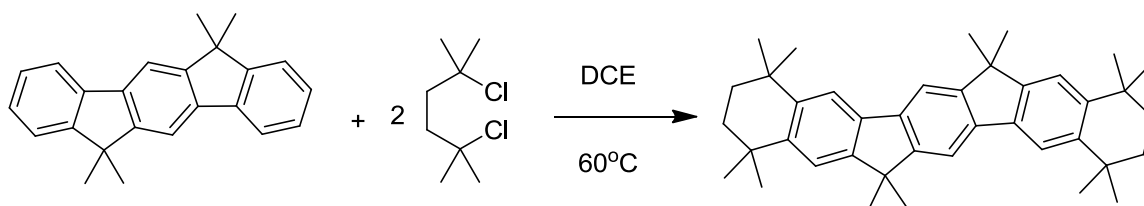
Compound IX



Triptycene(0.508 g, 2 mmol) was dissolved in 10 mL of dichloroethane and cooled to 0 °C in an ice bath and catalytic amount of anhydrous AlCl₃ was added under argon atmosphere. Then 2,5-dichloro-2,5-dimethylhexane (2.2 g, 12 mmol) in dichloroethane (10 mL) was added dropwise to the above mixture and heated to 60-80 °C under argon atmosphere for 2h while the reaction was monitored by NMR. Once the reaction was completed the reaction mixture was poured into a ice-HCl mixture(ice 100g : 10 mLHCl), stirred for 15 min, and the product was extracted to dichloromethane. The organic layer was dried over anhydrous MgSO₄, filtered through a short pad of silica and evaporated to isolate the crude product which was recrystallized with dichloromethane : methanol (1 :1) mixture to obtain pure product as white crystals.

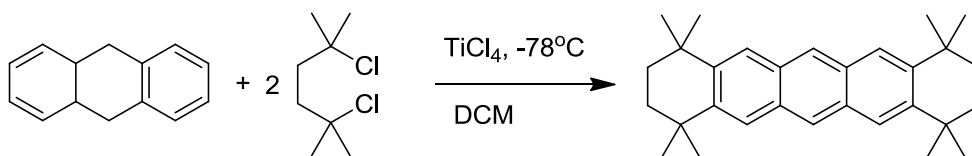
Yield (0.6 g, 54 %) ¹H NMR (CDCl₃) δ: 1.26 (s, 36 H), 1.64 (s, 12 H), 5.20 (s, 2 H), 7.28 (s, 6 H). ¹³C NMR (CDCl₃) δ: 32.16, 34.41, 35.46, 53.65, 121.58, 140.97, 142.98.

Compound X



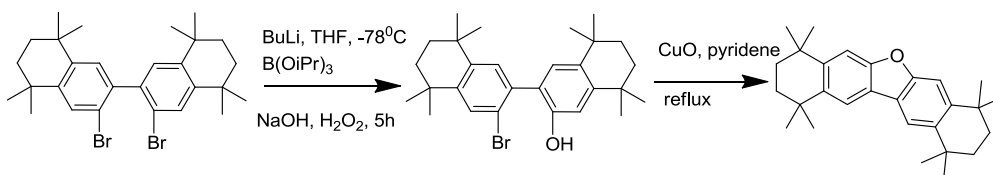
Yield : ¹H NMR (CDCl₃) δ: 1.34 (s, 12 H), 1.39 (s, 12 H), 1.53 (s, 12 H), 1.73 (s, 8 H), 7.34 (s, 2 H), 7.67 (s, 2 H), 7.69 (s, 2 H). ¹³C NMR (CDCl₃) δ: 27.93, 32.46, 34.76, 34.95, 35.56, 46.40, 113.88, 117.32, 120.45, 137.22, 138.71, 143.66, 143.96, 151.42, 153.42.

Compound III



9,10-Dihydroanthracene (4.0 g, 22.2 mmol) and 2,5-dichloro-2,5-dimethylhexane (11.0 g, 60 mmol) were placed in a Schlenk flask, and the contents were evacuated and back-filled with argon three times. Dry dichloromethane (100 mL) was added to the flask and the resulting solution was then cooled to -78°C . To the reaction mixture was then slowly added TiCl_4 (7.4 mL, 66.6 mmol) over a period of 10-20 min. The reaction mixture was stirred overnight and the contents of the reaction mixture were poured into ice-water (200 mL) and extracted with dichloromethane. The combined organic layers were washed with sat. NaHCO_3 and dried over MgSO_4 , passed through a short silica pad. After evaporation of the solvents the resulting solid was triturated in boiling EtOH (500 mL) and filtered and dried under vacuum to obtain pure product as a pale yellow solid (8.4 g) Yield : 95 %, $^1\text{H NMR}$ (CDCl_3) δ : 1.43 (s, 24 H), 1.79 (s, 8 H), 7.88 (s, 4 H), 8.19 (s, 2 H). $^{13}\text{C NMR}$ (CDCl_3) δ : 32.86, 34.88, 35.34, 123.92, 124.72, 130.65, 143.81.

Compound VI

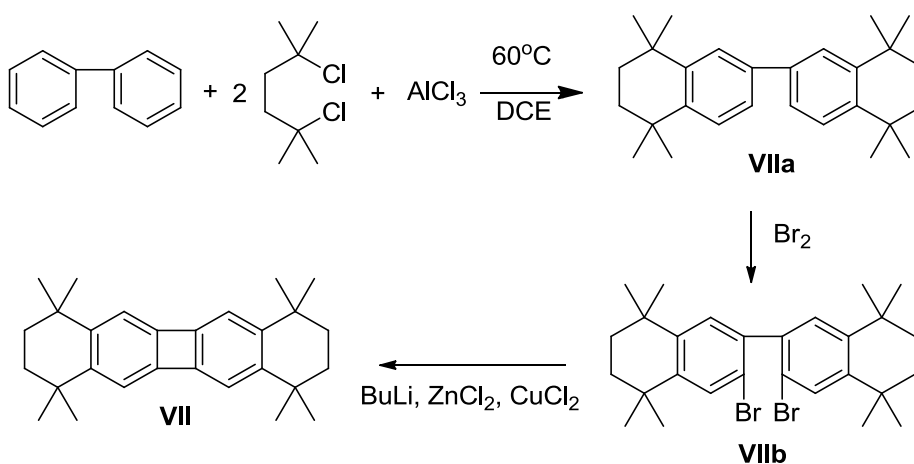


Cycloannulated dibromobiphenyl(0.40 g, 0.75 mmol) was dissolved in tetrahydrofuran(30 mL) and cooled to -78°C . one equivalent of butyl lithium (0.3 mL, 0.75 mmol) was added and stirred for 30 min and triisopropylborate (0.5 mL, 1.5 mmol) was added in one

portion and stirred overnight. A solution of NaOH() in H₂O₂() was added drop-wise to the above mixture at 0^oC and stirred for 5h. dilute hydrochloric acid (30 mL) was added and the formed product was extracted to dichloromethane (25 mL x2), dried over anhydrous MgSO₄ and evaporated to isolate crude product which was used in the next step without further purification. A mixture of the hydroxylated product (0.30 g, 0.6 mmol) , pyridine(15 mL) and CuO (0.047 g, 0.6 mmol) was refluxed overnight. The reaction mixture was cooled to room temperature and filtered through a short pad of silica gel and treated with dil HCl. The formed product was extracted to dichloromethane , dried over anhydrous MgSO₄ and evaporated to isolate crude product which was recrystallized with dichloromethane/ methanol(1:1) mixture to isolate pure product as a white solid.

Yield(0.23 g, 99%), ¹H NMR (CDCl₃) δ: 1.35 (s, 12 H), 1.39 (s, 12 H), 1.75 (s, 8 H), 7.41(s, 2H), 7.81(s, 2h). ¹³C NMR (CDCl₃) δ: 32.61, 32.85, 34.74, 35.32, 35.35, 35.50, 108.66, 118.04, 122.40, 139.65, 144.76, 155.36.

Compound VII



Diphenyl (14.0 g, 90.9 mmol) was dissolved in dichloroethane(80 mL and catalytic amount of anhydrous AlCl_3 was added under argon atmosphere. Then 2,5-dichloro-2,5-dimethylhexane (33.0 g, 180.3 mmol) in dichloroethane (30 mL) was added dropwise to the above mixture over 40 minutes at 27 °C .Then the reaction mixture was heated overnight at 45 °C under argon atmosphere. The reaction mixture was poured into a ice-.HCl mixture(ice 100g : 10 mLHCl), stirred for 15 min, and the product was extracted to dichloromethane. The organic layer was dried over anhydrous MgSO_4 , filtered through a short pad of silica and evaporated to isolate the crude product which was recrystallized with dichloromethane : methanol (1 :1) mixture to obtain pure product **VIIa** (33.0 g, 97 mmol) as colorless crystals. The obtained product (20.0 g, 53.5 mmol) was dissolved in dichloromethane (50 mL) and catalytic amount of Fe powder was added into it. Bromine (8.5 mL, 165.5 mmol) in dichloromethane (10 mL) was added slowly to the above mixture and stirred for 3h at room temperature. Then the reaction mixture was treated with NaHSO_3 solution (100 mL) and the product was extracted to dichloromethane (100 mL x 2), dried over anhydrous MgSO_4 , passed through a short pad of Silica and the solvent was evaporated to isolate the crude product which was recrystallized with dichloromethane:Methanol (1:1) to obtain pure product **VIIb** (25.2 g, 47.3 mmol). The brominated compound (5.32 g, 10 mmol) was dissolved in tetrahydrofuran (50 mL) and cooled to -78°C under argon atmosphere. BuLi (8.5 mL, 21.5 mmol) was added slowly to the above mixture, stirred for 30 min and the reaction mixture was allowed to warm to -20°C . Then the reaction mixture was stirred for 30 min at -20°C and cooled to -78°C . Anhydrous ZnCl_2 (1.5 g,11 mmol) in tetrahydrofuran (20 mL) was added into the above mixture and stirred for 20 min, anhydrous CuCl_2 (4.0 g, 30

mmol) was added and stirred for 30 min. The reaction mixture was poured into water (750 mL), stirred for 20 min, the product was extracted to dichloromethane (75 mL x 2), dried over anhydrous MgSO₄ and the solvent was evaporated to isolate the crude product which was recrystallized with dichloromethane : Methanol (1:1) to obtain pure product **VII** as white crystals.

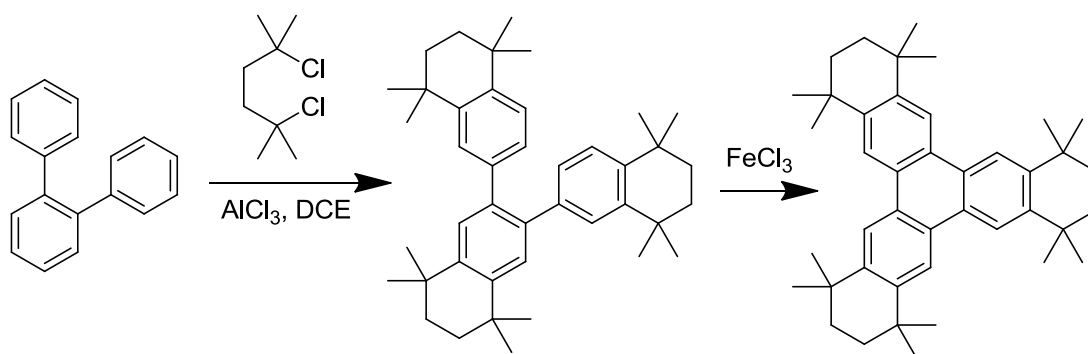
Compound **VIIb**

CA7-Br₂: ¹H NMR (CDCl₃) δ: 1.26 (s, 6 H), 1.28 (s, 6 H), 1.31 (s, 6 H), 1.33 (s, 6 H), 1.70 (s, 8 H), 7.24 (s, 2 H), 7.54 (s, 2 H). ¹³C NMR (CDCl₃) δ: 31.90, 31.91, 32.08, 34.41, 34.54, 35.11, 35.14, 120.50, 130.57, 130.59, 138.92, 143.99, 146.64.

Compound **VII**

¹H NMR (CDCl₃) δ: 1.48 (s, 36 H), 1.82 (s, 12 H), 8.44 (s, 6 H). ¹³C NMR (CDCl₃) δ: 32.64, 34.78, 35.50, 120.57, 127.71, 143.91.

Compound **IV**

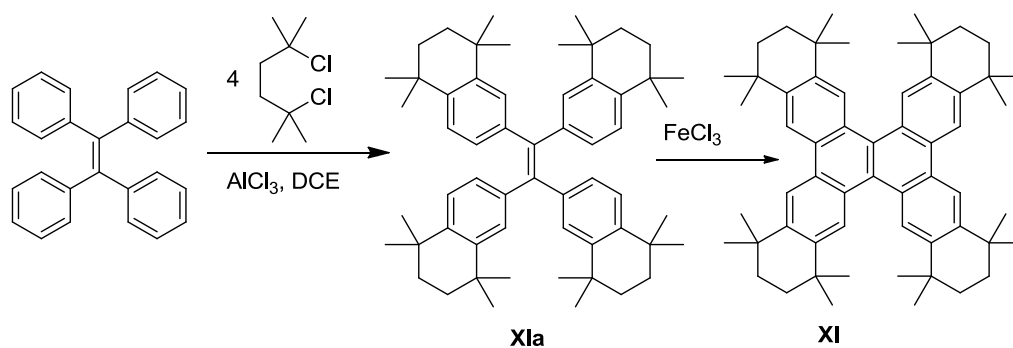


o-Terphenyl(1.0 g, 4.34 mmol) was dissolved in dichloroethane (8 mL) and cooled to 0 °C and catalytic amount of aluminum chloride was added into it. Then 2,5-Dichloro-2,5-dimethylhexane (2.78 g, 15.2 mmol) in dichloroethane (8 mL) was added

dropwise into the above solution and heated at 60-80 °C for 1h. The reaction mixture was cooled to room temperature and poured into ice (100g) and stirred for 15 minutes. The crude product was extracted to dichloromethane and dried over anhydrous MgSO₄ and filtered through a short pad of silica. The crude product was recrystallized with dichloromethane/hexane (1:1) to isolate the cycloannulated o-terphenyl as a white solid. The product (0.5 g, 0.89 mmol) was dissolved in a mixture of dichloromethane (50 mL) and nitromethane (5 mL) and catalytic amount of FeCl₃ was added and the reaction mixture was stirred for 3h. Methanol (50 mL) was added, stirred and the formed product was extracted to dichloromethane, dried over anhydrous MgSO₄ and evaporated to isolate the crude product which was recrystallized with dichloromethane/methanol(1:1) to isolate the cycloannulated triphenylene as a white solid.

Cycloannulated o-terphenyl : Yield (2.4 g, 83%) : ¹H NMR (CDCl₃) δ: 0.87 (s, 12 H), 1.24 (s, 12 H), 1.36 (s, 12 H), 1.56 (m, 8 H), 1.75 (s, 4 H), 6.75 (m, 2 H), 7.14- 7.20 (m, 2H), 7.24- 7.28 (m, 2H), 7.39 (s, 2H). ¹³C NMR (CDCl₃) δ: 31.81, 32.01, 32.14, 34.10, 24.42, 35.24, 35.34, 35.44, 126.29, 126.56, 128.51, 129.78, 138.56, 138.93, 142.62, 143.82, 143.95.

Cycloannulated triphenylene Yield(0.46 g, 94%) : ¹H NMR (CDCl₃) δ: 1.48 (s, 36 H), 1.82 (s, 12 H), 8.44 (s, 6 H). ¹³C NMR (CDCl₃) δ: 32.64, 34.78, 35.50, 120.57, 127.71, 143.91.

Compound **XI**

Tetraphenylethylene (0.5 g, 1.5 mmol) was dissolved in dichloroethane (8 mL) and cooled to 0 °C and catalytic amount of aluminum chloride was added into it. Then 2,5-Dichloro-2,5-dimethylhexane (1.65 g, 9 mmol) in dichloroethane (8 mL) was added dropwise into the above solution and heated at 60-80 °C for 2h. The reaction mixture was cooled to room temperature and poured into ice (100g) and stirred for 15 minutes. The crude product was extracted to dichloromethane and dried over anhydrous MgSO_4 and filtered through a short pad of silica. The crude product was recrystallized with dichloromethane/hexane (1:1) to isolate the product as a white solid. The product **XIa** (1.0 g, 1.3 mmol) was dissolved in dichloromethane (50 mL) and catalytic amount of FeCl_3 was added and the reaction mixture was stirred for 20 min. Methanol (50 mL) was added, stirred and filtered to isolate the pure product **XI** as a white solid.

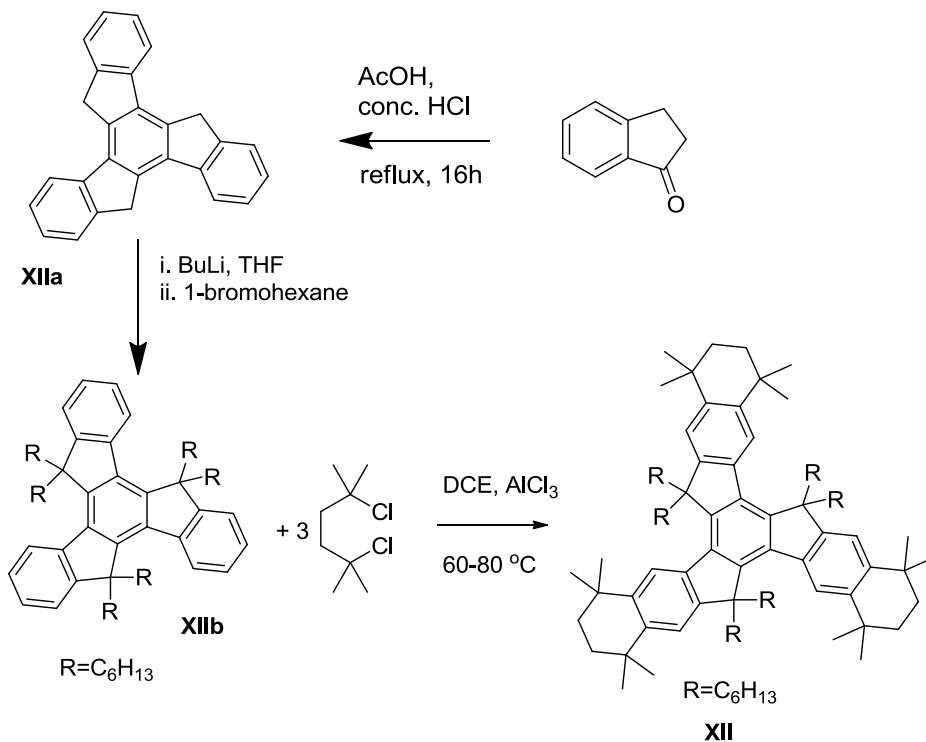
Compound **XIa** Yield: (0.83 g, 71%) ^1H NMR (CDCl_3) δ : 0.89 (s, 24 H), 1.18 (s, 24 H), 1.55 (m, 16 H), 6.74 (d, $J = 8.26$, 4 H), 6.88 (s, 4 H), 7.03 (d, $J = 8.26$, 4 H).

^{13}C NMR (CDCl_3) δ : 31.93, 33.96, 34.05, 35.38, 125.60, 128.23, 130.76, 141.11, 141.26, 142.22, 143.48.

Compound XI

^1H NMR (CDCl_3) δ : 1.40 (s, 24 H), 1.52 (s, 24 H), 1.83 (s, 16 H), 8.51 (s, 4 H), 8.53 (s, 4 H), ^{13}C NMR (CDCl_3) δ : 32.58, 32.80, 34.89, 35.43, 35.57, 121.19, 126.20, 127.21, 127.85, 128.80, 143.51, 143.87.

Compound XII



Synthesis of XIIIa

To a stirred mixture of acetic acid (16 mL) and conc. HCl (8.0 mL) was added 1-indane (3.5 g, 2.65 mmol) and the resulting mixture was refluxed for 16 h. The reaction mixture was cooled to room temperature and placed in ice-water (100 mL) and stirred for 10 mins. Then the product was filtered through a Buchner funnel, washed with water and then with acetone to isolate pure product as a white solid. Yield (2.4 g, 81%) ^1H NMR (CDCl_3) δ : 4.23 (s, 6 H), 7.38 (t, $J=7.4, 14.8$ Hz, 3 H), 7.50 (t, $J=7.4, 14.8$ Hz, 3 H), 7.68 (s, 3H), 2.98 (m, 6 H), 7.93 (s, 3 H).

Synthesis of XIIIb

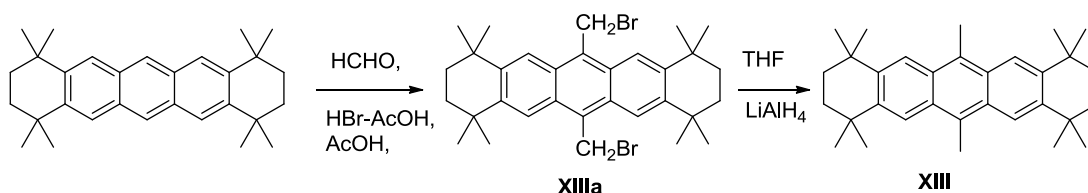
To a stirred solution of truxene (2.4 g, 7.01 mmol) in THF (50 mL) under argon atmosphere n-BuLi (10.6 mL, 2.5 M soln in hexane, 26.66 mmol) was added over a period of 25 min at room temperature. The reaction mixture was further stirred for half an hour and 1-bromohexane (3.74 mL, 26.7 mmol) was added over a 10 min period and stirred for four hours. The second portion of n-BuLi (10.6 mL, 2.5 M soln in hexane, 26.66 mmol) was added over a period of 25 min at room temperature and the second portion of 1-bromohexane (3.74 mL, 26.7 mmol) was added and stirred for 12 hours. Then aqueous solution of ammonium chloride was added and the formed product was extracted to petroleum ether, dried over anhydrous MgSO₄ and evaporated to isolate crude product as a yellow thick oil which was purified by passing through a short pad of silica to isolate the product as a pale yellow thick oil. Yield (5.9 g, 99%) ¹H NMR (CDCl₃) δ: 0.51 (m, 12 H), 0.61 (t, *J* = 6.6, 13.7 Hz, 18 H), 0.90 (m, 36 H), 2.09 (m, 6 H), 2.98 (m, 6 H), 7.33- 7.51 (m, 9 H), 8.38 (d, *J* = 7.6 Hz, 3H). ¹³C NMR (CDCl₃) δ: 14.11, 22.49, 24.10, 29.72, 31.71, 37.16, 55.80, 122.37, 124.84, 126.15, 126.53, 138.57, 140.55, 145.02, 153.85.

Synthesis of XII

Hexylated truxene (2.0 g, 2.36 mmol) was dissolved in 10 mL of dichloroethane and cooled to 0 °C in an ice bath and catalytic amount of anhydrous AlCl₃ was added under argon atmosphere. Then 2,5-dichloro-2,5-dimethylhexane (2.2 g, 12 mmol) in dichloroethane (10 mL) was added dropwise to the above mixture and heated to 60-80 °C under argon atmosphere for 2h. The reaction mixture was cooled to room temperature, poured into a ice-HCl mixture (ice 100g : 10 mL HCl), stirred for 15 min, and the product

was extracted to dichloromethane. The organic layer was dried over anhydrous MgSO_4 , filtered through a short pad of silica and evaporated to isolate the crude product which was recrystallized with dichloromethane : methanol (1 :1) mixture to obtain pure product as white crystals. Yield : (2.18 g, 79%) ^1H NMR (CDCl_3) δ : 0.56 (m, 30 H), 0.89 (m, 36 H), 1.36 (s, 18 H), 1.43 (s, 18 H), 1.77 (s, 12 H), 2.08 (m, 6 H), 2.86 (m, 6 H), 7.32 (s, 3 H), 8.22 (s, 3 H). ^{13}C NMR (CDCl_3) δ : 14.11, 22.47, 23.91, 29.61, 31.50, 32.34, 332.72, 34.58, 34.94, 35.62, 35.70, 37.09, 55.21.

Synthesis of XIII



A mixture of compound **III** (150 mg, 0.38 mmol), formaldehyde (226 mg, 7.6 mmol), HBr - AcOH (15 mL) and AcOH (35 mL) was heated at 40 °C for 12h and the reaction mixture was poured into water (500 mL). The product was extracted to dichloromethane and washed with dil. NaHCO_3 solution (50 mL), dried over anhydrous MgSO_4 and solvent was evaporated to isolate the product **XIIIa** as a yellow solid which was subjected to reduction with LiAlH_4 under reflux conditions in tetrahydrofuran to crude product. The crude product was recrystallized with dichloromethane: Methanol (1:1) under dark conditions to afford pure product **XIII** as yellow crystals.

Compound XIIIa

^1H NMR (CDCl_3) δ : 1.50 (s, 24 H), 1.84 (s, 8 H), 5.49 (s, 4 H), 8.23 (s, 4 H). ^{13}C NMR (CDCl_3) δ : 32.88, 35.20, 35.26, 121.23, 127.7, 128.35, 145.26.

Compound XIII

^1H NMR (CDCl_3) δ : 1.46 (s, 24 H), 1.82 (s, 8 H), 3.03 (s, 6 H), 8.18 (s, 4 H). ^{13}C

NMR (CDCl_3) δ : 33.07, 35.03, 35.52, 68.18, 121.95, 125.85, 128.68, 142.81.

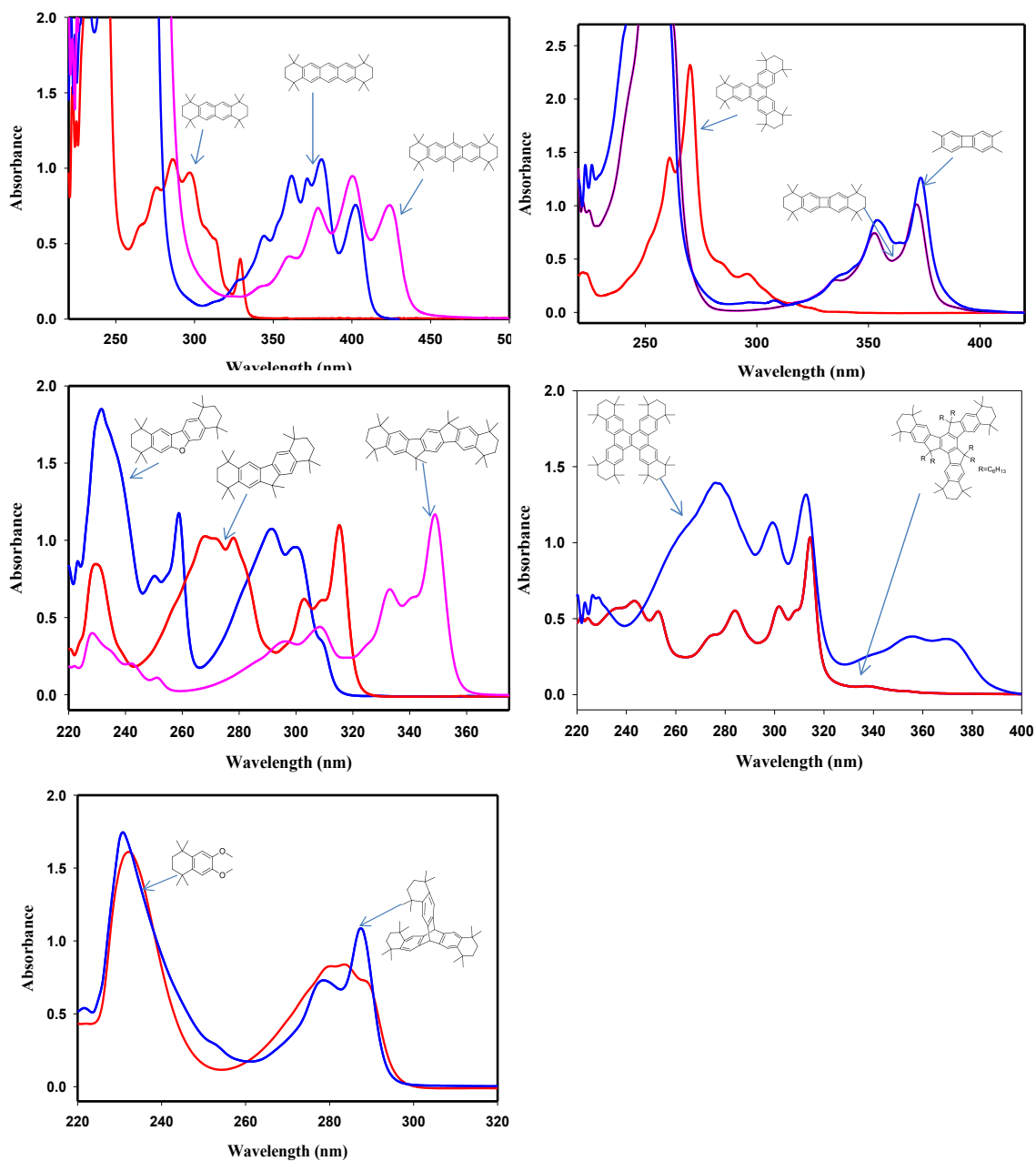
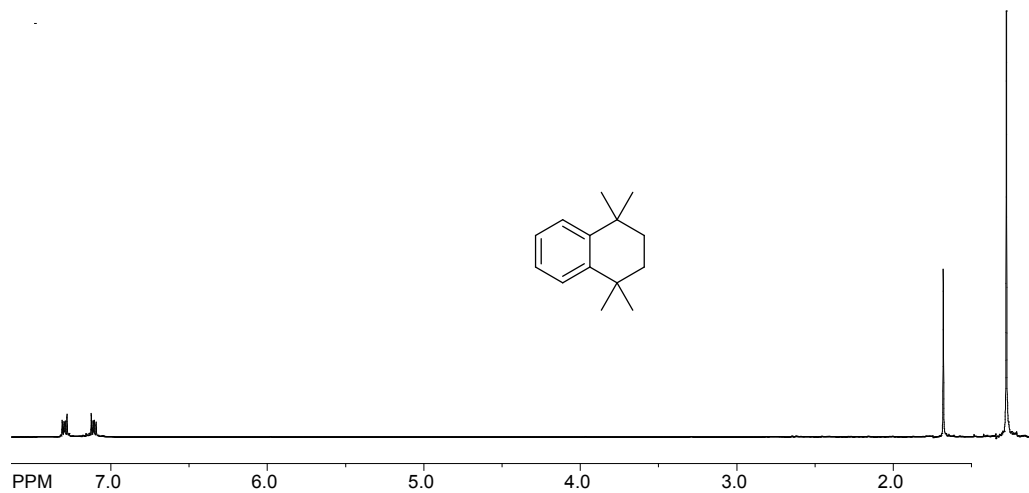
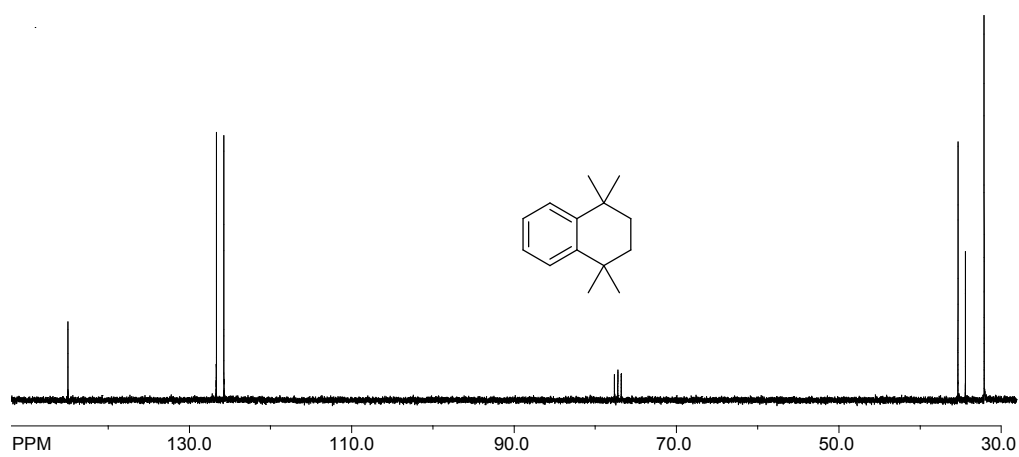
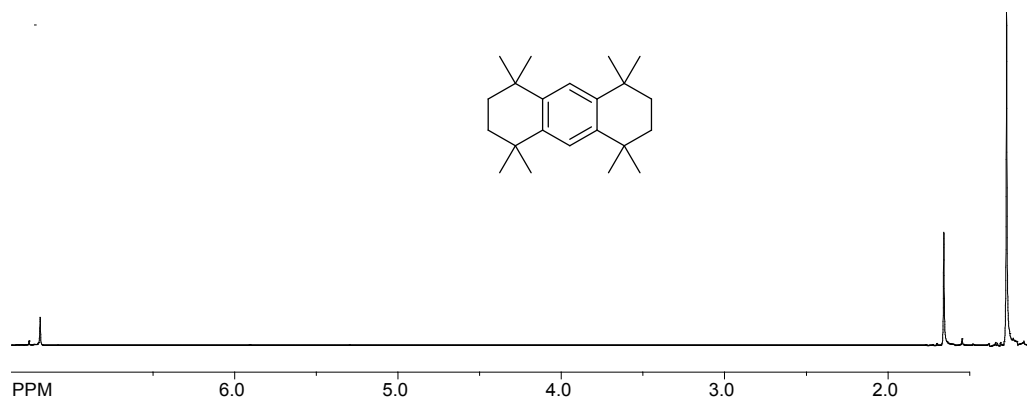
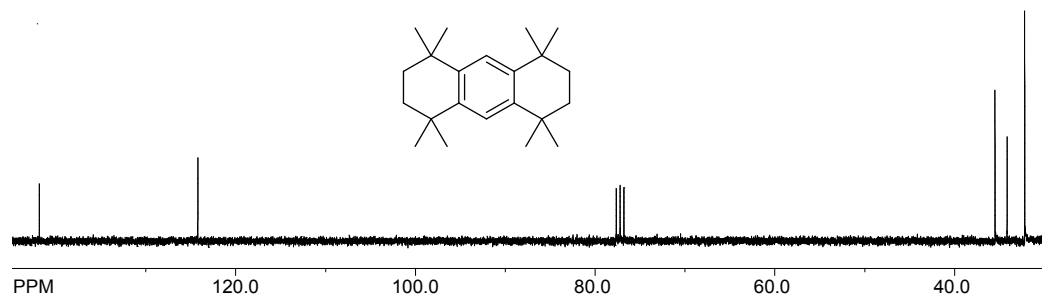
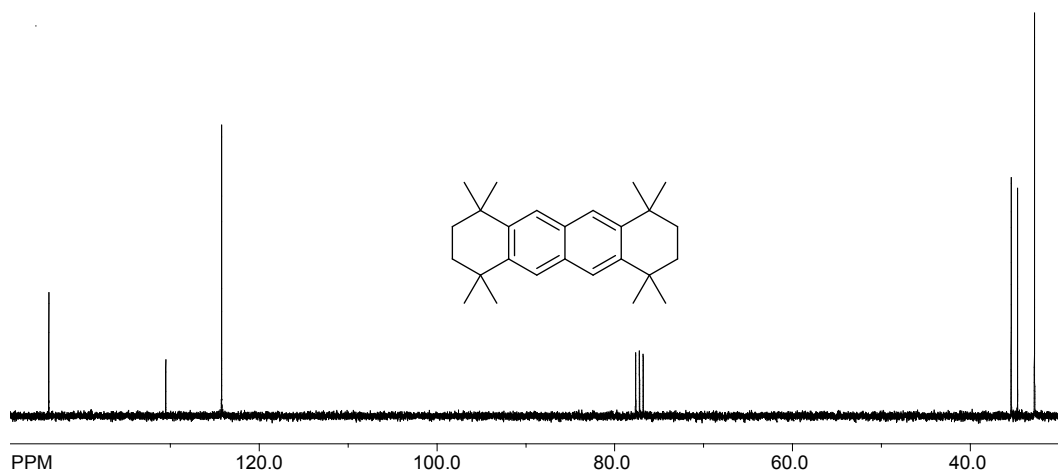
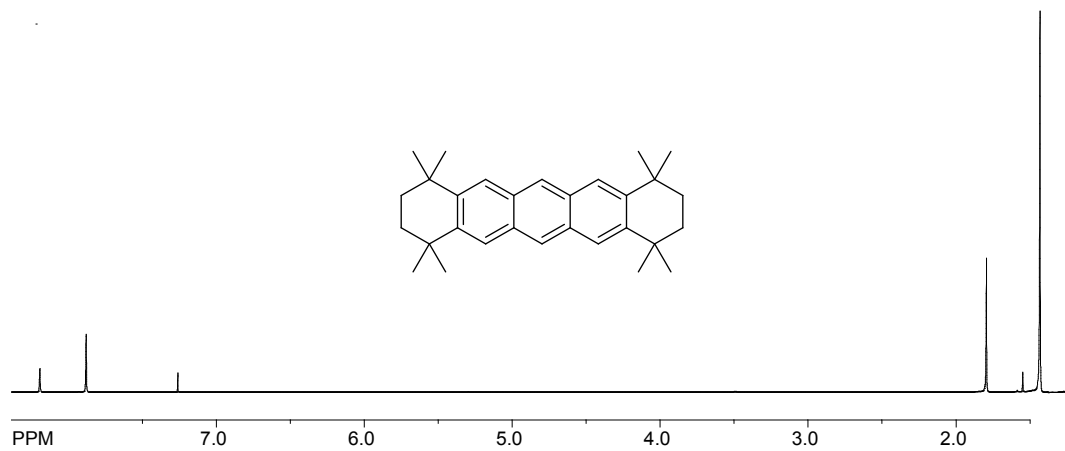
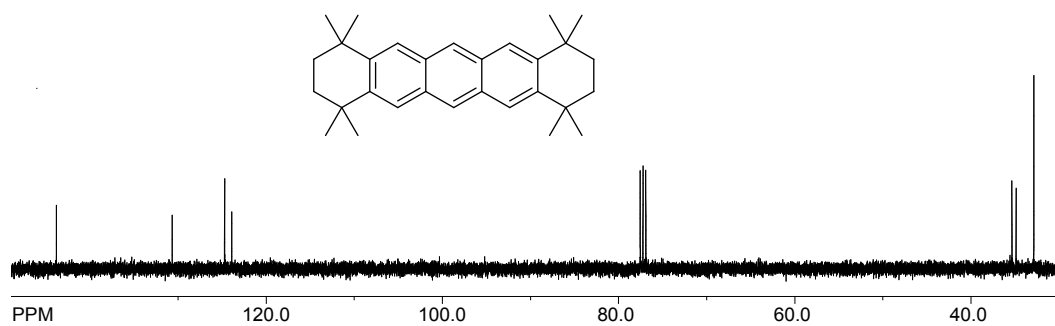
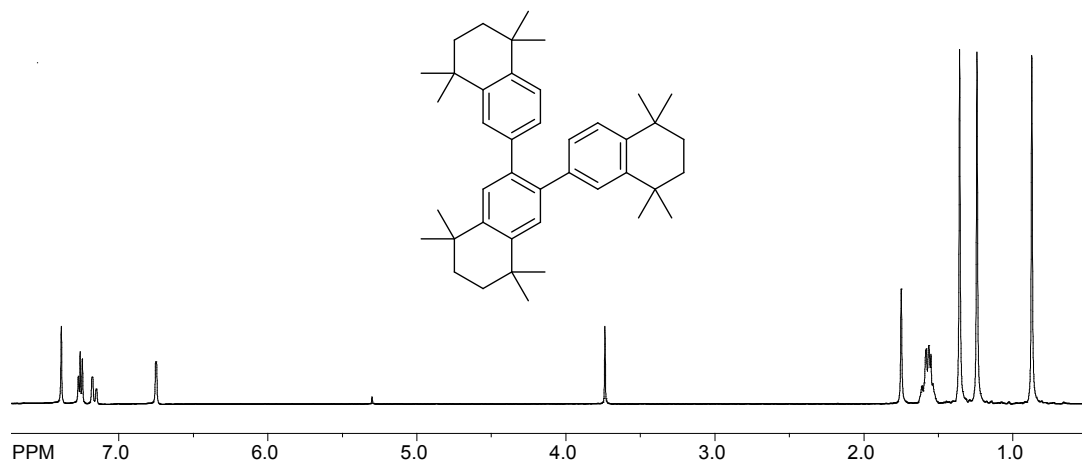
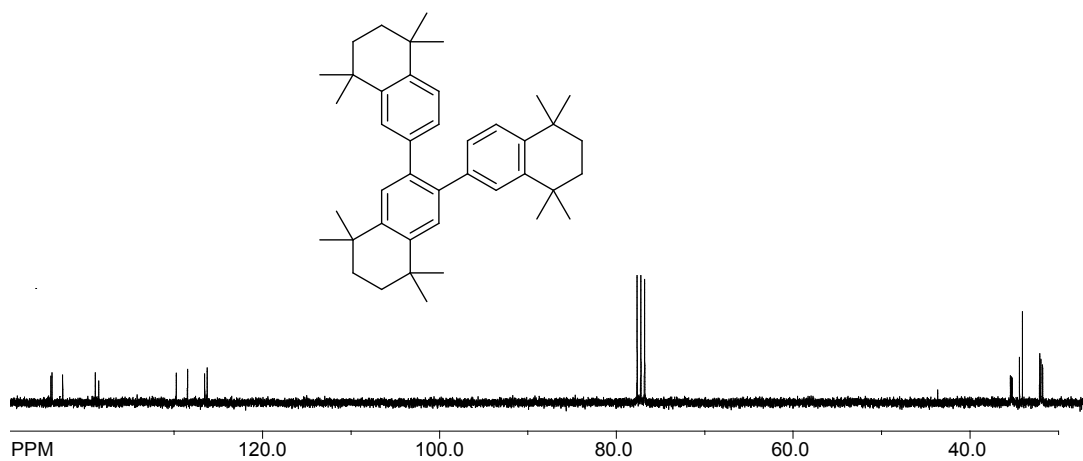
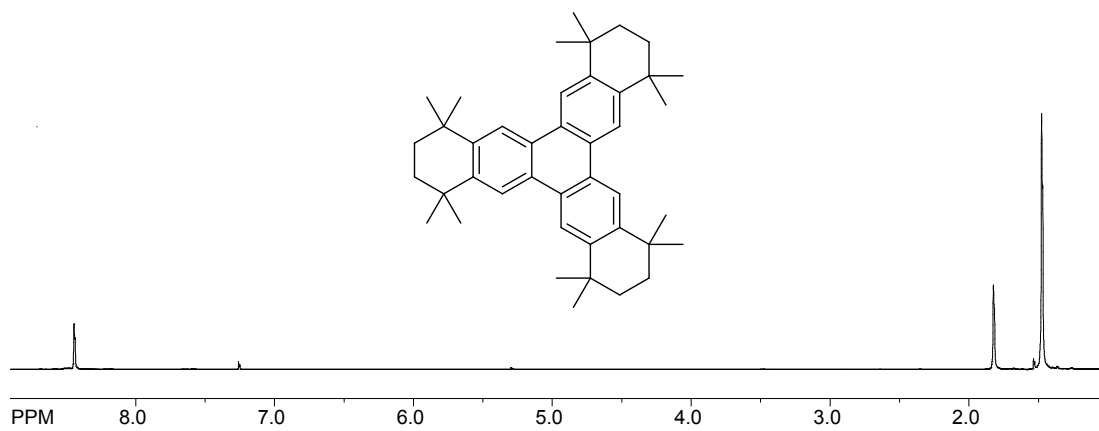
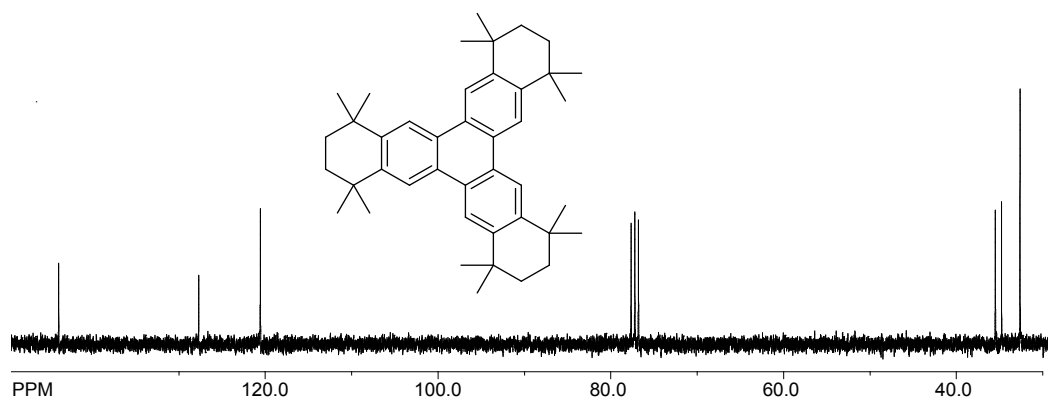


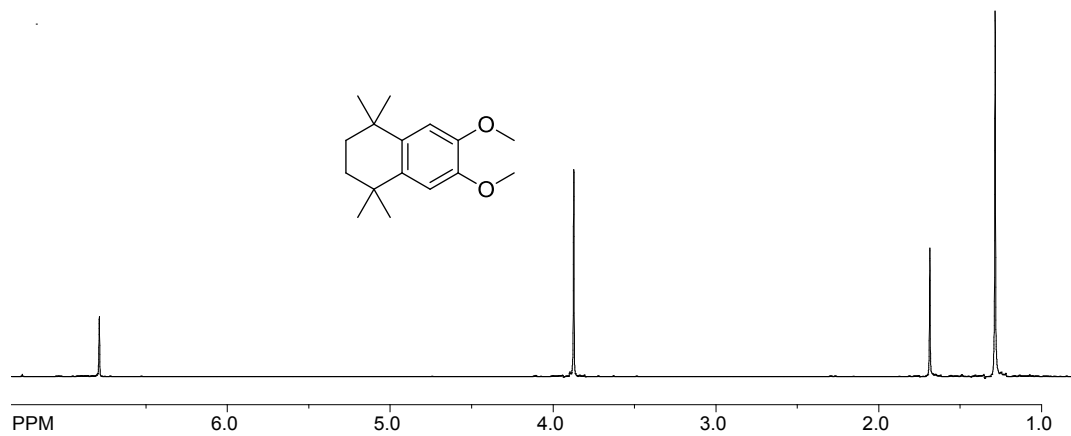
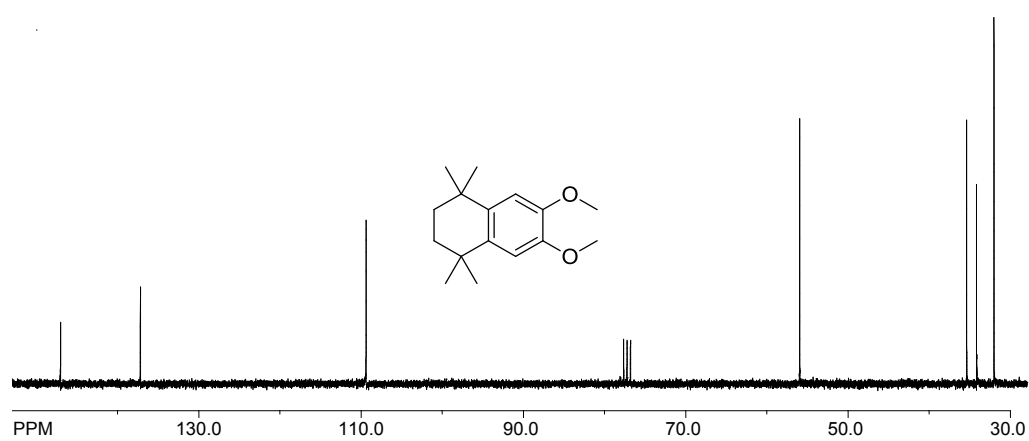
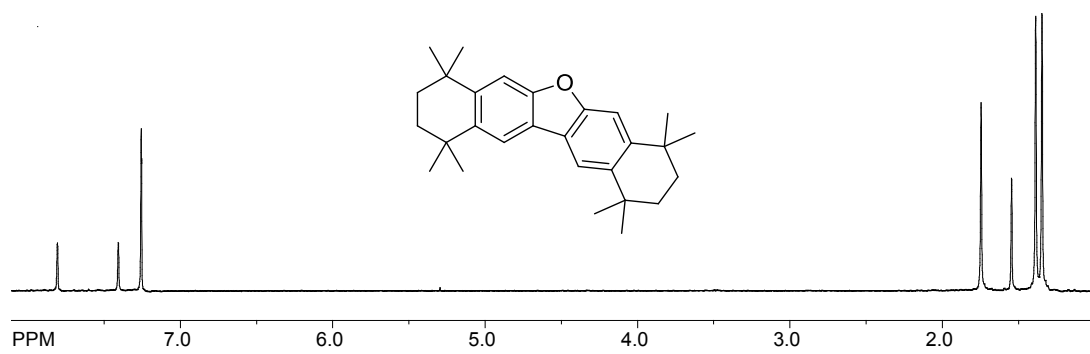
Figure 12. The UV-vis spectra of the compounds (I-XIII)

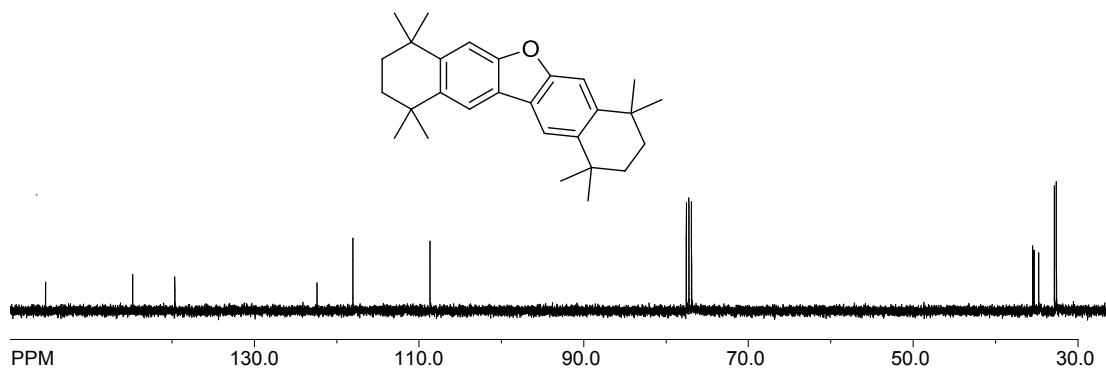
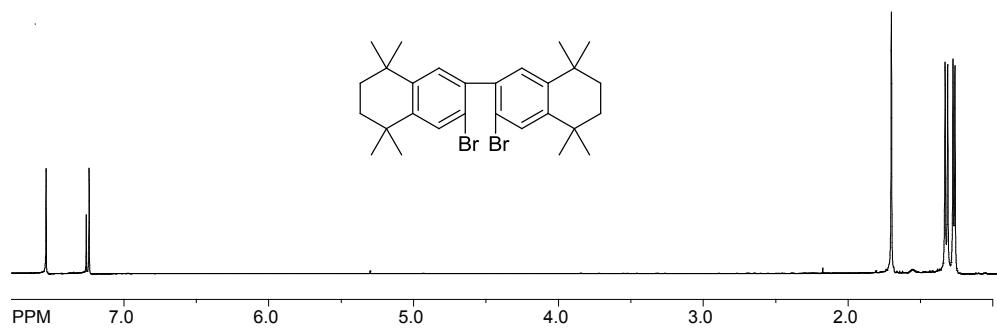
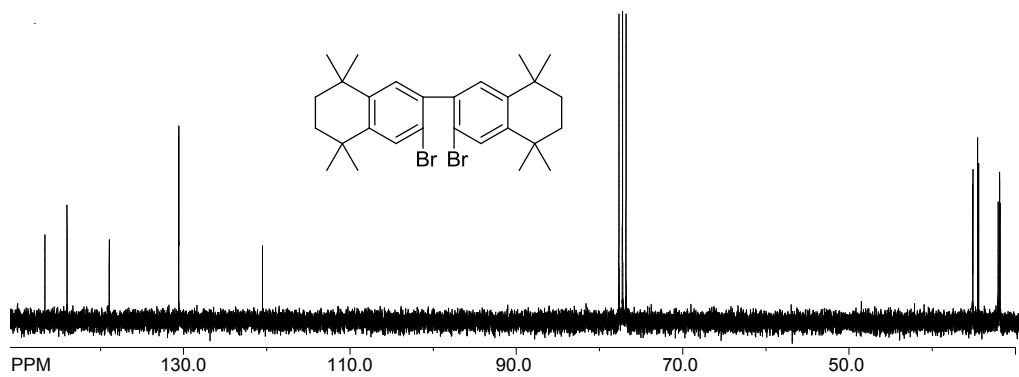
^1H NMR spectrum of Compound **Ia** ^1H NMR spectrum of Compound **Ia** ^1H NMR spectrum of Compound **I**

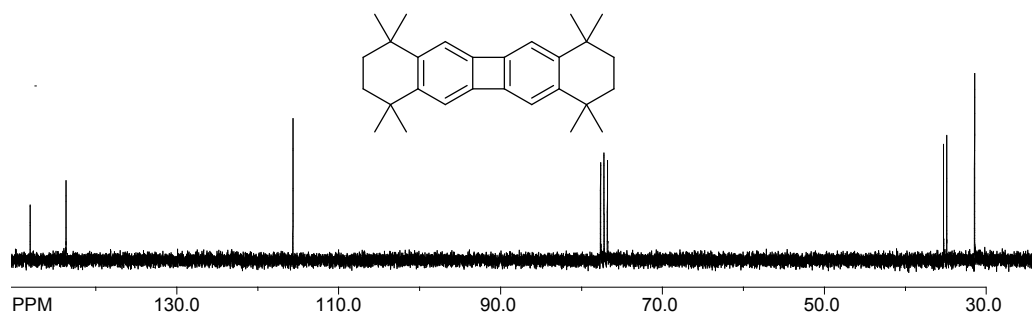
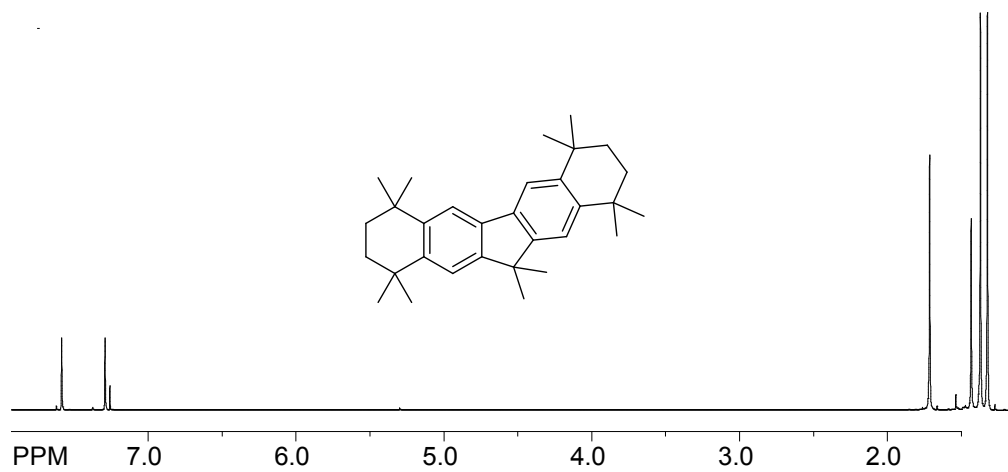
^{13}C NMR spectrum of Compound I ^1H NMR spectrum of Compound II ^{13}C NMR spectrum of Compound II

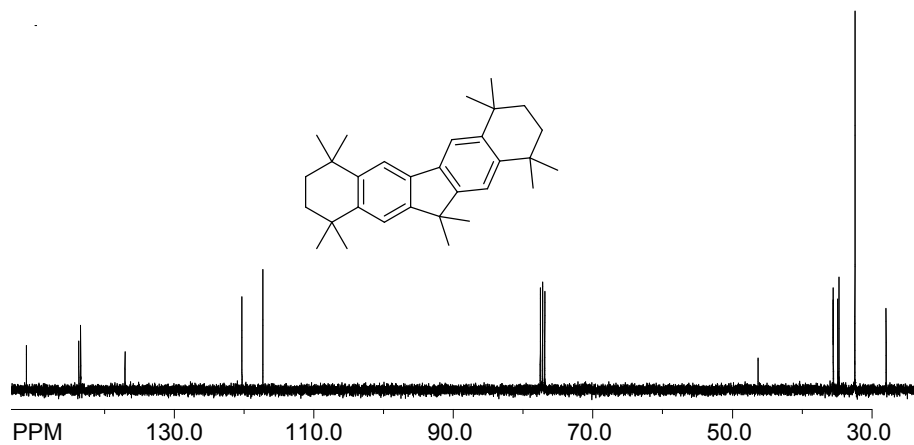
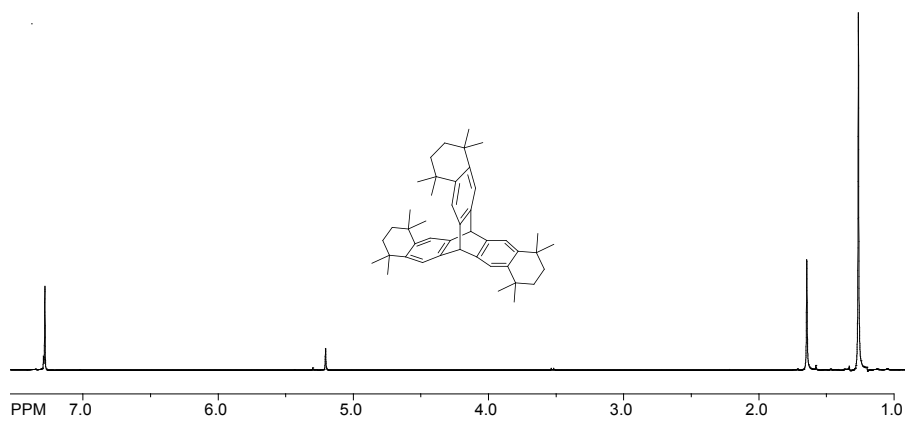
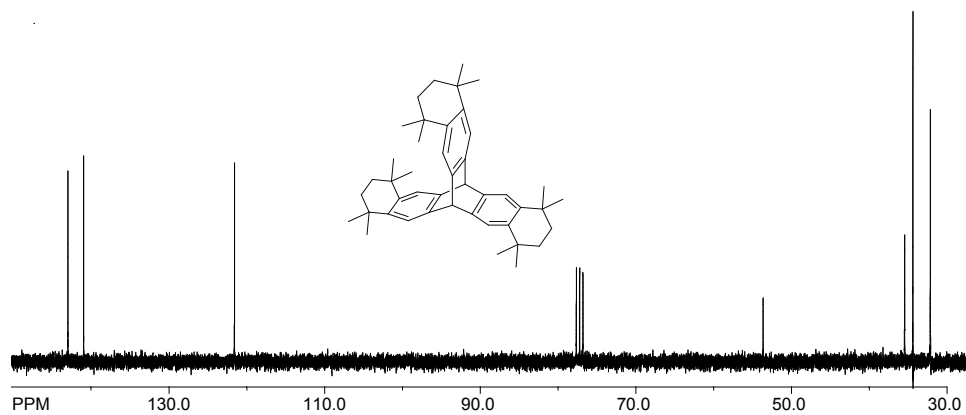
^1H NMR spectrum of Compound **III** ^{13}C NMR spectrum of Compound **III** ^1H NMR spectrum of **IVa**

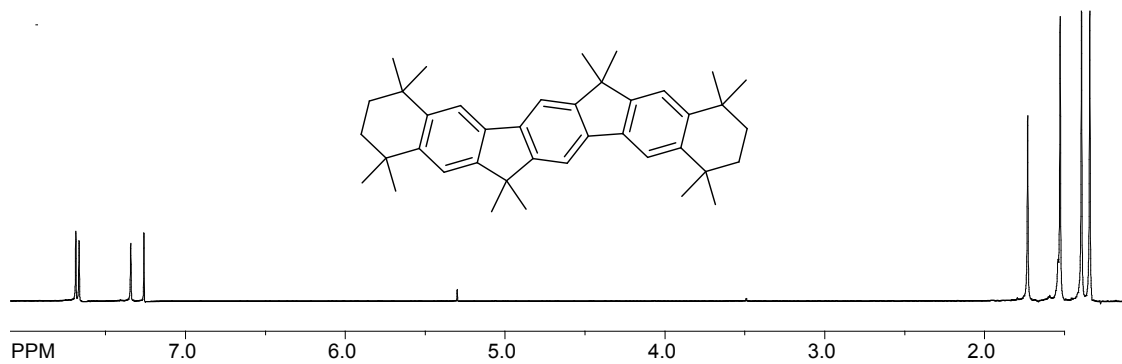
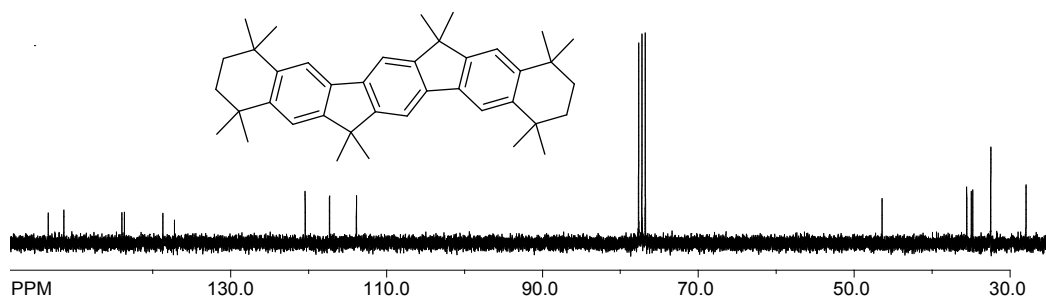
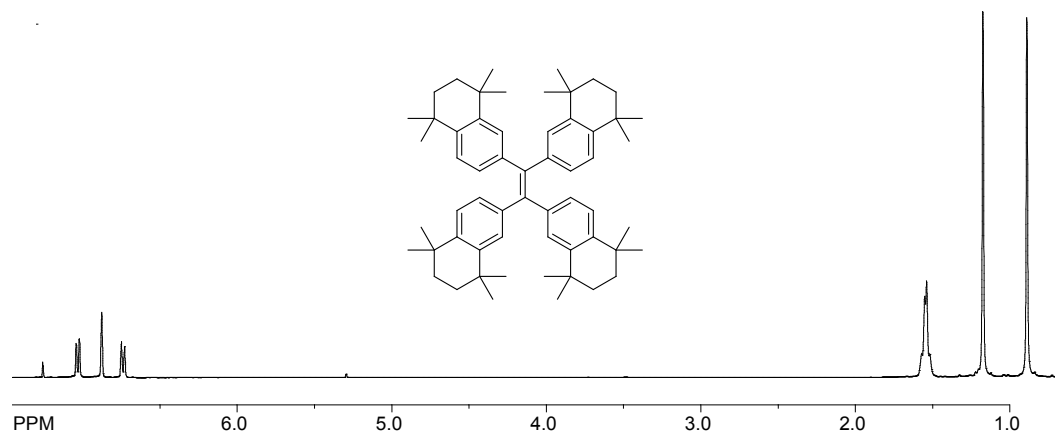
^{13}C NMR spectrum of **IVa** ^1H NMR spectrum of Compound **IV** ^{13}C NMR spectrum of Compound **IV**

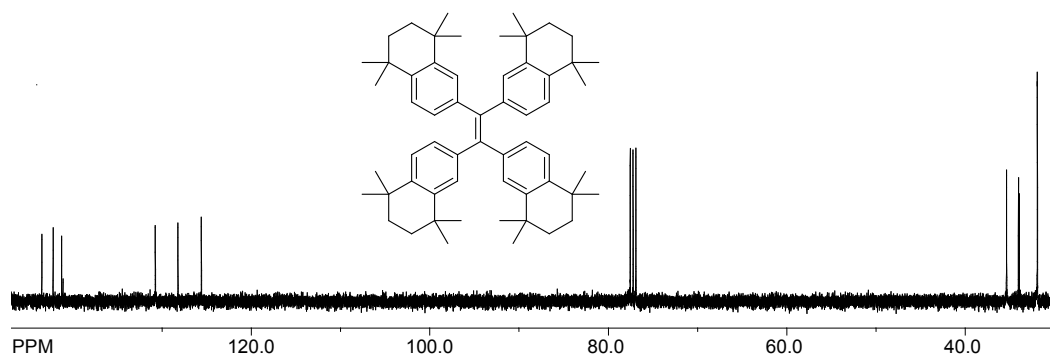
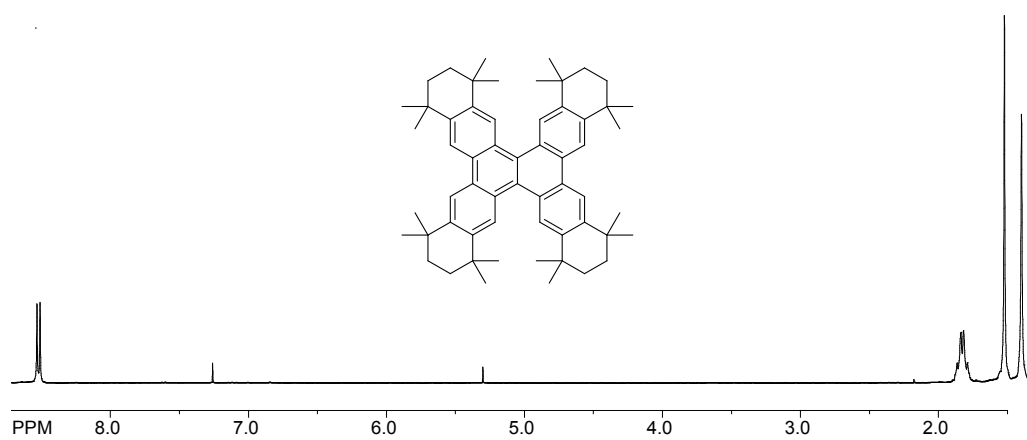
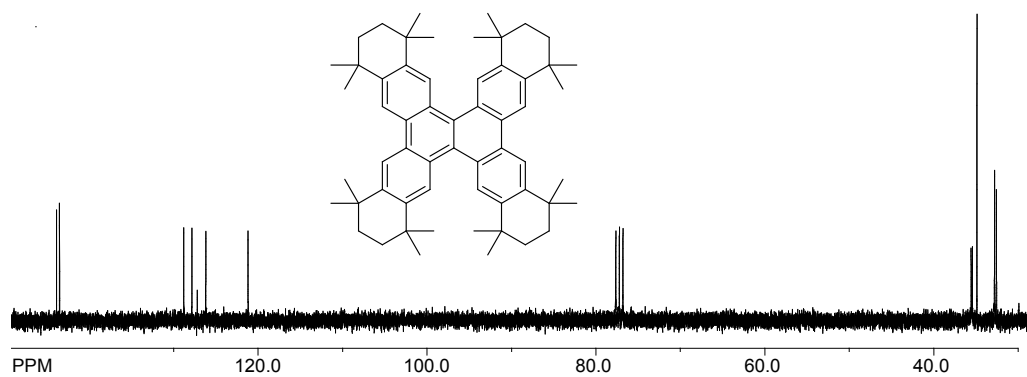
^1H NMR spectrum of Compound V ^{13}C NMR spectrum of V ^1H NMR spectrum of VI

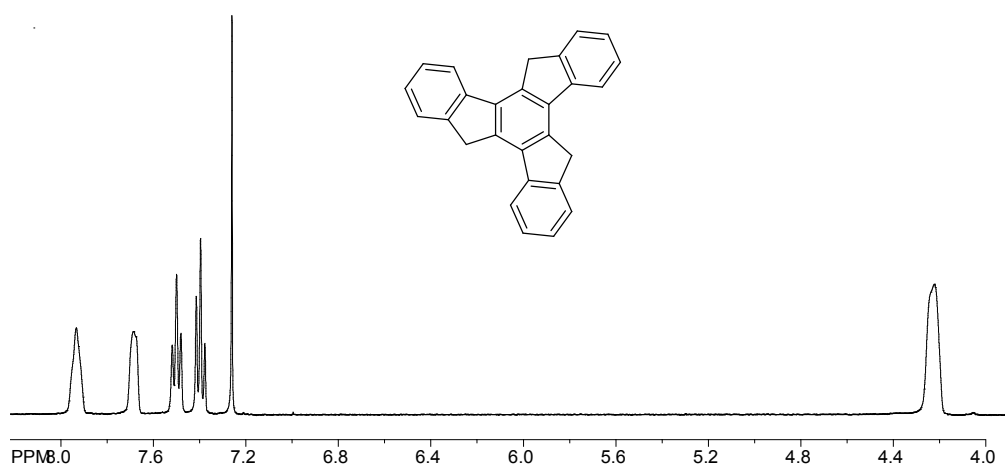
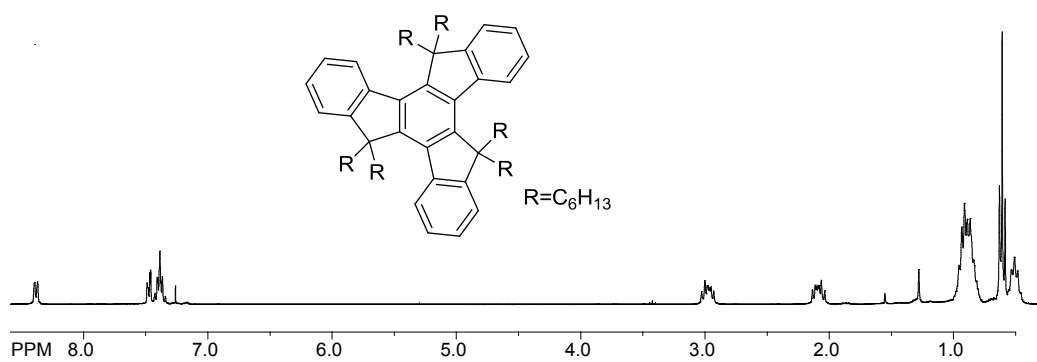
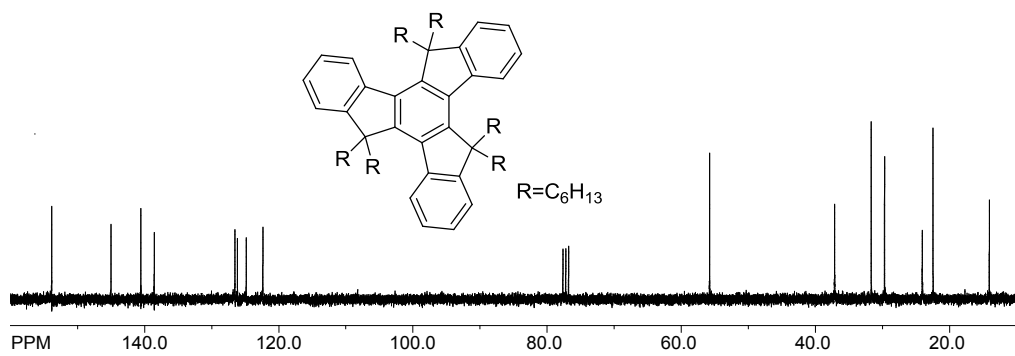
^{13}C NMR spectrum of **VI** ^1H NMR spectrum of compound **VIIIb** ^{13}C NMR spectrum of compound **VIIIb**

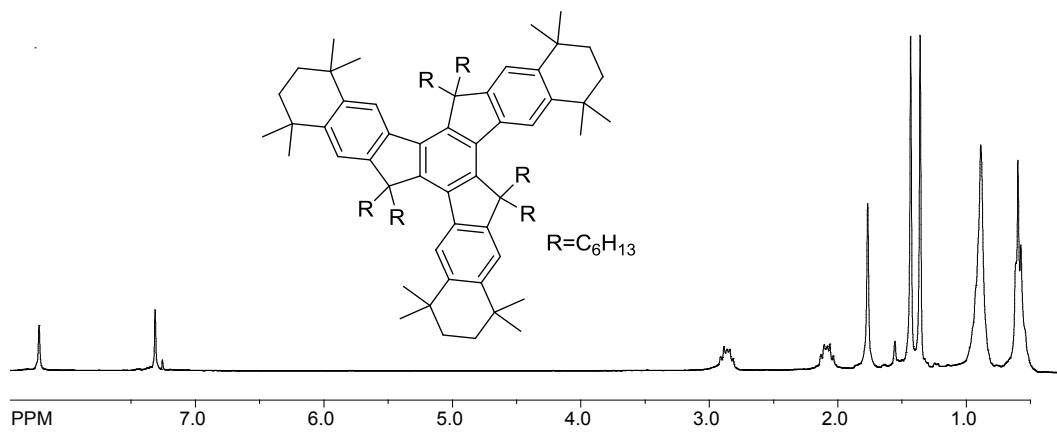
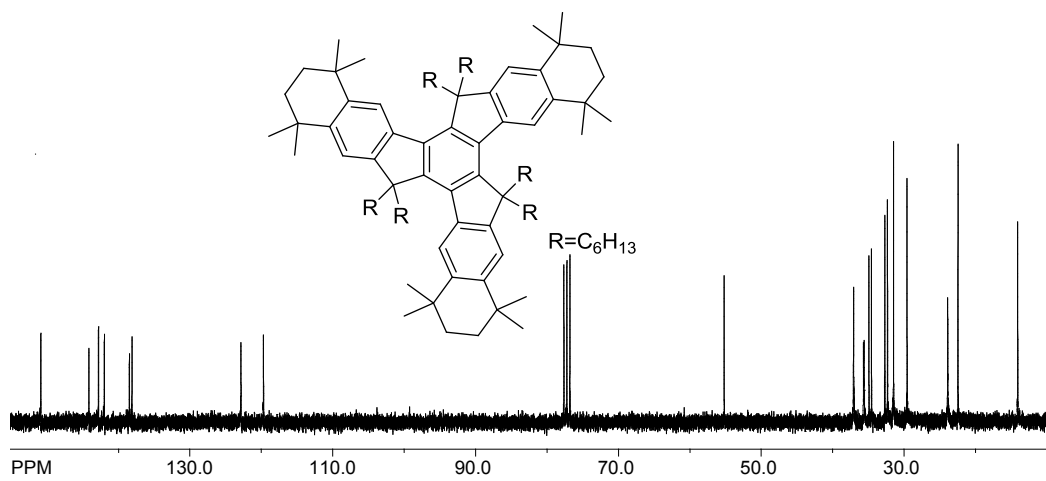
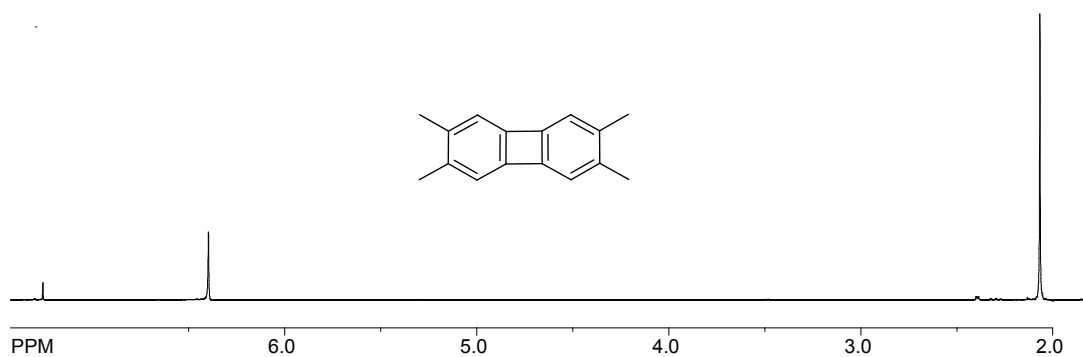
^1H NMR spectrum of Compound **VII** ^{13}C NMR spectrum of Compound **VII** ^1H NMR spectrum of Compound **VIII**

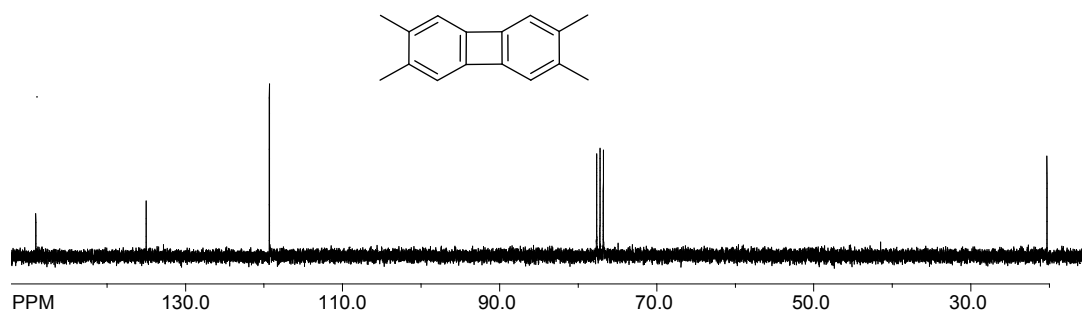
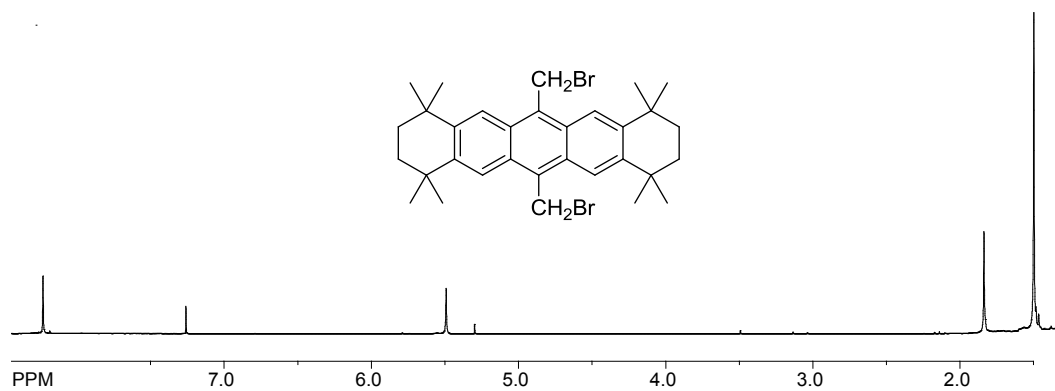
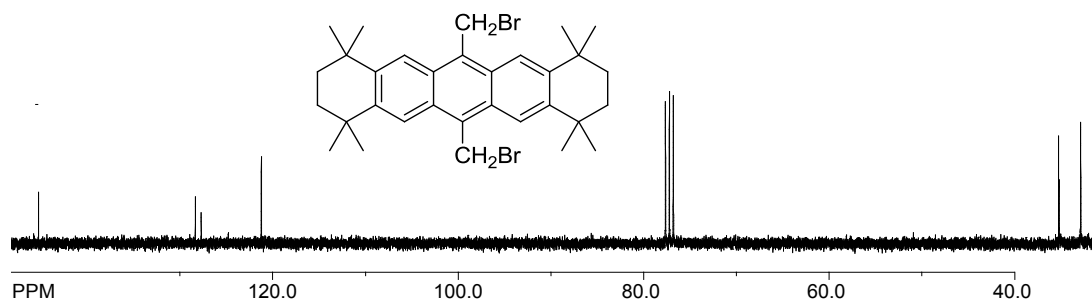
^{13}C NMR spectrum of Compound VIII ^1H NMR spectrum of Compound IX ^{13}C NMR spectrum of Compound IX

^1H NMR spectrum of Compound **X** ^{13}C NMR spectrum of Compound **X** ^1H NMR spectrum of Compound **XIa**

^{13}C NMR spectrum of Compound **XIa** ^1H NMR spectrum of Compound **XI** ^{13}C NMR spectrum of Compound **XI**

^1H NMR spectrum of truxene ^1H NMR spectrum of hexylated truxene ^1H NMR spectrum of hexylated truxene

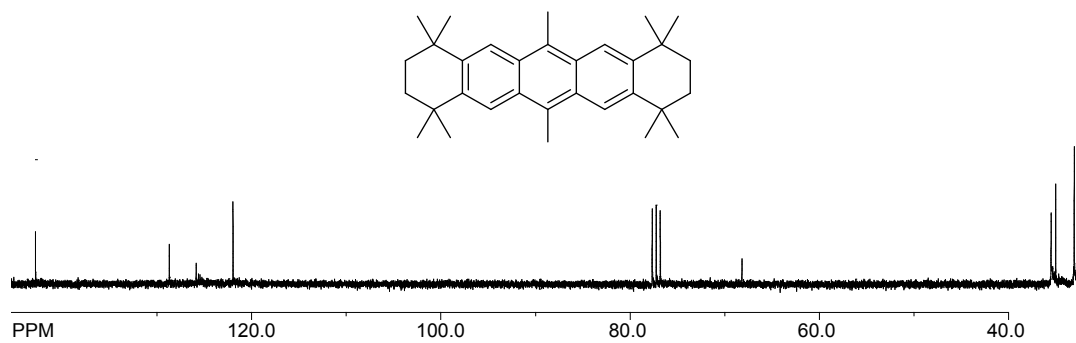
^1H NMR spectrum of Compound **XII** ^{13}C NMR spectrum of Compound **XII** ^1H NMR spectrum of tetramethylbiphenylene

^{13}C NMR spectrum of tetramethylbiphenylene ^1H NMR spectrum of Compound **XIIIa** ^{13}C NMR spectrum of Compound **XIIIa**

^1H NMR spectrum of Compound **XIII**



^{13}C NMR spectrum of Compound **XIII**



BIBLIOGRAPHY

(GENERAL INTRODUCTION)

1. (a) Kulkarni, A. P.; Tonzola, C. J.; Babel, A.; Jenekhe, S. A. *Chem. Mater.* **2004**, *16*, 4556. (b) Yu, W.-L.; Meng, H.; Pei, J.; Chua, S.-J.; Huang, W.; Lai, Y.-H. *Chem. Commun.* **1998**, *18*, 1957. (c) Shirota, Y.; Kinoshita, M.; Noda, T.; Okumoto, K.; Ohara, T. *J. Am. Chem. Soc.* **2000**, *122*, 11021. (d) Doi, H.; Kinoshita, M.; Okumoto, K.; Shirota, Y. *Chem. Mater.* **2003**, *15*, 1080.
2. (a) Tang, C. W.; VanSlyke, S. A.; Chen, C. H. *J. Appl. Phys.* **1989**, *65*, 3610. (b) Chen, C. H.; Shi, J.; Tang, C. W.; Klubek, K. P. *Thin Solid Films* **2000**, *363*, 327. (c) Tao, X. T.; Miyata, S.; Sasabe, H.; Zhang, G. J.; Wada, T.; Jiang, M. H. *Appl. Phys. Lett.* **2001**, *78*, 279. (d) Zhang, X. H.; Chen, B. J.; Lin, X. Q.; Wong, O. Y.; Lee, C. S.; Kwong, H. L.; Lee, S. T.; Wu, S. K. *Chem. Mater.* **2001**, *13*, 1565. (e) Li, J. Y.; Liu, D.; Hong, Z. R.; Tong, S. W.; Wang, P. F.; Ma, C. W.; Lengyel, O.; Lee, C. S.; Kwong, H. L.; Lee, S. T. *Chem. Mater.* **2003**, *15*, 1486.
3. Xia, C.; Advincula, R. C. *Macromolecules* **2001**, *34*, 6922.
4. Bredas, J. L.; Durrant, J. R. *Acc. Chem. Res.* **2009**, *42*, 1689.
5. Gunes, S.; Neugebauer, H.; Sariciftci N. S. *Chem. Rev.* **2007**, *107*, 1324.
6. (a) Wong, M. S.; Li, Z. H.; Tao, Y.; D'Iorio, M. *Chem. Mater.* **2003**, *15*, 1198-1203. (b) Morin, J. F.; Drolet, N.; Tao, Y.; Leclerc, M. *Chem. Mater.* **2004**, *16*, 4619-4626. (c) Leclerc, N.; Sanaur, S.; Galmiche, L.; Mathevet, F.; Attias, A. J.; Fave, J. L.; Roussel, J.; Hapiot, P.; Lemaitre, N.; Geffroy, B. *Chem. Mater.* **2005**, *17*, 502-513.
7. Gross, M.; Müller, D. C.; Nothofer, H.-G.; Scherf, U.; Neher, D.; Bräuchle, C.; Merrholz, K. *Nature* **2000**, *405*, 661.
8. Grimsdale, A. C.; Müllen, K. *Adv. Polym. Sci.* **2008**, *212*, 1.
9. (a) Oyaizu, K.; Iwasaki, T.; Tsukahara, Y.; Tsuchida, E. *Macromolecules* **2004**, *37*, 1257. (b) Bünnagel, T. W.; Nehls, B. S.; Galbrecht, F.; Schottler, K.; Kudla, C. J.; Volk, M.; Pina, J.; Seixas de Melo, J. S.; Burrows, H. D.; Scherf, U. *J. Polym. Sci., Part A: Polym. Chem.* **2008**, *46*, 7342. (c) Laquai, F.; Mishra, A. K.; Müllen, K.; Friend, R. H. *Adv. Funct. Mater.* **2008**, *18*, 3265. (d) Boudreault, P.-L. T.; Wakim, S.; Tang, M. L.; Tao, Y.; Bao, Z.; Leclerc, M. *J. Mater. Chem.* **2009**, *19*, 2921. (e) Wong, K.-T.; Chao, T.-C.; Chi, L.-C.; Chu, Y.-Y.; Balaiah, A.; Chiu, S.-F.; Liu, Y.-H.; Wang, Y. *Org. Lett.* **2006**, *8*, 5033. (f) Brown, D. W.; Mahon, M. F.; Ninan, A. *Tetrahedron* **1993**, *49*, 8919.

10. Burroughes J.H., Bradley D.D.C., Brown A.R, Marks R.N., Mackay K., Friend R.H., Burns P.L., Holmes A.B.: *Nature* **1990**, *347*, 539-541.
11. Braun D.; Heeger A.J.; *Appl Phys Lett.* **1991**, *58*, 1982-1984.
12. (a) Lu, J.; Liang, F.; Drolet, N.; Ding, J.; Tao, Y.; Movileanu, R. *Chem. Commun.* **2008**, 5315. (b) Tsai, J.-H.; Chueh, C.-C.; Lai, M.-H.; Wang, C.-F.; Chen, W.-C.; Ko, B.-T.; Ting, C. *Macromolecules* **2009**, *42*, 1897.
13. Nelson, J. *Science* **2001**, *293*, 1059-1060. (b) Hassheider, T.; Benning, S. A.; Lauhof, M.W.; Kitzerow, H. S.; Bock, H.; Watson, M. D.; Müllen, K. *Mol. Cryst. Liq. Cryst.* **2004**, *413*, 461-472. (c) Oukachmih, M.; Destruel, P.; Seguy, I.; Ablart, G.; Jolinat, P.; Archambeau, S.; Mabilia, M.; Fouet, S.; Bock, H. *Sol. Energy Mater. Sol. Cells* **2005**, *85*, 535-543.
14. (a) Hill, J. P.; Jin, W.; Kosaka, A.; Fukushima, T.; Ichihara, H.; Shimomura, T.; Ito, K.; Hashizume, T.; Ishii, N.; Aida. T. *Science* **2004**, *304*, 1481. (b) Yamamoto, Y.; Fukushima, T.; Suna, Y.; Ishii, N.; Saeki, A.; Seki, S.; Tagawa, S.; Taniguchi, M.; Kawai, T.; Aida. T. *Science* **2006**, *314*, 1761. (c) Xiao, S.; Tang, J.; Beetz, T.; Guo, X.; Tremblay, N.; Siegrist, T.; Zhu, Y.; Steigerwald, M.; Nuckolls. C. *J. Am. Chem. Soc.* **2006**, *128*, 10700.
15. Adam, D.; Schuhmacher, P.; Simmerer, J.; Häussling, L.; Siemensmeyer, K.; Etzbach, K. H.; Ringsdorf, H.; Haarer. D. *Nature* **1994**, *371*, 141.
16. (a) Feng, X.; Pisula, W.; Takase, M.; Dou, X.; Enkelmann, V.; Wagner, M.; Ding, N.; Mullen, K. *Chem. Mater.* **2008**, *20*, 2872-2874. (b) Wong, W.W. H.; Jones, D. J.; Yan, C.; Watkins, S.E.; King, S.; Haque, S. A.; Wen, X.; Ghiggino, K. P.; Holmes, A. B. *Org. Lett.* **2009**, *11*, 975-978. (c) Zhi, L.; Wu, J.; Müllen, K. *Org. Lett.* **2005**, *7*, 5761-5764. (d) Brand, J. D.; Kubel, C.; Ito, S.; Mullen, K. *Chem. Mater.* **2000**, *12*, 1638-1647. (a) Rathore, R.; Burns, C. L. *J. Org. Chem.* **2003**, *68*, 4071-4074. (b) Chebny, V. J.; Gwengo, C.; Gardinier, J. G.; Rathore, R. *Tetrahedron Lett.* **2008**, *49*, 4869-4872. (c) Wadumethrige, S.H.; Rathore, R. *Org. Lett.* **2008**, *10*, 5139-5142. (d) L. Zhai, R. Shukla, R. Rathore *Org. Lett.* **2009**, *11*, 3474-3477.
17. Yokoyama S.; Nakahama T.; Otomo A.; Mashiko, S. *J. Am. Chem. Soc.* **2000**, *122*, 3174.
18. Varnavski, O. P.; Ostrowski, J. C.; Sukhomlinova, L.; Twieg, R. J.; Bazan, G. C.; Goodson, T. *J. Am. Chem. Soc.* **2002**, *124*, 1736-1743.
19. Wolf, M. O.; Fox, H. H.; Fox, M. A. *J. Org. Chem.* **1996**, *61*, 287-294.
20. (a) Ma, J.; Dutt, G. B.; Waldeck, D. H.; Zimmt, M. B. *J. Am. Chem. Soc.* **1994**, *116*, 10619-10629; (b) Lenderink, E.; Duppen, K.; Wiersma, D. A. *J. Phys. Chem.* **1995**,

99, 8972–8977.

21. Wang, G.; Janssens, K.; Van Oosterwijck, C.; Yakimansky, A.; Van Beylen, M. *Polymer* **2005**, *46*, 295–302.
22. Jana, D.; Ghorai, B. K. *Tetrahedron letters*, **2012**, *53*, 196.
23. Roy, P.; Jana, D.; Ghorai, B. K. *Bull. Chem. Soc. Jpn.* **2010**, *83*, 1269-1271.
24. Huang, G.; Ma, B.; Chen, J.; Peng, Q.; Zhang, G.; Fan, Q.; Zhang, D. *Chem. Eur. J.* **2012**, ASAP.

CHAPTER 1

1. (a) *Organic Electronics*, Klauk, H., Ed.; Wiley-VCH: Weinheim, 2006. (b) *Introduction to Molecular Electronics*, M. C. Petty, M. R. Bryce, D. Bloor, Eds.; Oxford Univ. Press: New York, 1995. (c) Maiya, B.G.; Ramasarma, T. *Curr. Sci.* **2001**, *80*, 1523. (d) Tour, J. M. *Chem. Rev.* **1996**, *96*, 537
2. (a) Meldrum, A. N. *J. Chem. Soc.* **1899**, *75*, 1035. (b) Dischendorfer, O.; Verdino, A. *Monatsh. Chem.* **1936**, *68*, 41. (c) Domschke, G. *Chem. Ber.* **1966**, *99*, 930. (d) Dischendorfer, O.; Limontschew, W. *Monatsh. Chem.* **1949**, *80*, 58. (e) Japp, F. R.; Le Fevre, R. J. W.; Taylor, C. R.; Whittam, R. N. *J. Chem. Soc.* **1948**, 1992.
3. (a) Tsuji, H; Mitsui, C.; Ilies, L.; Sato, Y.; Nakamura, E. *J. Am. Chem. Soc.* **2007**, *129*, 11902. (b) Destrade, C.; Tinh, N.H.; Gasparoux, H.; Mamlok, L. *Liquid Crystals* **1987**, *2*, 229.
4. (a) Davis, W. B.; Svec, W. A.; Ratner, M. A.; Wasielewski, M. R. *Nature* **1998**, 396, 60. (b) Kraft, A.; Grimsdale, A. C.; Holmes, A. B. *Angew. Chem. Int. Ed.* **1998**, *37*, 402. (c) Van Hutten, P. F.; Krasnikov, V. V.; Hadziioannou, G. *Acc. Chem. Res.* **1999**, *32*, 257.
5. M. Banerjee, S. V. Lindeman, R. Rathore, *J. Am. Chem. Soc.*, 2007, **129**, 8070. (b) J. K. Kochi, R. Rathore, P. L. Magueres, *J. Org. Chem.*, 2000, **65**, 6826; (c) R. Rathore, S. H. Abdelwahed, I. A. Guzei, *J. Am. Chem. Soc.*, 2004, **126**, 13582; (d) P. Debroy, R. Shukla, S. V. Lindeman, R. Rathore, *J. Org. Chem.*, 2007, **72**, 1765.
6. Moylan, C.R.; Miller, R.D.; Twieg, R.J.; Betterton, K.M.; Lee, V.Y.; Matray, T.J.; Nguyen, C. *Chem. Mater.* **1993**, *5*, 1499.
7. Rathore, R.; Burns, C.L.; M.I. Deselnicu, M.I.; Denmark, S.E.; Bui, T. *Org. Synth.*, **2005**, *82*, 1. Also see Figure S9 in the SI section.
8. Rathore, R.; Burns, C. L.; M. I. Deselnicu *Org. Lett.* **2001**, *3*, 2887.

9. Sun, D.; Lindeman, S. V.; Rathore, R.; Kochi, J. K. *J. Chem. Soc., Perkin Trans. 2* **2001**, 1585-1594 and references cited therein.
10. Calculations were performed using 'Spartan 06' software package.
11. Compare: Banerjee, M.; Lindeman, S.V.; Rathore, R. *Chem. Commun.* **2008**, 1889.
12. (a) Weiss, E. A.; Tauber, M. J.; Kelley, R. F.; Ahrens, M. J.; Ratner, M. A.; Wasielewski, M. R. *J. Am. Chem. Soc.* **2005**, *127*, 11842-11850. (b) Dance, Z. E. X.; Mi, Q.; McCamant, D. W.; Ahrens, M. J.; Ratner, M. A.; Wasielewski, M. R. *J. Phys. Chem. B.* **2006**, *110*, 25163-25173 and reference cited therein.

CHAPTER 2A

1. (a) Berresheim, A. J.; Müller, M.; Müllen, K. *Chem. Rev.* **1999**, *99*, 1747-1785. (b) Watson, M. D.; Fichtenkotter, A.; Müllen, K. *Chem. Rev.* **2001**, *101*, 1267-1300. (c) Chebny, V. J.; Gwengo, C.; Gardinier, J. R.; Rathore, R. *Tetrahedron Lett.* **2008**, *49*, 4869-4872.
2. (a) *Introduction to Molecular Electronics*, M. C. Petty, M. R. Bryce, D. Bloor, Eds.; Oxford Univ. Press: New York, 1995. (b) B. G. Maiya, T. Ramasarma, *Current Science* **2001**, *80*, 1523-1530. (c) Gross, M.; Muller, D. C.; Nothofer, H. -G.; Scherf, U.; Neher, D.; Brauchle, C.; Meerholz, K. *Nature* **2003**, *405*, 661-665. (d) *Organic Electronics*, Klauk, H., Ed.; Wiley-VCH: Weinheim, 2006.
3. (a) Mori, Hiroyuki; *Proceedings of SPIE-The International Society for Optical Engineering* **2006**, 6135 (*Liquid Crystal Materials, Devices, and Applications XI*), 613503/1-613503/8. (b) Tschierske, C. *J. Mat. Chem.* **2001**, *11*, 2647-2671. (c) Goodby, J. W.; Saez, I. M.; Cowling, S. J.; Gortz, V.; Draper, M.; Hall, A. W.; Sia, S.; Cosquer, G.; Lee, S. -E.; Raynes, E. P. *Angew. Chem. Int. Ed.* **2008**, *47*, 2754-2787.
4. (a) Nelson, J. *Science* **2001**, *293*, 1059-1060. (b) Hassheider, T.; Benning, S. A.; Lauhof, M.W.; Kitzerow, H. S.; Bock, H.; Watson, M. D.; Müllen, K. *Mol. Cryst. Liq. Cryst.* **2004**, *413*, 461-472. (c) Oukachmih, M.; Destruel, P.; Seguy, I.; Ablart, G.; Jolinat, P.; Archambeau, S.; Mabilia, M.; Fouet, S.; Bock, H. *Sol. Energy Mater. Sol. Cells* **2005**, *85*, 535-543. (d) Bayer, A.; Zimmermann, S.; Wendorff, J. H. *Mol. Cryst. Liq. Cryst.* **2003**, *396*, 1-22. (e) Katsuhara, M.; Aoyagi, I.; Nakajima, H.; Mori, T.; Kambayashi, T.; Ofuji, M.; Takanishi, Y.; Ishikawa, K.; Takezoe, H.; Hosono, H. *Synth. Met.* **2005**, *149*, 219-223.
5. Zang, Q.; Prins, P.; Jones, S. C.; Barlow, S.; Kondo, T.; An, Z.; Siebbeles, L. D.; Marder, S. R. *Org. Lett.* **2005**, *7*, 5019-5022.

- 6.(a) Weiss, K.; Beernink, G.; Dötz, F.; Birkner, A.; Müllen, K.; Wöll, C. H. *Angew. Chem. Int. Ed.* **1999**, *38*, 3748-3752. (b) Dou, X.; Yang, X.; Bodell, G. J.; Wagner, M.; Enkelmann, V.; Müllen, K. *Org. Lett.* **2007**, *9*, 2485-2488.
7. Rathore, R.; Burns, C. L. *J. Org. Chem.* **2003**, *68*, 4071-4074.
8. A hydrogenation of **7b** (**4**) in ethyl acetate using Pd/C as a catalyst did not afford the corresponding hydroquinone **5** but a reduced indenofluorene derivative containing cyclohexanone moieties, see the Experimental section.
9. Rathore, R.; Abdelwahed, S. H.; Guzei, I. A. *J. Am. Chem. Soc.* **2004**, *126*, 13582-13583.
10. Takada, T.; Arisawa, M.; Gyoten, M.; Hamada, R.; Tohma, H.; Kita, Y. *J. Org. Chem.* **1998**, *63*, 7698-7706.
11. Rathore, R.; Kochi, J. K. *Acta. Chem. Scand.* **1998**, *52*, 114-130.
12. The ECE mechanism is also applicable to other (oxidative) biaryl syntheses, see: (a) Ronlan, A.; Hammerich, O.; Parker, V.D. *J. Am. Chem. Soc.* **1973**, *95*, 7132-7138. (b) Rathore, R.; Kochi, J. K. *J. Org. Chem.* **1995**, *60*, 7479-7490.
13. Compare: Chebny, V. J.; Shukla, R.; Rathore, R. *J. Phys. Chem. B* **2006**, *110*, 13003-13006 and references cited therein.
14. The distonic radical cations have ample literature precedent in the syntheses of a variety of biaryls, see: Hammerich, O.; Parker, V. D. *Adv. Phys. Org. Chem.* **1984**, *20*, 55-190 and references cited therein.
15. Cyclohexadienyl-type radicals are known to undergo oxidation at ~0 V (vs. SCE), see: Haddon, R. C.; Wudl, F.; Kaplan, M. L.; Marshall, J. H.; Cais, R. E.; Bramwell, F. B. *J. Am. Chem. Soc.* **1978**, *100*, 7629-7633.
16. N.G. Anderson, S. P. Maddaford; Keay, B. A. *J. Org. Chem.* **1996**, *61*, 9556-9559.
17. Owing to the large size of HBC **2**, the signals in its ¹H and ¹³C NMR spectra were broad at 22 °C, however, were sharpened at 90 °C (see Figure S5 in the Supporting Information section).

CHAPTER 2B

1. Scholl, R.; Mansfeld, J. *Ber. Dtsch. Chem. Ges.* **1910**, *43*, 1734-1746. Kovacic, P.; Jones, M. B. *Chem. Rev.* **1987**, *87*, 357.

2. (a) Berresheim, A. J.; Müller, M.; Müllen, K. *Chem. Rev.* **1999**, *99*, 1747. (b) Watson, M. D.; Fechtenkotter, A.; Müllen, K. *Chem. Rev.* **2001**, *101*, 1267. (c) Chebny, V. J.; Gwengo, C.; Gardinier, J. R.; Rathore, R. *Tetrahedron Lett.* **2008**, *49*, 4869.
3. (a) Rathore, R.; Burns, C. L. *J. Org. Chem.* **2003**, *68*, 4071. (b) Boden, N.; Bushby, R. J.; Headdock, G.; Lozman, O. R.; Wood, A. *Liq. Cryst.* **2001**, *28*, 139. (c) Boden, N.; Bushby, R. J.; Cammidge, A. N.; Duckworth, S.; Headdock, G. *J. Mater. Chem.* **1997**, *7*, 601.
4. Simpson, C. D.; Mattersteig, G.; Martin, K.; Gherghel, L.; Bauer, R. E.; Räder, H. J.; Muellen, K. *J. Am. Chem. Soc.* **2004**, *126*, 3139. Kübel, C.; Eckhardt, K.; Enkelmann, V.; Wegner, G.; Müllen, K. *J. Mater. Chem.* **2000**, *10*, 879.
5. McKillop, A.; Turrell, A. G.; Young, D. W.; Taylor, E. C. *J. Am. Chem. Soc.* **1980**, *102*, 6504.
6. Aylward, J. B. *J. Chem. Soc. B* **1967**, 1268.
7. Rathore, R.; Kumar, A. S.; Lindeman, S. V.; Kochi, J. K. *J. Org. Chem.* **1998**, *63*, 5847.
8. (a) Yang, J.-S.; Swager, T. M. *J. Am. Chem. Soc.* **1998**, *120*, 5321; (b) Yamaguchi, S.; Swager, T. M. *J. Am. Chem. Soc.* **2001**, *123*, 12087; (c) Rose, A.; Tovar, J. D.; Yamaguchi, S.; Nesterov, E. E.; Zhu, Z.; Swager, T. M. *Philos. Trans. R. Soc. London, Ser. A* **2007**, *365*, 1589, and references therein.
9. Kramer, B.; Fröhlich, R.; Waldvogel, S. R. *Eur. J. Org. Chem.* **2003**, 3549-3554. (b) Waldvogel, S. R.; Aits, E.; Holst, C.; Fröhlich, R. *Chem. Commun.* **2002**, 1278. (c) Kovacic, P.; Lange, R. M. *J. Org. Chem.* **1963**, *28*, 968.
10. L. Zhai, R. Shukla, R. Rathore *Org. Lett.* **2009**, *11*, 3474-3477.
11. (a) Rempala, P.; Kroulik, J.; King, B. T. *J. Am. Chem. Soc.* **2004**, *126*, 15002. (b) King, B. T.; Kroulik, J.; Robertson, C. R.; Rempala, P.; Hilton, C. L.; Korinek, J. D.; Gortari, L. M. *J. Org. Chem.* **2007**, *72*, 2279. (c) Ormsby, J. L.; Black, T. D.; Hilton, C. L.; Bharat; King, B. T. *Tetrahedron* **2008**, *64*, 11370 and references cited therein.
12. Dou, X.; Yang, X.; Bodell, G. J.; Wagner, M.; Enkelmann, V.; Müllen, K. *Org. Lett.* **2007**, *9*, 2485-2488 and references cited therein.
13. (a) Ronlan, A.; Hammerich, O.; Parker, V. D. *J. Am. Chem. Soc.* **1973**, *95*, 7132. (b) Ronlan, A.; Parker, V. D. *J. Org. Chem.* **1974**, *39*, 1014-1016. (c) Rathore, R.; Kochi, J. K. *J. Org. Chem.* **1995**, *60*, 7479. (d) Hammerich, O.; Parker, V. D. *Adv. Phys. Org. Chem.* **1984**, *20*, 55 and references cited therein.

CHAPTER 2C

1. (a) Harvey, R. G. *Poly Cyclic Aromatic Hydrocarbons*; Wiley: New York, 1996; (b) Baumgarten, M.; Mullen, K. *Top. Curr. Chem.* **1994**, *169*, 1 and references cited therein. (c) Berresheim, A. J.; Müller, M.; Müllen, K. *Chem. Rev.* **1999**, *99*, 1747. (d) Watson, M. D.; Fechtenkotter, A.; Müllen, K. *Chem. Rev.* **2001**, *101*, 1267 and references therein. (e) Cao, X.-Y.; Zi, H.; Zhang, W.; Lu, H.; Pei, J., *J. Org. Chem.* **2005**, *70*, 3645-3653.
2. (a) Mori, Hiroyuki; Proceedings of SPIE-The International Society for Optical Engineering **2006**, 6135 (Liquid Crystal Materials, Devices, and Applications XI), 613503/1-613503/8. (b) Tschierske, C. J. *Mat. Chem.* **2001**, *11*, 2647-2671. (c) Goodby, J. W.; Saez, I. M.; Cowling, S. J.; Gortz, V.; Draper, M.; Hall, A. W.; Sia, S.; Cosquer, G.; Lee, S. -E.; Raynes, E. P. *Angew. Chem. Int. Ed.* **2008**, *47*, 2754-2787
3. (a) Feng, X.; Pisula, W.; Takase, M.; Dou, X.; Enkelmann, V.; Wagner, M.; Ding, N.; Mullen, K. *Chem. Mater.* **2008**, *20*, 2872-2874. (b) Wong, W. W. H.; Jones, D. J.; Yan, C.; Watkins, S.E.; King, S.; Haque, S. A.; Wen, X.; Ghiggino, K. P.; Holmes, A. B. *Org. Lett.* **2009**, *11*, 975-978. (c) Zhi, L.; Wu, J.; Müllen, K. *Org. Lett.* **2005**, *7*, 5761-5764. (d) Brand, J. D.; Kubel, C.; Ito, S.; Mullen, K. *Chem. Mater.* **2000**, *12*, 1638-1647.
4. (a) Rathore, R.; Burns, C. L. *J. Org. Chem.* **2003**, *68*, 4071-4074. (b) Chebny, V. J.; Gwengo, C.; Gardinier, J. G.; Rathore, R. *Tetrahedron Lett.* **2008**, *49*, 4869-4872. (c) Wadumethrige, S.H.; Rathore, R. *Org. Lett.* **2008**, *10*, 5139-5142. (d) L. Zhai, R. Shukla, R. Rathore *Org. Lett.* **2009**, *11*, 3474-3477.
5. Baughman, R. H. *Synth. Met.* **1996**, *78*, 339 and references cited therein.
6. (a) *Introduction to Molecular Electronics*, M. C. Petty, M. R. Bryce, D. Bloor, Eds.; Oxford Univ. Press: New York, 1995. (b) Maiya, B. G.; Ramasarma, T. *Current Science* **2001**, *80*, 1523.
7. Wang, Z.; Dötz, F.; Enkelmann, V.; Müllen, K. *Angew. Chem. Int. Ed.* **2005**, *44*, 1247-1250.
8. Rathore, R.; Kochi, J. K. *J. Org. Chem.* **1995**, *60*, 4399.
9. Rathore, R.; Burns, C. L.; Deselnicu, M. I. *Org. Synth.* **2005**, *82*, 1.
10. Mio, M. J.; Kopel, L. C.; Braun, J. B.; Gadzikwa, T. L.; Hull, K. L.; Brisbois, R. G.; Markworth, C. J.; Grieco, P. A. *Org. Lett.* **2002**, *4*, 3199.
11. R. Shukla, S.V. Lindeman, R. Rathore *Chem. Comm.* **2007**, 3717-3719 and references cited therein.

12. (a) F. A. Bell, A. Ledwith, D. C. Sherrington, *J. Chem. Soc. C*, 1969, **13**, 2719. (b) F. A. Bell, A. Ledwith, D. C. Sherrington, *J. Org. Chem.*, 1976, **13**, 155.

CHAPTER 3A

1. (a) Peter, J. G.; Lance, J. T. *Supramolecular Chemistry*, **2003**, *15*, 5. (b) Donald, A. T.; Adel, M. N.; William, A. G. III *Angew. Chem. Int. Ed. Eng*, **1990**, *29*, 138. (c) Marco, F.; Fritz, V. *Angew. Chem. Int. Ed. Eng*, **1999**, *38*, 884.
2. Christopher, B. G.; Jennifer, C. S.; Michael, W. H.; Brandon, L. P.; Hanna, S. G.; Carol, A. H. *J. Am. Chem. Soc.*, **1999**, *121*, 9958.
3. (a) Philipp, W.; Jean, P. G.; Corinne, B.; François, D.; Maurice, G. *Angew. Chem. Int. Ed.*, **1999**, *38*, 3215. (b) Mutsumi, K.; Tetsuo, S.; Tsuyoshi, M.; Kenji, H.; Hirofusa, S. *Chem. Commun.*, **2000**, *11*. (c) Claudia, M. C.; Angel, E. K. *J. Am. Chem. Soc.*, **1998**, *120*, 4023.
4. Rosa, T.; José, M. Q.; Carlos, P.; Esteban, R.; Angel, E. K. *Chem. Commun.*, **2001**, 857.
5. (a) Schreivogel, A.; Maurer, J.; Winter, R.; Baro, A.; Laschat, S. *Eur. J. Org. Chem.* **2006**, *15*, 3395. (b) Wolf, M. O.; Fox, H. H.; Fox, M. A. *J. Org. Chem.* **1996**, *61*, 287.
6. (a) Shultz, D. A.; Fox, M. A. *Tetrahedron Lett.* **1988**, *29*, 4377. (b) Sun, Y.-P.; Fox, M. A. *J. Am. Chem. Soc.* **1993**, *115*, 747. (c) Schuddeboom, W.; Jonker, S. A.; Warman, J. M.; de Haas, M. P.; Vermeulen, M. J. W.; Jager, W. F.; de Lange, B.; Feringa, B. L.; Fessenden, R. W. *J. Am. Chem. Soc.* **1993**, *115*, 3286. (d) Ma, J.; Dutt, G. B.; Waldeck, D. H.; Zimmt, M. B. *J. Am. Chem. Soc.* **1994**, *116*, 10619. (e) Lenderink, E.; Duppen, K.; Wiersma, D. A. *J. Phys. Chem.* **1995**, *99*, 8972.
7. (a) Ito, A.; Nakano, Y.; Kato, T.; Tanaka, K. *Chem. Commun.* **2005**, 403. (b) Mori, T.; Inoue, Y. *J. Phys. Chem. A* **2005**, *109*, 2728.
8. Sengupta, S. *Synlett* **2004**, 1191.
9. (a) Masahiro, I. *Chem. Rev.* **2000**, *100*, 1685 and references therein. (b) Also see: *Introduction to Molecular Electronics*; Petty, M. C., Bryce, M. R., Bloor, D., Eds.; Oxford University Press: New York, 1995.
10. Vyas, V. S.; Rathore, R. ; *Chem Comm*, **2009**, In Press.

11. Buckles, R. E.; Hausman, E. A.; Wheeler, N. G. *J. Am. Chem. Soc.* **1950**, *72*, 2494.
12. Bashkin, J. K.; Kinlen, P. J. *Inorg. Chem.* **1990**, *29*, 4507-4509 and references cited therein.
13. (a) Bell, F. A.; Ledwith, A.; Sherrington, D. C. *J. Chem. Soc. C* **1969**, *13*, 2719. (b) Bell, F. A.; Ledwith, A.; Sherrington, D. C. *J. Org. Chem.* **1976**, *13*, 155.
14. Rathore, R.; Burns, C. L.; Deselnicu, M. I. *Org. Synth.* **2005**, *82*, 1.
15. Rathore, R.; Lindeman, S. V.; Kumar, A. S.; Kochi, J. K. *J. Am. Chem. Soc.* **1998**, *120*, 6931-6939.
16. Debroy, P.; Lindeman, S. V.; Rathore, R. *J. Org. Chem.* **2009**, *74*, 2080–2087

CHAPTER 3B

1. Shirakawa, H.; Louis, E. J.; MacDiarmid, A. G.; Chiang, C. K.; Heeger, A. J. *Chem. Commun.* **1977**, *16*, 578-580.
2. Hill, H. W.; Jr *Ind.Eng. Chem. Prod. Res. Dev.* **1979**, *18*, 252-253.
3. Ram, M. K.; Salerno, M.; Adami, M.; Faraci, P.; Nicolini, C. *Langmuir.* **1999**, *15*, 1252-1259.
4. Hill, H. W. In *High Performance Polymers: Their Origin and Development*; Seymour, R.B., Kirschbaum, G. S.. Eds.; Elsevier: New York, 1986,135-148.
5. Hill, H. W. Jr.; Brady, D. G. *J. Coatings Technol.* **1977**, *49*, 33.
6. Lux, F. *Polymer* **1994**, *14*, 2915.
7. MacDiarmid, A. G. *Synth. Met.* **1997**, *84*, 27.
8. Dezhnev, W.; Xiadong, W.; Riguang, J. *European polymer journal.* **2004**, *40*, 1223.

CHAPTER 4

1. Wurster, C; Schobig, E. *Ber. Dtsch. Chem. Ges.* **1879**, *12*, 1803-1807.
2. Weitz, E.; Fischer, K. *Angew.Chem.* **1925**, *38*, 1100.

3. Smith, M. B.; March, J. *Advanced Organic Chemistry, 5th edition*; Wiley: New York, 2011.
4. Zhai, L.; Shukla, R.; Wadumethrige, S. H.; Rathore, R. *J. Org. Chem.* **2010**, *75*, 4748-4760.
5. (a) Lewis, L. C.; and Singer, L. S. *Chem. Phys.* **1965**, *43*, 2712. (b) Erickson, R.; Benetis, N. P.; Lund, A.; Lindgren, M. *J. Phys. Chem.* **1997**, *101*, 2390. (c) Howarth, O. W.; Fraenkel, G. K. *J. Am. Chem. Soc.* **1966**, *88*, 4514. (d) Kochi, J. K.; Rathore, R.; Le Magueres, P. *J. Org. Chem.* **2000**, *65*, 6826.
6. (a) Stewart, R. *J. Chem. Educ.* **1961**, *38*, 308. (b) Hammerich, O.; Parker, V. D. *Advances in Physical Organic Chemistry*, **1984**, *20*, 55-182. (c) Kaiser, E. T.; Kevan, L. *Radical-Ions*, Wiley-Interscience, London, 1968.
7. Ledwith, A. *Accounts of Chemical Research*, **1972**, *5*, 133-139.4.
8. (a) Rathore, R.; Burns, C. L.; Deselnicu, M. I. *Org. Synth.* **2005**, *82*, 1. (b) Also see: Rathore, R.; Kochi, J. K. *J. Org. Chem.* **1995**, *60*, 4399.
9. (a) Badger, B.; Brocklehurst, B. *Trans. Faraday Soc.* **1969**, *65*, 2582 and 2588. (b) Badger, B.; Brocklehurst, B. *Trans. Faraday Soc.* **1970**, *66*, 2939. (c) Badger, B.; Brocklehurst, B. *Nature* **1968**, *219*, 263. (d) Rodgers, M. A. J. *J. Chem. Soc., Faraday Trans. 1* **1972**, *68*, 1278.
10. Navale, T. S.; Thakur, K.; Vyas, V. S.; Wadumethrige, S. H.; Shukla, R.; Lindeman, S. V.; Rathore, R. *Langmuir* **2012**, *28*, 71-83.
11. Matsuura, A.; Nishinaga, T.; Komatsu, K. *J. Am. Chem. Soc.* **2000**, *122*, 10007.
12. Rathore, R.; Loyd S. H.; Kochi, J. K. *J. Am. Chem. Soc.* **1994**, *116*, 8414-8415.
13. Rathore, R.; Kumar, A. S.; Lindeman, S. V.; Kochi, J. K. *J. Org. Chem.* **1998**, *63*, 5847.
14. Bruson, H. A.; Kroeger, J. W. *J. Am. Chem. Soc.* **1940**, *62*, 36-44
15. Kabir, S.M.H.; Hasegawa, M.; Kuwatani, Y.; Yoshida, M.; Matsuyama, H.; Iyoda, M. *J. Chem. Soc. Perkin Trans. I*, **2001**, *2*, 159-165.
16. Tashiro, M.; Yamato, T. *J. Org. Chem.* **1979**, *44*, 3037-41.
17. Buckles, R. E.; Serianz, A.; Naffziger, D. *Proceedings of the Iowa Academy of Science* **1973**, *80*, 45.